UNIVERSIDADE ESTADUAL DE CAMPINAS

INSTITUTO DE BIOLOGIA

BIANCA RIBEIRO DE SOUZA

"AVALIAÇÃO DA IMUNOTERAPIA COM O ONCOTHERAD® (MRB-CFI-1) E ASSOCIAÇÕES NO TRATAMENTO ONCOLÓGICO: CÂNCER DE BEXIGA E CÂNCER DE OVÁRIO"

"EVALUATION OF ONCOTHERAD® (MRB-CFI-1) IMMUNOTHERAPY AND ASSOCIATIONS IN ONCOLOGICAL TREATMENT: BLADDER CANCER AND OVARIAN CANCER"

CAMPINAS

2023

BIANCA RIBEIRO DE SOUZA

"AVALIAÇÃO DA IMUNOTERAPIA COM O ONCOTHERAD® (MRB-CFI-1) E ASSOCIAÇÕES NO TRATAMENTO ONCOLÓGICO: CÂNCER DE BEXIGA E CÂNCER DE OVÁRIO"

"EVALUATION OF ONCOTHERAD® (MRB-CFI-1) IMMUNOTHERAPY AND ASSOCIATIONS IN ONCOLOGICAL TREATMENT: BLADDER CANCER AND OVARIAN CANCER"

Ph.D. Thesis presented to the Institute of Biology of the University of Campinas in partial fulfillment of the requirements for the degree of Ph.D. in Molecular and Morphofunctional Biology in the concentration area Cell Biology.

Tese de doutorado apresentada ao Instituto de Biologia da Universidade Estadual de Campinas como parte dos requisitos exigidos para a obtenção do Título de Doutora em Biologia Molecular e Morfofuncional na área de concentração Biologia Celular.

Orientador: PROF. DR. WAGNER JOSÉ FÁVARO

ESTE ARQUIVO DIGITAL CORRESPONDE À VERSÃO FINAL DA TESE DEFENDIDA PELA ALUNA BIANCA RIBEIRO DE SOUZA E ORIENTADA PELO PROF. DR. WAGNER JOSÉ FÁVARO.

CAMPINAS

2023

Ficha catalográfica
Universidade Estadual de Campinas
Biblioteca do Instituto de Biologia
Gustavo Lebre de Marco - CRB 8/7977

So89a

Souza, Bianca Ribeiro de, 1993-
Avaliação da imunoterapia com o OncoTherad® (MRB-CFI-1) e associações no tratamento oncológico : câncer de bexiga e câncer de ovário / Bianca Ribeiro de Souza. – Campinas, SP : [s.n.], 2023.

Orientador: Wagner José Fávaro.
Tese (doutorado) – Universidade Estadual de Campinas, Instituto de Biologia.

1. Neoplasias da bexiga. 2. Neoplasias ovarianas. 3. Imunoterapia. 4. Receptores Toll-like. 5. OncoTherad. 6. Plasma rico em plaquetas. 7. Eritropoetina. I. Fávaro, Wagner José, 1980-. II. Universidade Estadual de Campinas. Instituto de Biologia. III. Título.

Informações Complementares

Título em outro idioma: Evaluation of OncoTherad® (MRB-CFI-1) immunotherapy and associations in oncological treatment : bladder cancer and ovarian cancer
Palavras-chave em inglês:
Bladder neoplasms
Ovarian neoplasms
Immunotherapy
Toll-like receptors
OncoTherad
Platelet-rich plasma
Erythropoietin
Área de concentração: Biologia Celular
Titulação: Doutora em Biologia Molecular e Morfofuncional
Banca examinadora:
Wagner José Fávaro [Orientador]
Murilo Vieira Geraldo
Ângela Cristina Malheiros Luzo
Telma Goncalves Carneiro Spera de Andrade
Gabriel Adan Araújo Leite
Data de defesa: 12-06-2023
Programa de Pós-Graduação: Biologia Molecular e Morfofuncional

Identificação e informações acadêmicas do(a) aluno(a)
- ORCID do autor: https://orcid.org/0000-0001-9373-6989
- Currículo Lattes do autor: http://lattes.cnpq.br/7432482920493423

Campinas, 12 de junho de 2023

COMISSÃO EXAMINADORA

Prof. Dr. Wagner José Fávaro (*Presidente*)

Prof. Dr. Murilo Vieira Geraldo

Prof.ª Dra. Ângela Cristina Malheiros Luzo

Prof.ª. Dra. Telma Goncalves Carneiro Spera de Andrade

Prof. Dr. Gabriel Adan Araújo Leite

Os membros da Comissão Examinadora acima assinaram a Ata de Defesa, que se encontra no processo de vida acadêmica do aluno.

A Ata da defesa com as respectivas assinaturas dos membros encontra-se no SIGA/Sistema de Fluxo de Dissertação/Tese e na Secretaria do Programa de Pós graduação em Biologia Molecular e Morfofuncional do Instituto de Biologia.

Dedico esse trabalho aos pacientes oncológicos e, em especial, às mulheres que estão na luta contra o câncer de ovário.

AGRADECIMENTOS

Primeiramente, agradeço a Deus, pela minha vida e saúde, e por iluminar meu caminho especialmente nos momentos mais difíceis. E a Nossa Senhora, que me protegeu em todos os percursos que trilhei até hoje.

Agradeço ao meu orientador, prof. Dr. Wagner José Fávaro, por todos os valiosos ensinamentos e por me inspirar na pesquisa. Obrigada por me mostrar o quanto é importante retornar o que recebemos na Universidade para a sociedade e por demonstrar na prática o valor da esperança. Muito obrigada, professor Wagner, por confiar e investir no meu potencial, bem como por todo o suporte para conclusão desse trabalho. Obrigada por nos enxergar como mais do que alunos de pós graduação e nos apoiar de forma tão prestativa também na vida pessoal.

Ao meu coorientador, Dr. Nelson Durán, pelos conhecimentos compartilhados e por estar sempre disponível, bem como pelas conversas que me inspiraram a ir mais longe.

Ao prof. Dr. Michael Anglesio por ter me orientado durante o estágio no exterior no Canadá, fornecendo grande suporte, apoio e ensinamentos sobre o câncer de ovário. *I truly thank you!*

Agradeço ao Conselho Nacional de Desenvolvimento Científico e Tecnológico (CNPq) (Processo nº 140695/2019-2) e à Fundação de Amparo à Pesquisa do Estado de São Paulo (FAPESP) (Processo nº 2020/15687-5 e BEPE Processo nº 2021/12357-7) pelo suporte financeiro sem o qual não seria possível a realização desse trabalho e o estágio no exterior. O presente trabalho também foi realizado com apoio da Coordenação de Aperfeiçoamento de Pessoal de Nível Superior – Brasil (CAPES) - Código de Financiamento 001.

À Universidade de Campinas (UNICAMP) pelo suporte e estrutura para a condução dessa pesquisa de doutorado e pela formação excelente que tive a oportunidade de obter.

À *University of British Columbia* (UBC) pela assistência e suporte ímpar durante o meu estágio como aluna visitante.

Aos meus pais, pelo amor e apoio incondicionais, pela paciência e incentivo durante toda a minha vida. Nenhuma palavra pode expressar o quanto sou grata a vocês.

Aos meus irmãos Mônica, Felipe e Tiago bem como meus avós e família que estão sempre torcendo pelo meu bem.

Ao Giuliano, pelo apoio emocional e também científico, como as nossas discussões de ciência e estatística e pela ajuda com os gráficos bonitos do R. Obrigada por todo o amor e dedicação.

À Ianny, que me acolheu gentilmente e me ensinou muito com tanta paciência, desde o início do doutorado. Obrigada por tudo, você é uma grande amiga e inspiração pra mim!

À Gabriela pós doc., pela amizade, parceria e apoio, especialmente nos momentos mais difíceis durante a pandemia do COVID-19 e dos trabalhos mais pesados.

Aos amigos do Laboratório de Carcinogênese Urogenital e Imunoterapia: Ianny, Sabrina, Gabriela pós doc., Gabriela mestranda, Giovana, Juliane, Felippe, Daniel Natália, Queila e Eduardo e à equipe do ensaio clínico do OncoTherad®: Dr. João, Juliana, Magali e Humberto por todo conhecimento compartilhado, por toda ajuda, apoio e amizade. Um ambiente de trabalho colaborativo sempre faz toda a diferença!

Às minhas amigas do laboratório do Dr. Michael Anglesio, Karolin e Anna, obrigada por me acolherem e ensinarem tanto. Obrigada também às técnicas científicas da UBC que tanto me ensinaram: Janine, Christine, Monica e Amy.

Aos meus amigos, Priscilla, Hanna, Larissa, Vinícius e William pela amizade sincera e apoio de tantos anos.

A todos os professores do Instituto de Biologia, muito obrigada pelos conhecimentos valiosos compartilhados e pela inspiração profissional.

Aos funcionários do Departamento de Anatomia, em especial ao técnico Roberto e à Tanaci, vocês são essenciais para todos nós!

Aos membros da banca pela atenção, disponibilidade e por aceitarem o convite. Estou muito honrada em poder contar com vocês.

Aos pacientes oncológicos em especial os participantes do ensaio clínico com o OncoTherad®, vocês são o que dão sentido ao trabalho na bancada todos os dias.

Aos animais utilizados na experimentação científica, sem os quais jamais conseguiríamos obter os avanços na saúde humana. Minha gratidão pela vida desses animais.

A todos que de alguma forma contribuíram para realização desse trabalho, meu muito obrigada!

RESUMO

Não há terapia de segunda linha eficaz para o câncer de bexiga não-músculo invasivo (CBNMI) quando ocorre falha do *Bacillus Calmette-Guérin* (BCG). Nesse cenário, uma nova perspectiva é representada pela imunoterapia OncoTherad® (MRB-CFI-1), um complexo nanoestruturado desenvolvido pela Universidade de Campinas, Brasil. Os efeitos antitumorais e imunomodulatórios do OncoTherad® atentam para análises em outros tumores sólidos que também estabelecem um estado de imunossupressão no microambiente tumoral, como o câncer de ovário. O termo carcinoma ovariano (CO) refere-se a uma coleção de cinco doenças distintas conhecidas como histotipos. Embora o tratamento histotipo-específico ainda seja um desafio clínico, modelos bem caracterizados são necessários para testar novas terapias. Nesse trabalho, nós avaliamos os efeitos histopatológicos e moleculares do OncoTherad® e associações terapêuticas (Plasma Rico em Plaquetas - PRP e Eritropoetina - EPO) no tratamento de diferentes cânceres do sistema urogenital (câncer de bexiga e câncer de ovário) em modelos animais. Além disso, nós caracterizamos o modelo de CO induzido quimicamente, avaliando sua representatividade da doença humana. Para o modelo de CBNMI, trinta e cinco camundongas C57BL/6J foram divididos em 5 grupos: Controle; Câncer (carcinógeno N-etil-N-nitrosoureia, 50 mg/ml); PRP (0,1 ml); OncoTherad (20 mg/ml); e OncoTherad+PRP (10 mg/ml). A modulação promovida na via de sinalização dos receptores *Toll-like* (TLRs), a atividade citotóxica (CX3CR1, IL-1β) e células Tregs FOXP3+ foram avaliadas por imuno-histoquímica (IHC). O tratamento com OncoTherad® isolado ou associado ao PRP aumentou as imunorreatividades de NF-kB, IL-6, TLR4, TBK1, IRF-3 e IFN-γ. Assim, a modulação do microambiente do CBNMI para um perfil citotóxico correlacionou-se com o aumento de IL-1β através da estimulação das vias imunes para produção de IFN-γ e a consequente ativação de células T CD8+ e redução de Tregs. No modelo de CO, trinta e cinco ratas *Fischer* foram distribuídas em 5 grupos: Controle (cirurgia *Sham*); Câncer (injeção de 7,12-dimetilbenzoantraceno – DMBA na bursa ovariana, 1,25 mg/kg); OncoTherad (20mg/kg IP); EPO (8,4 μg/kg IP); e OncoTherad+EPO (mesmas doses). A via dos TLRs (TLR2, TLR4, IL-6, IFN-γ) e o perfil da resposta inflamatória (iNOS, macrófagos totais F4/80+, macrófagos CD163+ M2, linfócitos Treg FOXP3+) foram avaliados por IHC. Além disso, avaliamos mutações genéticas e biomarcadores típicos de diferentes histotipos do CO bem como a densidade de linfócitos (CD3) por IHC. O OncoTherad® isolado ou associado à EPO foi capaz de prevenir lesões ovarianas e modular o microambiente do CO para um perfil citotóxico envolvendo a sinalização dos TLRs. A EPO também apresentou efeitos imunomoduladores, embora com caráter mais imunossupressor. O conjunto de características analisadas favoreceram a interpretação do modelo de CO induzido por DMBA como carcinoma seroso de baixo grau, no qual os tratamentos com OncoTherad® e EPO mostraram propriedades imunomoduladoras relacionadas à redução de lesões ovarianas. Dessa forma, foi possível demonstrar os efeitos antitumorais do OncoTherad® em cânceres do sistema urogenital bem como caracterizar um novo modelo animal de CO para o teste de novas drogas considerando o histotipo específico.

Palavras-chave: Neoplasias da bexiga; Neoplasias ovarianas; Imunoterapia; Receptores Toll-like; OncoTherad; Plasma rico em plaquetas; Eritropoetina.

ABSTRACT

There is no effective second-line therapy for non-muscle invasive bladder cancer (NMIBC) when Bacillus Calmette-Guérin (BCG) fails. In this scenario, a new perspective is represented by OncoTherad® immunotherapy (MRB-CFI-1), a nanostructured complex developed by the University of Campinas, Brazil. The antitumor and immunomodulatory effects of OncoTherad® draw attention to analyzes in other solid tumors that also establish a state of immunosuppression in the tumor microenvironment, such as ovarian cancer. The term ovarian carcinoma (OC) refers to a collection of five distinct diseases known as histotypes. Although histotype-specific treatment remains a clinical challenge, well-characterized models are needed to test new therapies. In this work, we evaluated the histopathological and molecular effects of OncoTherad® and therapeutic associations (Platelet Rich Plasma - PRP and Erythropoietin - EPO) in the treatment of different cancers of the urogenital system (bladder cancer and ovarian cancer) in animal models. Furthermore, we characterized the chemically induced OC model, assessing its representativeness of human disease. For the Bladder Cancer model, thirty-five C57BL/6J mice were divided into 5 groups: Control; Cancer (carcinogen N-ethyl-N-nitrosourea, 50 mg/ml); PRP (0.1 ml); OncoTherad (20 mg/ml); and OncoTherad+PRP (10 mg/ml). The modulation promoted in the signaling pathway of Toll-like receptors (TLRs), cytotoxic activity (CX3CR1, IL-1β), and FOXP3+ Tregs cells were evaluated by immunohistochemistry (IHC). Treatment with OncoTherad® alone or associated with PRP increased NF-kB, IL-6, TLR4, TBK1, IRF-3 and IFN-γ immunoreactivities. Thus, the modulation of the NMIBC microenvironment to a cytotoxic profile correlated with the increase of IL-1β through the stimulation of the immune pathways for the production of IFN-γ and the consequent activation of CD8+ T cells and reduction of Tregs. In the OC model, thirty-five Fischer rats were distributed into 5 groups: Control (Sham surgery); Cancer (7,12-dimethylbenzoanthracene – DMBA injection into the ovarian bursa, 1.25 mg/kg); OncoTherad (20mg/kg IP); EPO (8.4 µg/kg IP); and OncoTherad+EPO (same doses). The pathway of TLRs (TLR2, TLR4, IL-6, IFN-γ) and the profile of the inflammatory response (iNOS, total F4/80+ macrophages, CD163+ M2 macrophages, FOXP3+ Treg lymphocytes) were evaluated by IHC. In addition, we evaluated genetic mutations and typical biomarkers of different OC histotypes as well as lymphocyte density (CD3) by IHC. OncoTherad® alone or associated with EPO was able to prevent ovarian lesions and modulate the OC microenvironment to a cytotoxic immune profile involving TLR signaling. EPO also showed immunomodulatory effects, although with a more immunosuppressive character. The set of characteristics analyzed favored the interpretation of the DMBA-induced OC model as low-grade serous carcinoma, in which treatments with OncoTherad® and EPO showed immunomodulatory properties related to the reduction of ovarian lesions. In this way, it was possible to demonstrate the antitumor effects of OncoTherad® in cancers of the urogenital system, as well as to characterize a new animal OC model for testing new drugs considering the specific histotype.

Keywords: Bladder neoplasms; Ovarian neoplasms; Immunotherapy; Toll-like receptors; OncoTherad; Platelet rich plasma; Erythropoietin.

LISTA DE ILUSTRAÇÕES

LISTA DE TABELAS

LISTA DE ABREVIATURAS E SIGLAS

ANOVA: análise de variância

APCs: células apresentadoras de antígenos

ARID1A: AT-rich interactive domain-containing protein 1A

ATC: imunoterapia adotiva de células T

B7-1 (CD80): T-lymphocyte activation antigen CD80

B7-2 (CD86): T-lymphocyte activation antigen CD86

BAX: Apoptosis regulator BAX

BCG: *Bacillus Calmette-Guérin*

BCL-2: Apoptosis regulator Bcl-2

BRAF: B-Raf proto-oncogene, serine/threonine kinase

BRCA1: BRCA1 DNA repair associated

BRCA2: BRCA2 DNA repair associated

CB: câncer de bexiga urinária

CBNMI ou NMIBC: câncer de bexiga não músculo-invasivo

CCC: carcinoma ovariano de célula claras

CD163: Scavenger receptor cysteine-rich type 1 protein M130

CD28: T-cell-specific surface glycoprotein CD28

CD3: T-cell surface glycoprotein CD3 delta chain

CD40: Tumor necrosis factor receptor superfamily member 5

CD40L: ligante de CD40

CO ou OC: carcinoma ovariano

CpG-ODN: oligonucleotídeos CpG

CTLA-4: antígeno 4 associado a linfócito T citotóxico

CTLs: linfócitos T citotóxicos

CTNNB1: catenin beta 1

CX3CR1: receptor 1 de quimiocina CX3C

DAMP: padrões moleculares associados a danos

DC: células dendríticas

DMBA: 7,12-dimetilbenzoantraceno

ENU: N-etil-N-nitrosoureia

EPO: eritropoietina

ERKS: proteínas quinases reguladoras de sinalização extracelular

F4/80: Adhesion G protein-coupled receptor E1

FC: Fator(es) de crescimento

FDA: *Food and Drug Administration*

FFPE: formalin-fixed, paraffin-embedded

FGF: fator de crescimento de fibroblastos

FIGO: *International Federation of Gynecology and Obstetrics*

FOXP3: fator de transcrição *forkhead box protein* P3

GMCSF: fator estimulante de colônias de macrófagos

HE: hematoxilina & eosina

HER2: erb-b2 receptor tyrosine kinase 2

HGSC: carcinoma ovariano seroso de alto grau

HNF1B: Hepatocyte nuclear factor 1-beta

HPA: hidrocarboneto policíclico aromático

IC: intervalo de confiança

ICAM: moléculas de adesão intercelular

IFN-γ: interferon-γ

IGF-1: fator de crescimento semelhante à insulina 1

IHC: imuno-histoquímica

IKKα: Inhibitor of nuclear factor kappa-B kinase subunit alpha

IKKϵ (IKKi): Inhibitor of nuclear factor kappa-B kinase subunit epsilon

IL-10: interleucina-10

IL-12: interleucina-12

IL-1β: interleucina-1β

IL-6: interleucina-6

INCA: Instituto Nacional do Câncer

iNOS: óxido nítrico sintase induzível

INPI: Instituto Nacional da Propriedade Industrial

IRAK1: Interleukin-1 receptor-associated kinase 1

IRAK2: Interleukin-1 receptor-associated kinase-like 2

IRAK4: Interleukin-1 receptor-associated kinase 4

IRF-3: fator regulador de interferon-3

IRF-5: fator regulador de interferon-5

IRF-7: fator regulador de interferon-7

ISTH: *International Society on Thrombosis and Haemostasis*

JAKs: proteínas Janus Quinases

JNK: proteínas quinases c-jun-N-terminal

KRAS: KRAS proto-oncogene, GTPase

LGSC: carcinoma ovariano seroso de baixo grau

LL-37: Cathelicidin antimicrobial peptide

MAPKs: proteínas-quinases ativadas por mitógeno

MC: carcinoma ovariano mucinoso

MDSCs: células supressoras derivadas da linhagem mieloide

MHC: complexo principal de histocompatibilidade

micro-CT: microtomografia computadorizada de raios X

MNU: N-metil-N-nitrosoureia

MRB-CFI-1: Modificador de Resposta Biológica - Complexo de Fosfato Inorgânico 1

MyD88: proteína de resposta primária de diferenciação mielóide 88

NF-κB: fator nuclear kappa B

NK: células *Natural Killer*

NO: óxido nítrico

OMS: Organização Mundial da Saúde

OPG: osteoprotegerina

p38: p38 mitogen-activated protein kinases

p53: Cellular tumor antigen p53

PAMPs: padrões moleculares associados a patógenos

PARP: Poly [ADP-ribose] polymerase

PCR: Reação em Cadeia da Polimerase

PD-1: proteína de morte celular programada 1

PDGF: fator de crescimento derivado de plaquetas

PD-L1: ligante de morte programada-1

PF4: fator plaquetário 4

PIK3CA: phosphatidylinositol-4,5-bisphosphate 3-kinase catalytic subunit alpha

P-MAPA: agregado polimétrico anidrídico fosfolinoleato-palmitoleato de magnésio e amônio proteico

PMNs: neutrófilos polimorfonucleares

PolyP: polifosfatos

PR: progesterone receptor

pT1: carcinoma urotelial confinado à mucosa e submucosa da bexiga

pT1G2-3: carcinoma urotelial confinado à mucosa e submucosa da bexiga grau 2 – 3

pTa: carcinoma urotelial papilar não invasivo

pTaG2-3: carcinoma urotelial papilar não invasivo grau 2 - 3

PTEN: phosphatase and tensin homolog

pTis: carcinoma urotelial *in situ*

RANK: receptor ativador de NF-κB

RANKL: ligante do receptor ativador de NF-κB

rHuEPO: eritropoetina recombinante humana

ROS: espécies reativas de oxigênio

RPC: resposta patológica completa

RTU: ressecção transuretral

SIAH-2: E3 ubiquitin-protein ligase SIAH2

SLR: sobrevida livre de recorrência

STATs: Transdutores de Sinal e Ativadores de Transcrição

STING: via do fator estimulador do complexo gênico do interferon

TAK1: TGF-beta-activated kinase 1 and MAP3K7-binding protein 1

TAMs: macrófagos associados a tumores *(tumor-associated macrophages)*

TBK1: quinase 1 de ligação ao TANK

TCD4: linfócito T *helper*

TCD8: linfócito T citotóxico

TGF-β: fator de crescimento transformante β

TIL: infiltrado linfocitário tumoral

TIR: domínio do receptor Toll-interleucina-1

TIRAP: proteína adaptadora contendo domínio receptor de toll-interleucina 1 (TIR)

TLRs: receptores *Toll Like*

TMA: Microarranjo de tecido (*Tissue Microarray)*

TNF-α: fator de necrose tumoral α

TNM: Classificação de Tumores Malignos

TP53: tumor protein p53

TPI: inibição da progressão tumoral

TRAF3: TNF receptor-associated factor 3

TRAF6: TNF receptor-associated factor 6

TRAIL: ligante indutor de apoptose relacionado ao TNF

TRAM: proteína de membrana associada à cadeia de translocação

Tregs: células T regulatórias

TRIF: proteína adaptadora indutora de interferon-β contendo domínio TIR

UICC: *Union for International Cancer Control's*

USPTO: *United States Patent and Trademark Office*

VEGF: fator de crescimento endotelial vascular

WT1: Wilms tumor protein

SUMÁRIO

1. INTRODUÇÃO

1.1. Câncer de Bexiga Urinária

1.1.1. Visão Geral

O câncer de bexiga urinária (CB) é o décimo tipo de câncer mais comum no mundo, com mais de 500 mil novos casos diagnosticados por ano (Bray et al., 2018). A Sociedade Americana para o Câncer estimou para 2022 cerca de 81.180 novos casos de CB nos Estados Unidos, sendo 61.700 em homens e 19.480 em mulheres (*American Cancer Society*, 2022a). A estimativa também previu 17.100 mortes por CB, sendo 12.120 homens e 4.980 mulheres. Segundo dados do Instituto Nacional do Câncer (INCA, 2022a), a estimativa para o Brasil no ano de 2023 é de 11.370 novos casos de CB, sendo 7.870 homens e 3.500 mulheres. No ano de 2020 foram notificadas 4.595 mortes por CB (3.097 homens e 1.498 mulheres) no país. A mortalidade por câncer de bexiga proporcional em relação a todas as mortes por câncer tem aumentado nos últimos 30 anos no Brasil (**Figura 1**; INCA, 2022b).

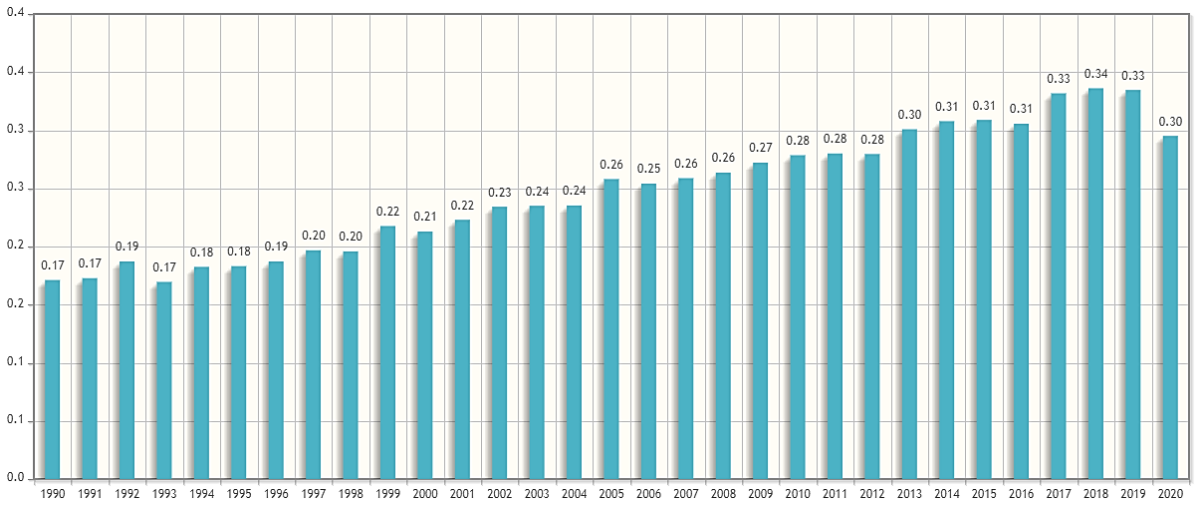

Figura 1. Mortalidade proporcional por câncer de bexiga no Brasil entre os anos de 1990 e 2020. Gráfico gerado através do Atlas on-line de mortalidade do site do INCA (INCA, 2022b). Valores expressos em porcentagem (eixo y).

Mais de 70% da incidência de CB é superficial, denominado câncer de bexiga não-músculo invasivo (CBNMI), e a ocorrência de uma doença invasiva é ocasional (Askeland et al., 2012). Os tumores superficiais são classificados em três estágios: Tis - carcinoma in situ; Ta - papilífero e T1 - tumor confinado a mucosa e submucosa da bexiga, ocorrendo em 10%, 70% e 20%, respectivamente (Epstein et al., 1998). Contudo, 50% dos tumores não-músculo

invasivos recorrem em 4 anos após o tratamento padrão e 11% evoluem para o fenótipo invasivo (Askeland et al., 2012). O estadiamento histológico do CB é determinado pela profundidade de invasão tumoral da parede vesical e dependerá da ressecção transuretral (RTU) do tumor, por via endoscópica, para seu diagnóstico correto. Fragmentos de ressecção superficiais e profundos devem ser analisados separadamente (Epstein et al., 1998).

Um número significativo de fatores de risco tem sido relacionado ao desenvolvimento de CB. Segundo dados do registro da base populacional do INCA, o maior fator de risco para o desenvolvimento do CB é o tabagismo, presente em cerca de 50 - 70 % dos casos (INCA, 2022c). Na meta-análise de estudos epidemiológicos de Zeegers et al. (2000) sobre o impacto das características do tabagismo ao risco de câncer do trato urinário, o cigarro foi apontado como um fator que aumenta substancialmente o risco para o desenvolvimento do câncer de bexiga. O cigarro possui dezenas de substâncias tóxicas, dentre elas aminas aromáticas e compostos N-nitrosos, potentes carcinógenos. Outro fator de risco potencial para o desenvolvimento do CB é a exposição ocupacional às aminas aromáticas por trabalhadores de indústrias de borracha, têxtil e de tinta e a infecção por *Schistosoma haematobium*, sendo este endêmico em países mediterrâneos como o Egito (Poon et al., 2015; Rosenquist & Grollman, 2016; Zeegers et al., 2000). A exposição a certas substâncias tais como o arsênio, que pode estar presente em águas de abastecimento, o ácido aristolóquico presente em muitas plantas de uso medicinal e a pioglitazona presente em fármacos para tratamento de diabetes estão associados como um fator de risco (Poon et al., 2015; Rosenquist & Grollman, 2016).

Em geral, o CB é cerca de 3 a 4 vezes mais comum em homens do que em mulheres. Por outro lado, a sobrevida das mulheres é pior com esse tipo de tumor. Especula-se que a alta agressividade do câncer de bexiga nas mulheres é decorrente de fatores hormonais, além do diagnóstico mais tardio (Dobruch et al., 2016). Embora a bexiga urinária seja secundariamente regulada por hormônios sexuais esteroides, o urotélio normal e os tumores uroteliais são responsivos aos andrógenos e estrógenos (Garcia et al., 2015). Garcia et al. (2015) demonstraram pela primeira vez em ratas induzidas quimicamente ao CBNMI que os níveis proteicos aumentados da ubiquitina ligase Siah-2 supraregularam os receptores androgênicos e diminuíram os níveis dos receptores estrogênicos, culminando com o escape das células uroteliais neoplásicas do sistema imune. Esses mesmos autores verificaram que os níveis dos receptores do sistema imune, *Toll-like receptors* (TLRs), foram diminuídos no CBNMI e associaram esse efeito ao aumento dos níveis de Siah-2 e dos receptores androgênicos.

1.1.2. Terapêutica

O tratamento primário do CBNMI baseia-se no procedimento cirúrgico através da ressecção transuretral (RTU), seguido da imunoterapia intravesical com *Bacillus Calmette-Guérin* (BCG), para diminuição da recidiva e prevenção da progressão tumoral (Askeland et al., 2012). No entanto, as taxas de recidiva e progressão após ressecção endoscópica são elevadas para o câncer de bexiga (Askeland et al., 2012). Em torno de 20% a 30% dos tumores superficiais (pTis, pTa e pT1) apresentam progressão e 70% recorrência pós-tratamento exclusivo com RTU (Askeland et al., 2012; Kemp et al., 2005). Por outro lado, sabe-se que a terapia adjuvante com BCG pode diminuir esses índices para 30% (Askeland et al., 2012; Hall et al., 2007). Morales e Eidinger (1976) foram pioneiros em comprovar o sucesso no tratamento do CBNMI com BCG. Desde então, BCG é o tratamento de escolha para o CBNMI de alto risco, sendo considerada atualmente a imunoterapia que apresenta melhores resultados, superior inclusive à quimioterapia intravesical com relação às taxas de recorrência e progressão do tumor (Askeland et al., 2012; Bohle; Brandau, 2003; Hall et al., 2007).

A imunoterapia com BCG resulta em resposta imune massiva caracterizada pela indução dos receptores do sistema imune, receptores *Toll-like* 2 e 4 (TLRs 2 e 4), com consequente indução da expressão de citocinas tanto na urina quanto na bexiga e influxo de células inflamatórias na parede vesical (Bohle; Brandau, 2003; Garcia et al., 2015; 2016; Schamhart et al., 2000). Citocinas como Fator de Necrose Tumoral – α (TNF-α), fator estimulante de colônias de macrófagos (GMCSF), interferon (IFN) e interleucinas (ILs) induzem resposta de linfócitos T–*helper* e das células *Natural Killer* (NK) na bexiga (Bohle; Brandau, 2003; Garcia et al., 2015; 2016). De acordo com Schamhart et al. (2000), após a instilação de BCG, a parede vesical apresenta infiltrado celular granulomatoso, envolto por linfócitos e granulócitos com indução de resposta imune de longa duração, a qual pode persistir por mais de 1 ano. Contudo, tal resposta varia amplamente nos pacientes e a possível correlação entre expressão de citocinas e resultado da terapia é alvo de intensa investigação (Schamhart et al., 2000).

No entanto, o uso de organismos vivos e atenuados pode causar efeitos colaterais e dificuldade em predizer a resposta imune e antitumoral. O uso do BCG é limitado no CBNMI devido à falha do tratamento, efeitos adversos e intolerância que ocorrem em mais de dois terços dos pacientes (Perabo et al., 2005). Ainda, complicações severas e óbito relacionados ao tratamento foram descritos (Berry et al., 1996; Kamat et al., 2017). Estima-se que

aproximadamente 5-10% dos pacientes não conseguem completar o tratamento de indução com BCG, acarretando na interrupção do esquema terapêutico (Bohle et al., 2003; Ojea et al., 2007). A toxicidade da imunoterapia intravesical com BCG pode ser dividida em efeitos colaterais locais e sistêmicos. Os efeitos colaterais locais mais comuns incluem disúria (71%), hematúria (29%) e contratura vesical (3%) (Hall et al., 2007). Já os efeitos colaterais sistêmicos podem ser divididos em infecciosos (cistite bacteriana, epididimite, prostatite, infecções uretrais, sepse) e não-infecciosos (artralgias, reações cutâneas, anafilaxia), sendo que os sintomas de febres e calafrios ocorrem em 30% dos pacientes; epididimite, prostatite e infecções uretrais em 4%; sepse em 1%; e artralgias e reações cutâneas em 6% (Hall et al., 2007; O'Donnell. & Boehle, 2006).

Embora o uso da RTU com quimioterapia ou imunoterapia adjuvantes represente um importante avanço no tratamento do CBNMI, o manejo deste tumor, principalmente para tumores de alto grau, continua sendo um desafio devido às altas taxas de recorrência e progressão para os fenótipos músculo invasivo e/ou metastáticos (Garcia et al., 2016). Diferentes agentes quimioterápicos convencionais têm sido utilizados na recorrência do CBNMI após uso da imunoterapia intravesical com BCG (Lightfoot et al., 2011; Steinberg et al., 2011). A valrubicina, um análogo semissintético da doxorrubicina, foi aprovada pelo órgão regulador norte-americano FDA (*Food and Drug Administration*) para uso em casos específicos de tumores pTis refratários ao BCG, sendo efetiva em menos de 10% dos pacientes (Steinberg et al., 2011). Além disso, protocolos baseados nas imunoterapias com IFN-α ou IFN-α associado ao BCG também têm sido utilizados (Lightfoot et al., 2011). Contudo, nenhum destes esquemas terapêuticos foi superior ao uso isolado do BCG.

Um problema adicional é o frequente desabastecimento de BCG tanto no Brasil, como no mundo devido às suspensões, restrições e dificuldades na produção. Assim, os pacientes com CBNMI estão sujeitos a mudanças e/ou interrupções no tratamento e até mesmo desamparados totalmente na falta de BCG. Os desafios impostos frente à escassez de BCG apontam para a necessidade de desenvolvimento de novas opções de tratamento para o CBNMI (Guallar-Guarrido; Julián et al., 2020).

1.1.3. Modelo de Indução

Para o desenvolvimento de novos fármacos faz se necessário modelos animais bem caracterizados para estudos pré-clínicos. Alterações neoplásicas podem ser iniciadas na bexiga urinária de camundongas e ratos no período de algumas semanas de tratamento com doses

baixas de carcinógenos químicos (Crallan et al., 2006; Reis et al., 2009) que são instilados diretamente na bexiga dos animais (Crallan et al., 2006). Hicks & Wakefield (1972) utilizaram 4 doses do carcinógeno N-metil-N-nitrosoureia (MNU) para rápida indução do CBNMI em ratos, demonstrando que este é um carcinógeno completo. As nitrosouréias podem atuar como iniciadoras e promotoras da neoplasia podendo causar persistente metilação do DNA (Steinberg et al., 1990). Estudos com animais pré-tratados com MNU confirmaram que as células tumorais preferencialmente se implantam na superfície urotelial alterada (Soloway et al., 1983; Weldon & Soloway, 1975).

A carcinogênese urotelial induzida com nitrosouréias em murinos é semelhante à carcinogênese humana, pois envolve o efeito de agentes ambientais (o mesmo carcinógeno presente no cigarro de tabaco) num substrato geneticamente susceptível. Além disso, a carcinogênese urotelial induzida com nitrosouréias sofre uma sequência de alterações morfológicas, iniciando com hiperplasia simples seguida de hiperplasia nodular e papilar, progredindo posteriormente para papiloma e, ocasionalmente, carcinomas não invasivos e, finalmente, neoplasias invasivas (Cohen et al., 2002; Dias et al., 2016; Fávaro et al., 2012; Garcia et al., 2015; 2016; Oliveira et al., 2006; Reis et al., 2009; 2010; 2012).

Os experimentos com CBNMI realizados por nosso grupo de pesquisa utilizaram incialmente o modelo animal (ratas Fischer 344 ou camundongas com fundo C57BL/6J) de indução química com N-metil-N-nitrosoureia (MNU). No entanto, no ano de 2017, a produção do N-metil-N-nitrosoureia (MNU –N1517 Sigma Aldrich®) foi descontinuada e o N-etil-N-nitrosoureia (ENU - Sigma, St. Louis, MO, EUA) passou a ser usado nos modelos experimentais, demonstrando a mesma eficácia que o MNU. Likhachev e seu grupo de pesquisa, em um experimento com hamsters *Syrian Golden*, também demonstraram que tanto o MNU quanto o ENU provocaram metilação no DNA em diversos tecidos, induzindo o câncer (Likhachev et al., 1983).

Em estudos empregando tanto o MNU como o ENU, o modelo animal induzido apresentou vantagens particulares para os estudos da carcinogênese urogenital. A saber: 1- carcinógeno conhecido por agir diretamente sobre o urotélio, sem necessidade de ativação metabólica; 2- reproduziu tumores de bexiga clinicamente observados em humanos, os quais tiveram origem exclusiva no urotélio, foram espontâneos e não implantados e histologicamente equivalentes ao carcinoma de células transicionais; 3- pôde ser administrado por via intravesical em doses de pulso quantificáveis; 4- possui baixo custo, reprodutível e utiliza um hospedeiro imunocompetente, o que é importante quando se estuda o tratamento com imunomoduladores, como

por exemplo, o *Bacillus Calmette-Guerin* (BCG); 5- modelo de câncer mais controlado do que aqueles que usam carcinógenos na dieta ou na água potável (Dias et al., 2016; Fávaro et al., 2012; Garcia et al., 2015; 2016; Perabo et al., 2005; Reis et al., 2010; 2012).

1.2. Câncer de Ovário

1.2.1. Visão Geral

O câncer de ovário (CO) é a segunda neoplasia ginecológica de maior incidência em mulheres, seguindo o câncer de colo de útero (INCA, 2022d) e apresenta a maior mortalidade dentre as neoplasias do sistema genital feminino (*American Cancer Society*, 2022b). As estimativas para o ano de 2022 nos Estados Unidos foram de 19.880 novos diagnósticos e 12.810 mortes por CO (*American Cancer Society,* 2022b). No Brasil, as estimativas do Instituto Nacional do Câncer (INCA, 2022a) são de 7.310 novos casos de câncer de ovário. Entre as mulheres, o CO ocupa o quinto lugar em morte por câncer e os levantamentos de dados do Instituto Nacional do Câncer (INCA) revelam uma crescente mortalidade no Brasil nos últimos anos com taxas variáveis entre os estados (**Figura 2**). Em 2015 foram registrados 3.536 óbitos, em 2017, 3.879 óbitos e 4.123 em 2019 (INCA, 2022b). Cerca de 75% dos casos são avançados quando descobertos, devido às dificuldades de detecção precoce do CO, contribuindo para o pior prognóstico dentre as malignidades ginecológicas (Meinhold-Heerlein; Hauptmann, 2014; INCA, 2022d).

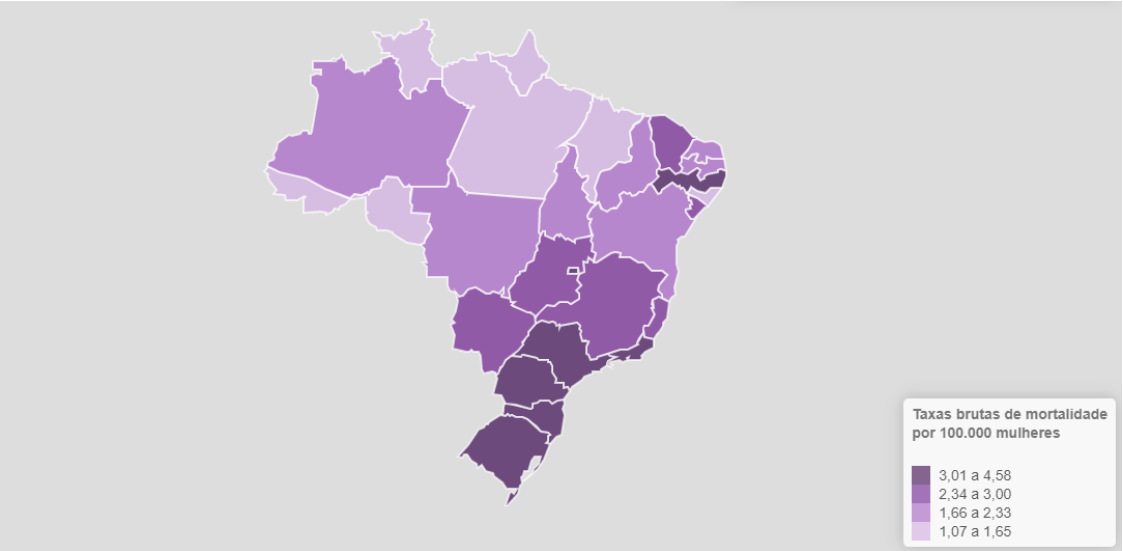

Figura 2. Representação espacial das taxas brutas de mortalidade por câncer de ovário, por 100.000 mulheres, pelas unidades da federação do Brasil, entre os anos 2000 e 2020. Mapa gerado através do Atlas on-line de mortalidade do site do INCA (INCA, 2022b).

O termo câncer de ovário compreende um grupo heterogêneo de tumores malignos que acometem a gônada feminina e diferem em etiologia, prognóstico, morfologia e patologia (Prat, 2015; Meinhold-Heerlein et al., 2016). As causas são multifatoriais, mas há fatores de risco que facilitam o desenvolvimento da neoplasia tais como a idade, o histórico familiar e mutações herdadas em genes específicos como o *BCRA1* e *BCRA2* (Andrews; Mutch, 2017; Webb; Jordan, 2017). Algumas pesquisas apontam para a relação existente entre a ovocitação e o câncer de ovário, sendo condições relacionadas com maior número de ovulações tais como nuliparidade, infertilidade, menopausa tardia e menarca precoce associadas com maiores taxas de CO, enquanto que condições que acarretam em menor número de ciclos ovulatórios tais como menarca tardia, menopausa precoce, gravidez e uso de hormônios contraceptivos são fatores indiretamente relacionados com a incidência de CO (Kurman; Shih, 2010; Gong et al., 2013; Webb; Jordan, 2017).

Os tumores ovarianos podem ser classificados por tipo histológico (de acordo com a Organização Mundial da Saúde, OMS) e quanto ao estágio do tumor (segundo a Federação Internacional de Ginecologia e Obstetrícia - *International Federation of Gynecology and Obstetrics*, FIGO). A classificação da OMS é baseada na histogênese do ovário de acordo com o possível tecido de origem do tumor, podendo ser: (1) tumores epiteliais, originados das células que recobrem a superfície externa do ovário as quais derivam do epitélio celômico; (2) tumores de células germinativas, originadas das células germinativas primordiais que migram a partir do saco vitelino até os ovários originando os gametas femininos denominados de ovócitos; ou (3) tumores do estroma e do cordão sexual, derivados dos cordões sexuais de origem mesonéfrica e do mesênquima (Kumar et al., 2010; Kurman et al., 2014).

Entre os três tipos principais da classificação histológica da OMS, os tumores epiteliais são os mais frequentes (85 a 90% dos tumores ovarianos malignos) e podem ser constituídos de um ou mais tipos distintos de epitélios com uma quantidade variável de estroma (Kurman et al., 2014). Baseada na histopatologia, imunohistoquímica e perfil molecular, a classificação dos tumores epiteliais ovarianos mais comumente utilizada pelos patologistas inclui cinco subtipos principais ou histotipos, que contabilizam mais de 97% dos carcinomas epiteliais ovarianos: (1) carcinoma seroso de alto grau, 70%; (2) carcinoma endometrioide, 10%; (3) carcinoma de células claras, 10%; (4) carcinoma mucinoso, 3%; e (5) carcinoma seroso de baixo grau, menos de 5% (Clarke; Gilks, 2011; Prat, 2012; Javadi et al., 2016).

O estadiamento e avaliação da malignidade do tumor de ovário são realizadas cirurgicamente conforme as orientações da FIGO (estádio I a IV) e no sistema TNM utilizado

pela União Internacional Contra o Câncer (*Union for International Cancer Control's* - UICC), ambos levam em consideração a capacidade de disseminação do tumor desde seu local de origem e refletem a extensão da doença, o tipo de tumor e sua relação com o hospedeiro (Prat, 2015). Dentre essas orientações tem-se a inspeção, classificação e realização de inventário da cavidade abdominal (incluindo seu conteúdo) e das estruturas que têm alguma relação anatômica com os ovários como: peritônio, espaços retroperitoneais e linfonodos (Prat, 2015).

1.2.2. Terapêutica

A conduta mais comum utilizada no tratamento de tumores de ovário é uma combinação entre cirurgia e quimioterapia baseada em platina (Grisham et al., 2014). Primeiramente, realiza-se o estadiamento do tumor e o seu grau de extensão, posteriormente é realizada uma cirurgia de ressecção que geralmente leva à retirada do ovário afetado, seguida de uma quimioterapia associada (Stewart et al., 2019). Entretanto, os métodos atuais apesar de melhorados com o passar dos anos, não previnem as altas taxas de recorrência além dos efeitos colaterais adversos. O uso combinado de carboplatina e paclitaxel como adjuvantes após a cirurgia de retirada do tumor tem se mostrado como o tratamento quimioterápico mais comum atualmente (Stewart et al., 2019).

Outras abordagens aliadas podem tornar o tratamento ainda mais eficiente como a intraperitoneal, visto que o peritônio é o primeiro local para onde o CO dissemina-se e, na maior parte dos casos, fica confinado nesta cavidade (Ledermann, 2018). Apesar das estratégias convencionais de cirurgia aliada à quimioterapia e também o uso de radioterapia serem eficientes em alguns casos, os mesmos são pouco específicos considerando a heterogeneidade do CO, com vários subtipos histológicos que divergem em suas características moleculares e taxas de resposta à quimioterapia (Grisham et al., 2014; Prat, 2015, Cortez et al., 2018). Além disso, os tratamentos convencionais possuem alta ação citotóxica, portanto, atacam tanto células tumorais quanto células saudáveis, podendo levar ao aparecimento de diversos efeitos colaterais e ao desenvolvimento de mecanismos de resistência (Cortez et al., 2018).

Os efeitos colaterais mais comuns são fadiga, perda de peso, infecções, anemia, náuseas e vômitos, diarreias, disfunções sexuais e na fertilidade, sendo mais comum dormência nos membros (58,6%), fadiga (55%), perda de cabelo (49,9%) e falta de apetite (46,3%) nas combinações de taxano e carboplatina (Hsu et al., 2017). Outros efeitos colaterais graves nos tecidos saudáveis incluem nefrotoxicidade (Liu et al., 2006), hepatoxicidade (Pratibha et al., 2006), neurotoxicidade (Amptoulach; Tsavaris, 2011), cardiotoxicidade (Sawant et al., 2015),

ototoxicidade (Rademaker-Lakhai et al., 2006), toxicidade gastrointestinal, mielosupressão e imunossupressão além de resistência adquirida à droga após um tempo de tratamento (Florea; Büsselberg, 2011; Galluzzi et al., 2014). A toxicidade ao sistema nervoso periférico, que pode persistir após um tempo ou ser permanente, é o maior fator limitante para a dose de cisplatina e a ausência de uma estratégia eficaz estabelecida para gerenciar esse efeito colateral atenta para a urgência de se encontrar novas estratégias (Amptoulach; Tsavaris, 2011).

Outro ponto importante é o fato de, mesmo que transitoriamente, os tratamentos convencionais como cirurgia e quimioterapia podem causar supressão imunológica. No caso de alguns tratamentos com quimioterapia, esse efeito acontece por reduzir o número de células do sistema imune da paciente, inclusive células T (Vinay et al, 2015). A atividade normal do sistema imune pode retornar após cerca de 2 ou 3 semanas do término do tratamento com o quimioterápico, no entanto a recuperação não é observada nos casos em que a paciente é submetida a tratamento de longo prazo (Vinay et al, 2015). Em relação à cirurgia, esse trauma causa aumento de citocinas pró inflamatórias e riscos de infecções (Vinay et al, 2015).

A maioria das pacientes de CO recai dentro de 16–18 meses após o término do tratamento com quimioterapia baseada em platina e morrem da doença, 15% deles já no primeiro ano (Lavoué et al., 2013). A resistência à cisplatina adquirida após alguns ciclos de tratamento como no caso do CO (Köberle et al., 2010) é o principal fator que dificulta a sensibilidade das células cancerígenas fazendo com que não respondam à droga o que, consequentemente, diminui a eficácia do tratamento de longo prazo (Florea; Büsselberg, 2011). A alta taxa de resistência à quimioterapia que aparece na maioria dos pacientes com carcinoma serosos de alto grau (Bowtell et al., 2015; Kurman; Shih, 2016; Christie; Bowtell, 2017) é um motivo inegável na busca por tratamentos diferenciados como intervenções de base imunológica. A grande maioria (90%) dos pacientes que apresentam disseminação das células tumorais além dos ovários, apresenta recaída durante o tratamento e vem à óbito devido ao desenvolvimento da resistência (Agarwal; Kaye, 2003). No Brasil, cerca de 80% das pacientes com tumor epitelial avançado apresentam recorrência devido ao desenvolvimento de resistência, que acomete a maioria dos pacientes com o tipo mais frequente de CO - o carcinoma seroso de alto grau (Ministério da Saúde, 2019).

Inibidores da poli (adenosina difosfato [ADP] ribose) polimerase (PARPs), como o Olaparib, inibem o crescimento tumoral em carcinomas ovarianos serosos de alto grau associados às mutações nos genes *BCRA1* e *BCRA2*, bloqueando o reparo do DNA promovido por essa via e promovendo consequente citotoxicidade nas células cancerosas (Ledermann et

al., 2012). Os inibidores de PARPs mostraram bons resultados melhorando a sobrevida livre de progressão (PFS) e inibindo o crescimento tumoral (Ledermann et al., 2012). De acordo com as diretrizes atuais para o manejo de inibidores de PARP em CO, eles não devem ser repetidos se o paciente progredir após o tratamento, não há indicação para uso em cânceres em estágio inicial e provavelmente não serão eficazes nos carcinomas de células claras ou mucinoso (Tew et al., 2020). Mesmo com o desenvolvimento dos inibidores de PARP, há uma necessidade substancial de terapias direcionadas adicionais, bem como superar a resistência a essas drogas.

Novas abordagens surgiram nas últimas décadas que implementaram o uso da imunoterapia no combate ao câncer de ovário como, por exemplo anticorpos, que podem identificar proteínas específicas das células tumorais e ativar a resposta humoral e celular do paciente contra elas (Liu et al., 2010) e inibidores de *checkpoints* imunológicos, que modulam a tolerância de linfócitos T aos antígenos próprios, regulagem perdida em condições de neoplasia (Krishnan et al., 2017). Outra abordagem é a incorporação de drogas anti-angiogênicas no tratamento do CO, tais como o Bevacizumab que foi consideração *pela Food and Drug Administration* (FDA) como uma opção de tratamento de primeira linha para o CO nos EUA (Ledermann, 2018; Genentech, 2017).

Outras estratégias que envolvem o sistema imune da paciente estão em desenvolvimento como a imunoterapia adotiva de células T (ATC), baseada no isolamento de células T infiltrantes do tumor ou da corrente sanguínea que são isoladas, expandidas e injetadas como efetores imunes específicos (Genta et al., 2018; Ghisoni et al., 2019). A utilização de neoantígenos tumorais, moléculas imunogênicas não expressas em tecidos saudáveis, pode expandir as células T preexistentes, ampliando o combate imune e controle do tumor (Napoletano; Bellati, 2019). No entanto, nem sempre os neoantígenos tumorais identificados são imunogênicos, inclusive no CO (Napoletano; Bellati, 2019; Liu et al., 2019). Nesse sentido, há ainda as terapias fundamentadas em vacinas, que, a partir da injeção de células dentríticas (baseadas no tumor), recombinantes virais, peptídeos ou derivados de ácidos nucleicos, estimulam o reconhecimento das células cancerígenas pelo sistema imune além de estabelecer memória imunológica (Krishnan et al., 2017). Apesar dos inúmeros esforços, a aprovação para novas drogas destinadas ao tratamento do CO é lenta, enquanto tem sido desafiante melhorar a sobrevivência geral dos pacientes acometidos por essa síndrome (Liu; Metulonis, 2014).

1.2.3. Modelo de Indução

Um modelo animal válido com características histológicas semelhantes aos tumores ovarianos humanos é necessário para avaliar a eficácia de compostos químicos com possível potencial terapêutico, visto que o tratamento específico para o CO ainda é um desafio clínico (Chuffa et al., 2013). Os experimentos envolvendo o câncer de ovário realizados por nosso grupo de pesquisa utiliza o modelo animal isogênico (ratas *Fischer* 344) com indução química através de 7,12-dimetilbenzoantraceno (DMBA). O período de desenvolvimento do CO após a aplicação do DMBA na bursa ovariana compreende em torno de 120 dias (Chuffa et al., 2018; Zonta et al., 2017). O tipo histológico dos tumores ovarianos formados pode variar de acordo com a espécie e idade dos animais, dose do carcinógeno, via de administração e método de indução (Chuffa et al., 2013). No entanto, a maioria dos tumores desenvolvidos após a aplicação do protocolo adotado (Chuffa et al., 2018) são carcinomas denominados como papilíferos serosos de alto grau, os quais são semelhantes ao CO mais recorrente em mulheres – o carcinoma seroso de alto grau (Javadi et al., 2016).

O DMBA é um hidrocarboneto policíclico aromático (HPA) originado no ambiente a partir da combustão de compostos orgânicos tais como o carvão, gasolina e cigarro (Bhattacharya; Keating, 2012; Zhou et al., 2018). Os efeitos imunossupressores e carcinogênicos do DMBA trazem prejuízos à saúde humana inclusive sobre aspectos reprodutivos (Anderson et al., 2014) e seu potencial carcinogênico está relacionado ao desenvolvimento dos cânceres decorrentes da fumaça do cigarro e poluição urbana (Kwon et al., 2018). Em roedores, o DMBA causa imunotoxicidade aos folículos ovarianos de modo dose-dependente (Zhou et al., 2018) através de estresse oxidativo nas células da granulosa e da teca e apoptose (Tsai-Turton et al., 2007); e alteração na expressão de proteínas das junções *gap* (Ganesan et al., 2013), de oncogenes e de genes supressores tumorais (Madden et al., 2014). Devido às suas propriedades de indução, promoção e progressão de tumores, o DMBA é utilizado como carcinógeno para modelos experimentais há vários anos (Nishida et al., 1998).

A utilização do DMBA para indução química da carcinogênese em roedores é um método efetivo para o estudo do CO, principalmente os de origem epitelial (Marion et al., 2013). O DMBA é capaz de induzir a formação de neoplasias de origem epitelial com padrões histológicos, moleculares e de disseminação semelhantes ao CO em humanos (Nishida et al., 1998; Stewart et al., 2004). Os tumores desenvolvidos em ratos após o tratamento com o DMBA apresentaram marcadores epiteliais e metabólicos (Crist et al., 2005) e mutações nos genes *Tp53*

e *Ki-Ras* (Stewart et al., 2004) característicos do CO em mulheres. Dessa forma, o modelo de CO via indução química com DMBA é apropriado para o estudo dos componentes estruturais e funcionais do microambiente tumoral, inclusive aspectos do sistema imune (Chuffa et al., 2017; Zonta et al., 2017).

1.3. Sistema Imune e Câncer

A relação entre tumores malignos e o sistema imune é muito estreita visto que o câncer, inclusive o câncer de bexiga e de ovário, é imunogênico, ou seja, capaz de desencadear uma resposta inflamatória. Vários antígenos tumorais, com ou sem mutações, já foram identificados em diferentes tipos de tumores, os quais são adquiridos pelas células tumorais no processo de transformação neoplásica e induzem uma resposta imune específica das células T do hospedeiro (Lavoué et al., 2013). Uma das evidências mais fortes de que ligam a imunidade antitumoral e o câncer foi, inclusive, observada no câncer de ovário humano (Liu et al., 2010). Em 2003, Zhang et al. demonstraram a presença de algumas populações de linfócitos infiltrados em carcinomas ovarianos em diferentes estágios, denominando de infiltrado linfocitário tumoral (TIL) (Zhang et al., 2003). Zhang et al. (2003) correlacionaram a presença desse infiltrado com uma positiva evolução do quadro clínico dos pacientes. Posteriormente, outros estudos confirmaram que a contagem desses TILs era um importante fator para um prognóstico favorável (Liu et al., 2010).

No microambiente de um tumor podem ser encontradas diversas células imunes como: neutrófilos, eosinófilos, células dendríticas, linfócitos, células *natural killer* (NK) e macrófagos associados a tumores - *tumor-associated macrophages* (TAMs) (Gata; Laurentiu, 2017). Essas células estão associadas ao aparecimento de respostas tanto da imunidade inata como adaptativa e criam um complexo microambiente inflamatório, o qual pode inibir ou estimular o crescimento tumoral (Disis, 2010). Na resposta imunológica inata, as protagonistas dessa interação com o tumor são as células NK e os macrófagos (Abbas, 2012). As células NK, em especial, são capazes de destruir diversos tipos de células malignas que expressam uma quantidade pequena de complexo principal de histocompatibilidade (MHC) classe I ou ligantes ativadores de células NK apresentados pelas células apresentadoras de antígenos (APCs) como as dendríticas e macrófagos (Abbas, 2012).

Os macrófagos podem ter uma atuação mais ampla dependendo do seu estado de ativação que é determinado pelo conjunto de estímulos do microambiente. Em resposta a sinais

oriundos de produtos bacterianos ou interferon gama (IFN-γ), os macrófagos adaptam-se ao fenótipo M1 (Heusinkveld; Burg, 2011). A polarização do tipo M1 é imunoestimulatória, caracterizada pela produção de fatores citotóxicos pelos macrófagos como espécies reativas de oxigênio (ROS) e óxido nítrico (NO) via óxido nítrico sintase induzida (iNOS), liberação de enzimas lisossomais, produção de TNF (fator de necrose tumoral) e IL-12 (interleucina 12), além de induzir a atividade citotóxica de células NK e atrair e ativar células do sistema imunológico adaptativo (Heusinkveld; Burg, 2011; Abbas, 2012). O perfil M2 de macrófagos atua na eliminação de parasistas e cicatrização de feridas, no entanto também resulta em funções imunossupresoras como polarização de células T para o pefil Th (T *helper*) 2; produção do fator de cresimento endotelial vascular (VEGF), fator de crescimento transformante β (TGF-β) e IL-10; atenuação da resposta imune e, consequentemente, facilita a progressão tumoral (Heusinkveld; Burg, 2011; Bellora et al., 2014).

A resposta imune adaptativa antitumoral é específica a antígenos associados aos tumores e essencialmente constituída da atividade citotóxica via linfócitos T citotóxicos (CTLs) CD8+ e células T CD4+ Th1 (Disis, 2010; Abbas; 2012). O início da resposta imune adaptativa requer dois sinais: o primeiro via apresentação de antígenos envolvendo o MHC nas APCs e o receptor de células T (Sinal 1); e o segundo via co-estimulação do receptor CD28 nas células T com ligantes B7-1 (CD80) ou B7-2 (CD86) expressos nas APCs (Sinal 2), o que acarreta em expansão clonal das células T, secreção de citocinas e execução de funções efetoras (Seliger et al., 2008; Taube et al., 2018). Os macrófagos M1 tem papel na geração da imunidade adaptativa atraindo a ativando células Th1 que tem efeito citotóxico direto às células tumorais (Disis, 2010). Por outro lado, os TAMs, em geral de fenótipo M2, e células supressoras derivadas da linhagem mieloide (MDSCs) podem inibir a resposta imune adaptativa a partir da secreção de citocinas que afetam diretamente a atividade de células T bem como recrutando células supressoras como as células T regulatórias (Tregs) (Disis, 2010; Yang, 2015).

As células Tregs FOXP3+ diminuem a imunovigilância dos tumores e suprimem as respostas imunes antitumorais (Wang et al., 2022). FOXP3, um fator de transcrição de hélice de garfo, é o principal marcador de células Tregs envolvido na diferenciação e função dessas células. No microambiente tumoral, as Tregs secretam TGF-β que é um mediador chave na indução de FOXP3, diferenciação e atividade de outras células Tregs (Wang et al., 2022). Dessa forma, o microambiente tumoral envolve uma complexa rede de citocinas e fatores solúveis que podem suprimir a imunidade. Esse ambiente inflamatório associado com uma população de leucócitos imunossupressores, previne a maturação de células da linhagem mieloide, favorece

o desenvolvimento de células Tregs e restringe a atividade citotóxica de linfócitos efetores, permitindo assim a evasão do câncer da ação do sistema imune e tornando possível sua progressão (Cubillos-Ruiz et al., 2010).

O mecanismo de detecção imune inata de tumores imunogênicos que levam às respostas de células T adaptativas permanece indefinido, embora os interferons (IFNs) estejam implicados neste processo (Woo et al., 2014). Woo et al. (2014) identificaram que a ativação espontânea de células T CD8+ contra tumores foi defeituosa em camundongas sem o fator estimulador do complexo de genes de interferon (STING), mas não em outras vias de sinalização inatas, sugerindo o envolvimento de uma via de detecção de DNA citosólico. *In vitro*, a produção de IFNs e a ativação de células dendríticas foram desencadeadas por DNA derivado de células tumorais, através de STING e do fator regulador de interferon IRF-3 (Woo et al., 2014). No microambiente tumoral *in vivo*, o DNA de células tumorais foi detectado no interior de células apresentadoras de antígeno do hospedeiro, o que se correlacionou com a ativação da via de STING e a produção de IFNs (Woo et al., 2014). Assim, o trabalho de Woo et al. (2014) demonstrou que o mecanismo principal para a detecção imune inata do câncer ocorre através da via hospedeira STING, com implicações para o uso de imunoterapias.

1.3.1. Receptores *Toll Like* (TLRs): Alvos promissores no tratamento oncológico

A população de células da imunidade inata e adaptativa tem sua atividade associada com a presença de *Toll-like Receptors* (TLRs), que também são expressos em células endoteliais e epiteliais (Bhardwaj et al., 2010; Dajon et al., 2017). Os TLRs fazem parte da família de receptores transmembrana que reconhecem padrões moleculares associados a patógenos (PAMPs) e associados a danos (DAMPs) e têm atividade tanto na lesão quanto na reparação tecidual decorrentes da inflamação (Kumar et al., 2011; Galli et al., 2010; Satoh; Akira, 2016). Dentre os tipos de TLRs, os que estão localizados na membrana plasmática e reconhecem lipídios e proteínas ligantes são: TLR1, TLR2, TLR4, TLR5 e TLR6; já os que são encontrados em compartimentos intracelulares e detectam ácidos nucleicos virais incluem TLR3, TLR7, TLR8 e TLR9 (Satoh; Akira, 2016; Duan et al., 2022).

A função clássica dos TLRs consiste no recrutamento de leucócitos para os tecidos infectados com posterior indução de respostas imunes adaptativas (Akira; Takeda, 2004; Galli et al., 2010; Takeda; Akira, 2004). A ativação dos TLRs na superfície das células epiteliais induz a expressão de moléculas de adesão intercelular (ICAM), as quais desempenham um

papel fundamental na implantação e adesão de leucócitos (Satoh; Akira, 2016). Muitos dos efeitos conhecidos da sinalização dos TLRs ocorrem através da produção de moléculas inflamatórias e moléculas para sobrevivência celular, como TNF-α e interleucinas IL-6, IL-1β e IL-10, bem como a expressão de moléculas co-estimulatórias em células dendríticas e macrófagos (Akira; Takeda, 2004; Galli et al., 2010). Coletivamente, cada TLR recruta uma combinação específica de moléculas adaptadoras para ativar diferentes fatores de transcrição que darão origem à resposta apropriada e efetiva contra o patógeno estimulador (Akira; Takeda, 2004; Satoh; Akira, 2016; Takeda; Akira, 2004).

A transdução de sinais dos TLRs ocorre através de diferentes proteínas adaptadoras, as quais desencadeiam uma cascata de sinalização envolvendo o fator de transcrição nuclear kβ (NF-κβ), proteínas-quinases ativadas por mitógeno (MAPKs), p38, proteínas quinases c-jun-N-terminal (JNKs), proteínas quinases reguladoras de sinalização extracelular (ERKs) e os fatores regulatórios de interferon (IRF-3, IRF-5 e IRF-7) (Akira; Takeda, 2004; Satoh; Akira, 2016; Takeda; Akira, 2004). Agumas das moléculas adaptadoras envolvidas na sinalização dos TLRs são: fator 88 de diferenciação mielóide (MyD88), proteína adaptadora contendo domínio receptor de toll-interleucina 1 (TIR) (TIRAP), adaptador indutor de interferon-β contendo domínio TIR (TRIF) e proteína de membrana associada à cadeia de translocação (TRAM) (Akira; Takeda, 2004; Satoh; Akira, 2016; Takeda; Akira, 2004). A proteína MyD88 é utilizada por todos os TLRs, a exceção do TLR3, e ativa NF-κβ e as vias das MAPKs para induzir a produção de citocinas inflamatórias (Satoh; Akira, 2016; Takeda; Akira, 2004). TRAM e TIRAP são moléculas adaptadoras utilizadas pelo TLR4 para recrutar TRIF e pelos TLRs 2 e 4 para recrutar MyD88, respectivamente (Satoh; Akira, 2016; Takeda; Akira, 2004).

Assim, a sinalização dos TLRs (**Figura 3**) pode ser classificada de duas formas: via dependente de MyD88 (via canônica) para a produção de citocinas inflamatórias e via dependente de TRIF (via não-canônica) para a produção de interferons tipo 1 e citocinas inflamatórias (Satoh; Akira, 2016; Duan et al., 2022). TLR4 é o único receptor que utiliza as quatro moléculas adaptadoras (MyD88, TRIF, TIRAP e TRAM) para desencadear sua sinalização podendo ser tanto a via canônica como a não-canônica (Akira; Takeda, 2004).

A ativação de TLR4 em macrófagos resulta na produção de várias citocinas inflamatórias diferentes que interferem no crescimento tumoral. A sinalização de TLR4 induz a produção de interferon (IFN) que têm efeitos antitumorais por indução do ligante indutor de apoptose relacionado ao TNF (TRAIL), um potente indutor de morte de células tumorais (Luo et al., 2004). Shankaran et al., (2001) mostraram que a função supressora tumoral do sistema

imune depende criticamente das ações de IFN-γ, as quais, pelo menos em parte, são direcionadas para regular a imunogenicidade de células tumorais. IFN-γ estimula várias vias antiproliferativas e tumoricidas em macrófagos e em linhagens de células tumorais, bem como possui um profundo impacto no crescimento de tumores sólidos e metástases e aparentemente desempenha um papel precoce na proteção contra metástases (Alshaker & Matalka, 2011; Li et al., 2007; Martini et al., 2010; Tate et al., 2012).

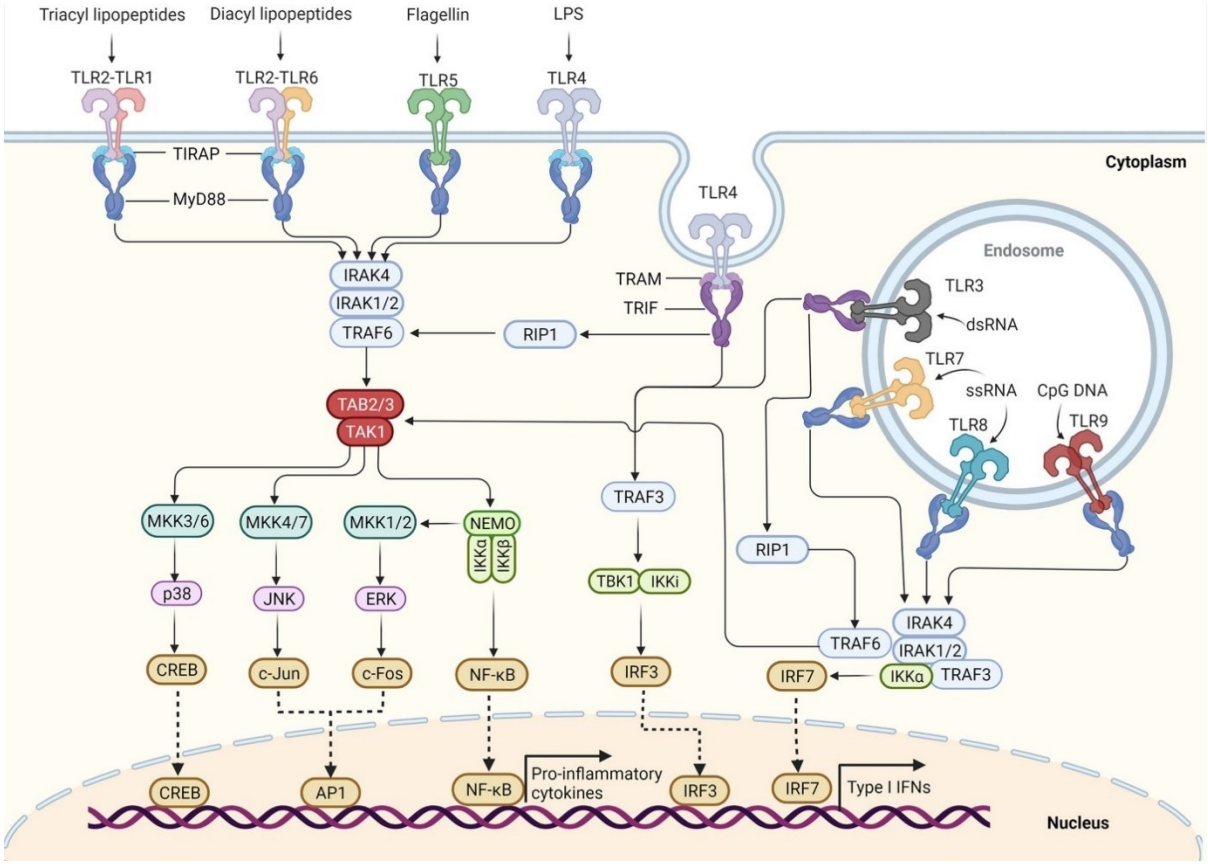

Figura 3. Sinalização dos Receptores Toll like. TLR5, TLR4 e os heterodímeros TLR2–TLR1 e TLR2–TLR6 reconhecem componentes da membrana de patógenos enquanto TLR3, TLR7–TLR8 e TLR9, localizados nos endossomos, reconhecem ácidos nucleicos. TLR4 localiza-se na membrana, mas é endocitado em endossomos após ativação. A sinalização é iniciada através da dimerização e interação do domínio TIR dos receptores com TIRAP e MyD88 (ou diretamente com MyD88) ou com TRAM e TRIF (ou diretamente com TRIF). A sinalização desencadeada por TLR4 muda de MyD88-dependente para TRIF-dependente quando o receptor se encontra em compartimento intracelular. O envolvimento de MyD88 desencadeia uma cascata de reação envolvendo IRAK4, IRAK1/2, TRAF6 e ativação do complexo TAK1. TAK1 ativado fosforila e ativa o complexo canônico IKK que leva à ativação de NF-kB ou também ativa as MAPKs (MKK4/7 e MKK3/6) que, por sua vez, ativam JNK e p38. As vias MAPKs ativam importantes fatores de transcrição como CREB e AP1, os quais auxiliam NF-kB a promover indução das citocinas pro-inflamatórias. O envolvimento de TRIF recruta TRAF6 e TRAF3,

e depois RIP1, ativa os complexos TAK1 e IKK, levando a ativação de NF-kB e MAPKs. TRIF também promove ativação de TBK1 e IKKϵ (ou IKKi) (dependente de TRAF3) o que posteriormente, fosforila e ativa IRF3. Na sinalização de TLR7, TLR8 e TLR9, IRF7 pode ser ativado diretamente por IRAK1 e IKKϵ. Ativação de IRF3 e IRF7 leva à indução de IFNs tipo I (Duan et al., 2022).

Os tumores de bexiga urinária, especialmente o CBNMI, mostraram expressão diminuída de TLRs (Ayari et al., 2011; Stopiglia et al., 2015). A imunoterapia com BCG mediada por TLRs para o tratamento do CBNMI constitui uma estratégia bem-sucedida para este tipo de tumor. Infiltração linfocítica local e produção de citocinas inflamatórias foram encontradas na parede da bexiga urinária da maioria dos pacientes que receberam BCG intravesical, resultando em uma complexa resposta imune local (Sander et al., 1996; Yu et al., 2007). O ligante indutor de apoptose relacionado ao TNF (TRAIL) é produzido a partir de neutrófilos polimorfonucleares (PMNs) através da estimulação de TLR2 por BCG (Steinberg et al., 2011). Garcia et al. (2016) demonstraram em experimentos com ratos induzidos para o CBNMI que a imunoterapia intravesical com BCG aumentou os níveis proteicos de TLR2 e TLR4, com consequente aumento dos níveis de MyD88, IKKα e NF-kB, resultando no aumento de IL-6 e TNF-α. Esses mesmos autores concluíram que a ativação do sistema imune local através do tratamento intravesical com BCG, via MyD88, foi essencial para reduzir a progressão tumoral nesses animais.

Em humanos, TLR2, TLR3, TLR4 e TLR5 são expressos fortemente no epitélio de superfície do ovário e esse padrão de expressão é relacionado com a proteção contra infecções principalmente bacterianas e reflete também o papel fisiológico desses receptores na reparação tecidual após a ovocitação (Zhou et al., 2009). As células epiteliais das tubas uterinas também expressam TLRs (1-10), principalmente nas células ciliadas, onde a estimulação com agonistas de TLR2, TLR3, TLR5, TLR7 e TLR9 induziu a secreção de citocinas pró-inflamatórias como interleucina 6 e 8 (IL-6 e IL-8) (Amjad et al., 2018). Em células tumorais do CO, foi encontrada expressão de TLR3, 4, 5 e 9 (Dajon et al., 2017) e altos níveis de determinados TLRs em células do CO podem estar associados à progressão do câncer, metástase, resistência ao tratamento e prognóstico ruim devido ao recrutamento de citocinas e indução de quimiocinas de leucócitos imunossupressores e pró-angiogênicos para o local do tumor (Kelly et al., 2006; Berger et al., 2010). Block et al. (2018) mostraram que a forte expressão de MyD88 é relacionada com menor sobrevida em pacientes com carcinoma ovariano seroso de alto grau, porém a maior expressão

de TLR4 e MyD88 é associada com uma maior taxa de sobrevida em pacientes com carcinoma ovariano seroso de baixo grau.

A modulação da sinalização de TLR pode ter efeitos antitumorais ou pró-tumorais, dependendo do TLR, do subtipo de câncer e das células imunes que se infiltram no tumor (Dajon et al., 2017). Em geral, a expressão de TLR em células tumorais resulta em imunossupressão, resistência à quimioterapia e crescimento tumoral, enquanto a expressão em células imunes facilita um microambiente inflamatório antitumoral e aumenta a resposta imune contra tumores mediada por células (Muccioli; Benencia, 2014; Zhou et al., 2009). Dessa forma, as pesquisas sobre a atividade dos TLRs na progressão do CO indicam que tanto a inibição de certos TLRs em células cancerígenas ou a estimulação de TLR em células imunes podem funcionar como estratégicas terapêuticas (Muccioli; Benencia, 2014). Em células imunes, como macrófagos e células dendríticas, após o reconhecimento de PAMP pelos TLRs, ocorre uma resposta imune que pode desencadear uma mudança no perfil inflamatório, diminuindo a imunossupressão, aumentando a capacidade das APCs e facilitando a ativação de células T (células NK e CTLs) que podem combater os tumores (Muccioli; Benencia, 2014). Efeitos antitumorais da sinalização de TLR, tais como a produção do fator de necrose tumoral alfa (TNFα), aumento da atividade de células NK e neutrófilos e aumento da infiltração linfocitária foram relatados em estudos *in vitro* e *in vivo* com ligantes TLR (Zhou et al., 2009).

Compostos que são capazes de agir como agonistas dos *Toll-like Receptors* (TLRs) podem representar candidatos promissores a serem desenvolvidos como medicamentos contra o câncer (Husseinzadeh; Davenport, 2014). Considerando a imunossupressão do microambiente tumoral, a estimulação da resposta imune efetiva contra as células cancerígenas é uma estratégia terapêutica e a ativação de TLRs com agonistas pode influenciar a progressão do tumor através da resposta imune adaptativa e expressão gênica relacionada com mediadores inflamatórios (Chuffa et al., 2018). Adams et al. (2005) descreveram pela primeira vez os benefícios da utilização de agonistas de TLR3 no CO em estágio avançado. Outros estudos com uso dos agonistas de TLRs conjuntamente com outros agentes imunoestimulantes como vacinas (Morse et al., 2011) ou quimioterapia (Chuffa et al., 2018) mostraram resultados promissores da estimulação de TLR no CO. A estimulação com agonistas de TLR3 e CD40 aumentou a secreção de IL-12 e IFN tipo I, melhorou a capacidade de processamento de antígenos e capacidade migratória das células dendríticas em amostras de CO de camundongas e humanos (Scarlett et al., 2009). Pesquisas com agonistas de TLR8 em humanos (Lu et al., 2012) e de

TLR9 em murinos (Chuang et al., 2009; Cesare et al., 2008) demonstraram o aumento da atividade da imunidade inata contra o CO através do aumento da atividade das células NK.

O P-MAPA (agregado polimétrico anidrídico fosfolinoleato-palmitoleato de magnésio e amônio proteico, desenvolvido pela Farmabrasilis) é capaz de atuar como agonista de TLR2 e TLR4 e desencadear efeitos antitumorais (Fávaro et al., 2012). A combinação de imunoterapia com P-MAPA e cisplatina em ratas com câncer de bexiga não-músculo invasivo (CBNMI) induzido foi eficaz na redução das lesões neoplásicas e não houve antagonismo entre as drogas (Dias et al., 2016). Além disso, o P-MAPA estimula a via de sinalização dos interferons (TRIF-dependente), que foi eficaz no tratamento do CBNMI em modelos animais (Garcia et al., 2016). No CO, o P-MAPA induziu a expressão de genes inflamatórios mediados por TLR4 via MyD88 e TRIF-dependente e potencializou os efeitos da cisplatina na sinalização TLR, sendo a terapia com P-MAPA associado à cisplatina mais efetiva na redução dos tumores e adesões peritoneais do que os tratamentos isolados (Chuffa et al., 2018).

1.3.2. O papel dos *Checkpoints* imunológicos na imunidade antitumoral

O início da resposta imune adaptativa requer dois sinais, o primeiro via apresentação de antígenos envolvendo o complexo principal de histocompatibilidade (MHC) e o receptor de células T (Sinal 1), e o segundo via co-estimulação de CD28 com B7 (CD80 ou CD86) (Sinal 2) (Taube et al., 2018). Uma vez que uma resposta imune é iniciada, a duração e a amplitude da resposta são moduladas por diferentes pontos de checagem (*checkpoints*). Um deles é o CTLA-4 (antígeno 4 associado a linfócito T citotóxico), que possui maior afinidade pelas moléculas B7 em relação ao CD28. O CTLA-4 é suprarregulado 48h após a ativação das células T e leva à atenuação da resposta imune na fase inicial, verificando a ativação precoce de células T *naive* e de memória via sinalização dominante negativa (Taube et al., 2018). Outro importante ponto de checagem é a via de morte programada-1 (PD-1) / ligante de morte programada-1 (PD-L1), que atua nos tecidos periféricos na fase efetora da resposta imune (Taube et al., 2018). Acredita-se que seu papel seja suprimir a resposta imune e evitar possíveis danos autoimunes após exposição de antígenos a longo prazo, como durante infecções virais crônicas (Taube et al., 2018).

O ponto de checagem PD-1/ PD-L1 é de particular interesse, pois os tumores podem cooptar este caminho para atenuar a resposta imune do hospedeiro no microambiente tumoral (Taube et al., 2018). A resistência à imunidade adaptativa mediada por PD-L1 foi descrita pela primeira vez no melanoma (Taube et al., 2012). Neste mecanismo, a vigilância das células T

reconhece os neoantígenos tumorais como estranhos e se torna ativada, regulando positivamente o PD-1 e secretando IFN-γ (Taube et al., 2018). Em resposta ao IFN-γ, as células tumorais e as células imunes no microambiente tumoral expressam PD-L1. O PD-L1 então liga-se ao PD-1, que é altamente expresso nos TILs, e inativa as células T de vigilância (Taube et al., 2012; 2018). Dessa forma, células tumorais que expressam FOXP3 podem ativar a transcrição de PD-L1 e inibir diretamente a atividade de células T CD8+ no microambiente tumoral, além da inibição indireta pelo recrutamento de mais células Tregs FOXP3+ que também inibem as células T efetoras através da secreção de TGF-β, IL-10, IL-35 e moléculas citolíticas (Wang et al., 2022).

O PD-1 é expresso em diversas células imunológicas incluindo também os linfócitos B e células NK e o bloqueio terapêutico dessa via também pode influenciar a ação dessas células (Postow et al., 2015). Imunoterapias que tem como alvo esses *checkpoints* funcionam bloqueando os inibidores imunológicos como CTLA-4 e PD-1/ PD-L1, permitindo que a resposta imune do paciente atue na eliminação do tumor, o que leva à melhora na sobrevida mesmo em casos de cânceres avançados (Taube et al., 2018). Em 2011, o primeiro inibidor de *checkpoint* foi aprovado pela FDA (*Food and Drug Administration*): o Ipilimumab (anti-CTLA-4) para pacientes com melanoma e, em 2014, o Nivolumab e o Pembrolizumab (ambos anti PD-1) também foram aprovados. Em 2015, os agentes anti-PD-1/ PD-L1 para outros tipos de cânceres foram aprovados pela primeira vez (Taube et al., 2018).

Quando a expressão de PD-L1 tanto na célula tumoral quanto na célula imune foi avaliada como potenciais biomarcadores de resposta à terapia no carcinoma urotelial, os pesquisadores descobriram que a expressão de PD-L1 na célula imune é mais preditiva da resposta à inibição da sinalização PD1/ PD-L1 do que a expressão de PD-L1 na célula tumoral (Rosenberg et al., 2016). Tal fato pode ser explicado pela existência de um componente da expressão constitutiva de PD-L1 nas células tumorais, como tem sido relatado em tumores que surgem do epitélio do tipo escamoso (Malm et al., 2015). Mais recentemente, o sucesso da terapia de bloqueio PD-1/ PD-L1 no carcinoma urotelial levou à aprovação do FDA para certas condições clínicas desse tipo de tumor (Taube et al., 2018).

Uma evidência de que a expressão de PDL-1 em células tumorais suprime a resposta antitumoral já foi descrita também para o câncer de ovário por Hamanishi et al., (2007), os quais observaram uma correlação inversa entre a contagem de linfócitos T CD8+ intraepiteliais e a expressão de PDL-1 nas células tumorais. Além disso, um pior prognóstico foi associado significativamente com pacientes que apresentaram maior expressão de PDL-1

nas células tumorais ovarianas (Hamanishi et al., 2007). Maiores níveis de PDL-1 em monócitos no líquido ascitíco e sangue foram encontrados em pacientes com CO epitelial do que em pacientes com tumores de ovário benignos ou limítrofes (Maine et al., 2014).

Em ensaios publicados com pacientes de CO epitelial recidivado, resistentes à platina e tratados unicamente com inibidores de *checkpoints*, a taxa de resposta total não excedeu 15%, sugerindo que associações de estratégicas terapêuticas seriam mais eficientes tais como o tratamento com anticorpos anti CTLA-4 e inibidores de PARP, combinação efetiva em modelos animais de CO (Mittica et al., Higuchi et al., 2016) ou a associação de inibidores como Ipilimumab e Nivolumab que acarretaram em uma resposta de 34% em pacientes com CO epitelial e resistentes à platina (Burger et al., 2018). A terapêutica de bloqueio de *checkpoints*, no entanto, não atua somente sobre a resposta imune específica contra o tumor, mas também efeitos adversos podem decorrer da ativação inespecífica como eventos dermatológicos, gastrointestinais, hepáticos, endócrinos ou outros inflamatórios mais raros, embora a toxicidade seja inferior aos tratamentos oncológicos convencionais como quimioterapia e radioterapia (Postow et al., 2015).

1.3.3. Vias de sinalização associadas à resposta imune: STAT/JAK1/JAK2 e RANK/RANKL/OPG

A via STAT/JAK-1/JAK-2 é uma importante via de sinalização celular, atuante no desenvolvimento e diferenciação celular, em especial do sistema imunológico, promovendo a transdução de sinais de citocinas, interleucinas e fatores de crescimento (Tefferi, 2008). Estes fatores interagem com receptores transmembrana constitutivamente associados a proteínas Janus Quinases (JAKs). Estas são convertidas em uma forma ativa no momento da interação ligante-receptor e fosforilam resíduos tirosina na região citoplasmática do receptor, criando sítios para a fosforilação dos chamados Transdutores de Sinal e Ativadores de Transcrição (STATs), que ao formarem dímeros ativos, acumulam-se no núcleo e ligam-se ao DNA, modulando a expressão de genes relacionados ao ciclo celular (Rawlings et al., 2004).

O papel desta via na oncogênese é ainda objeto de discussão, sendo encontradas alterações no nível de JAKs em alguns tipos de câncer, como tumores epiteliais ovarianos e adenocarcinoma gástrico. Além disso, mutações ativadoras de STAT foram encontradas em 40% dos casos de leucemia linfocítica granular. Baixos níveis de inibidores da atividade de STATs foram encontrados em glioblastomas, provocando aumento da expressão proteica (Rawlings et al., 2004). Atividades antitumorais mediadas por IFN-γ são intermedidas por

STAT1 e STAT2, enquanto STAT3 tem sido relacionado com imunossupressão e sobrevivência das células tumorais inclusive em tumores da bexiga urinária (Owen et al., 2019; Brooks; Putoczki, 2020). A via STAT/JAK-1/JAK-2 é uma das vias envolvidas na regulação da expressão de PD-L1 induzida por IFN-γ (Mimura et al., 2018).

A via de sinalização RANK/RANKL/OPG é assim denominada em referência aos seus componentes chave: O Receptor Ativador de NF-κB (RANK), uma proteína transmembrana; seu ligante (RANKL) e o receptor Osteoprotegerina (OPG) que atuam na regulação do metabolismo ósseo, permitindo o crescimento e diferenciação de osteoclastos e a reabsorção óssea (Cheng; Fong, 2014). O OPG produzido pelos osteoblastos e células estromais atua como um receptor para o RANKL solúvel e, portanto, impede a diferenciação e ativação dos osteoclastos ao interferir na interação entre RANKL e RANK. Curiosamente, essa via de sinalização é também atuante no sistema imunológico, incluindo o desenvolvimento dos linfonodos, diferenciação de linfócitos, sobrevivência de células dendríticas, ativação de células T e indução de tolerância (Cheng; Fong, 2014). Em experimentos com ratos RANK/RANKL *knockout*, não houve desenvolvimento dos linfonodos (Kong et al., 1999). Além disso, células T CD4+ e CD8+ expressam RANKL após ativação e essa expressão está conectada à sobrevivência através de mecanismos anti-apoptóticos de células dendríticas as quais expressam RANK (Groot et al., 2017).

A relação da via RANK/RANKL/OPG com a carcinogênese se dá de várias maneiras. É bem descrito o envolvimento dessa via no processo metastático para o osso, por meio de um *feedback* recíproco entre proliferação tumoral e reabsorção óssea (Groot et al., 2017). Por outro lado, o sistema RANK/RANKL também apresenta efeitos na carcinogênese independente dos osteoclastos, visto que RANK e RANKL são expressos por células tumorais como no câncer renal, melanoma, próstata, mama e no CO, utilizando essa expressão em vantagem para sobrevivência e migração (Cheng; Fong, 2014; Renema et al., 2016). Essa via está ligada aos estágios iniciais de formação do câncer e metástase (Renema et al., 2016) e a expressão de RANK/RANKL em células tumorais é correlacionada com a progressão tumoral e metástase no câncer de mama (Cheng; Fong, 2014). A expressão de RANK também é maior no câncer de bexiga em comparação com o urotélio saudável (Mass et al., 2022). Da mesma forma, os níveis de OPG sérico em pacientes com câncer de bexiga são maiores comparativamente a humanos saudáveis e se correlacionam com um maior estágio e grau do tumor (Mizutani et al., 2004).

RANKL é envolvido na carcinogênese da mama relacionada com a progesterona (Hu et al., 2014; Tanos et al., 2013) e a sinalização RANK/RANKL atua nos tumores mamários relacionados com mutações *BRCA1* (Sigl et al., 2016). Mutações no gene *BRCA1* são implicadas não somente no câncer de mama como também no CO que, apesar de ser uma entidade clínica distinta, recentes evidências sobrepõem alterações genéticas e epigenéticas comuns às duas síndromes (Longacre et al., 2016). Células epiteliais e estromais de CO expressam RANK, RANKL e OPG, e RANKL tem expressão elevada nas células tumorais especialmente oriundas de tumores com mutações em *BRCA1/2* e essa expressão foi correlacionada significativamente com uma menor sobrevida em pacientes (Weiser et al., 2019). A inibição de RANKL culmina em efeitos antitumorais, bloqueando os efeitos diretos de RANKL nas células tumorais que expressam RANK (Groot et al., 2017) como também pode tornar mais efetivo o tratamento com inibidores de *checkpoints* quando associados (Van Dam et al., 2019).

O estabelecimento de um ambiente favorável para o desenvolvimento das células tumorais ocorre também através da acumulação de macrófagos associados a tumores, que expressam RANK e através da sinalização por RANKL alteram a resposta imune, induzindo a angiogênese (Renema et al., 2016). Este fenômeno é exacerbado pelo VEGF, que é frequentemente secretado pelas células tumorais e regula positivamente a expressão de RANK das células endoteliais (Min et al., 2007). A sinalização de RANK/RANKL nos macrófagos de perfil M2 induz a produção de quimiocinas, promovendo a proliferação de linfócitos Treg contribuindo para um microambiente imunossuprimido (Fujimura et al., 2015). Células Tregs CD4+CD25+FOXP3+ infiltradas no tumor são associadas com fenótipos mais agressivos de câncer de mama as quais também são uma fonte importante de produção de RANKL (Cheng; Fong, 2014). Wieser et al. (2019) demonstraram o envolvimento da sinalização de RANK na imunopatogênese do CO, no qual citocinas pró inflamatórias como IL-1β e TNFα induzem expressão de RANK e OPG nas células tumorais.

1.4. MRB-CFI-1 (Modulador de Resposta Biológica – Complexo Fosfato Inorgânico I) ou OncoTherad®: Uma nova nano-imunoterapia para o tratamento do câncer de bexiga e potencial no câncer no ovário

A nanoterapia é uma nova estratégia para o tratamento de neoplasias, na qual nanopartículas podem ser sintetizadas como agentes citotóxicos ou podem funcionar como carreadoras de reagentes imunomoduladores (Cubillos-Ruizet al., 2010). O magnésio e o

amônio quando associados ao fosfato configuram estratégias para o tratamento do câncer, seja de forma macro ou nanoestruturada (Durán; Fávaro, 2018). A literatura especializada tem demonstrado que a administração intratumoral de determinados compostos de fosfato ativam o sistema imune no microambiente tumoral, levando a uma importante regressão do tumor (Corrales et al., 2015; Shirota et al., 2012). Shirota et al. (2012) demonstraram que a administração intratumoral de oligonucleotídeos CpG (CpG-ODN) reduz a atividade imunossupressora de MDSCs, visto que as MDSC monocíticas do microambiente tumoral expressaram TLR9 e responderam à estimulação de CpG por intermédio da perda de sua capacidade supressora da função das células T, pela produção de citocinas Th1 e pela sua diferenciação em macrófagos com capacidade tumoricida, contribuindo para a regressão tumoral.

Similarmente, Corrales et al. (2015) demonstraram que a administração intratumoral de derivados dinucleotídeos cíclicos sintéticos ativou o fator estimulador do complexo de genes de interferon (STING), induzindo uma significativa regressão de tumores estabelecidos em camundongos, bem como uma reposta imune sistêmica capaz de reduzir e eliminar as metástases à distância e promover uma memória imunológica de longa duração. Inclusive em tumores ovarianos, oligodesoxinucleotídeos CpG (ligantes sintéticos de TLR9) associados com o peptídeo LL-37 promoveram efeitos antitumorais e melhoraram a sobrevivência de camundongas com CO, principalmente através do aumento da proliferação e ativação de células NK no peritônio dos animais (Chuang et al., 2009).

Considerando a importância do desenvolvimento de fármacos que atuem como agonistas dos TLRs, o laboratório de Carcinogênese Urogenital e Imunoterapia - LCURGIM (Instituto de Biologia – UNICAMP), liderado pelo professor Dr. Wagner José Fávaro, em parceria com o NANOBIOSS (Instituto de Química – UNICAMP), liderado pelo Prof. Nelson Duran, desenvolveu um composto sintético com propriedades antitumorais e imunológicas denominado Modificador de Resposta Biológica – Complexo Fosfato Inorgânico 1 (MRB-CFI-1) ou OncoTherad®. O OncoTherad® é um composto nanométrico de fosfato e sais metálicos associado a uma proteína glicosídica, com tamanho de 477,1 ± 127,1 nm e fórmula química: $C_{14}NO_8Mg_2(PO_4)_2$ (Fávaro et al., 2023). O nanofármaco possui patente depositada no Brasil (BR1020170127680) pela agência de inovação INOVA – UNICAMP no Instituto Nacional da Propriedade Industrial (INPI) (Fávaro; Duran, 2017) e na Europa no *European Patent Office* (WO2018227261), as quais estão em fases avançadas de análise. A patente americana já foi

concedida nos Estados Unidos pelo *United States Patent and Trademark Office* (USPTO) (US20200156951A1).

O OncoTherad® atua como um Modificador de Resposta Biológica, desencadeando a estimulação do sistema imune através da fosforilação de aminoácidos hidroxilados como serina, treonina e tirosina por compostos que apresentam sais de fosfato (Fávaro; Durán, 2017). Além disso, o OncoTherad® promove a ativação local do sistema imune no microambiente tumoral e um efeito antitumoral principalmente devido às induções de IFN (Fávaro; Durán, 2017; Fávaro et al., 2019).

Para verificar a capacidade de ativação local do sistema imune, a administração intraperitoneal do OncoTherad® foi avaliada em ratas *Fischer* 344. As análises macroscópicas dos peritônios revelaram que os animais tratados com o OncoTherad® apresentaram sinais intensos de inflamação peritoneal tais como rubor, aumento da vascularização, pontos hemorrágicos e pequenos aglomerados de cristais de fosfatos na cavidade abdominal (Fávaro; Durán, 2017). Pela via intravesical, diferentes doses promoveram inflamação dose-dependente na bexiga, ureteres e rins de ratos, camundongas e coelhos, mas não mostrou sinais de genotoxicidade, hepatotoxicidade e nefrotoxicidade, nem alterou nenhum parâmetro bioquímico nas três doses testadas (20 mg/kg, 50 mg/kg e 100 mg/kg) (Fávaro; Durán, 2017; Durán et al., 2019; Fávaro et al., 2023). Tais resultados pré-clínicos revelaram que o composto OncoTherad® foi capaz de induzir a resposta inflamatória local, o que justifica sua classificação como um imunomodulador.

O potencial antitumoral e imunomodulatório do OncoTherad® (MRB-CFI-1) em ratas *Fischer* 334 induzidas quimicamente ao CBNMI foram demostrados pela capacidade de impedir a progressão tumoral e recuperação histológica da bexiga urinária em torno de 70% dos animais (Durán et al., 2019; Fávaro et al., 2019; Fávaro et al., 2023). Em relação à atividade imunomodulatória, o OncoTherad® levou à ativação distinta do sistema imune inato mediada por TLRs 2 e 4 (Durán et al., 2019), resultando no aumento da via de sinalização para interferon (TLR4, TRIF, TBK1, IRF3, INF-γ) e iNOS, a qual está relacionada com a maior eficácia desse nanocomposto no tratamento do CBNMI (Fávaro; Durán, 2017; Fávaro et al., 2019; Fávaro et al., 2023). Em modelo de CBNMI em camundongas C57Bl/6J, o uso do OncoTherad® levou a uma inibição da progressão tumoral superior ao uso de BCG, o que esteve relacionado com a estimulação da via não canônica através de TLR4 enquanto BCG estimulou apenas a via canônica via TLR2 (Reis et al., 2022a). Além disso, em experimentos realizados em roedores, o OncoTherad® foi capaz de diminuir a expressão do sistema RANK/RANKL e,

consequentemente impedir a formação de metástases e/ ou impedir a progressão das mesmas, além de reduzir os níveis do *checkpoint* PD-1/PD-L1 (Fávaro et al., 2019; Reis et a., 2022b; Fávaro et al., 2023). Em consequência, níveis da proteína Bax foram aumentados e de Bcl-2 diminuíram após o tratamento com o OncoTherad®, indicando uma maior atividade apoptótica e menor proliferativa (Fávaro et al., 2023).

Após os resultados de segurança e eficácia em estudos pré-clínicos, foi desenvolvido um ensaio clínico-veterinário em cães com câncer de bexiga espontâneo. Os animais receberam uma aplicação semanal por seis semanas consecutivas de OncoTherad® pelas vias intravesical (44 mg/ml) e intramuscular (22 mg/ml); depois uma aplicação quinzenal (intravesical e intramuscular) por 6 meses e uma aplicação mensal (intravesical e intramuscular) por mais 6 meses, totalizando 24 aplicações. Após as seis primeiras aplicações de OncoTherad®, a massa tumoral reduziu cerca de 62,34% e no final da 24ª, a redução foi de 84,54% de seu volume em relação ao ultrassom inicial. Ao final da 24ª instilação, 100% dos pacientes apresentaram remissão parcial da doença e a taxa de sobrevida livre de recidiva/ progressão foi de 100% ao longo dos 402 dias do ensaio. Ainda, o tratamento com OncoTherad® não apresentou sinais de toxicidade sistêmica nas doses terapêuticas propostas (Böckelmann et al., 2017).

Após os resultados promissores em cães, a segurança do OncoTherad® foi observada no uso compassivo em seres humanos. O ensaio clínico (RBR-6swqd2) fase I/II de braço único contou com vinte e nove pacientes (18 homens, 11 mulheres) com CBNMI de alto grau refratário e/ ou recidivante (≥ 1 curso anterior de terapia intravesical com onco-BCG). Os pacientes receberam uma aplicação semanal por seis semanas consecutivas de OncoTherad® pelas vias intravesical (120 mg/ml) e intramuscular (25 mg/ml); depois uma aplicação quinzenal (intravesical e intramuscular) por 3 meses e uma aplicação mensal (intravesical e intramuscular) até completar 24 meses de tratamento. O acompanhamento foi realizado com mapeamento sistemático de biópsias da bexiga, cistoscopia e ultrassonografia. O desfecho primário foi a resposta patológica completa (RPC) e a sobrevida livre de recorrência (SLR). A recorrência foi definida como recidiva tumoral comprovada histologicamente (qualquer grau) e monitorada em intervalos de 3 meses. A idade média dos 29 pacientes foi de 64 anos, variando de 34 a 94 anos. No início do estudo, pTis, pTaG2-3, pT1G2-3 ocorreram em 10%, 59% e 31% dos pacientes, respectivamente. O tratamento com o OncoTherad® levou a taxas de RPC (IC 95%) de 100% em 3, 6 e 9 meses e de 89,6% (26/29) em 12 e 24 meses. A taxa de SLR de 24 meses em todos os pacientes foi de 79,3%. Além disso, o tempo médio para a recorrência da doença para os

pacientes foi de 459 dias (15,3 meses; IC 95%) em 24 meses de acompanhamento. Os eventos adversos relacionados ao tratamento foram em sua maioria (95%) de Grau 1 ou 2, sendo os mais comumente relatados: disúria (51,7%), cistite (34,5%), prurido (44,8%), erupção cutânea (27,6 %), artralgia (27,6%) e fadiga (27,6%) (Fávaro et al., 2019a; Alonso et al., 2020).

Considerando que o CO apresenta a maior letalidade dentre os cânceres ginecológicos e que não houve nenhuma redução substancial na taxa de mortalidade nas últimas décadas, há uma necessidade urgente do desenvolvimento de novas abordagens de tratamento eficazes (Adams et al., 2005; Lavoué et al., 2013; Muccioli; Bernencia, 2014). Em face do papel estratégico dos imunoterápicos e dos avanços da nanotecnologia para produção de novas moléculas com atividade farmacológica, destacam-se os compostos que atuam como agonistas dos TLRs, os quais representam candidatos promissores contra o câncer. Atualmente há diferentes exemplos dos benefícios da ativação dos TLRs em células imunes inclusive no microambiente de tumores ovarianos (Muccioli; Bernencia, 2014). O CO exibe metástase na cavidade peritoneal, apontando para o uso da via intraperitoneal como um excelente alvo para imunoterapias localizadas (Lengyel et al., 2010). Sendo assim, os efeitos antitumorais e imunomodulatórios do OncoTherad® (MRB-CFI-1) são promissores e atentam para análises em outros tipos de câncer que também estabelecem estado de imunossupressão no microambiente tumoral, tais como o câncer de ovário.

1.5.Associações Terapêuticas

1.5.1. Plasma Rico em Plaquetas (PRP) como potencial agente na resposta antitumoral

As plaquetas são fragmento celulares anucleados derivados de megacariócitos encontradas no sangue periférico (Foster et al, 2009; Ribatti; Crivellato, 2007). Além de desempenharem um papel crucial na hemostasia - resposta fisiológica frente a danos em vasos sanguíneos que mantém a integridade do fluxo vascular e o controle da hemorragia e trombose - as plaquetas também estão implicadas em outros processos fisiológicos como inflamação e cicatrização de feridas (Nurden, 2011). Após uma lesão vascular, as plaquetas se aderem à matriz extracelular exposta, resultando na ativação e agregação plaquetária para formação do tampão plaquetário (Bross et al., 2011). Fatores de coagulação se agregam na superfície pró-coagulante das plaquetas ativadas e asseguram a estabilização do tampão hemostático através da formação de uma malha de fibrina reticulada, obtida da conversão do fibrinogênio pela

trombina (Bross et al., 2011). Quando as plaquetas são ativadas, ocorre a degranulação de grânulos alfa e liberação de fatores de crescimento (FC) os quais se ligam à superfície das membranas celulares e ativam a hemostasia por sinalização celular, contribuindo para a regeneração de tecidos a partir da angiogênese e aumento das propriedades quimiotáticas e mitóticas das células indiferenciadas (Anitua et al, 2013; Küçük et al, 2014).

O plasma rico em plaquetas (PRP) é um produto biológico obtido por centrifugação do sangue periférico, obtendo-se uma concentração de plaquetas mais alta em comparação com os valores basais (Luzo et al., 2023). A partir da centrifugação do sangue total, um preparado de PRP contém uma alta concentração de plaquetas e, consequentemente, de FC que podem auxiliar na regeneração de tecidos variados como ossos, tendões, músculos (Küçük et al, 2014). Dentre os FC plaquetários destacam-se: o fator de crescimento derivado de plaquetas (PDGF), fator de crescimento de transformação β (TGF- β), fator de crescimento de insulina 1 (IGF-1), fator de crescimento de fibroblastos (FGF) e fator de crescimento endotelial vascular (VEGF) (Küçük et al, 2014; Naderi et al, 2020). Devido aos benefícios relacionados, o PRP tem sido empregado em muitas terapias regenerativas nas áreas da medicina, cirurgia, estética, odontologia, biologia molecular e celular e engenharia de biomateriais (Chou et al, 2020; Naderi et al, 2020; Vendramim et al, 2006; Luzo et al., 2023).

Apesar das variações nos métodos de preparação do PRP, de maneira geral os protocolos seguem uma sequência genérica que consiste em: 1) coleta do sangue em tubos com anticoagulante; 2) centrifugação inicial leve para separação em 3 camadas - uma camada superior contendo plaquetas e glóbulos brancos, uma camada intermediária rica em glóbulos brancos (*buffy coat*) e uma camada inferior que consiste principalmente de hemácias e 3) coleta do plasma sobrenadante acima da faixa de glóbulos brancos (ou incluindo o *buffy coat*) e nova centrifugação para obtenção das plaquetas concentradas que corresponde a 1/2 ou 1/3 inferior (Dohan Ehrenfest et al, 2009; Perez et al, 2013, Luzo et al., 2023). Com o uso de agonistas ou durante a própria centrifugação ocorre a ativação mecânica das plaquetas, liberando os FCs para o plasma. A presença de leucócitos remanescentes, devido à densidade ser parecida com a das plaquetas, é uma das características que podem ser utilizadas na classificação do tipo de PRP obtido (Ubezio et al., 2014; Dohan Ehrenfest et al, 2009; Mishra et al., 2012). As diferenças na força e no tempo de centrifugação usados nos diferentes protocolos de preparação do PRP resultam em diferenças significativas no rendimento, concentração, pureza, viabilidade e estado de ativação das plaquetas, os quais afetam sua aplicabilidade clínica (Harrison et al., 2018).

Existem diferentes classificações do PRP de acordo com o protocolo utilizado e o produto final obtido o qual pode variar na quantidade de plaquetas, leucócitos e fatores de crescimento dependendo da técnica de preparação (Cecerska-Heryć et al., 2022). Dessa forma, uma classificação que englobe as características que facilitem a utilização terapêutica do PRP é imprescindível para padronização em ensaios clínicos (Luzzo et al., 2023). A classificação da *International Society on Thrombosis and Haemostasis* (ISTH) é uma das mais abrangentes, considerando as condições de coleta da amostra (com uso ou não de anticoagulantes), a pureza (teor de glóbulos vermelhos ou glóbulos brancos), o número de plaquetas no produto, se as plaquetas foram ou não ativadas, ou se o produto foi congelado/descongelado antes do uso (Harrison et al., 2018). A classificação de Acebes-Huerta et al., (2020) propôs de forma mais aprofundada a consideração dos componentes associados aos eventos adversos (plaquetas intactas, glóbulos brancos, hemácias e *debris* celulares) e se o produto PRP é aplicado fresco, ativado ou congelado/descongelado. Por análise proteômica, Lee et al (2020) classificaram todas as proteínas do PRP detalhadamente por suas funções (cicatrização de feridas, angiogênese relacionada à cicatrização de feridas, migração de fibroblastos, biossíntese de colágeno, biossíntese de glicosaminoglicanos, ligação de glicosaminoglicanos e outras), seguidas pela identificação de funções potenciais do PRP.

As plaquetas desempenham um papel ativo na imunidade inata e adaptativa através de interações adesivas com leucócitos e células endoteliais via P-selectina, o que pode levar a eventos pró-inflamatórios, incluindo ativação de leucócitos, produção de citocinas em cascata e recrutamento de leucócitos para locais de lesão tecidual (Semple; Freedman, 2010). Além disso, estudos demonstraram que tanto as plaquetas humanas quanto as murinas podem expressar TLR2, TLR4 e TLR9 (Semple; Freedman, 2010). A expressão plaquetária do TLR4 medeia a trombocitopenia induzida por lipopolissacarídeos (LPS) e a produção de TNF-α por leucócitos, indicando que esses eventos podem ser responsáveis pela ativação do sistema imune inato (Semple; Freedman, 2010). Na doença aterosclerótica, a adesão de plaquetas ativadas ao endotélio libera moléculas pró-inflamatórias e citocinas, como IL-1β e CD40L, citocina CCL5/RANTES e fator plaquetário 4 (PF4), que são depositadas no endotélio vascular por um processo dependente da P-selectina, com consequente recrutamento de monócitos para o local da lesão (Semple; Freedman, 2010). Hua et al. (2012) compararam o tratamento convencional para ectopia cervical (laser) e um tratamento com aplicação de PRP ativado em gel em humanos. Os resultados mostraram eficácia terapêutica idêntica para os dois tratamentos, mas o grau de efeitos adversos do grupo PRP foi mais leve. O mecanismo exato do PRP na

reepitelização escamosa da ectopia cervical não está bem claro, mas os autores atribuem o efeito aos FCs presentes como o PDGF, TGF-β, IGF-1, FGF, VEGF e também à presença de leucócitos restantes da obtenção do PRP, que promovem a fagocitose de microrganismos, removem tecidos necrosados e inibem a reação inflamatória.

Nosso grupo de pesquisa investigou o envolvimento do PRP na modulação do sistema imune no tratamento do CBNMI quimicamente induzido em ratos (Dias et al., 2018). Nossos resultados demonstraram que o tratamento intravesical com PRP isolado ou associado ao BCG desencadeou citotoxicidade significativa em células de carcinoma de bexiga (HTB-9). Animais tratados com PRP associado ao BCG mostraram melhor recuperação histopatológica e diminuição da progressão de lesões neoplásicas uroteliais em 70% dos animais quando comparados aos grupos que receberam as terapias administradas isoladamente. Além disso, essa associação terapêutica promoveu ativação distinta do sistema imune mediado por TLRs 2 e 4, resultando no aumento das imunorreatividades para MyD88, TRIF, IRF3, IFN-γ (Dias et al., 2018).

Os grupos fosfato presentes no OncoTherad®, são importantes na prática clínica, pois existe uma nítida relação entre alguns fosfatos (Polifosfatos - PolyP) e plaquetas. Os PolyP são secretados por plaquetas ativadas ou mastócitos, e desempenham importante atividade pró-inflamatória (Morrissey, 2012; Morrissey et al., 2012a; Müller et al., 2009). Os PolyP desencadeiam a coagulação, aceleram a ativação do fator V, aumentam a estrutura do coágulo de fibrina e aceleram a retroativação do fator XI pela trombina. Recentemente, foi descrito que PolyP modula a resposta imune inata ao suprimir o complemento, interferindo também na complexa relação entre coagulação e imunidade inata mediada por PF4 (Wat et al., 2014). Em nossos estudos piloto, análises de caracterizações físico-químicas mostraram haver uma importante interação entre as proteínas do PRP e os fosfatos presentes no OncoTherad®, além de maior concentração de proteínas após essa interação, possivelmente devido à capacidade do componente inorgânico (CFI-1) de induzir a liberação de proteínas pelas plaquetas. Assim, os promissores efeitos do PRP e sua potencial associação com grupos fosfato presentes no OncoTherad® podem constituir uma importante alternativa terapêutica, principalmente nos casos de pacientes não responsivos aos tratamentos convencionais.

1.5.2. Eritropoietina: além das propriedades hematopoiéticas

A Eritropoietina (EPO) é uma proteína glicosilada de 34 kDa e 165 aminoácidos que desempenha funções como hormônio, citocina e fator de crescimento (Chateauvieux et al.,

2011). A EPO é produzida majoritariamente pelos rins em adultos e pelo fígado durante o período fetal, neonatal e em casos de anemia severa, no entanto células do baço, medula óssea, cérebro e pulmão também podem expressar RNA mensageiro de EPO em pequenas quantidades (Jelkmann, 2016). O processo de eritropoiese (produção de eritrócitos ou células vermelhas do sangue) nos mamíferos requer a presença de EPO que, em condições normais, apresenta concentração de 10-11mol/l no plasma sanguíneo que aumenta em condições de hipóxia (Jelkmann, 2016). A EPO regula a sobrevivência, proliferação e diferenciação de eritrócitos a partir de células tronco hematopoiéticas CD34+ na medula óssea e mantém as concentrações de hemoglobina no sangue em níveis normais, visto que a deficiência em sua produção resulta em anemia (Jelkmann, 2013).

A produção de EPO humana depende da transcrição do gene de EPO (localizado no cromossomo 7) e condições como hipóxia e anemia são capazes de induzir sua expressão (Chateauvieux et al., 2011; Jelkmann, 2013). A EPO sintetizada interage com os homodímeros dos receptores de EPO (EPOR) na superfície de células eritrocíticas, o que estimula a eritropoiese através de uma complexa rede de sinais moleculares relacionados com controle da diferenciação, proliferação e morte celular (Chateauvieux et al., 2011). Em condições de anemia decorrente de doenças inflamatórias crônicas e câncer, citocinas pró-inflamatórias como IL-1β e TNF-α causam falha na produção de EPO através dos fatores de transcrição GATA-2 e NF-kB que podem inibir o promotor do gene de EPO (Chateauvieux et al., 2011).

O gene humano de EPO foi clonado através da tecnologia de recombinação de DNA, tornando possível a produção em larga escala desse recombinante de EPO (rHuEPO) como análogos estimulantes de eritropoiese (ESAs), tais como alfaepoetina ou darbepoetina alfa, que podem ser utilizadas terapeuticamente em casos de anemia crônica alternativamente às transfusões sanguíneas (Cantrell et al., 2011; Jelkmann, 2013). Os ESAs mimetizam a função fisiológica e ativam os EPORs nas células eritrocíticas, sendo uma das opções de tratamento para atenuar os sintomas de fadiga e da anemia associada ao câncer ou decorrente do próprio tratamento com quimioterapia (Chateauvieux et al., 2011; Jelkmann, 2013). Durante o tratamento quimioterápico, caso a concentração de hemoglobina do paciente for menor que 100 g/l pode-se iniciar o tratamento com ESAs, que também pode ser utilizado para pacientes com AIDS e em casos específicos em pré e pós operatórios (Jelkmann, 2013). O tratamento da anemia leva a um melhor prognóstico por reduzir um dos efeitos colaterais da quimioterapia, uma vez que essa complicação subsequente do tratamento leva à exaustão celular dos

eritrócitos, piorando a qualidade de vida do paciente e até diminuindo a sensibilidade do tumor à radioterapia e quimioterapia (Pronzato, 2006).

A EPO também apresenta efeitos não hematopoiéticos como a capacidade de proteção tecidual contra determinados traumas, toxinas e outros danos hereditários ou não hereditários e esse efeito citoprotetor foi relatado principalmente no sistema cardiovascular e nervoso (Chateauvieux et al., 2011). Essa proteção é mediada principalmente por inibição da apoptose, atividade anti-inflamatória e indução da angiogênese, fatores que evitam o estresse tecidual. Os efeitos anti-inflamatórios da EPO foram descritos em diferentes modelos animais, através da redução da expressão de citocinas pró-inflamatórias e do processo apoptótico (Lombardero et al., 2011). Além disso, o uso de ESAs é associado com aumento no número de plaquetas e estimulação de sua ativação (Lombardero et al., 2011; Jelkmann, 2013).

EPO e EPOR também são expressos em células do cérebro e nos sistemas cardiovascular, digestório, endócrino, respiratório e inclusive no genital feminino (útero, tubas uterinas e ovário) (Yasuda et al., 2000; Lombardero et al., 2011). O receptor de eritropoetina é presente nos folículos ovarianos de vários estágios, incluindo diferentes tipos celulares como o ovócito, camada granulosa, teca interna e células luteínicas, onde contribui no processo de mudanças cíclicas do sistema genital feminino (Yasuda et al., 2000). A EPO apresenta efeitos protetores e antioxidantes também nos ovários de ratas e camundongas, auxiliando nos danos aos tecidos causados por isquemia e estresse oxidativo e melhorando a sobrevivência e funcionamento folicular (Ergun et al., 2010; Manizheh et al., 2011; Mahmoodi et al., 2014). O efeito protetor de EPO também foi relatado em ratas submetidas à quimioterapia com cisplatina, sendo capaz de melhorar a função ovariana e prevenir a infertilidade (Sayan et al., 2017).

A EPO também pode influenciar mecanismos imunes exercendo um papel imunomodulador. Em modelos experimentais murinos, a EPO aumentou resposta imune, atuando sobre a atividade dos linfócitos B (Katz et al., 2007), células dendríticas (Lifshitz et al., 2009) e macrófagos (Lifshitz et al., 2010). Lifshitz et al. (2010) demostraram em camundongos que uma disponibilidade excessiva de EPO resultou no aprimoramento do fenótipo pró-inflamatório e da função dos macrófagos peritoneais do baço tanto em estado latente como inflamatórios (induzidos). O tratamento *in vivo* levou a um aumento no número de macrófagos esplênicos e dos macrófagos que expressam CD11b, CD80 e MHC classe II. Os macrófagos inflamatórios peritoneais obtidos de camundongos tratados com EPO mostraram aumento da expressão de F40, CD11b, CD80 e MHC classe II e maior atividade fagocítica

(Lifshitz et al., 2010). A EPO foi utilizada até mesmo para estimular linfócitos T em terapia celular adotiva (Vinanica et al., 2020).

A questão crítica e ainda controversa é até que ponto o uso de ESAs pode favorecer o crescimento tumoral devido à atividade angiogênica e estimulação de EPOR nas células tumorais. Dado que EPOR não é um oncogene, várias pesquisas demonstraram não haver vantagens seletivas da superexpressão desse receptor pelas células tumorais (Fandrey, 2008; Lombardero et al., 2011). Além disso, determinadas células tumorais carecem da proteína funcional EPOR, embora expressem baixos níveis de EPOR RNAm, sendo que a presença desses receptores é um dos fatores condicionais para os efeitos colaterais (Jelkmann, 2013). Swift et al., (2010) mostraram que o receptor de EPO em mais de 200 linhagens de células tumorais humanas não foi induzido ou ativado por tratamento com ESAs. Por outro lado, recentemente foi mostrado em cultura de células humanas de adenocarcinoma ovariano que na ausência de EPO os EPOR protegem as células cancerígenas da morte celular induzida por Tamoxifeno além do tratamento associado com a EPO apresentar maior redução da proliferação celular do que o Tamoxifeno isolado (Kimáková et al., 2018).

A vascularização do tumor apresenta estrutura e função anormais e, em condições de fluxo sanguíneo reduzido, ocorre hipóxia especialmente em concentrações baixas de hemoglobina (Lombardero et al., 2011). A hipóxia tumoral é um fator em geral associado a uma pior sobrevida e, ao mesmo tempo que pode restringir a proliferação celular, estimular apoptose e necrose; algumas células podem adaptar-se ao estresse hipóxico através de modificações na expressão gênica e adquirir um fenótipo agressivo com facilitação da propagação local e à distância pela diminuição da expressão de moléculas de adesão e aquisição de resistência à quimioterapia ou radioterapia (Lombardero et al., 2011). Hardee et al. (2005) mostraram que a aplicação de rHuEPO em ratas com tumores mamários não promoveu crescimento tumoral ou aumento da angiogênese em comparação com o placebo. Outras pesquisas demonstraram um efeito antitumoral da EPO, na diminuição de massa tumoral em modelos murinos de linfoma (Katz et al., 2005) e mieloma (Mittelman et al., 2001) e tumores de mama, na qual quando associada com Tamoxifeno promoveu maior regressão tumoral do que o tamoxifeno isolado (Sairah et al., 2008). Nanocarreadores lipídicos de tamoxifeno e conjugados com EPO na superfície têm resultados promissores com maior atividade citotóxica *in vitro* em células de adenocarcinoma de mama humano (Beh et al., 2017) e em modelos de adenocarcinoma de mama em ratas (Beh et al., 2019).

Estudos clínicos e meta-análises demonstraram que o uso de ESAs não causa efeitos significativos na progressão da doença e crescimento tumoral em pacientes que trataram anemia decorrente do câncer ou da quimioterapia (Glaspy et al., 2010; Aapro et al., 2012; Jelkmann, 2013). Cantrell et al. (2011) relataram que o uso ou não ESAs para tratamento da anemia decorrente da quimioterapia por pacientes de CO não alterou a sobrevida livre de progressão nem a sobrevida global. Mulheres com cânceres ginecológicos compreendem um subgrupo de pacientes que potencialmente se beneficiam com o uso de ESAs (Cornes; Boiangiu, 2007). Além disso, pacientes com CO em geral apresentam idade avançada, estão na pós menopausa e apresentam baixa tolerância à anemia (Lombardero et al., 2011). Do mais, o tipo de câncer e as terapias conjuntas às quais o paciente é submetido influenciam os efeitos da EPO exógena assim como o tempo e dose de tratamento (Lombardero et al., 2011; Jelkmann, 2013).

2. HIPÓTESES e OBJETIVOS

A hipótese geral desse trabalho de doutorado é: *O nanofármaco OncoTherad® apresenta efeitos antitumorais e imunomodulatórios no tratamento do câncer de diferentes órgãos do sistema urogenital e esses efeitos podem ser aprimorados com associações terapêuticas específicas.* Sendo assim, o objetivo geral foi avaliar os efeitos histopatológicos e moleculares do complexo nanoestruturado OncoTherad® e associações terapêuticas (Plasma Rico em Plaquetas e Eritropoetina) no tratamento de diferentes cânceres do sistema urogenital (câncer de bexiga e câncer de ovário) em modelos animais. Para tanto, a tese de doutorado divide-se em duas principais partes:

2.1. Projeto Câncer de Bexiga: OncoTherad® e Plasma Rico em Plaquetas (PRP) (CNPq 140695/2019-2)

Os objetivos principais deste estudo foram caracterizar os efeitos histopatológicos e moleculares do complexo nanoestruturado OncoTherad® (MRB-CFI-1) associado ao PRP no tratamento do câncer de bexiga não-músculo invasivo (CBNMI) induzido quimicamente em camundongas C57BL/6J, bem como estabelecer os possíveis mecanismos de ação dessa associação terapêutica relacionando as vias de sinalização dos TLRs 2 e 4; fatores de crescimento VEGF e IGF-1; e população de linfócitos T regulatórios FOXP3+ e linfócitos T CD8+ CX3CR1+. Para tanto, os objetivos específicos foram:

a) Analisar o peso corporal inicial e final, ganho de peso e consumo de ração e água dos animais durante o período experimental;

b) Analisar as características físico-químicas da urina dos animais;

c) Descrever macroscopicamente e quantificar as alterações das bexigas urinárias dos diferentes grupos experimentais;

d) Caracterizar a histopatologia do CBNMI de camundongas induzidos quimicamente e comparar a progressão tumoral frente aos tratamentos intravesicais com OncoTherad®, PRP e OncoTherad+PRP®;

e) Caracterizar e comparar os efeitos dos tratamentos intravesicais com OncoTherad®, PRP e OncoTherad®+PRP nas vias de sinalização dos TLRs 2 e 4 (TLR2, TLR4, MyD88, NF-κB, IL-6, IL-1β, TRIF, TBK1, IRF-3, IFN-γ) por imunohistoquímica;

f) Caracterizar e comparar os efeitos dos tratamentos intravesicais com OncoTherad®, PRP e OncoTherad®+PRP nos fatores de crescimento relacionados com a progressão tumoral VEGF e IGF-1 por imunohistoquímica;

g) Caracterizar e comparar os efeitos dos tratamentos intravesicais com OncoTherad®, PRP e OncoTherad®+PRP na população de linfócitos T regulatórios FOXP3+ e linfócitos T CD8 CX3CR1+, por imunohistoquímica.

2.2. Projeto Câncer de Ovário: OncoTherad® e Eritropoetina (EPO) (FAPESP 2020/15687-5)

O objetivo fundamental do projeto foi avaliar os efeitos histopatológicos e moleculares da imunoterapia com OncoTherad® (MRB-CFI-1) associada à Eritropoetina (EPO) no tratamento do câncer de ovário induzido quimicamente em ratas *Fischer* 344. Para tanto, foram investigados os possíveis mecanismos de ação dessa associação terapêutica no funcionamento de fatores e vias de sinalização inter-relacionadas e implicadas no complexo microambiente da carcinogênese ovariana, constituindo um panorama informativo sobre o perfil da resposta inflamatória frente aos tratamentos. Dentre esses fatores, foram avaliados a via dos receptores *Toll-like* e o perfil da resposta inflamatória. Dessa forma, os objetivos específicos foram:

a) Monitorar o ciclo estral, peso corporal inicial e final, ganho de peso e consumo de ração e água das fêmeas durante o período experimental;

b) Avaliar e caracterizar os tipos de alterações histopatológicas induzidas quimicamente nas ratas e comparar a progressão tumoral após os tratamentos com OncoTherad®, EPO e OncoTherad®+EPO;

c) Caracterizar a via dos receptores *Toll-like* no microambiente tumoral do CO e avaliar a modulação após os diferentes tratamentos a partir da imunolocalização e imunorreatividade dos receptores TLR2, TLR4, MyD88, NF-κB, TRIF e IRF-3 por imuno-histoquímica;

d) Avaliar a resposta inflamatória citotóxica no microambiente tumoral e após tratamentos a partir da imunolocalização e imunorreatividade de IFN-γ, iNOS e macrófagos totais F4/80+ por imuno-histoquímica;

e) Avaliar o perfil de imunossupressão no microambiente tumoral e após os tratamentos a partir da imunolocalização e imunorreatividade de IL-6, macrófagos M2 CD163+ e Linfócitos T regulatórios (Tregs) FOXP3+ por imuno-histoquímica;

2.2.1. Caracterização do modelo de câncer de ovário: Projeto de estágio no exterior (BEPE FAPESP 2021/12357-7)

Um subprojeto foi desenvolvido na Universidade de British Columbia (UBC) sob a orientação do Dr. Michael Anglesio (BEPE FAPESP: Processo número 2021/12357-7) com o objetivo de avaliar se o modelo de câncer de ovário induzido quimicamente com DMBA era representativo da doença em humanos, definindo molecularmente o(s) tipo(s) histológico(s) encontrado(s). Para tanto, avaliamos biomarcadores mutacionais e imuno-histoquímicos (IHC) usados rotineiramente para o CO humano e usamos as características observadas para fornecer um melhor contexto para a avaliação dos efeitos dos tratamentos com o OncoTherad® e EPO. Para atingir esses propósitos, os objetivos específicos foram:

a) Pesquisar *hotspots* de mutação equivalente entre genes humanos e seus parálogos em ratos para desenhar primers apropriados para ensaios de sequenciamento;

b) Extrair o DNA dos ovários incluídos nos blocos de parafina e avaliar a presença das mutações alteradas recorrentemente no câncer de ovário diretamente (*Kras, Pik3ca* e *Ctnnb1*) por reação em cadeia da polimerase (PCR) e sequenciamento Sanger.

c) Construir os *Tissue Microarrays* (TMA) a partir dos blocos doadores contendo os ovários dos animais dos grupos Controle, Câncer, OncoTherad, EPO, OncoTherad+EPO;

d) Avaliar mutações genéticas típicas indiretamente com substitutos imuno-histoquímicos de mutação (Arid1a e p53) e a expressão proteica de biomarcadores típicos de diferentes tipos de câncer de ovário (Wt1, Hnf1b e Pr) por imuno-histoquímica;

e) Examinar e quantificar a infiltração de células imunes por imuno-histoquímica

utilizando marcador de linfócitos T CD3+.

3. MATERIAIS E MÉTODOS

Para o trabalho de doutorado em geral, os materiais e métodos de acordo com os objetivos podem ser resumidos no esquema da **Figura 4**. Dado o tamanho da tese de doutorado e suas subdivisões bem como para se evitar exaustivas repetições, os resultados/discussão foram apresentados em formato de artigo. Dessa forma, os materiais e métodos específicos e utilizados para cada parte desse trabalho estão detalhados em cada respectivo artigo. Os dois artigos apresentados nessa tese de doutorado estão em processo de revisão/submissão.

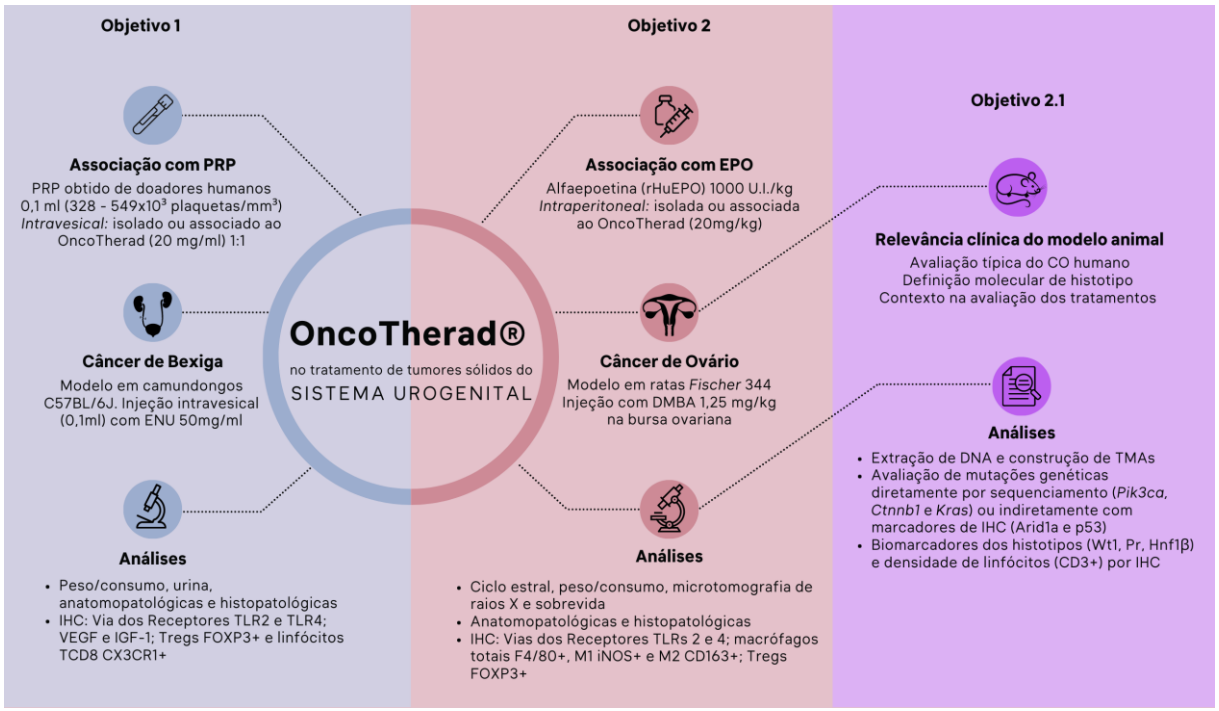

Figura 4. Design experimental de acordo com os objetivos. O trabalho de doutorado foi dividido em duas principais partes: 1) câncer de bexiga e 2) câncer de ovário. Um subprojeto (objetivo 2.1) foi desenvolvido a partir o objetivo 2. ENU: N-etil-N-nitrosouréia. DMBA: 7,12-dimetilbenzoantraceno IHC: análises de imunohistoquímica. CO: Câncer de ovário. TMAs: *Tissue Microarrays*.

4. CAPÍTULO I

Revista para submissão: **TRANSLATIONAL RESEARCH**

A Potential New Therapeutic Strategy for Non-Muscle Invasive Bladder Cancer: Combination of Intravesical OncoTherad® Immunotherapy and Platelet Rich Plasma

Bianca Ribeiro de Souza[1]; Ianny Brum Reis[2], Gabriela Cardoso de Arruda Camargo[1], Gabriela Oliveira[1], Queila Cristina Dias[1], Nelson Durán[1,3], Wagner José Fávaro[1]

[1]Department of Structural and Functional Biology, Institute of Biology – University of Campinas (UNICAMP), Campinas, São Paulo, Brazil.

[2]Department of Diagnosis and Surgery, School of Dentistry - São Paulo State University (UNESP), Araraquara, São Paulo, Brazil.

[3]Nanomedicine Research Unit (Nanomed), Federal University of ABC (UFABC), Santo André, São Paulo, Brazil

Running head: *OncoTherad® and PRP in Bladder Cancer Treatment*

Key words: bladder cancer; immunotherapy; OncoTherad; histopathology; immunohistochemistry, Toll-Like receptors.

Corresponding author: Bianca Ribeiro de Souza. 255, Monteiro Lobato Street, University City - University of Campinas (UNICAMP) - Laboratory of Urogenital Carcinogenesis and Immunotherapy. ZIP/Postal Code: 13083-862, Campinas, São Paulo, Brazil. E-mail: biancarsbio@gmail.com. Phone: +55 (18) 98193-8916.

Co-authors' emails: Ianny Brum Reis (iannybrumreis@yahoo.com.br), Gabriela Cardoso de Arruda Camargo (gcacamargo0@gmail.com), Queila Cristina Dias (queilaspg@yahoo.com.br), Gabriela Oliveira (gabrielaufscar@gmail.com), Nelson Durán (nelsonduran1942@gmail.com), Wagner José Fávaro (favarowj@unicamp.br).

ABSTRACT

There is no effective second-line therapy for non-muscle-invasive bladder cancer (NMIBC) when Bacillus Calmette-Guérin (BCG) fails. A new perspective is represented by OncoTherad® (MRB-CFI-1) immunotherapy, a nanostructured inorganic phosphate complex associated with glycosidic protein, developed by University of Campinas in Brazil. Previous studies have shown that Platelet Rich Plasma (PRP) also acts on immune activation and exerts antitumor effects. This study characterized the effects of the OncoTherad® associated with PRP in the treatment of NMIBC chemically induced in mice. When treated intravesically with PRP only, mice showed 28.6% of tumor progression inhibition rate; with OncoTherad® 85.7%; and with OncoTherad®+PRP 71.4%. Intravesical treatments led to distinct activation of Toll like Receptors (TLRs) 2 and 4-mediated innate immune system in the interleukins (canonical) and interferons (non-canonical) signaling pathways. OncoTherad® isolated or associated with PRP upregulated TLR4 and its downstream cascade mediators as well as increased interleukins 6 (IL-6) and 1β (IL-1β), and interferon-γ (IFN-γ). In this way, the NMIBC microenvironment was modulated to a cytotoxic profile correlated with the IL-1β increase by stimulating immune pathways for IFN-γ production and consequent cytotoxic T lymphocytes (as CD8+ T-cells) activation and regulatory T-cells (Tregs) reduction. In addition, PRP did not trigger carcinogenic effects through the biomarkers evaluated. Considering the possibility of personalizing the treatment with the PRP use as well as the antitumor properties of OncoTherad®, we highlight this association as a potential new therapeutic strategy for NMIBC, mainly in cases of relapse and/or resistance to BCG.

ABBREVIATIONS

ANOVA, analysis of variance; BCG, Bacillus Calmette-Guérin; CTLs, cytotoxic T lymphocytes; CX3CR1, CX3C chemokine receptor 1; DC, dendritic cells; FOXP3, transcription factor forkhead box protein P3; IFN-γ, interferon-γ; IGF-1, insulin-like growth factor 1; IL-1β, interleukin-1β; IL-6, interleukin-6; iNOS, inducible nitric oxide synthase; IRF-3, interferon regulatory factor-3; MyD88, myeloid differentiation primary-response protein 88; MRB-CFI-1, Biological Response Modifier - Inorganic Phosphate Complex 1; NF-κB, nuclear factor kappa B; NMIBC, non-muscle-invasive bladder cancer; PF4, platelet factor 4; PolyP, polyphosphates; pTis, urothelial carcinoma in situ, pTa, noninvasive papillary urothelial carcinoma; pT1, urothelial carcinoma confined to the bladder mucosa and submucosa; STING, interferon gene complex-stimulating factor pathway; TBK1, tank-binding kinase 1; TNF-α, tumor necrosis factor α; TPI, tumor progression inhibition; TIR, Toll-interleukin-1 receptor domain; TLRs, Toll-like receptors; Tregs, regulatory T-cells; TRIF, TIR-domain-containing adaptor protein that induces IFN-γ; VEGF, vascular endothelial growth factor.

AT A GLANCE COMMENTARY

Souza BR, et al.

Background

Effective intravesical therapies remain lacking for non-muscle invasive bladder cancer (NMIBC) when the first-line therapy fails. Considering the immunosuppression of the tumor microenvironment, the stimulation of an effective immune response against cancer cells with Toll-like Receptors (TLRs) agonists is a promising strategy.

Translational Significance

We have characterized the mechanisms of action of the therapeutic association between OncoTherad® immunotherapy and Platelet Rich Plasma (PRP) in a NMIBC animal model. The associated treatment significantly inhibited tumor progression by acting on the TLR signaling pathway and modulating the microenvironment to a cytotoxic profile. This association may constitute a new therapeutic strategy for BCG-unresponsive NMIBC patients.

INTRODUCTION

More than 70% of the incidence of bladder cancer is superficial, called non-muscle invasive bladder cancer (NMIBC).[1] The primary treatment of NMIBC is based on the surgical procedure through transurethral resection, followed by intravesical immunotherapy with Bacillus Calmette-Guérin (BCG).[2] 20% to 30% of superficial tumors (pTis - carcinoma *in situ*, pTa – papillary, and pT1 - tumor confined to the bladder mucosa and submucosa) show progression to invasive phenotype and 70% recurrence after transurethral resection while adjuvant therapy with BCG can decrease these rates.[2–4] However, it is estimated that approximately 5-10% of patients are unable to complete the treatment with BCG due to the side effects.[5,6] An additional problem is the frequent worldwide BCG shortage due to suspensions, restrictions and difficulties in production. Thus, NMIBC patients are subject to changes and/or interruptions in treatment and even completely helpless in the absence of BCG. The challenges imposed by the BCG scarcity highlight the need to develop new treatment options for NMIBC.[7]

Compounds that are able to act as Toll-like Receptors (TLRs) agonists may represent promising candidates to be developed as cancer drugs.[8] Considering the immunosuppression of the tumor microenvironment, the activation of TLRs with agonists can influence tumor progression through adaptive immune response against cancer cells and gene expression related to inflammatory mediators.[9] The classic function of TLRs is the recruitment of leukocytes to infected tissues with subsequent induction of adaptive immune responses.[10–12] Collectively, each TLR recruits a specific combination of adapter molecules to activate different transcription factors that will give rise to the appropriate and effective response against the stimulatory pathogen.[10,12,13] TLRs signaling pathways comprise two different pathways: the canonical or MyD88 (myeloid differentiation primary-response protein 88)-dependent and the non-canonical or TRIF (TIR-domain-containing adaptor protein that induces IFN-γ)-dependent.[13]

Many of the known effects of TLR signaling occur through the production of inflammatory molecules and molecules for cell survival, such as tumor necrosis factor α (TNF-α) and interleukins IL-6, IL-1β and IL-10, as well as the expression of costimulatory molecules in dendritic cells and macrophages.[10,11] Urinary bladder tumors, especially NMIBC, showed decreased expression of TLRs.[14,15] Immunotherapy with BCG mediated by TLRs is a successful strategy in NMIBC which involves the canonical pathway by activating MyD88 and NF-κB (nuclear factor kappa B). Local lymphocytic infiltration and production of inflammatory

cytokines were found in the urinary bladder wall of most patients who received intravesical BCG, resulting in a complex local immune response.[16,17]

The Laboratory of Urogenital Carcinogenesis and Immunotherapy - LCURGIM (University of Campinas) developed a synthetic nanostructured compound with antitumor and immunological properties called Biological Response Modifier - Inorganic Phosphate Complex 1 (MRB-CFI-1, for its acronym in Portuguese). MRB-CFI-1, registered as OncoTherad®, is composed of phosphate and metal salts associated with a glycosidic protein, with a size of 477.1 ± 127.1 nm and chemical formula: $C_{14}NO_8Mg_2(PO_4)_2$.[18,19] The nanopharmaceutical has patents granted in Brazil[18] (BR102017012768B1) and the USA[20] (US11572284B2, US11136242B2); and is being tested in a clinical trial for bladder cancer (Brazilian Clinical Trials Registry -RBR-6swqd2, UTN U1111-1226-9096).[21] OncoTherad® stimulates the immune system through the phosphorylation of hydroxylated amino acids such as serine, threonine and tyrosine by compounds that present phosphate salts.[18] In this way, this immunotherapy promotes local activation of the immune system in the tumor microenvironment and exhibits antitumor effects mainly due to TLR4-mediated IFNs induction.[19,22–24]

The mechanism of innate immune detection of immunogenic tumors leading to adaptive T-cell responses remains elusive, although interferons (IFNs) are implicated in this process.[25] The main mechanism for the innate immune detection of cancer occurs through the host interferon gene complex-stimulating factor pathway (STING), with implications for the use of immunotherapies.[25] The type I and II IFN responses induced by STING are related to the activation of tank-binding kinase 1 (TBK1) through TLRs receptors. IFNs promote M1 macrophage polarization and CD8+ T-cell expansion and activation, increasing immune surveillance. Recently, CX3C chemokine receptor 1 (CX3CR1) was discovered to be a T-cell differentiation marker.[26] On the other hand, regulatory T cells (Tregs), identified by the transcription factor forkhead box protein P3 (FOXP3) marker, allow immune tolerance.[27]

Platelet-rich plasma (PRP) is a platelet lysate concentrated in a small volume of plasma with the presence of growth factors, which are released when activated.[28] It is obtained from whole blood centrifugation, in which red and white blood cells and platelets are separated, where platelets have a higher concentration in a small volume of plasma compared to baseline values.[29] Due to related benefits, PRP has been used in many regenerative therapies in the areas of medicine such as surgery, aesthetics, dentistry, molecular and cellular biology, and biomaterials engineering.[30,31] Our research group investigated the involvement of PRP in

modulating the immune system in the treatment of chemically induced NMIBC in rats.[32] Intravesical treatment with PRP alone or associated with BCG triggered significant cytotoxicity in bladder carcinoma cells (HTB-9). Further, animals treated with PRP associated with BCG showed better histopathological recovery and a decrease in the progression of urothelial neoplastic lesions in 70% of the animals when compared to the groups that received the therapies administered alone. In addition, this therapeutic association promoted distinct activation of the immune system mediated by TLRs 2 and 4, resulting in increased immunoreactivity for MyD88, TRIF, IRF-3 (Interferon regulatory factor-3), and IFN-γ.[32]

The phosphate groups present in OncoTherad® are important in clinical practice, as there is a clear relationship between some phosphates (Polyphosphates - PolyP) and platelets. PolyP are secreted by activated platelets or mast cells, and play an important proinflammatory activity.[33,34] PolyP modulates the innate immune response by suppressing the complement system, also interfering in the complex relationship between coagulation and platelet factor 4 (PF4)-mediated innate immunity.[35] In our pilot studies (data not shown), analyzes of physicochemical characterizations showed that there is an important interaction between PRP proteins and phosphates present in OncoTherad®, in addition to a higher concentration of proteins after this interaction, possibly due to the ability of the inorganic component (CFI-1) to induce protein release from platelets. Thus, the promising effects of PRP and its potential association with phosphate groups present in OncoTherad® may constitute a therapeutic alternative, especially in cases of patients unresponsive to conventional treatments.

Given this context, we characterized the histopathological and molecular effects of the OncoTherad® associated with PRP in the treatment of NMIBC chemically induced in mice and described the mechanisms of action of this association involving the TLRs 2 and 4 signaling pathways. To construct a panel of immune response in the NMIBC microenvironment, we also evaluated indicators of the cytotoxic activity (TBK1, CX3CR1, IL-1β), FOXP3+ Tregs, and cancer progression biomarkers VEGF (vascular endothelial growth factor) and IGF-1 (insulin-like growth factor 1).

MATERIAL AND METHODS

Obtaining Platelet Rich Plasma (PRP), OncoTherad®, and Dosages

To obtain PRP, the peripheral blood of four human volunteers without use of drugs for 72 h, aged over 18 years and with no history of diseases that compromise the number of platelets in the basal blood, was used. Following the published protocol[32], blood was collected in 6 ml samples in EDTA K3 vacuum blood collection tubes (K50-1306M – KASVI, Olen). After blood collection, it was centrifuged (Routine 380R, Hettich Zentrifugen, Munich, Germany) at 100g (700 rpm) for 5 min (Supplemental Fig 1). The plasma fraction resulting from this centrifugation was transferred to a dry tube (15 ml volume) and a new centrifugation was performed at 401g (1400 rpm) for 17 min. At the end of this process, the supernatant with the platelet concentration (corresponding to 328,103 – 549,103 platelets/mm^3) was collected with a micropipette as PRP and transferred to a sterile tube. To prevent degradation of proteins in the sample, an aliquot of protease inhibitor cocktail at 1% (v/v) was added and the contents were stored in a freezer at -20°C until use. The peripheral blood and PRP were characterized[32] by counting white and red blood cells in hematological counter (ABX Micron ES 60, Horiba Medical, Montpellier, France). The intravesical injections of PRP applied to the animals were 0.1 ml. The project is associated with the protocol approved by the Ethics Committee for Research with Human Beings – UNICAMP (CAAE number: 51774515.0.0000.5404).

OncoTherad® (MRB-CFI-1) was synthesized and characterized[18,19], suspended in 0.9% saline solution, at a concentration of 20 mg/ml and the established dosage was therapeutic (20 mg/kg), which corresponds to intravesical applications of an average of 0.1 ml. For the association, OncoTherad® complex suspensions produced in saline solution were later diluted in PRP, in a 1:1 ratio, and the generated product was characterized by chemical-physical analyses.[18,19] Intravesical applications of 0.1 ml were then composed of 0.05 ml of OncoTherad® (20mg/ml) and 0.05 ml of PRP, resulting in a final concentration of 10 mg/ml and dosage of 10 mg/kg of OncoTherad® suspended in PRP. The chemical characterization data demonstrated an important interaction of the OncoTherad® compound with the PRP proteins (data not shown). Based on these results, we decided to reduce the concentration of OncoTherad® by half (10 mg/ml) to verify whether its association with PRP would be effective.

Experimental Groups: NMIBC Induction and Treatment

In the present study, thirty-five female C57BL/6J mice, aged 7 weeks, weighing on average 20 g, obtained at the Biotherism Center of the State University of Campinas (CEMIB/UNICAMP) were used. For NMIBC induction, 28 animals were anesthetized with 2% Xylazine Hydrochloride (5mg/kg i.m.; König, São Paulo, Brazil) and 10% Ketamine Hydrochloride (60mg/kg, i.m.; Fort Dodge, Iowa, USA), maintained in this state for 45 min to avoid spontaneous urination, and a dose of 50 mg/ml of N-ethyl-N-nitrosourea (ENU - N3385 ISOPAC®, Sigma, St. Louis, MO, USA) dissolved in 0.3 ml of sodium citrate (1M pH 6.0) every 15 days, totaling 3 doses.[36] The other 15 animals that did not receive ENU were considered as the Control Group. After CBNMI induction with ENU, the animals were divided into 5 groups (n=7 animals per group; Fig 1): (a) Control Group (**Control**): the animals were at rest, with *ad libitum* consumption of food and water; (b) ENU Group (**Cancer**): the animals were rested for one week and then euthanized; (c) ENU + PRP group (**PRP**): the animals received an intravesical dose of 0.1 ml of PRP (corresponding to 328 103 – 549 103 platelets/mm^3) for 6 consecutive weeks[32]; (d) ENU + MRB-CFI-1 group (**OncoTherad**): the animals received an intravesical dose of 20 mg/ml of the compound MRB-CFI-1 (OncoTherad®) suspended in 0.9% saline solution for 6 consecutive weeks; (e) Group ENU + MRB-CFI-1 + PRP (**OncoTherad+PRP**): the animals received an intravesical dose of 10 mg/mL of the compound MRB-CFI-1 (OncoTherad®) suspended in PRP (corresponding to 316 – 515 103 platelets/mm^3), in the ratio 1:1 (OncoTherad:PRP), for 6 consecutive weeks.

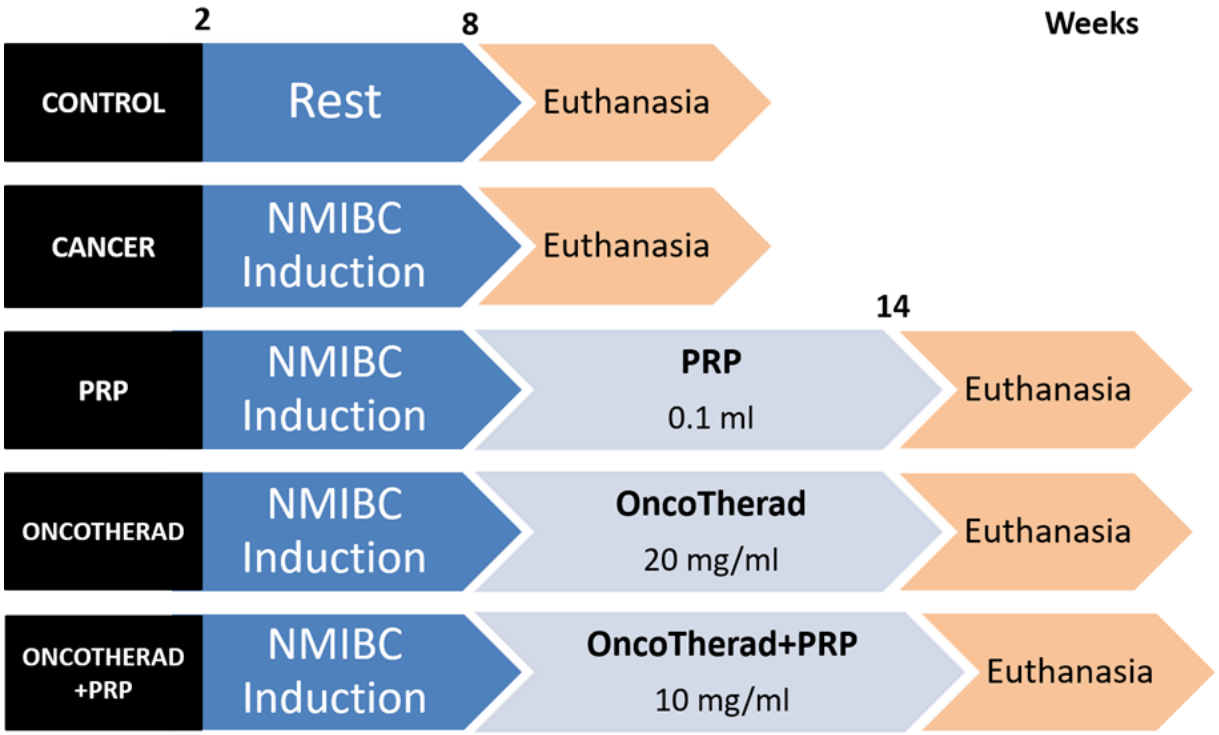

Figure 1. Experimental groups. The 2nd week corresponds to the beginning of the chemical induction of NMIBC (3 intravesical doses with N-ethyl-N-nitrosurea 250 mg/kg every 15 days); the 8th week corresponds to the euthanasia of the Control and Cancer groups and the beginning of treatments with OncoTherad, PRP, OncoTherad associated with PRP (10mg/ml) (1 intravesical dose/week for 6 consecutive weeks) and the 14th week corresponds to the euthanasia of the treated groups.

The intravesical doses in the different experimental groups were instilled via a 20-*gauge* flexible catheter (Abocath, São Paulo, Brazil) and correspond to a volume of 0.1 ml (Supplemental Fig 2). The animals were kept in an animal facility with adequate and individualized facilities in propylene boxes lined with shavings (5 animals/box), in an enriched environment (Supplemental Fig 3) and in sterile ventilated mini-isolators under controlled conditions of temperature (22 ± 2ºC) and luminosity (light cycle/ 12h dark, 200 lux). Animals in all groups received water and the same solid diet *ad libitum* (Nuvilab, Colombo, PR, Brazil). After the treatment periods, the animals were euthanized and the urinary bladders collected and submitted to histopathological and immunohistochemical analysis. The experimental protocol followed the ethical principles in animal research according to the National Research Council's Guide for the Care and Use of Laboratory Animals[37] and the project was approved by the Ethics Committee on Animal Use at UNICAMP – CEUA/UNICAMP (protocol number 4871-1/2018).

Weight and Consumption Analysis and Anatomopathological Evaluation

The body weight of all animals was evaluated at the beginning of the experiment, after the NMIBC induction, and at the end of the treatments. Body weight gain, as well as feed and water consumption were measured weekly throughout the experimental period and calculated per animal from the average of each group. Anatomopathological evaluation was performed and macroscopic alterations were quantified at the time of euthanasia of the animals.

Urinalysis

Mice urine was collected in 1.5 ml microtubes before euthanasia. Due to the very small urinary volume, the samples were collected in pool form for each experimental group. The urinary content was immediately used for reaction in Uri-Color Check ® urine reactive strips (WAMA Diagnóstica, São Carlos, SP, Brazil), processed according to the manufacturer's information and then read in specific URICLIN 101 urine preparation equipment (Laborclin, Pinhais, PR, Brazil). The parameters evaluated were: color, hemoglobin/red blood cells (mg/dl; cell/µl), pH, density, protein (mg/dl), ketone bodies (mg/dl), glucose (mg/dl), bilirubin (mg/dl). dl), urobilinogen (EU/dl; 1mg corresponds to approximately 1 Ehrlich Unit - EU), nitrite (mg/dl) and esterases/leukocytes (cel/µl). The detectable values in the Control group, in which the animals did not have cancer, were defined as a control parameter of normal values.

Samples processing and Histopathology

Urinary bladders from animals of the experimental groups were collected and fixed in Bouin for 12 h. After fixation, the tissues were washed in 70% ethanol, with subsequent dehydration in an increasing series of ethanol concentrations. Subsequently, the fragments were cleared with xylene for 2 h and embedded in plastic polymers (Paraplast Plus, ST. Louis, MO, USA). Then, the materials were sectioned using a Slee CUT5062 RM 2165 microtome (Slee Mainz, Mainz, Germany) with a thickness of 5 µm, stained with Hematoxylin-Eosin and photographed using a DM2500 photomicroscope (Leica, Munich, Germany). The diagnosis of urothelial lesions was classified according to the staging proposed by the consensus of the World Health Organization/International Society of Urological Pathology.[39]

The tumor progression inhibition index (TPI) obtained for each treatment was calculated through the percentage of animals in the group that did not present malignant lesions compared to the Cancer group without treatment.

Immunohistochemistry of Toll-Like receptor signaling pathway (TLR2, TLR4, MyD88, NF-kB, TRIF, TBK1, IRF-3, IFN-γ, IL-6, and IL-1β); immune biomarkers (CX3CR1 and FOXP3); and growth factors (VEGF and IGF-1) in NMIBC

Urinary bladder samples from animals of the experimental groups, the same used for histopathological analyses, were used for immunostaining. They were sectioned at 5 μm thickness using a Slee CUT5062 RM 2165 rotary microtome (Slee Mainz, Mainz, Germany) and collected on silanized slides. Antigenic retrieval was performed by incubating the sections in citrate buffer (pH 6.0) at 100°C in a microwave oven. Endogenous peroxidase was blocked using Peroxidase Blocker (EP12-20523) with subsequent incubation in 5% Goat Serum blocking solution (EP-12-20532) for 10 minutes at room temperature. Subsequently, the TLR2, MyD88, NF-κB, IL-6, TLR4, TRIF, IRF-3, IFN-γ, TBK1, CX3CR1, IL-1β, FOXP3, VEGF, and IGF-1 antigens were located using specific primary antibodies (Supplemental Table 1), diluted in Goat Serum (EP-12 -20532) 1% and stored overnight at 4°C. EasyLink One (Easy Path EP-12-20504) was used for antigen detection according to the manufacturer's instructions. After washing with TBS-T buffer, the sections were incubated with HRP-polymer (EP-12-20503) from the EasyLink One kit for 25 min and, subsequently revealed with diaminobenzidine (DAB), counterstained with Harris Hematoxylin and evaluated on the DM2500 photomicroscope (Leica, Munich, Germany).

To evaluate the intensity of antigen immunoreactions in the urothelial cells of the urinary bladder, five fields were selected with 400x magnification for each animal and each antibody. The immunostaining results were analyzed using the Image J software (https://imagej.nih.gov/ij/) in Macro Profile Analysis from the selection of the urothelium and quantification of positive urothelial cells (adapted from previous protocol).[32] Quantitative data were evaluated in two ways: Total Immunoreactivity and Immunoreactivity Intensity. Total immunoreactivity was obtained as the result of the percentage of urothelial cells negative for a given antibody subtracted from 100%, that is, the values represent the total number of urothelial cells in the field that showed immunoreaction for the evaluated antibody. The analysis of the

Immunoreactivity Intensity was performed from the categorization of the immunoreaction occurring in the urothelial cells by intensity criterion. The categories defined in the Image J software were: absent (Negative), weak (Low Positive), moderate (Positive) and strong (High Positive). The values obtained in the different intensity categories were represented in column graphs and are equivalent to the percentage of urothelial cells in the field that showed marking at each level (absent, weak, moderate or strong) for a given antibody.

Statistical Analyses

The parameters of weight and consumption of food and water were represented as mean ± standard deviation and evaluated using the Kruskal-Wallis non-parametric analysis of variance (ANOVA) complemented with the Student-Newman-Keuls test due to the lack of data normality (evaluated previously by the Shapiro-Wilk normality test). The analysis of weight gain over time was performed using the two-way ANOVA test, complemented by the Tukey test. Histopathological diagnoses and the index of inhibition of tumor progression were analyzed using the Chi Square Test (Z Proportion Test). For the immunohistochemical analyses, the total immunoreactivity average was calculated for each group and for each antibody and the data were submitted to the Kruskal-Wallis non-parametric analysis of variance followed by the Student-Newman-Keuls post hoc test. Immunoreactivities by category of staining intensity were represented in column graphs and data were evaluated using analysis of variance (ANOVA), complemented by Tukey's test for each level of immunoreaction (absent, weak, moderate or strong). The software used for analysis and graphing were GraphPad Prism, version 7.00 (GraphPad Software Inc., San Diego, California, USA) and BioEstat 5.0 (Sociedade Civil Mamirauá/CNPq, Belém, PA, Brazil). Statistical significance was 5% ($p<0.05$) for all applied tests.

RESULTS

Intravesical treatments with OncoTherad® and PRP recovered weight loss caused by NMIBC induction

The body weight of animals in all experimental groups was statistically equal ($p>0.05$) at the beginning of the experiment (Table 1). After chemical induction of NMIBC, all groups

that received the carcinogen had lower body weight ($p<0.05$) compared to the Control group (Table 1). The analysis of weight gain over time showed a significant difference ($p<0.01$) between the animals that were not submitted to the chemical induction of NMIBC compared to the animals induced from the 3rd week to the 8th week, that is, from the first induction dose with the carcinogen and this reduction in weight gain was maintained throughout the induction period (Fig 2). The final body weight of the animals did not differ between the groups ($p>0.05$), showing that the six weeks of treatment were enough to recover the weight in values similar to the healthy group. Furthermore, during the period from the 9th to the 14th week, there were no significant differences ($p>0.05$) in weight gain over time between the treated groups (Fig 2).

The Cancer group showed a higher feed intake ($p<0.05$) compared to all treated groups (PRP, OncoTherad, and OncoTherad+PRP) (Table 1). Animals treated with OncoTherad® alone had a higher water intake ($p<0.05$) than Control, PRP, and OncoTherad+PRP groups.

Table 1. Body weight (g), weight gain (g), and feed (g) and water (ml) consumption of different experimental groups.

Parameters	Experimental groups (n=7/group)				
	Control	**Cancer**	**PRP**	**OncoTherad**	**OncoTherad +PRP**
Initial Body weight (g)	20.73 ± 0.9 **a**	21.11 ± 1.2 **a**	20.19 ± 1.4 **a**	20.00 ± 1.4 **a**	20.39 ± 1.3 **a**
Body weight after NMIBC induction (g)	22.47 ± 0.8 **a**	21.39 ± 1.3 **b**	21.06 ± 1.3 **b**	20.60 ± 1.3 **b**	20.83 ± 1.2 **b**
Final body weight (g)	22.47 ± 0.8 **a**	21.39 ± 1.3 **a**	21.93 ± 2.6 **a**	21.67 ± 1.5 **a**	22.00 ± 1.4 **a**
Feed intake/week (g)	27.2 ± 0.9 **ab**	30.4 ± 0.9 **b**	25.9 ± 5.2 **a**	25.4 ± 8.2 **a**	26.6 ± 5.5 **a**
Water intake/week (ml)	32.8 ± 4.9 **a**	35.7 ± 5.7 **ab**	35.5 ± 5.9 **a**	37.2 ± 7.6 **b**	31.9 ± 4.7 **a**

Values expressed as mean ± standard deviation. Nonparametric Kruskal-Wallis Analysis of Variance, Student-Newman-Keuls Test. In the same line, values followed by different letters indicate statistically significant differences between groups ($p<0.05$).

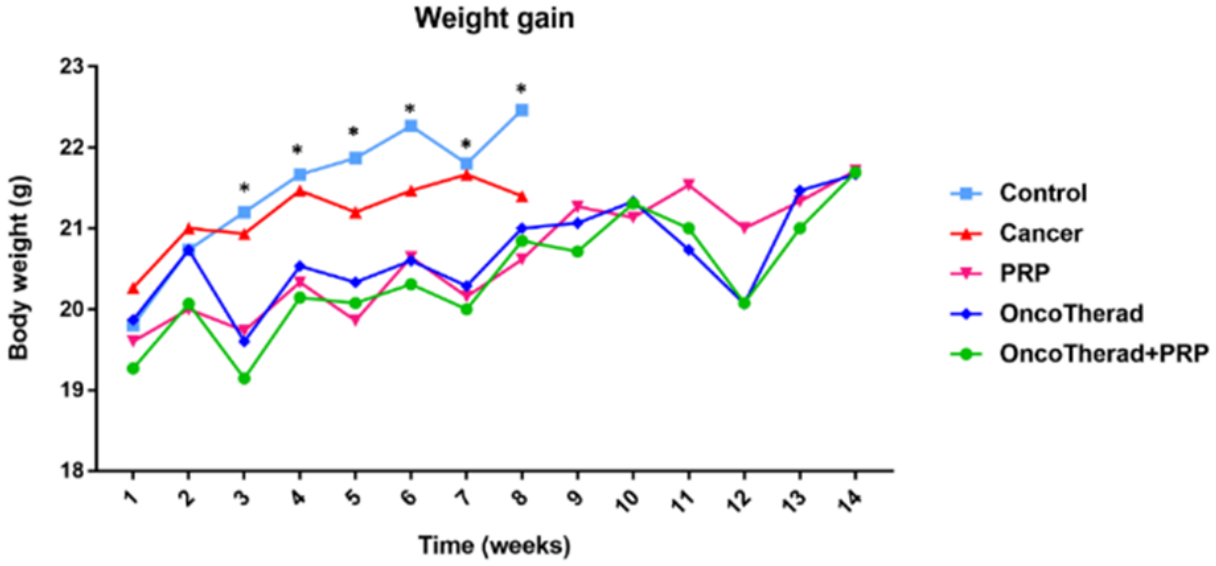

Figure 2. Analysis of body weight gain over the weeks of the experimental period. The experimental period comprises the 1st to the 14th week: the 2nd week corresponds to the beginning of the chemical induction of NMIBC (3 intravesical doses with N-ethyl-N-nitrosourea 250 mg/kg every 15 days); the 8th week corresponds to the euthanasia of the Control and Cancer groups and the beginning of treatments with OncoTherad®, PRP and OncoTherad® associated with PRP (1 intravesical dose/week for 6 consecutive weeks) and the 14th week corresponds to the euthanasia of the treated groups. * $p<0.01$ in the comparison between the Control group and the other groups that were induced to NMIBC. From the 9th to the 14th week there was no significant difference between the groups ($p>0.05$). Values expressed as mean per group. Two-way ANOVA. Tukey test.

Urinalysis indicated alterations in the NMIBC model

The biochemical elements analyzed from the animals' urine are shown in Table 2. The Control group, in which the animals did not have cancer and did not receive intravesical treatments, was considered as a parameter of normal values. The urine of healthy animals was yellowish, and the presence of blood was not detected. The absence of hematuria or color change in the urine of the animals with NMIBC that received or not treatments indicates that the bladder catheterization process did not cause mechanical injuries to the urinary tract. A slight acidification of the urine occurred in all groups with NMIBC with or without treatment compared to the Control (pH=7), more markedly in the PRP group. There were subtle changes

in urine density (specific gravity) in animals with NMIBC compared to the Control. The groups with the highest density values were those that received treatment with OncoTherad®, alone or associated with PRP.

Proteinuria values ranged from traces to 30 mg/dl in groups regardless of intravesical treatment. With treatment with OncoTherad® alone there was a higher protein concentration than when the nanodrug was associated with PRP or PRP alone. The presence of ketone bodies was verified as traces in the Cancer group at a concentration of 15 mg/ml. However, all animals received a solid diet and water *ad libitum* throughout the experimental period. Glucose and bilirubin in normal parameters are not found in the urine, and they were not detected in the urine of any experimental group. Urobilinogen was detected in a very variable way between the groups, with a value of 8 EU in the Control and presenting normal values (0.2 to 2 EU) in the PRP, OncoTherad, and OncoTherad+PRP groups. The presence of nitrite was verified in the Cancer, OncoTherad, and OncoTherad+PRP groups. However, nitrites are produced by bacteria that may have been contaminants in the collection process, leading to a false positive. Leukocytes were verified only in the urine of animals in the Cancer group.

Table 2. Analysis of biochemical parameters in the urine of animals from different experimental groups.

	Experimental Groups				
Parameters	**Control**	**Cancer**	**PRP**	**OncoTherad**	**OncoTherad+PRP**
Color	yellow	yellow	yellow	yellow	yellow
Blood	negative	negative	negative	negative	negative
pH	7.0	6.0	5.0	6.0	6.0
Specific gravity	1.015	1.025	1.025	≥ 1.030	≥ 1.030
Protein	trace	30 mg/dl	trace	30 mg/dl	trace
Ketone bodies	negative	trace	negative	negative	negative
Glucose	negative	negative	negative	negative	negative
Bilirubin	negative	negative	negative	negative	negative
Urobilinogen	≥ 8.0 EU/dl	≥ 8.0 EU/dl	≥ 0.2 EU/dl	1.0 EU/dl	≥ 0.2 EU/dl
Nitrite	absent	present	absent	present	present
Leukocytes	absent	trace	absent	absent	absent

The values correspond to the parameters detected in the pool urine of each experimental group. Parameters: color; blood (hemoglobin mg/dl, red blood cells; cel/µl); pH; density; protein (mg/dl); ketone bodies (mg/dl); glucose (mg/dl); bilirubin (mg/dl); urobilinogen (EU/dl, 1mg corresponds to approximately 1 Ehrlich Unit - EU); nitrite (mg/dl) and esterases/leukocytes (cel/µl). The detectable values in the Healthy group, in which the animals did not have cancer and did not receive intravesical treatments, was defined as a control parameter for normal values.

OncoTherad® alone or associated with PRP changed the macroscopic appearance of the urinary bladders of NMIBC-induced animals

At the time of euthanasia, a macroscopic description of the urinary tract organs was performed (Table 3, Supplemental Fig 4). The animals in the Control group did not show any apparent structural alteration in the kidneys, ureters or urinary bladders, which exhibited a thin wall with a semi-translucent appearance and normal vascularization (Table 3, Fig 3A). On the

other hand, the urinary tract of animals in the Cancer group showed several macroscopic alterations such as cystic renal lesions, dilation of both ureters - bilateral hydroureter - and thickening of the urinary bladder wall with increased vascularity (Table 3, Fig 3B).

In the PRP group, some animals had discrete hydroureter and urinary bladders with regions or points of thickening (Table 3, Fig 3C), although normal ureters and bladders without apparent macroscopic lesions were also identified. Structural features of the urinary tract in the OncoTherad group included kidneys without apparent lesions in most of the animals, discret hydroureters and normal ureters. Some urinary bladders of the animals in the OncoTherad group showed slightly increased vascularization and thickening points (Fig 3D), as well as other bladders exhibited similar aspects to the control group, with no apparent lesions or thickening (Fig 3E). In the OncoTherad group associated with PRP, the kidneys did not show apparent macroscopic changes in most animals and discrete unilateral or bilateral hydrouretes were present, as well as normal ureters (Table 3). The wall of the urinary bladders of some animals in this group was vascularized and slightly thickened or with points of thickening (Fig 3F). In the other animals, bladders without thickening or lesions were identified.

Table 3. Anatomopathological evaluation of the urinary system of the animals.

	Experimental groups (n=7 animals/group)				
Macroscopic parameters	**Control**	**Cancer**	**PRP**	**OncoTherad**	**OncoTherad +PRP**
Urinary bladder thickening					
Absent	7/7	0	1/7	4/7	2/7
Slight	0	4/7	2/7	3/7	5/7
Intense	0	3/7	4/7	0	0
Macroscopic lesion					
Abent	7/7	5/7	2/7	6/7	6/7
Present	0	2/7	5/7	1/7	1/7
Vascularization					
Normal	6/7	2/7	6/7	4/7	1/7
Slightly increased	1/7	1/7	0	3/7	5/7
Accentuated	0	4/7	1/7	0	1/7
Ureters					
Normal	4/7	0	1/7	1/7	2/7
Unilateral hydroureter	1/7	0	5/7	5/7	2/7
Bilateral hydroureter	2/7	7/7	1/7	1/7	3/7
Kidneys					
No lesions	7/7	6/7	5/7	6/7	6/7
Some apparent alteration	0	1/7	2/7	1/7	1/7

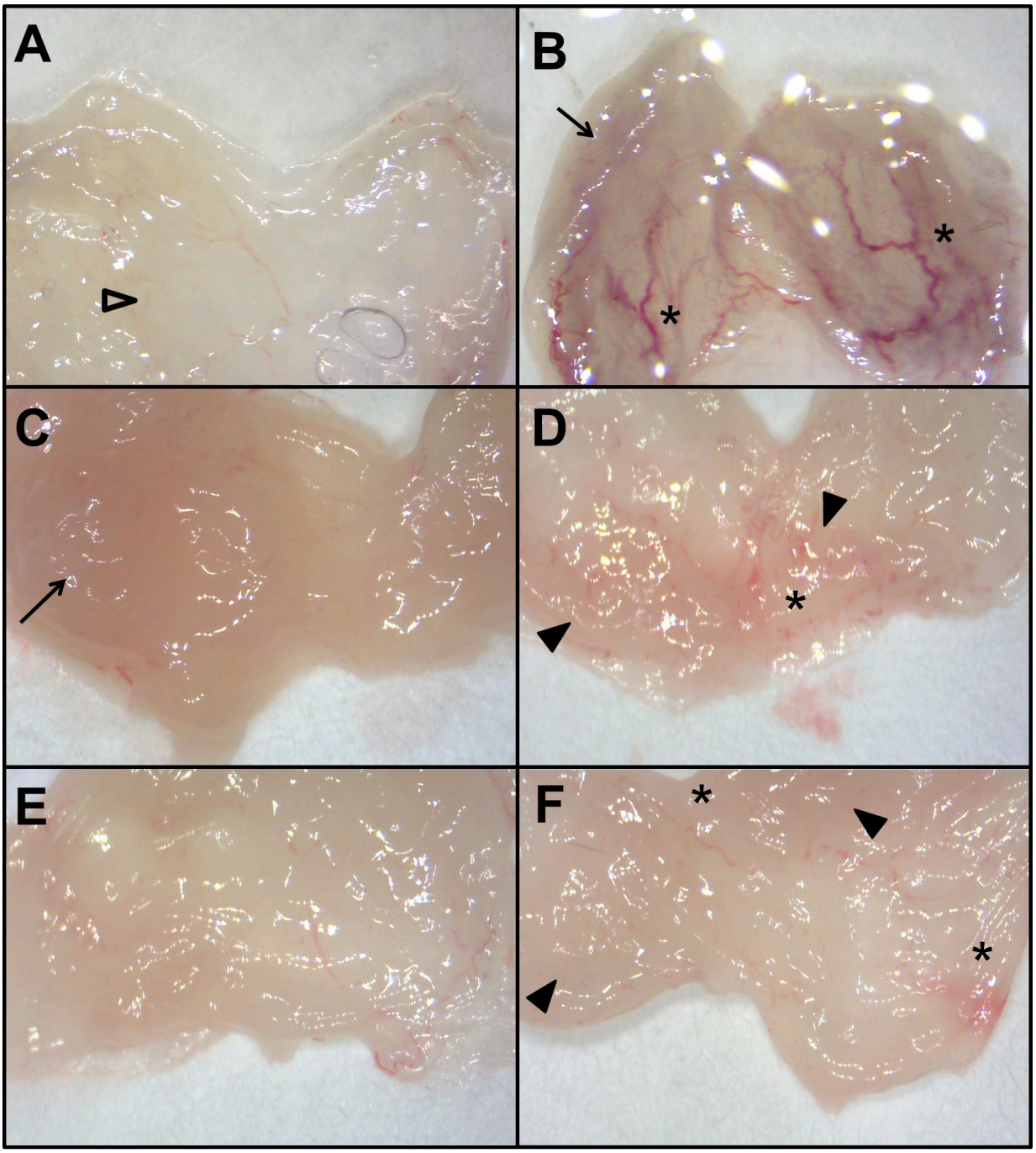

Figure 3. Photographs of the urinary bladders of the different experimental groups: Control (A); Cancer (B); PRP (C); Oncotherad (D, E) and OncoTherad+PRP (F). (A) Healthy bladder showing thin wall and semi-translucent appearance as well as normal vascularity. (B) Highly vascularized bladder (*) with a thickened wall (arrow). (C) Bladder with regions of thickening (arrow). (D) Bladder slightly vascularized (*) and with thickening points (arrowhead). (E) Normal bladder. (F) Bladder slightly vascularized (*) and with a slightly thickened wall (arrowhead). The bladers were sectioned longitudinally and the photographs show the inner surface of the urinary bladder wall (frontal plane). Photographs taken with a stereomicroscope. 3.5x magnification.

Immunotherapy with OncoTherad® associated or not with PRP inhibited tumor progression in NMIBC model

The urinary tract of the Control group did not show histopathological alterations (Fig 4A, Table 4). Healthy urothelium was composed of 2 to 3 layers, with a basal cell layer, an intermediate cell layer, and a superficial or apical layer of umbrella cells facing the lumen of the organ (Fig 4A). The basal cells were supported on a basal membrane and below this there is the lamina propria or mucosa, which is made up of dense to loose connective tissue and, more internally, the muscular layer was found. In contrast, the urinary tract in the Cancer group showed neoplastic lesions classified as carcinoma *in situ* (pTis) in all animals (Table 4). The pTis carcinoma (Fig 4B) was characterized by disorderly cell proliferation in a flat urothelium and the presence of marked cell atypia found from the base to the apex of the urothelium, such as enlarged nuclei, reduced cytoplasm and multiple, prominent nucleoli.

The neoplastic lesions found in the PRP Group were papillary urothelial carcinoma (pTa) and carcinoma *in situ* (pTis) (Table 4). pTa carcinoma was characterized by papillary or non-papillary, exophytic or endophytic lesions consisting of urothelial cells with disorderly arrangement and loss of polarity, hyperchromatic, pleomorphic nuclei and prominent nucleoli (Fig 4C). The other animals had low-grade intraurothelial neoplasia, characterized by the presence of few atypia such as large nuclei, but without loss of polarity. Thus, treatment with PRP alone promoted 28.57% inhibition of tumor progression (Table 4).

In the OncoTherad group, there were no malignant lesions in most animals such as flat hyperplasia (Fig 4D) and normal urothelium (Fig 4E), indicating that the nanodrug inhibited tumor progression in 85.71% of the animals (Table 4). Flat hyperplasia was characterized by urothelial thickening and absence of cytological atypia (Fig 4D). Most animals in the OncoTherad+PRP group did not exhibit malignant lesions such as flat hyperplasia and low-grade intraurothelial neoplasia (Fig 4F), indicating that the associated treatment promoted 71.42% inhibition of tumor progression (Table 4).

Table 4. Histopathological changes in the urinary bladder of mice from different experimental groups and Tumor Progression Inhibition Rate (%) obtained after treatments.

	Experimental groups (n=7/group)				
Histopathology	**Control**	**Cancer**	**PRP**	**OncoTherad**	**OncoTherad+PRP**
Normal	7 (100%) *	-	-	2 (28.57%) *	-
Flat Hyperplasia	-	-	-	3 (42.85%) *	3 (42.85%) *
Low-grade Intraurothelial Neoplasia	-	-	2 (28.57%) #	1 (14.28%) *	2 (28.57%) *
Carcinoma in situ (pTis)	-	7 (100%)	1 (14.28%)	-	1 (14.28%)
Papillary Urothelial Carcinoma (pTa)	-	-	4 (57.14%)	1 (14.28%)	1 (14.28%)
Tumor Progression inhibition (TPI)	-	0% **a**	28.57% **ac**	85.71% **b**	71.42% **bc**

* Statistical significance compared to the Cancer Group ($p < 0.05$). # Statistical significance in relation to the OncoTherad group ($p < 0.05$). Tumor Progression Inhibition: Percentage of animals that did not have malignant lesions compared to the Cancer group. In the same line, values followed by different letters indicate a significant difference between groups ($p < 0.05$). Chi square Test (Proportion Z Test). Benign lesions: Flat hyperplasia. Premalignant Lesions: Low-Grade Intraurothelial Neoplasia. Malignant lesions: pTis e pTa.

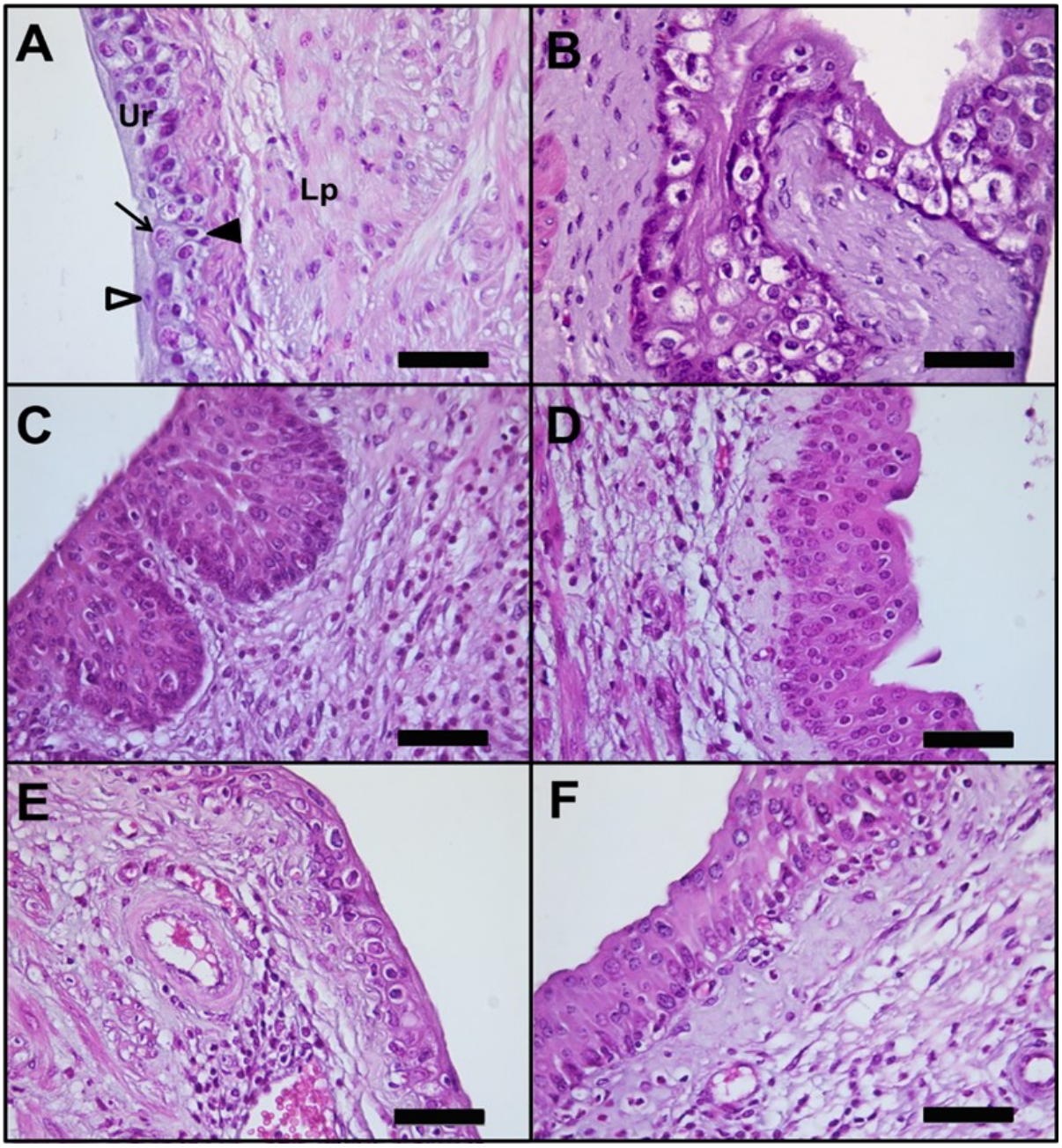

Figure 4. Photomicrographs of urinary bladders from different experimental groups: Control (A); Cancer (B); PRP (C); Oncotherad (D, E) and OncoTherad+PRP (F). (A) Healthy urothelium (Ur) composed of 2 to 3 layers: basal cells (closed arrowhead), intermediate cells (arrow) and a superficial or apical layer composed of umbrella cells (open arrowhead); and the lamina propria (Lp) consisting of connective tissue. (B) Carcinoma pTis (circle), characterized by disordered proliferation of the urothelium and marked cellular atypia: enlarged nuclei with reduced cytoplasm and prominent nucleoli. (C) pTa carcinoma, characterized by endophytic or exophytic papillary lesions consisting of urothelial cells with disorderly arrangement and loss of polarity. (D) Flat hyperplasia, urothelium thickening without atypia. (E) Normal urothelium. (F) Low-grade intraurothelial neoplasia, presence of few atypia without loss of polarity. Hematoxylin-Eosin. Bars = 50 µm.

PRP modulated OncoTherad® effects on TLR signaling by enhancing stimulation of canonical and non-canonical pathways through TLR4

The total cytoplasmic immunoreactivity for the TLR2, MyD88, NF-κB, IL-6, TLR4, TRIF, IRF-3 and IFN-γ antigens in the urothelium of the urinary bladders are presented in Table 5 and the different intensities of the immunoreaction for these antigens in Fig 5. The immunolocalization of the antigens in histological sections of the urinary bladders is shown in Figs 6 and 7.

The total TLR2 immunoreactivity did not show significant differences ($p>0.05$) among the experimental groups (Table 5), however in the analysis of the intensity of the immunoreactivity it was possible to find significant differences in the intensity of the immunoreactivity for TLR2. In the Cancer and PRP groups, the intensity was weaker ($p<0.05$) than in healthy animals (Fig 5A). On the other hand, the groups treated with OncoTherad® alone or associated with PRP showed a pattern of labeling intensity similar ($p>0.05$) to the Control (Fig 5A). For the TLR2 immunoreaction, regardless of the group, it was possible to observe that animals with neoplastic lesions such as pTis (Fig 6B) showed weaker immunoreaction than premalignant lesions such as low-grade intraurothelial neoplasia (Fig 6C and E) and these, in turn, less intense than benign lesions such as hyperplasia (Fig 6D).

The total percentage of MyD88-positive urothelial cells was higher ($p<0.05$) in the PRP group compared to the Control, Cancer, and OncoTherad+PRP groups; but when compared to the OncoTherad group, there was no significant difference ($p>0.05$) in the total immunoreactivity (Table 5). In the analysis of immunoreactivity intensity, the groups that received the isolated treatments with OncoTherad® or PRP presented greater intensity ($p<0.05$) of the immunoreaction for MyD88 compared to the combined treatment (Fig 5B). There was heterogeneous expression between animals with different histopathological diagnoses, however, it was possible to observe that the same type of lesion in animals from different groups exhibited different intensities of immunoreactivity, such as a stronger staining in low-grade intraurothelial neoplasia of the PRP group (Fig 6H) than that found in OncoTherad+PRP (Figure 6J) and, likewise, hyperplasia in the OncoTherad group (Fig 6I) compared to that occurring in the associated group.

The total immunoreactivity for NF-kB was higher ($p<0.05$) in all groups that received treatments with Oncotherad® and PRP, alone or together, compared to animals with NMIBC without treatment (Table 5). Furthermore, the OncoTherad and OncoTherad+PRP groups also

had a higher percentage ($p<0.05$) of NF-kB positive urothelial cells compared to the Control group (Table 5). From the immunoreaction intensity variation data, it was possible to verify that treatment with OncoTherad® alone or associated with PRP promoted an increase ($p<0.05$) in the intensity of NF-kB expression when compared to the Control, Cancer, and PRP (Fig 5C). In the same group, there was heterogeneous expression intensity among animals with different histopathological diagnoses. The animals with benign lesions such as hyperplasia in the OncoTherad group (Fig 6N) showed a stronger immunoreaction than premalignant lesions such as low-grade intraurothelial neoplasia in the PRP (Fig 6M) and OncoTherad+PRP groups (Fig 6O), which also showed stronger immunoreaction compared with malignant lesions as in pTis carcinoma (Fig 6L).

The total percentage of IL-6 positive urothelial cells was similar ($p>0.05$) among all experimental groups (Table 5), however in the analysis of immunoreactivity intensity the Cancer and PRP groups, which did not differ ($p>0$ .05) to each other, exhibited weaker staining ($p<0.05$) compared to the Control (Fig 5D). On the other hand, the OncoTherad and OncoTherad+PRP groups did not differ ($p>0.05$) from the healthy animals and showed a stronger immunoreaction ($p<0.05$) than the Cancer and PRP groups (Fig 6D). IL-6 appeared as a weaker expression in neoplastic lesions such as pTis (Fig 6Q) than benign lesions such as hyperplasia (Fig 6S). However, the same type of lesion in animals from different groups exhibited different intensities of immunoreactivity as a stronger staining in the low-grade intraurothelial neoplasia of the OncoTherad+PRP group (Figure 6T) than that found in the group that received PRP alone (Fig 6R).

The total immunoreactivity for TLR4 was higher ($p<0.05$) in the OncoTherad+PRP group compared to the Cancer group and the isolated treatments and did not differ ($p>0.05$) from the Control group (Table 5). In addition, the PRP group also showed a lower ($p<0.05$) percentage of positive urothelial cells compared to that found in healthy animals, but did not show a significant difference ($p>0.05$) compared to the Cancer group (Table 5). By analysis of intensity of immunoreactivity, animals with induced NMIBC exhibited weaker intensity ($p<0.05$) of staining for TLR4 compared to the Control group (Fig 5E). As with total immunoreactivity, the OncoTherad+PRP group showed a stronger immunoreaction intensity ($p<0.05$) in comparison with the Cancer and the groups that received isolated treatments (Figure 5E). In the PRP group, the marking intensity for TLR4 was similar ($p>0.05$) to Cancer and weaker ($p<0.05$) than in the Control while OncoTherad promoted a stronger expression ($p<0.05$) of TLR4 compared to the Cancer group (Fig 5E). It was possible to observe a variation in

the intensity of expression according to the histopathological diagnoses, since neoplastic lesions such as pTis (Fig 7B) or pTa (Fig 7C) showed weaker immunoreaction than non-malignant lesions such as hyperplasia (Fig 7D) and low-grade intraurothelial neoplasia (Fig 7E).

Total TRIF immunoreactivity showed no significant differences ($p>0.05$) between experimental groups (Table 5). Although the OncoTherad group exhibited a higher absolute percentage of TRIF-positive urothelial cells with moderate intensity immunoreaction compared to the other groups (Fig 5F), these differences were not statistically significant ($p>0.05$). In the visual analysis of the histological sections after immunoreaction for TRIF, it was possible to observe, regardless of the group, that animals with neoplastic lesions such as pTis (Fig 7G) or pTa (Fig 7H) showed weaker immunoreaction than non-malignant lesions such as hyperplasia (Fig 7I) and low-grade intraurothelial neoplasia (Fig 7J).

For IRF-3, total immunoreactivity was higher ($p<0.05$) in the OncoTherad+PRP group compared to the group treated with PRP alone (Table 5). In addition, the PRP group also showed a lower ($p<0.05$) percentage of positive urothelial cells compared to the Control group, but did not show a significant difference ($p>0.05$) compared to Cancer (Table 5). In the analysis of the intensity, the animals with induced NMIBC exhibited weaker intensity ($p<0.05$) of the immunoreaction compared to the Control group (Fig 5G). However, all groups that received treatments with OncoTherad and PRP, alone or in combination, showed a different pattern ($p<0.05$) of marking intensity compared to both the Control and Cancer groups, showing higher levels of weakly labeled and moderately labeled minors (Fig 5G). Comparing the treatments, although the OcoTherad group and the PRP group did not differ ($p>0.05$) in the intensity of the immunoreaction for IRF-3, the associated treatment promoted a stronger labeling ($p<0.05$) compared to PRP treatment alone (Fig 5G). It was possible to observe a variation in the intensity of IRF-3 expression in animals induced to NMIBC with or without treatment and in healthy animals, which showed more intense staining mainly in the apical region of the urothelium in the umbrella cells (Fig 7K).

OncoTherad® immunotherapy alone or combined with PRP showed the highest percentages of positive cells for IFN-γ ($p<0.05$) in comparison with the Cancer group (Table 5), showing strong immunoreaction in the urothelium (Fig 7). In contrast, the Cancer group showed the lowest IFN-γ total immunoreactivity ($p<0.05$) and weak immunoreaction. In the same way, the analysis of immunoreactivity intensity (Fig 5H) showed that IFN-γ staining in the Cancer Group was weaker ($p<0.05$) compared with the groups that received treatments with OncoTherad alone or associated with PRP. Neoplastic lesions such as pTa (Figure 7R) showed

a weaker IFN-γ immunoreaction than non-malignant lesions such as hyperplasia (Figure 7S) and low-grade intraurothelial neoplasia (Figure 7T).

Table 5. Total immunoreactivity (%) for each antigen in the different experimental groups.

	Experimental Groups				
Antigens	**Control**	**Cancer**	**PRP**	**OncoTherad**	**OncoTherad+PRP**
TLR2	88.38 **a**	81.17 **a**	74.94 **a**	89.38 **a**	91.18 **a**
MyD88	91.22 **a**	87.13 **a**	96.40 **b**	93.96 **ab**	88.55 **a**
NF-kB	88.54 **ac**	90.31 **c**	95.11 **ab**	96.97 **b**	97.03 **b**
IL-6	96.28 **a**	92.83 **a**	88.97 **a**	96.49 **a**	94.00 **a**
TLR4	90.94 **ac**	85.35 **ab**	72.91 **b**	84.89 **ab**	96.42 **c**
TRIF	85.85 **a**	87.95 **a**	81.89 **a**	90.58 **a**	90.50 **a**
IRF-3	92.97 **a**	86.12 **ab**	77.18 **b**	84.79 **ab**	92.13 **a**
IFN-γ	85.61 **a**	68.78 **b**	86.03 **a**	91.31 **a**	90.09 **a**

Values are equivalent to the mean percentage of urothelial cells positive for the antigens per group (n=5 sections/animal/group). Kruskal-Wallis ANOVA, Student-Newman-Keuls Test. Along the same lines, values followed by different letters indicate a significant difference between groups ($p<0.05$).

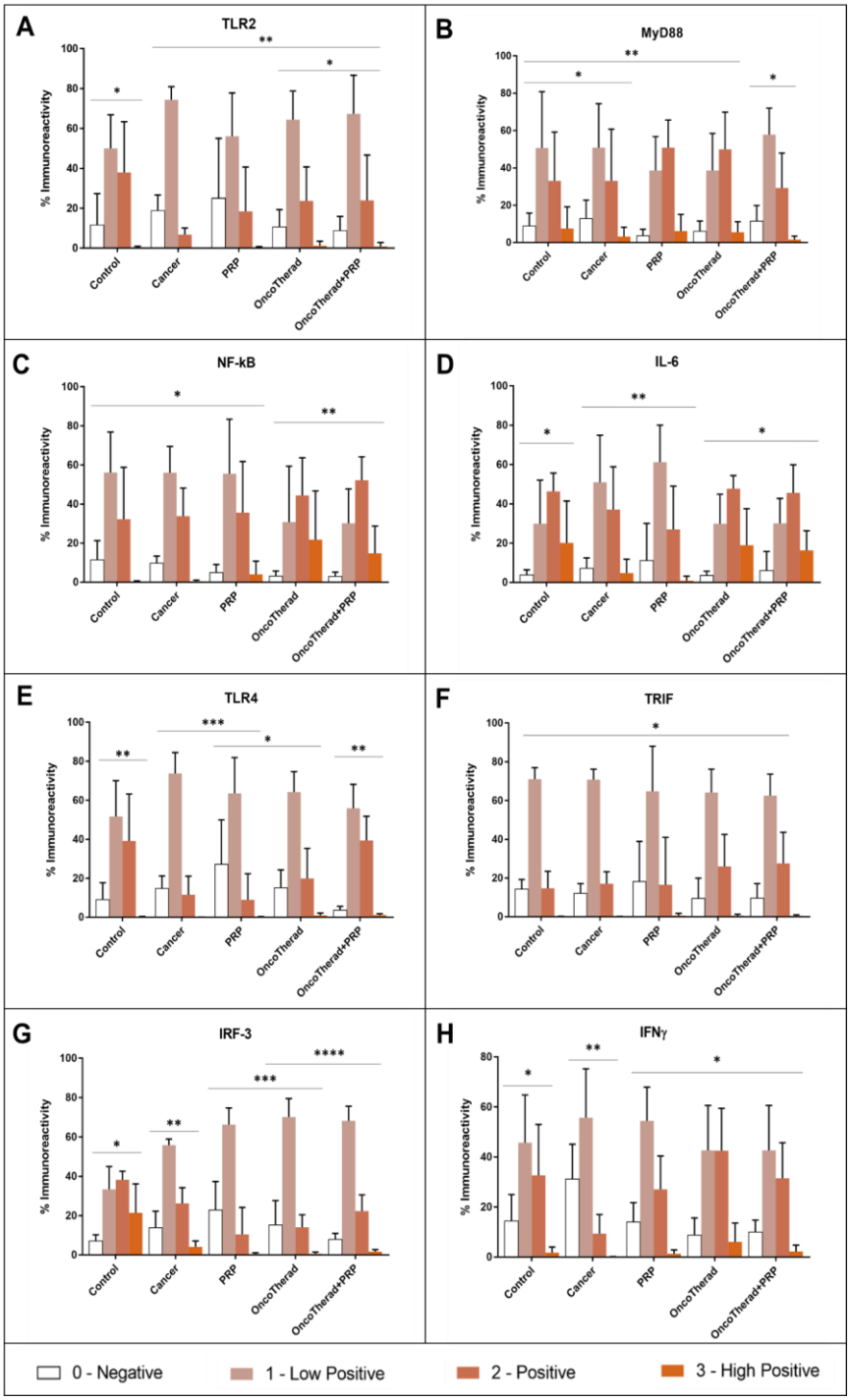

Figure 5. Immunoreactivities (%) in different intensity categories for antigens: TLR2 (A), MyD88 (B), NF-kB (C), IL-6 (D), TLR4 (E), TRIF (F), IRF-3 (G) and IFN-γ (H). */**/***/****Different symbols indicate a significant difference ($p<0.05$) between groups, when statistically differ in any category of immunoreactivity. ANOVA, Tukey test (n = 5 sections/animal/group). Immunoreactivity was classified into four categories: Negative (0): absence of labeling; Low Positive (1): weak immunoreaction; Positive (2): moderate immunoreaction and High Positive (3) strong immunoreaction.

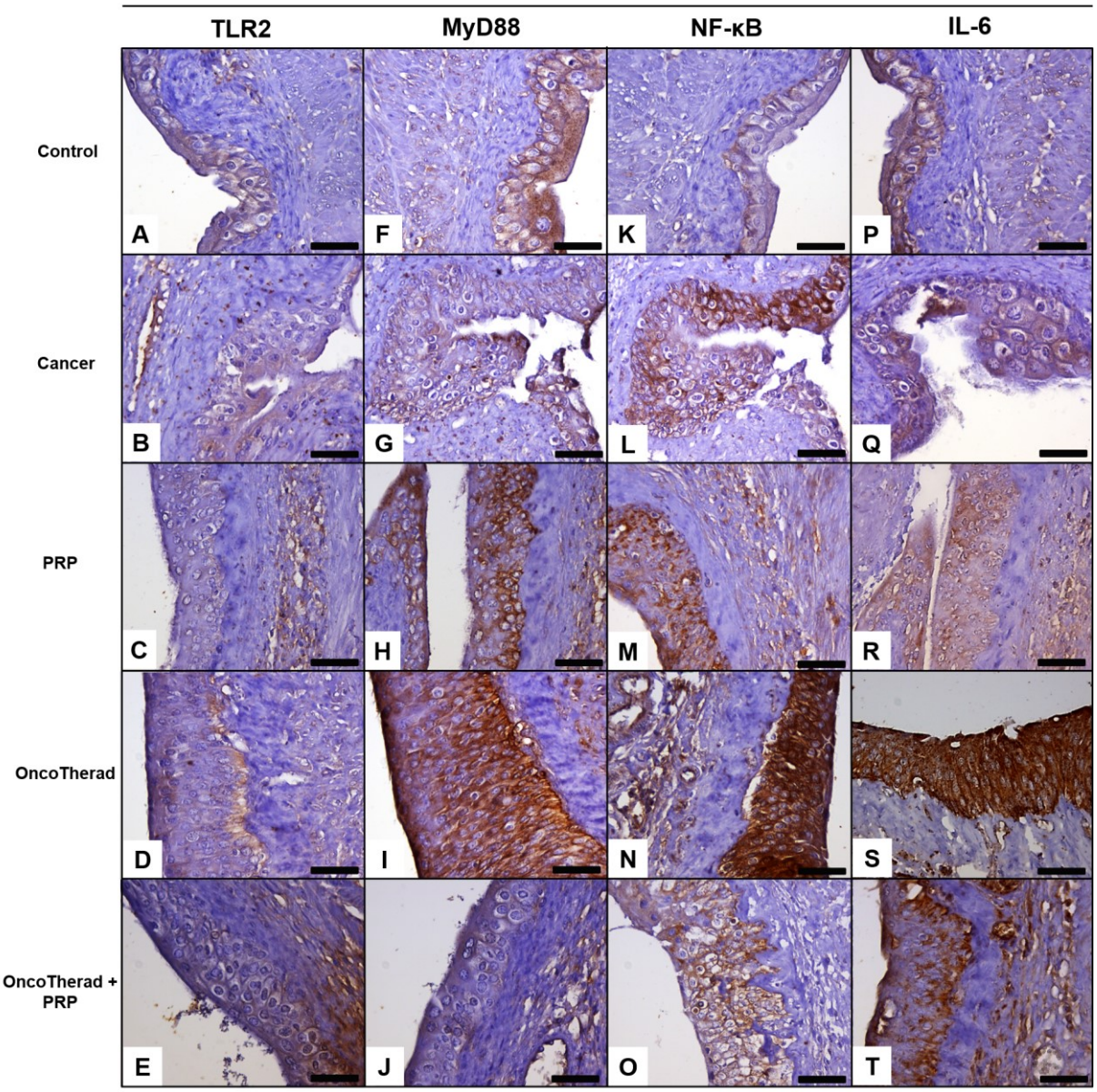

Figure 6. Immunolocalization of TLR-2 (A-E), MyD88 (F-J), NF-κB (K-O) and IL-6 (P-T) antigens in the urinary bladders of different experimental groups. Control (healthy urothelium: A,F,K,P); Cancer (urothelial carcinoma in situ or pTis: B,G,L,Q); PRP (Low Grade Intraurothelial Neoplasia: C,H,M,R); Oncotherad (Flat Hyperplasia: D,I,N,S) and OncoTherad+PRP (Low Grade Intraurothelial Neoplasia: E,J,O,T). Bars = 50 μm.

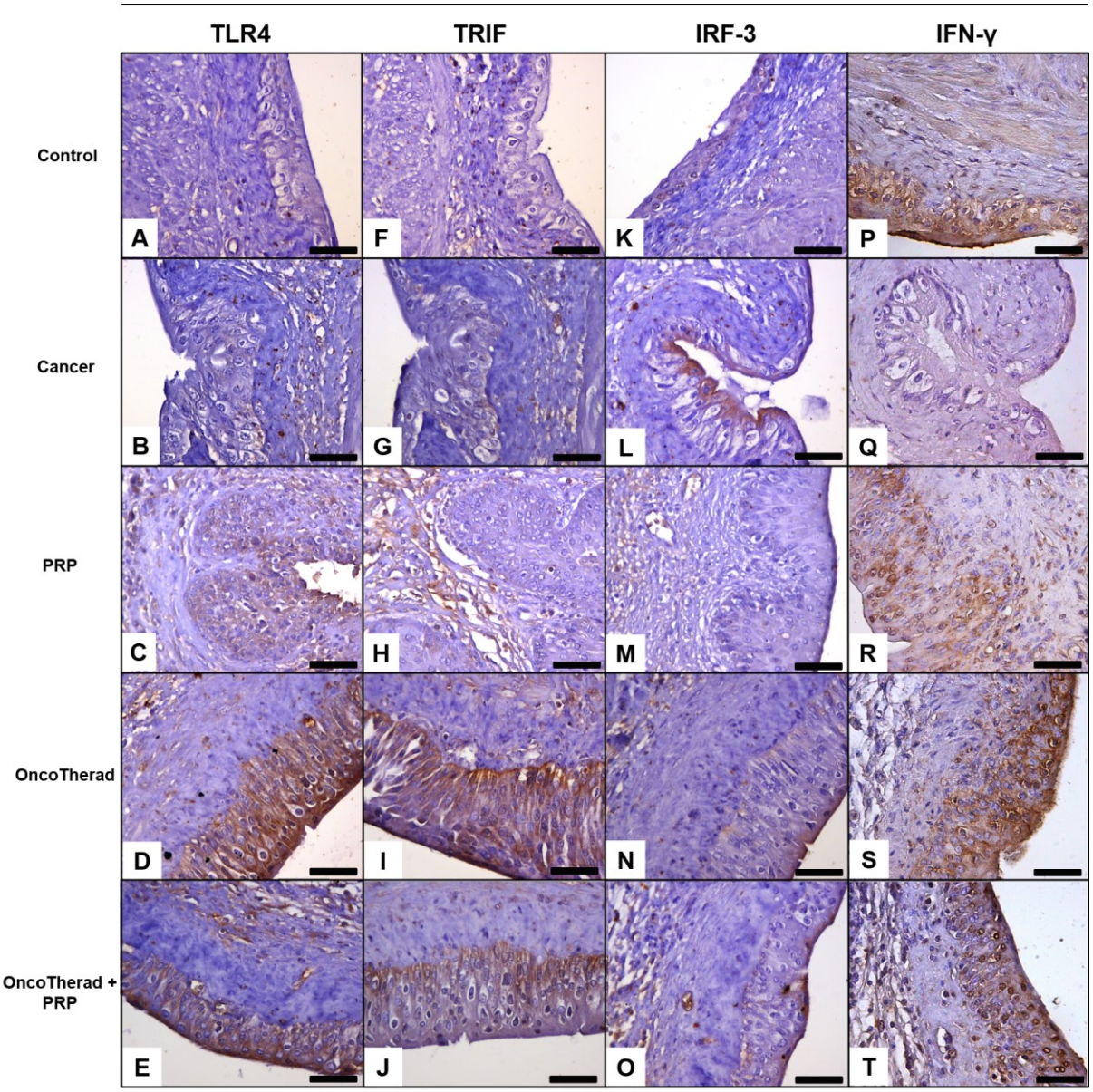

Figure 7. Immunolocalization of TLR-4 (A-E), TRIF (F-J), IRF-3 (K-O), IFN-γ (P-T) antigens in the urinary bladders of different experimental groups. Control (healthy urothelium: A,F,K,P); Cancer (urothelial carcinoma in situ or pTis: B,G,L,Q); PRP (non-invasive urothelial carcinoma pTa: C,H,M,R); Oncotherad (Flat Hyperplasia: D,I,N,S) and OncoTherad+PRP (Low Grade Intraurothelial Neoplasia: E,J,O,T). Bars = 50 µm.

OncoTherad® plus PRP modulated the NMIBC microenvironment to a cytotoxic profile involving CD8+ T-cell activation and Tregs reduction

TBK1 immunoreactivity and the immunoreaction intensity were increased ($p<0.01$) by OncoTherad and OncoTherad+PRP (Table 6, Figs 8 and 9). There was an increase ($p<0.01$) in the number of CX3CR1+ cells and the immunostaining intensity after OncoTherad® treatment (Table 6, Figs 8 and 9). Both total immunoreactivity and IL-1β intensity decreased ($p<0.01$) in the Cancer group. However, the OncoTherad+PRP group showed a higher ($p<0.01$) percentage of IL-1β positive cells and a stronger immunoreaction compared to the Cancer (Table 6, Figs 8 and 9). OncoTherad® and OncoTherad plus PRP decreased ($p<0.01$) the percentage of FOXP3+ cells and reduced the reaction intensity compared to the Cancer and PRP groups (Table 6, Figs 8 and 9).

Table 6. Total immunoreactivity (%) for each antigen in the different experimental groups.

	Experimental Groups				
Antigens	**Control**	**Cancer**	**PRP**	**OncoTherad**	**OncoTherad+PRP**
TBK1	69.72 **ac**	58.32 **ab**	52.97 **b**	79.76 **c**	70.63 **ac**
IL-1β	69.75 **a**	54.26 **b**	64.45 **ab**	62.44 **ab**	69.57 **a**
CX3CR1	86.06 **a**	87.09 **a**	94.57 **bc**	95.58 **b**	90.29 **ac**
FOXP3	74.37 **a**	93.41 **b**	90.55 **b**	78.08 **a**	75.58 **a**

Values are equivalent to the mean percentage of urothelial cells positive for the antigens per group (n=5 sections/animal/group). Kruskal-Wallis ANOVA, Student-Newman-Keuls Test. Along the same lines, values followed by different letters indicate a significant difference between groups ($p<0.05$).

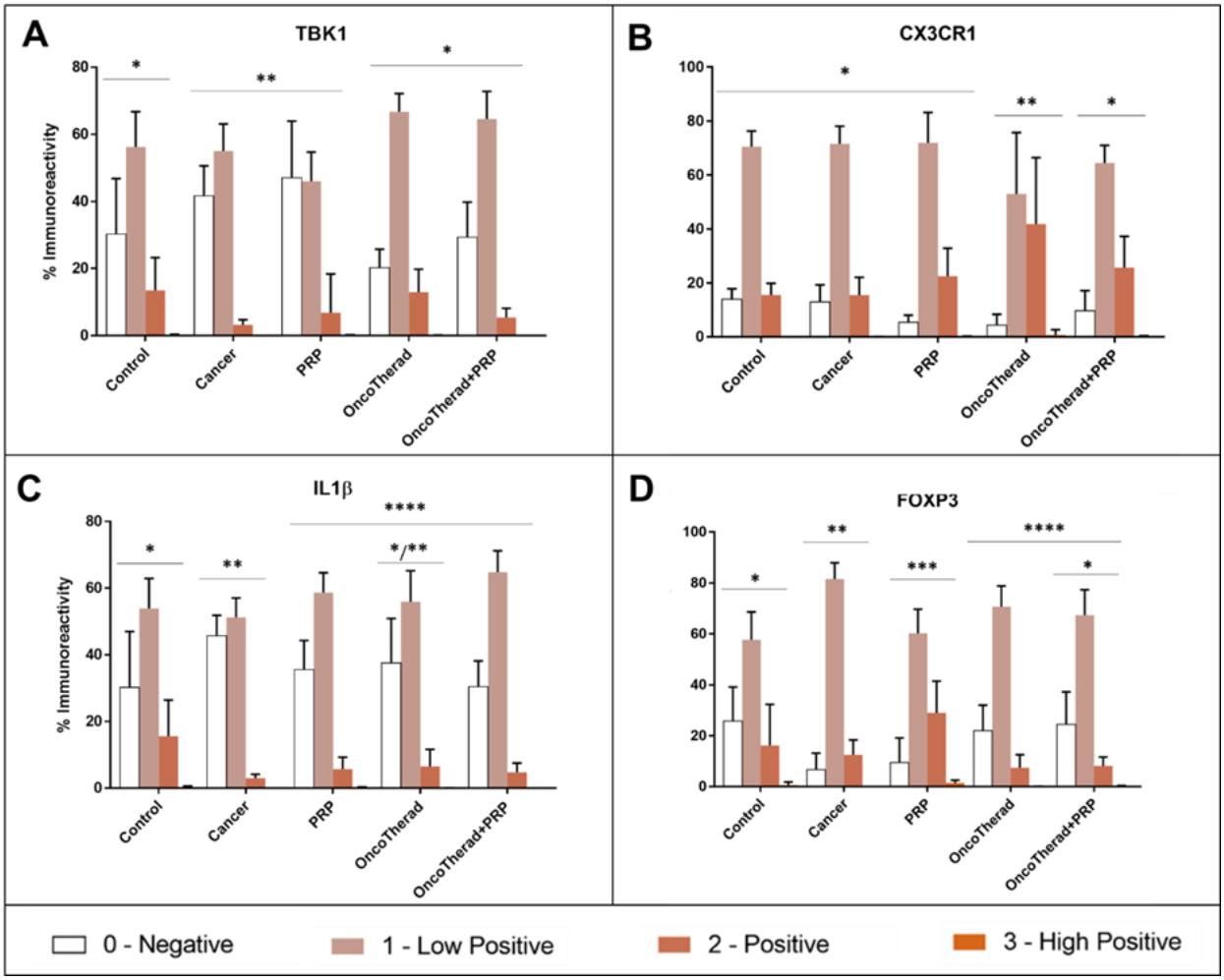

Figure 8. Immunoreactivities (%) in different intensity categories for antigens: TBK1 (A), CX3CR1 (B), IL-1β (C) and FOXP3 (D). */**/***/****Different symbols indicate a significant difference ($p<0.05$) between groups, when statistically differ in any category of immunoreactivity. ANOVA, Tukey test (n = 5 sections/animal/group). Immunoreactivity was classified into four categories: Negative (0): absence of labeling; Low Positive (1): weak immunoreaction; Positive (2): moderate immunoreaction and High Positive (3) strong immunoreaction.

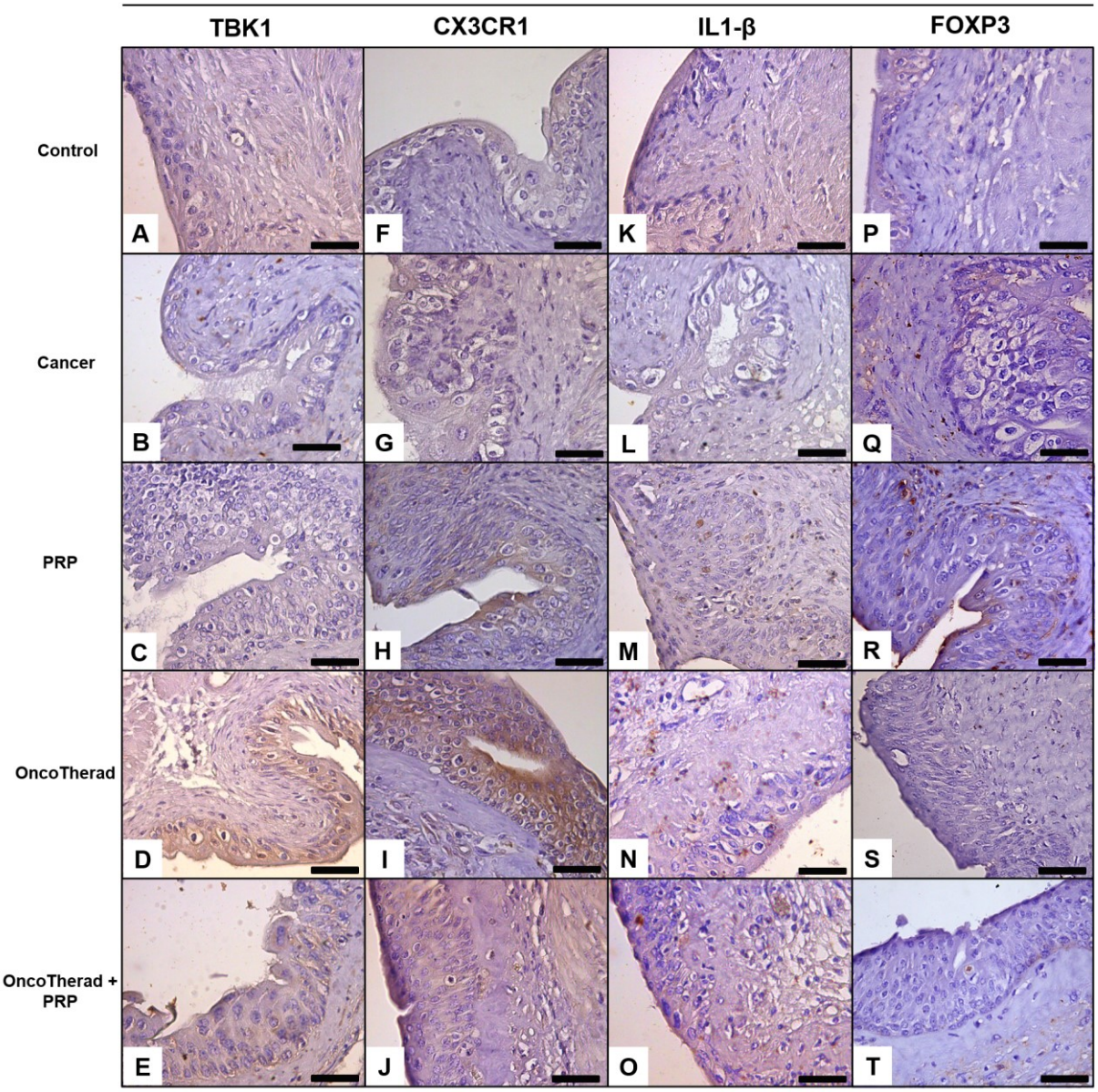

Figure 9. Immunolocalization of TBK1 (A-E), CX3CR1 (F-J), IL-1β (K-O), FOXP3 (P-T) antigens in the urinary bladders of different experimental groups. Control (healthy urothelium: A,F,K,P); Cancer (urothelial carcinoma in situ or pTis: B,G,L,Q); PRP (non-invasive urothelial carcinoma pTa: C,H,M,R); Oncotherad (Flat Hyperplasia: D,I,N,S) and OncoTherad+PRP (Flat Hyperplasia: E,J,O,T). Bars = 50 µm.

Intravesical treatment with PRP did not increase cancer progression biomarkers in mice with NMIBC

PRP alone or with OncoTherad® did not increase ($p>0.05$) VEGF and IGF-1 growth factors. There was no statistical difference ($p>0.05$) among the groups regarding the total

immunoreactivity and intensity of the immunoreactions for VEGF (Table 7, Figs 10 and 11). Immunoreactivities of IGF-1 were similar ($p>0.05$) among the groups (Table 7). The Control, Cancer, PRP, and OncoTherad+PRP groups showed different patterns of intensity for the IGF-1 immunoreaction (Figs 10 and 11). However, the intensity in the Cancer was stronger ($p<0.05$) when compared with the PRP group.

Table 7. Total immunoreactivity (%) for each antigen in the different experimental groups.

	Experimental Groups				
Antigens	**Control**	**Cancer**	**PRP**	**OncoTherad**	**OncoTherad+PRP**
VEGF	84.45 **a**	87.35 **a**	86.87 **a**	89.92 **a**	90.29 **a**
IGF1	92.77 **a**	88.47 **a**	85.14 **a**	88.16 **a**	84.71 **a**

Values are equivalent to the mean percentage of urothelial cells positive for the antigens per group (n=5 sections/animal/group). Kruskal-Wallis ANOVA, Student-Newman-Keuls Test. Along the same lines, values followed by different letters indicate a significant difference between groups ($p<0.05$).

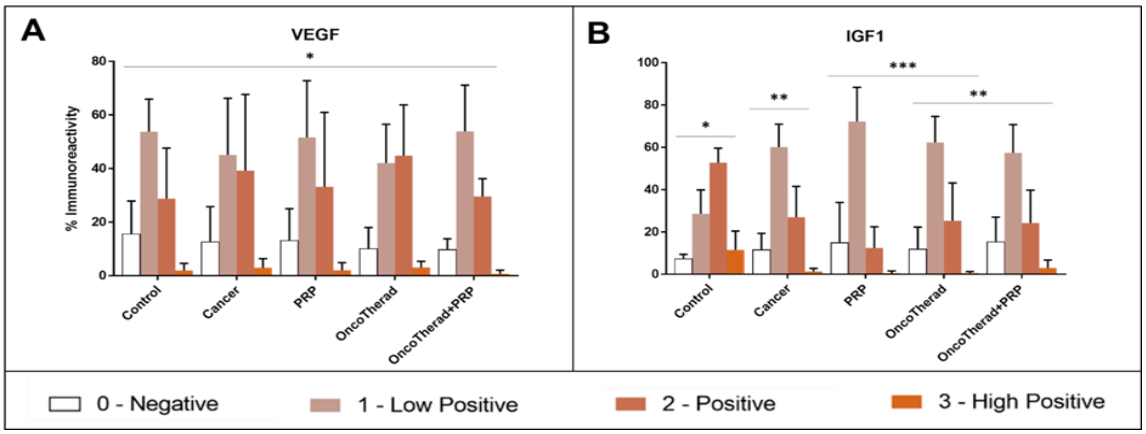

Figure 10. Immunoreactivities (%) in different intensity categories for antigens VEGF (A) and IGF-1 (B). */**/***Different symbols indicate a significant difference ($p<0.05$) between groups, when statistically differ in any category of immunoreactivity. ANOVA, Tukey test (n = 5 sections/animal/group). Immunoreactivity was classified into four categories: Negative (0): absence of labeling; Low Positive (1): weak immunoreaction; Positive (2): moderate immunoreaction and High Positive (3) strong immunoreaction.

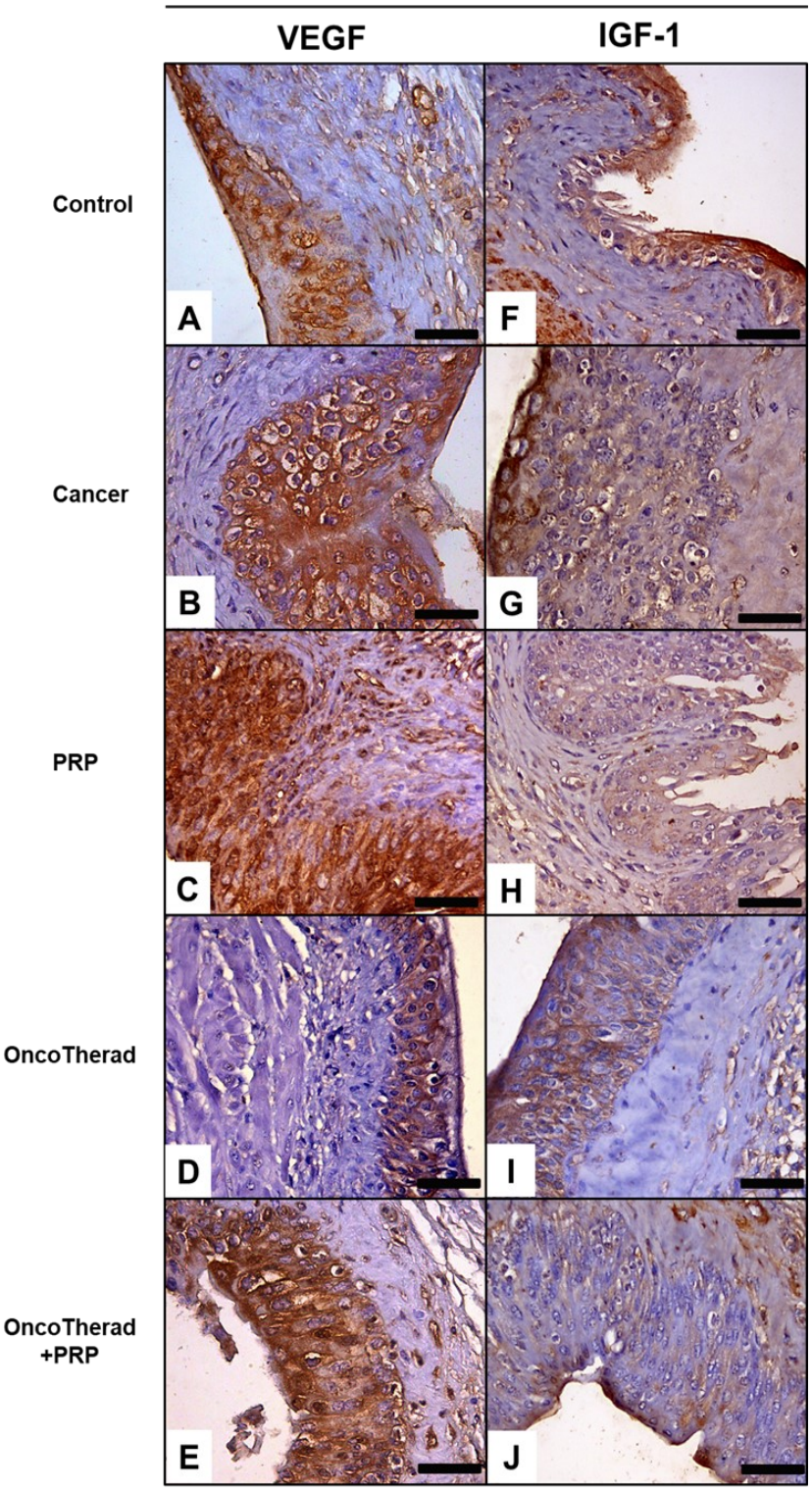

Figure 11. Immunolocalization of VEGF (A-E) and IGF-1 in the urinary bladders of different experimental groups. Control (healthy urothelium: A,F); Cancer (urothelial carcinoma in situ or pTis: B,G); PRP (non-invasive urothelial carcinoma pTa: C,H); Oncotherad (Flat Hyperplasia: D,I) and OncoTherad+PRP (Flat Hyperplasia: E,J). Bars = 50 μm.

Immunomodulation and antitumor response in NMIBC microenvironment promoted by OncoTherad® associated with PRP involves TLR-mediated IFN-γ production

Collectively, the interpretation of these data supported the mechanism of action triggered by OncoTherad® immunotherapy (alone or associated with PRP) summarized in Fig 12.

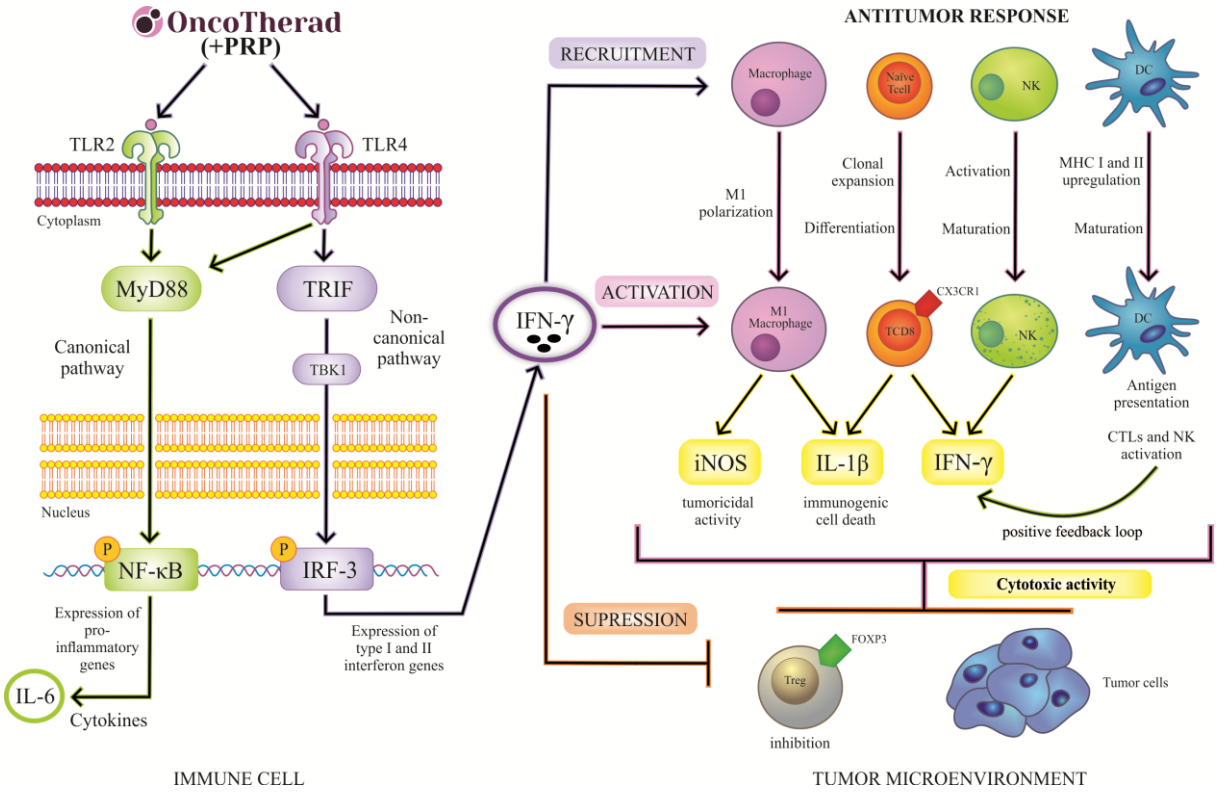

Figure 12. Antitumor response triggered by OncoTherad® immunotherapy associated with PRP. OncoTherad® (isolated or associated with PRP) stimulates Toll like Receptors 2 and 4 in immune cells. TLR2 signaling involves MyD88 and activation of NF-kB that will be phosphorylated and translocated to the nucleus. This is the canonical pathway (MyD88-dependent), where activated NF-kB leads to the production of pro-inflammatory cytokines as IL-6. TLR4 can recruit MyD88 in the canonical pathway or recruit TRIF to trigger the non-canonical pathway (MyD88-independent). TRIF will promote TBK1 Activation which will phosphorylate and activate IRF-3. IRF-3 in the nucleus will induce the expression of type I and II interferon genes as IFN-γ. IFN-γ triggers antitumor effects directly on tumor cells and indirectly by interacting and recruiting IFN-γ-producing cells, such as T-cells, macrophages, NK cells, and dendritic cells (DC) in the NMIBC microenvironment. IFN-γ stimulates

polarization of macrophages toward M1 phenotype. M1 macrophages show proinflammatory and tumoricidal activity with iNOS expression and enhanced capacity for cytokines secretion as IL-1β. IFN-γ is required for maturation of naïve T-cells to effector CD8+ T-cells and also promotes maturation and activations of NK cells. IFN-γ also promotes maturation and MHC I and II up-regulation in dendritic cells (DC). Through a positive feedback loop IFN-γ stimulates its own production in cytotoxic T lymphocytes (CTLs) as TCD8 and NK cells activated after the antigen presentation of DCs. IFN-γ also inhibits immune-suppressive T regulatory cells (Tregs) which are related to immune escape of the tumor cells.

DISCUSSION

In this study, we used a chemically induced NMIBC model to evaluate the association of OncoTherad® immunotherapy and PRP as an antitumor strategy. We fully characterized the NMIBC model both therapy-free as well as under the different intravesical treatments. The NMIBC induction may have delayed weight gain in the animals, even though the feed intake in the Cancer group was higher. Other studies have also reported a decrease in body weight in rodents resulting from chemical induction with other N-nitroso carcinogens.[39,40] Despite this, the administration of OncoTherad® associated or not with PRP recuperated the body weight, indicating absence of general toxicity and an effective treatment of the cancer state.

OncoTherad®, alone or associated with PRP, led to the highest urinary density. After OncoTherad® treatment, there was also a higher protein concentration. Proteins present in the urine may lead to an increase in density[41] and may even have originated from OncoTherad® itself. However, a variation of 1.0 to 1.03 in murine urinary density is considered minimal and still indicates a normal glomerular filtration rate.[42] In addition, leukocyturia was observed in the Cancer group only. Under normal conditions, small numbers of leukocytes may be found in murine urine.[42] Leukocyturia can occur due to urogenital tract inflammation resulting from urinary infection as well as non-infectious conditions such as lithiasis and neoplastic lesions.[43]

The absence of macroscopic renal lesions indicates that there was no acute toxicity in the organs due to the treatments at the doses used, since renal alterations are common in preclinical studies of drug toxicity.[44] A more edematous and reddish appearance (hyperemia) of urinary bladders due to dilation of blood vessels is described in cases of acute cystitis in mice.[45] Several urinary bladders of animals treated with OncoTherad® alone or associated with PRP showed hyperemia, indicating the stimulation of an inflammatory response. Thickening of the

urinary bladder wall may indicate the presence of neoplasia, especially when found focally; whereas when it is diffuse and/or symmetrical, it is usually related to benign conditions such as cystitis, immune infiltrate, edema in the lamina propria, urothelial hyperplasia, or being reactionary to intravesical treatments.[46–48] Therefore, the thickening found in the wall of the bladders in the present study are due to both neoplastic processes and the acute inflammation caused by the treatments with OncoTherad® only or when it was associated with PRP.

After the induction period with ENU, the presence of neoplasia (pTis) was found in 100% of the animals, confirming the representativeness of this NMIBC model. The animals in the OncoTherad group exhibited mostly non-malignant lesions after 6 weeks of treatment. Thus, OncoTherad® intravesical treatment (20 mg/ml) not only inhibited tumor progression but also promoted a regression of induced malignant lesions. The antitumor effect of this nanodrug was already reported for bladder cancer induced in rats[19,22] and spontaneous in dogs[49] and humans.[23,24] The association of OncoTherad® (10 mg/ml) with PRP resulted in an inhibition of tumor progression statistically equivalent with the group that received the therapeutic dose (20mg/ml). In this way, an effect of PRP was demonstrated as the association was effective in reducing neoplastic lesions even with the OncoTherad® concentration reduced by half.

Platelets play an active role in innate and adaptive immunity through adhesive interactions with leukocytes and endothelial cells, which can lead to pro-inflammatory events including leukocyte activation and recruitment as well as cascade cytokine production.[50] The antitumor potential of PRP is possibly related to the modulation of the immune system that involves the action of growth factors and the chemotactic activity of platelets.[32,50] In addition, the effectiveness of its association with OncoTherad® can be explained mainly by the relationship between platelets and polyphosphates (PolyP) which play an important proinflammatory activity.[33,34,51] In our pilot studies, analyzes of physicochemical characterizations showed a higher concentration of PRP proteins upon interaction with OncoTherad®, possibly due to the ability of the phosphates present in the immunotherapy to induce the release of proteins by platelets. Another possible interaction is that OncoTherad® acts as agonist of TLR2 and TLR4[18,19] while both human and murine platelets can express TLRs such as TLR2, TLR4, and TLR9.[50] Platelet expression of TLR4 mediates lipopolysaccharide (LPS)-induced thrombocytopenia and TNF-α production by leukocytes, indicating that these events may be responsible for activation of the innate immune system.[50]

Decreased expression of Toll-like receptors in bladder cancer occurred for both TLR2 and TLR4 in the NMIBC model which is consistent with previous data in patients and correlates

with tumor progression.[14,15,52] This correlation may explain the decrease in the intensity of the TLRs immunoreaction according to the severity of the histopathological lesions in this study. Further, the decrease of IL-6 and IL-1β as well as IRF-3 in this NMIBC model support that both canonical and non-canonical pathways are involved in bladder carcinogenesis and related to the suppression of the immune response, allowing proliferation and survival of tumor cells.[53–55] However, TLR2 and TLR4 expression were recovered with Oncotherad® treatment as previously reported by our group [19,22,23] or when it was associated with PRP, which is related to the effectiveness in inhibiting tumor progression.

OncoTherad® alone or plus PRP stimulated the canonical pathway, given the significant increases in the expression of NF-kB and IL-6. This activation may have occurred mainly through TLR4, also significantly up-regulated. The TLR4 stimulation with LPS induces an intracellular signaling that stimulates the expression of IL-6 in bladder cancer cells.[56] On the other hand, after intravesical treatment with PRP alone, the levels of TLR2 expression and others mediators of the canonical pathway were not different from the group with NMIBC without treatment. Thus, PRP did not reverse the reduced pattern of TLR2 expression nor was it able to promote significant tumor inhibition when used alone. Previous studies in NMIBC models demonstrate that treatment with BCG mainly induces the canonical pathway, promoting an increase in the levels of TLR2 and TLR4, activation of MyD88 and NF-kB, and an increase in inflammatory cytokines such as TNF-α.[36,57–59] Nonetheless, when PRP was associated with immunotherapy with BCG, it promoted activation through TLR4 and increased TRIF and IRF-3, immunomodulating in favor of the non-canonical pathway.[32]

The associated treatment also modulated the non-canonical or TRIF-dependent pathway in a more accentuated way, presenting the highest values of both total immunoreactivity and intensity for TLR4, even compared with the isolated treatments. Further, only the associated therapy recovered the TLR4 expression pattern found in healthy animals. Such results reinforce previous data from our group describing the stimulation of TLR4 by OncoTherad®[19,22,23], but probably the associated treatment co-opted pathways through this receptor even more intensely. This occurrence can be explained since TLR4 is the only one of the TLRs that can trigger both the canonical and non-canonical pathways.[60] Studies in murine models have shown that stimulation of TLR4 expression promotes antitumor effects in bladder cancer.[57,59,61,62] Fungal compounds that act as TLR4 ligands induced maturation of dendritic cells and stimulated antigen presentation by these cells and subsequent specific T-cell response against bladder cancer in murine models.[63,64]

Previous studies have shown that OncoTherad® promotes distinct activation of the immune system mediated by TLRs, being able to increase protein levels for TLR4, TRIF, IRF-3 and IFN-γ in the urinary bladder of rats with chemically induced NMIBC.[19,22,23] In this study, intravesical treatments with OncoTherad® associated or not with PRP increased both total immunoreactivity and intensity of the immunoreaction for IFN-γ. Stimulation with fungal-derived compounds associated with DNA vaccines promoted stimulation of dendritic cells and antitumor Th1 profile response through IFN-γ production by activated T cells *in vitro* and *in vivo* in C57BL/6J mice with bladder cancer.[64,65] IFN-γ induces the expression of macrophage-derived cytokines through the upregulation of TLR4 in human bladder cancer cell lines.[66] This is an important regulatory mechanism, where TLR4 stimulation induces the production of cytokines such as IL-12 which stimulates the production of IFN-γ T-cells.[67]

TBK1 were also increased by OncoTherad® isolated or associated with PRP which is consistent with the stimulation of TLR4-mediated IFN-γ production[68] by OncoTherad®. The presence of IFN-γ in the tumor microenvironment attracts T-cells and promotes the development of a Th1 profile CD4 T-cell antitumor response which can give rise to a cytotoxic antitumor response via CD8+ T-cells and a direct tumoricidal activity related to M1 macrophages expressing iNOS.[69] As IFN-γ is central to CD8+ T cell activation[70] the stimulation of its production by OncoTherad® treatment is related to the increase in the number of CX3CR1+ T-cells. Further, OncoTherad® and OncoTherad® plus PRP decreased FOXP3+ cells which is also implicated with the IFN-γ suppression effect on these cells.[70]

The increase of IL-1β promoted by OncoTherad® plus PRP may be related to the immunogenic cell death as this interleukin is a key pro-inflammatory mediator and crucial during pyroptosis (inflammatory cell death).[71] The induction of the non-canonical pathway by the Protein aggregate magnesium-ammonium phospholinoleate-palmitoleate anhydride (a biological response modifier obtained by fermentation from *Aspergillus oryzae*) increased iNOS levels as well as the apoptotic process, inducing immunogenic cell death in a NMIBC murine model.[36] Likewise, OM-174 (TLR2/TLR4 agonist) induced the release of cytokines and IFN-γ by macrophages and monocytes, which led to iNOS expression in tumor cells followed by apoptosis in a model of colon cancer in mice.[69] Furthermore, despite the presence of the growth factors in the PRP, intravesical treatment with PRP alone or associated with OncoTherad® did not increase VEGF and IGF-1 which are reported as progression biomarkers in bladder cancer.[72,73]

In this study, the TLR4 non-canonical pathway for the production of interferons was stimulated mainly by the association of treatments, given the significant increases in its mediators as well as IFN-γ itself, and three hypotheses may explain the results obtained: (1) the role of PRP in immunomodulating the response by stimulating mainly the non-canonical pathway, since PRP alone also increased IFN-γ immunoreactivity compared to Cancer, but the effects on the canonical pathway were not expressive, except for NF-kB. This may be explained by the late activation of NF-kB occurs in both canonical or non-canonical pathways after TRIF recruitment by TLR3 or TLR4, which culminates in the activation of IRF-3 and production of type I and II interferons.[10,60] (2) Stimulation of the canonical and non-canonical pathway by OncoTherad® through TLR4, given the increase in expression of TLR4, NF-kB, IL-6, and IFN-γ in comparison with the Cancer group. (3) Stimulation of the canonical and non-canonical pathway by the associated treatment OncoTherad+PRP through TLR4.

Our findings confirmed the antitumor and immunomodulatory effects of OncoTherad® associated with PRP in the NMIBC model. OncoTherad+PRP led to activation of TLRs-mediated innate immune system mainly in the TRIF-dependent signaling pathway. The NMIBC microenvironment was modulated to a cytotoxic profile correlated with the IL-1β increase by stimulating immune pathways for IFN-γ production and consequent CD8+ T-cell activation and Tregs reduction. These mechanisms support the significant inhibition of tumor progression obtained with OncoTherad® alone or associated with PRP. In addition, PRP did not trigger carcinogenic effects in this NMIBC model. Therefore, this association may constitute a potential new therapeutic strategy for BCG-unresponsive NMIBC patients.

ACKNOWLEDGEMENTS

The present research was carried out with the financial support of the São Paulo Research Foundation - FAPESP, Brazil (Process Number: 2020/15687-5) and National Council for Scientific and Technological Development - CNPq, Brazil (Funding number: 140695/2019-2).

All authors have read the journal's authorship agreement and the journal's policy on conflicts of interest and have declared no conflicts of interest.

DATA STATEMENT

The data supporting the findings of this current study are available from the corresponding author upon reasonable request.

REFERENCES

1. Babjuk M, Burger M, Compérat EM, et al. European Association of Urology Guidelines on Non-muscle-invasive Bladder Cancer (TaT1 and Carcinoma In Situ) - 2019 Update. *European Urology*. 2019;76(5):639-657. doi:10.1016/j.eururo.2019.08.016

2. Askeland EJ, Newton MR, O'Donnell MA, Luo Y. Bladder Cancer Immunotherapy: BCG and Beyond. *Advances in Urology*. 2012;2012:1-13. doi:10.1155/2012/181987

3. Hall MC, Craig Hall M, Chang SS, et al. Guideline for the Management of Nonmuscle Invasive Bladder Cancer (Stages Ta, T1, and Tis): 2007 Update. *Journal of Urology*. 2007;178(6):2314-2330. doi:10.1016/j.juro.2007.09.003

4. Kemp TJ, Ludwig AT, Earel JK, et al. Neutrophil stimulation with Mycobacterium bovis bacillus Calmette-Guérin (BCG) results in the release of functional soluble TRAIL/Apo-2L. *Blood*. 2005;106(10):3474-3482. doi:10.1182/blood-2005-03-1327

5. Böhle A, Brandau S. Immune mechanisms in bacillus Calmette-Guerin immunotherapy for superficial bladder cancer. *J Urol*. 2003;170(3):964-969. doi:10.1097/01.ju.0000073852.24341.4a

6. Ojea A, Nogueira JL, Solsona E, et al. A multicentre, randomised prospective trial comparing three intravesical adjuvant therapies for intermediate-risk superficial bladder cancer: low-dose bacillus Calmette-Guerin (27 mg) versus very low-dose bacillus Calmette-Guerin (13.5 mg) versus mitomycin C. *Eur Urol*. 2007;52(5):1398-1406. doi:10.1016/j.eururo.2007.04.062

7. Guallar-Garrido S, Julián E. Bacillus Calmette-Guérin (BCG) Therapy for Bladder Cancer: An Update. *Immunotargets Ther*. 2020;9:1-11. doi:10.2147/ITT.S202006

8. Husseinzadeh N, Davenport SM. Role of Toll-like receptors in cervical, endometrial and ovarian cancers: A review. *Gynecologic Oncology*. 2014;135(2):359-363. doi:10.1016/j.ygyno.2014.08.013

9. Chuffa LG de A, de Almeida Chuffa LG, de Moura Ferreira G, Lupi LA, da Silva Nunes I, Fávaro WJ. P-MAPA immunotherapy potentiates the effect of cisplatin on serous ovarian carcinoma through targeting TLR4 signaling. *Journal of Ovarian Research*. 2018;11(1). doi:10.1186/s13048-018-0380-5

10. Akira S, Takeda K. Toll-like receptor signalling. *Nat Rev Immunol*. 2004;4(7):499-511. doi:10.1038/nri1391

11. Galli R, Starace D, Busà R, et al. TLR stimulation of prostate tumor cells induces chemokine-mediated recruitment of specific immune cell types. *J Immunol*. 2010;184(12):6658-6669. doi:10.4049/jimmunol.0902401

12. Takeda K, Akira S. TLR signaling pathways. *Semin Immunol*. 2004;16(1):3-9. doi:10.1016/j.smim.2003.10.003

13. Satoh T, Akira S. Toll-Like Receptor Signaling and Its Inducible Proteins. *Microbiol Spectr*. 2016;4(6). doi:10.1128/microbiolspec.MCHD-0040-2016

14. Ayari C, Bergeron A, LaRue H, Ménard C, Fradet Y. Toll-like receptors in normal and malignant human bladders. *J Urol*. 2011;185(5):1915-1921. doi:10.1016/j.juro.2010.12.097

15. Stopiglia RM, Matheus WE, Garcia PV, et al. Molecular Assessment of Non-Muscle Invasive and Muscle Invasive Bladder Tumors: Mapping of Putative Urothelial Stem Cells and Toll-Like Receptors (TLR) Signaling. *Journal of Cancer Therapy*. 2015;06(02):129-140. doi:10.4236/jct.2015.62014

16. Sander B, Damm O, Gustafsson B, Andersson U, Håkansson L. Localization of IL-1, IL-2, IL-4, IL-8 and TNF in superficial bladder tumors treated with intravesical bacillus Calmette-Guerin. *J Urol*. 1996;156(2 Pt 1):536-541. doi:10.1097/00005392-199608000-00078

17. Yu DS, Lee CF, Chang SY. Immunotherapy for orthotopic murine bladder cancer using bacillus Calmette-Guerin recombinant protein Mpt-64. *J Urol*. 2007;177(2):738-742. doi:10.1016/j.juro.2006.09.074

18. Fávaro WJ, Caballero NED. PROCESS FOR OBTAINING NANOSTRUCTURED COMPLEX (CFI-1), NANOSTRUCTURED COMPLEX ASSOCIATED WITH PROTEIN (MRB-CFI-1). *Patent*. Published online August 23, 2022. Accessed March 12, 2023. https://patentimages.storage.googleapis.com/dd/0e/84/5ce8e5594dd259/BR102017012768B1.pdf

19. Fávaro WJ, Alonso JCC, de Souza BR, et al. New synthetic nano-immunotherapy (OncoTherad®) for non-muscle invasive bladder cancer: Its synthesis, characterization and anticancer property. *Tissue and Cell*. 2023;80:101988. doi:10.1016/j.tice.2022.101988

20. Favaro WJ, Caballero NED. Method for producing a nanostructured complex (CFI-1), a protein-associated nanostructured complex (MRB-CFI-1) and use. *US Patent*. Published online October 5, 2021. Accessed March 12, 2023. https://patentimages.storage.googleapis.com/a9/1b/77/72686d2d9d735a/US11136242.pdf

21. REBEC. Accessed March 12, 2023. https://ensaiosclinicos.gov.br/rg/RBR-6swqd2

22. Reis IB, Tibo LHS, Socca EAR, de Souza BR, Durán N, Fávaro WJ. OncoTherad® (MRB-CFI-1) nano-immunotherapy reduced tumoral progression in non-muscle invasive bladder cancer through activation of Toll-like signaling pathway. *Tissue Cell*. 2022;76:101762. doi:10.1016/j.tice.2022.101762

23. Alonso JCC, Ribeiro de Souza B, Leme G, et al. Crosstalk among T-cell CX3CR1, immune checkpoints and toll-like receptor 4 signaling pathway in BCG-unresponsive nonmuscle invasive bladder cancer: Mechanism of action of OncoTherad Nano-Immunotherapy. *J Clin Oncol*. 2022;40(16_suppl):e16551-e16551. doi:10.1200/jco.2022.40.16_suppl.e16551

24. Alonso JCC, Reis IB, Gonçalves JM, et al. Oncotherad immunotherapy elicits promising responses in Bacillus Calmette-Guérin-unresponsive non–muscle invasive bladder cancer: Results from phase I/ II study. *J Clin Oncol*. 2020;38(15_suppl):e17048-e17048. doi:10.1200/jco.2020.38.15_suppl.e17048

25. Woo SR, Fuertes MB, Corrales L, et al. STING-dependent cytosolic DNA sensing mediates innate immune recognition of immunogenic tumors. *Immunity*. 2014;41(5):830-842. doi:10.1016/j.immuni.2014.10.017

26. Yamauchi T, Hoki T, Oba T, et al. T-cell CX3CR1 expression as a dynamic blood-based biomarker of response to immune checkpoint inhibitors. *Nat Commun*. 2021;12(1):1402. doi:10.1038/s41467-021-21619-0

27. Lu L, Barbi J, Pan F. The regulation of immune tolerance by FOXP3. *Nat Rev Immunol*. 2017;17(11):703-717. doi:10.1038/nri.2017.75

28. Merchán WH, Gómez LA, Chasoy ME, Alfonso-Rodríguez CA, Muñoz AL. Platelet-rich plasma, a powerful tool in dermatology. *J Tissue Eng Regen Med*. 2019;13(5):892-901. doi:10.1002/term.2832

29. Dhurat R, Sukesh MS. Principles and methods of preparation of platelet-rich plasma: A review and author′s perspective. *Journal of Cutaneous and Aesthetic Surgery*. 2014;7(4):189. doi:10.4103/0974-2077.150734

30. Chou TM, Chang HP, Wang JC. Autologous platelet concentrates in maxillofacial regenerative therapy. *Kaohsiung J Med Sci*. 2020;36(5):305-310. doi:10.1002/kjm2.12192

31. Naderi N, Griffin MF, Mosahebi A, Butler PE, Seifalian AM. Adipose derived stem cells and platelet rich plasma improve the tissue integration and angiogenesis of biodegradable scaffolds for soft tissue regeneration. *Molecular Biology Reports*. 2020;47(3):2005-2013. doi:10.1007/s11033-020-05297-7

32. Dias LP, Luzo ÂCM, Volpe BB, et al. Effects of intravesical therapy with platelet-rich plasma (PRP) and Bacillus Calmette-Guérin (BCG) in non-muscle invasive bladder cancer. *Tissue Cell*. 2018;52:17-27. doi:10.1016/j.tice.2018.03.011

33. Morrissey JH. Polyphosphate: a link between platelets, coagulation and inflammation. *International Journal of Hematology*. 2012;95(4):346-352. doi:10.1007/s12185-012-1054-5

34. Müller F, Mutch NJ, Schenk WA, et al. Platelet polyphosphates are proinflammatory and procoagulant mediators in vivo. *Cell*. 2009;139(6):1143-1156. doi:10.1016/j.cell.2009.11.001

35. Wat JM, Foley JH, Krisinger MJ, et al. Polyphosphate suppresses complement via the terminal pathway. *Blood*. 2014;123(5):768-776. doi:10.1182/blood-2013-07-515726

36. Garcia PV, Seiva FRF, Carniato AP, et al. Increased toll-like receptors and p53 levels regulate apoptosis and angiogenesis in non-muscle invasive bladder cancer: mechanism of action of P-MAPA biological response modifier. *BMC Cancer*. 2016;16:422. doi:10.1186/s12885-016-2474-z

37. National Research Council, Division on Earth and Life Studies, Institute for Laboratory Animal Research, Committee for the Update of the Guide for the Care and Use of Laboratory Animals. *Guide for the Care and Use of Laboratory Animals: Eighth Edition*. National Academies Press; 2011. https://books.google.com/books/about/Guide_for_the_Care_and_Use_of_Laboratory.html?hl=&id=GyxkAgAAQBAJ

38. Epstein JI, Amin MB, Reuter VR, Mostofi FK. The World Health Organization/International Society of Urological Pathology Consensus Classification of Urothelial (Transitional Cell) Neoplasms of the Urinary Bladder. *The American Journal of Surgical Pathology*. 1998;22(12):1435-1448. doi:10.1097/00000478-199812000-00001

39. Ekambaram G, Rajendran P, Magesh V, Sakthisekaran D. Naringenin reduces tumor size and weight lost in N-methyl-N'-nitro-N-nitrosoguanidine-induced gastric carcinogenesis in rats. *Nutr Res*. 2008;28(2):106-112. doi:10.1016/j.nutres.2007.12.002

40. Sivaramakrishnan V, Shilpa PNM, Praveen Kumar VR, Niranjali Devaraj S. Attenuation of N-nitrosodiethylamine-induced hepatocellular carcinogenesis by a novel flavonol-Morin. *Chem Biol Interact*. 2008;171(1):79-88. doi:10.1016/j.cbi.2007.09.003

41. Chadha V, Garg U, Alon US. Measurement of urinary concentration: a critical appraisal of methodologies. *Pediatr Nephrol*. 2001;16(4):374-382. doi:10.1007/s004670000551

42. Abdel-Alim AAF, Kamel MA, Elsayed RAA. Some pharmacological studies of ciproflo. *Zagazig Vet J*. 2017;45(1):172-180. doi:10.21608/zvjz.2017.28662

43. de Oliveira Cezar G, dos Santos VD, Funchal C. Avaliação da Compatibilidade entre Bulas de Diferentes Marcas de Tiras Reagentes de Urina. *RBM*. 2012;15(1):87-100. doi:10.25061/2527-2675/ReBraM/2012.v15i1.73

44. Frazier KS, Seely JC, Hard GC, et al. Proliferative and nonproliferative lesions of the rat and mouse urinary system. *Toxicol Pathol*. 2012;40(4 Suppl):14S - 86S. doi:10.1177/0192623312438736

45. Ambite I, Puthia M, Nagy K, et al. Molecular Basis of Acute Cystitis Reveals Susceptibility Genes and Immunotherapeutic Targets. *PLoS Pathog*. 2016;12(10):e1005848. doi:10.1371/journal.ppat.1005848

46. Cohan RH, Caoili EM, Cowan NC, Weizer AZ, Ellis JH. MDCT Urography: Exploring a new paradigm for imaging of bladder cancer. *AJR Am J Roentgenol*. 2009;192(6):1501-1508. doi:10.2214/AJR.09.2344

47. Nicolau C, Bunesch L, Sebastia C, Salvador R. Diagnosis of bladder cancer: contrast-enhanced ultrasound. *Abdom Imaging*. 2010;35(4):494-503. doi:10.1007/s00261-009-9540-9

48. Pan Y, Lavelle JP, Bastacky SI, et al. Detection of tumorigenesis in rat bladders with optical coherence tomography. *Med Phys*. 2001;28(12):2432-2440. doi:10.1118/1.1418726

49. Böckelmann PK, Tizziani SHS, Durán N, Fávaro WJ. New therapeutic perspective for bladder cancer in dogs: Toxicological and clinical effects of OncoTherad nanostructured immunotherapy. *J Phys Conf Ser*. 2019;1323(1):012022. doi:10.1088/1742-6596/1323/1/012022

50. Semple JW, Freedman J. Platelets and innate immunity. *Cell Mol Life Sci*. 2010;67(4):499-511. doi:10.1007/s00018-009-0205-1

51. Morrissey JH, Choi SH, Smith SA. Polyphosphate: an ancient molecule that links platelets, coagulation, and inflammation. *Blood*. 2012;119(25):5972-5979. doi:10.1182/blood-2012-03-306605

52. LaRue H, Ayari C, Bergeron A, Fradet Y. Toll-like receptors in urothelial cells--targets for cancer immunotherapy. *Nat Rev Urol*. 2013;10(9):537-545. doi:10.1038/nrurol.2013.153

53. Garcia-Lora A, Algarra I, Garrido F. MHC class I antigens, immune surveillance, and tumor immune escape. *J Cell Physiol*. 2003;195(3):346-355. doi:10.1002/jcp.10290

54. Sheu J, Shih IM. HLA-G and immune evasion in cancer cells. *J Formos Med Assoc*. 2010;109(4):248-257. doi:10.1016/S0929-6646(10)60050-2

55. Teicher BA. Transforming growth factor-beta and the immune response to malignant disease. *Clin Cancer Res*. 2007;13(21):6247-6251. doi:10.1158/1078-0432.CCR-07-1654

56. Qian Y, Deng J, Xie H, et al. Regulation of TLR4-induced IL-6 response in bladder cancer cells by opposing actions of MAPK and PI3K signaling. *J Cancer Res Clin Oncol*. 2009;135(3):379-386. doi:10.1007/s00432-008-0478-z

57. Fávaro WJ, Nunes OS, Seiva FR, et al. Effects of P-MAPA Immunomodulator on Toll-Like Receptors and p53: Potential Therapeutic Strategies for Infectious Diseases and Cancer. *Infect Agent Cancer*. 2012;7(1):14. doi:10.1186/1750-9378-7-14

58. Kumar P, Tyagi R, Das G, Bhaskar S. Mycobacterium indicus pranii and Mycobacterium bovis BCG lead to differential macrophage activation in Toll-like receptor-dependent manner. *Immunology*. 2014;143(2):258-268. doi:10.1111/imm.12306

59. Garcia PV, Apolinário LM, Böckelmann PK, da Silva Nunes I, Duran N, Fávaro WJ. Alterations in ubiquitin ligase Siah-2 and its corepressor N-CoR after P-MAPA immunotherapy and anti-androgen therapy: new therapeutic opportunities for non-muscle invasive bladder cancer. *Int J Clin Exp Pathol*. 2015;8(5):4427-4443. https://www.ncbi.nlm.nih.gov/pubmed/26191134

60. Kawai T, Akira S. Toll-like receptors and their crosstalk with other innate receptors in infection and immunity. *Immunity*. 2011;34(5):637-650. doi:10.1016/j.immuni.2011.05.006

61. Takeuchi A, Kamiryou Y, Yamada H, et al. Oral administration of xanthan gum enhances antitumor activity through Toll-like receptor 4. *Int Immunopharmacol*. 2009;9(13-14):1562-1567. doi:10.1016/j.intimp.2009.09.012

62. Zhang GW, Qin GF, Han B, et al. Efficacy of Zhuling polyporus polysaccharide with BCG to inhibit bladder carcinoma. *Carbohydr Polym*. 2015;118:30-35. doi:10.1016/j.carbpol.2014.11.012

63. Lin CC, Yu YL, Shih CC, et al. A novel adjuvant Ling Zhi-8 enhances the efficacy of DNA cancer vaccine by activating dendritic cells. *Cancer Immunol Immunother*. 2011;60(7):1019-1027. doi:10.1007/s00262-011-1016-4

64. Chen MH, Li WS, Lue YS, et al. Clitocybe nuda Activates Dendritic Cells and Acts as a DNA Vaccine Adjuvant. *Evid Based Complement Alternat Med*. 2013;2013:761454. doi:10.1155/2013/761454

65. Li Z, Pradera F, Kammertoens T, Li B, Liu S, Qin Z. Cross-talk between T cells and innate immune cells is crucial for IFN-gamma-dependent tumor rejection. *J Immunol*. 2007;179(3):1568-1576. doi:10.4049/jimmunol.179.3.1568

66. Yamada H, Odonnell MA, Matsumoto T, Luo Y. Interferon-gamma up-regulates toll-like receptor 4 and cooperates with lipopolysaccharide to produce macrophage-derived chemokine and interferon-gamma inducible protein-10 in human bladder cancer cell line RT4. *J Urol*. 2005;174(3):1119-1123. doi:10.1097/01.ju.0000168619.25341.96

67. Ikeda H, Old LJ, Schreiber RD. The roles of IFN gamma in protection against tumor development and cancer immunoediting. *Cytokine Growth Factor Rev*. 2002;13(2):95-109. doi:10.1016/s1359-6101(01)00038-7

68. Sameer AS, Nissar S. Toll-Like Receptors (TLRs): Structure, Functions, Signaling, and Role of Their Polymorphisms in Colorectal Cancer Susceptibility. *Biomed Res Int*. 2021;2021. doi:10.1155/2021/1157023

69. Garay RP, Viens P, Bauer J, et al. Cancer relapse under chemotherapy: why TLR2/4 receptor agonists can help. *Eur J Pharmacol*. 2007;563(1-3):1-17. doi:10.1016/j.ejphar.2007.02.018

70. Jorgovanovic D, Song M, Wang L, Zhang Y. Roles of IFN-γ in tumor progression and regression: a review. *Biomark Res*. 2020;8:49. doi:10.1186/s40364-020-00228-x

71. Ju X, Yang Z, Zhang H, Wang Q. Role of pyroptosis in cancer cells and clinical applications. *Biochimie*. 2021;185:78-86. doi:10.1016/j.biochi.2021.03.007

72. Roudnicky F, Dieterich LC, Poyet C, et al. High expression of insulin receptor on tumour-associated blood vessels in invasive bladder cancer predicts poor overall and progression-free survival. *J Pathol*. 2017;242(2):193-205. doi:10.1002/path.4892

73. Kopparapu PK, Boorjian SA, Robinson BD, et al. Expression of VEGF and its receptors VEGFR1/VEGFR2 is associated with invasiveness of bladder cancer. *Anticancer Res*. 2013;33(6):2381-2390. https://www.ncbi.nlm.nih.gov/pubmed/23749886

SUPPLEMENTARY MATERIAL

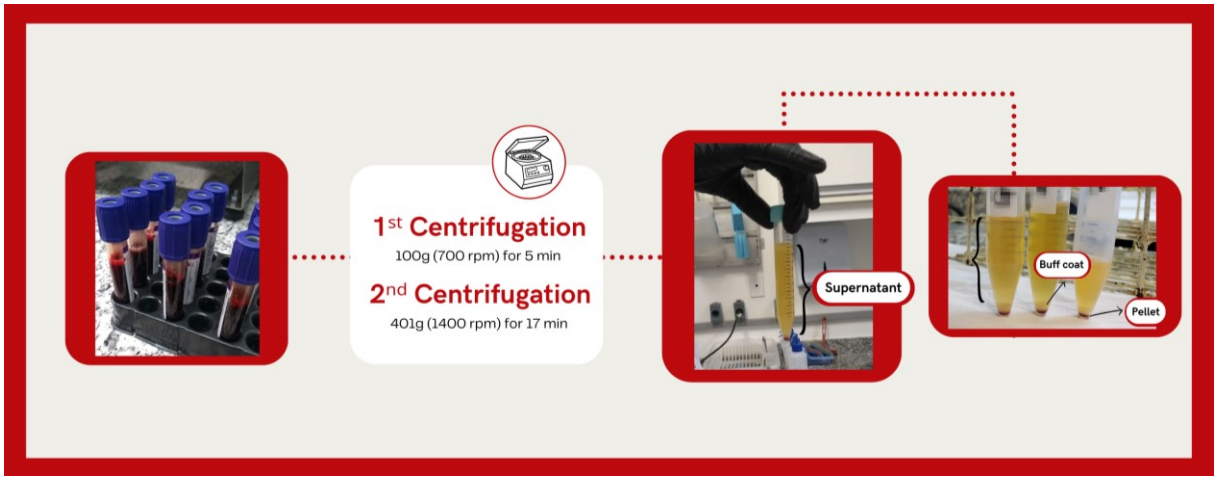

Supplemental Figure 1. Obtaining Platelet Rich Plasma (PRP). Peripheral blood was collected and transferred in specific collection tubes. After the centrifugations, the blood was separated into three layers: Plasma and platelets with a few white blood cells dispersed in the plasma (supernatant), an intermediate layer composed of white blood cells (buff coat), and pellet composed of red blood cells.

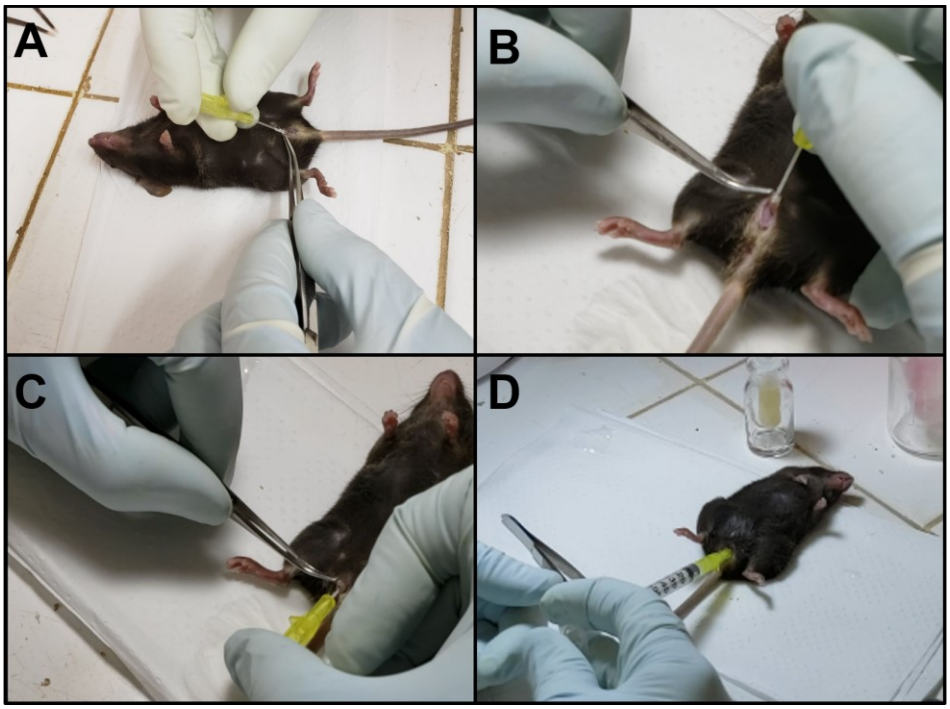

Supplemental Figure 2. Steps of the procedure for catheterization of the urethra and urinary bladder used in the induction of non-muscle invasive bladder cancer (NMIBC) and in intravesical treatments. (A) Positioning of the flexible catheter. (B) Insertion of the catheter into the external urethral ostium. (C) Complete insertion of the catheter reaching the interior of the bladder. (D) Intravesical instillation.

Supplemental Figure 3. Examples of environmental enrichment spaces used for mice. Environmental enrichment provides quality of life and well-being to experimental animals, as well as a more active behavior similar to the species' natural behavior[1].

1. Garbin LC, Faleiros RR, Do Lago LA. ENRIQUECIMENTO AMBIENTAL EM ROEDORES UTILIZADOS PARA A EXPERIMENTAÇÃO ANIMAL: REVISÃO DE LITERATURA. Revista Acadêmica Ciência Animal. 2012;10(2):153. doi:10.7213/academica.7692

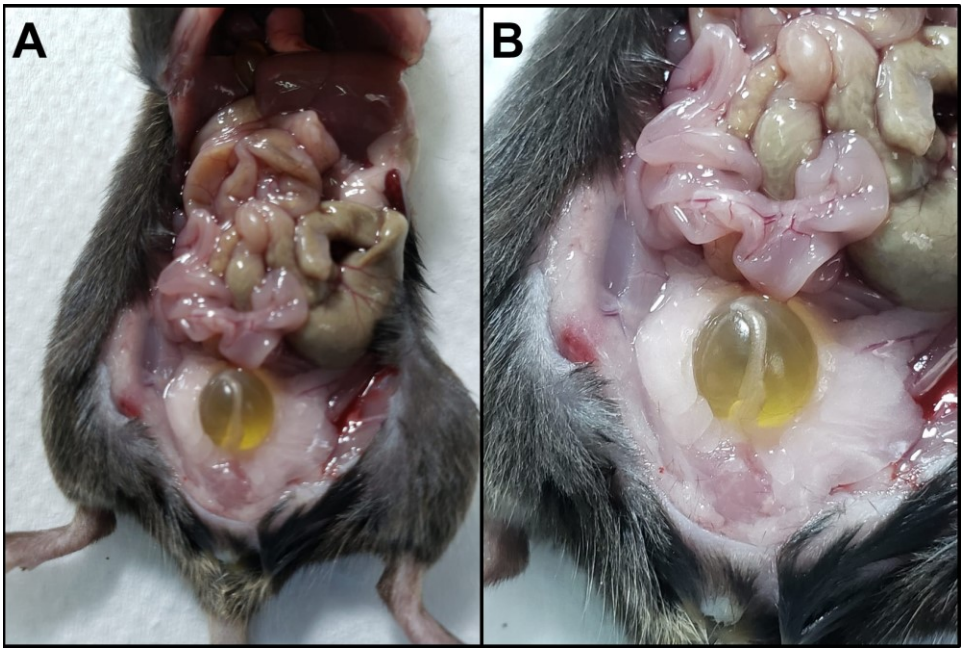

Supplemental Figure 4. Macroscopic evaluation of the urinary bladder at the time of euthanasia. (A) Examination of the abdominal cavity and urinary tract. (B) Detail of the urinary bladder with normal vascularization, translucent wall and no externally apparent thickening.

Supplemental Table 1. Primary antibodies for Immunohistochemistry.

Antibody	Clonality	Code	Distributor	Dilution
TLR2	polyclonal	sc-10739	Santa Cruz Biotechnology, USA	1:100
MyD88	polyclonal	sc-11356	Santa Cruz Biotechnology, USA	1:50
NF-κB	polyclonal	ab-7970	Abcam, USA	1:300
IL-6	polyclonal	bs-0782R	Bioss, USA	1:50
TLR4	monoclonal	sc-293072	Santa Cruz Biotechnology, USA	1:50
TRIF	polyclonal	sc-67061	Santa Cruz Biotechnology, USA	1:75
IRF-3	monoclonal	sc-376455	Santa Cruz Biotechnology, USA	1:75
IFN-γ	monoclonal	sc-12755	Santa Cruz Biotechnology, USA	1:50
TBK1	monoclonal	sc-398366	Santa Cruz Biotechnology, USA	1:50
CX3CR1	monoclonal	sc-377227	Santa Cruz Biotechnology, USA	1:50
IL-1β	monoclonal	sc-12742	Santa Cruz Biotechnology, USA	1:50
FOXP3	monoclonal	sc-53876	Santa Cruz Biotechnology, USA	1:200
VEGF	monoclonal	sc-7269	Santa Cruz Biotechnology, USA	1:50
IGF-1	polyclonal	sc-9013	Santa Cruz Biotechnology, USA	1:50

5. CAPÍTULO II

Revista para submissão: **LIFE SCIENCES**

A novel Low-Grade Serous Ovarian Carcinoma Model induced by DMBA: Results from OncoTherad® preclinical testing

Bianca Ribeiro de Souza[1*]; Gabriela Oliveira[1]; Giovana Leme[1]; Ianny Brum Reis[2]; Felippe Augusto Tossini Cabral[1]; Juliane Lima Baggio de Paula[1]; Daniel Henrique da Silva Santos[1]; Claudia Ronca Felizzola[1], Nelson Durán[1,3], Michael Anglesio[4]; Wagner José Fávaro[1]

[1]Department of Structural and Functional Biology, Institute of Biology – University of Campinas (UNICAMP), Campinas, SP, Brazil.

[2]Department of Diagnosis and Surgery, School of Dentistry - São Paulo State University (UNESP), Araraquara, SP, Brazil.

[3]Nanomedicine Research Unit (Nanomed), Federal University of ABC (UFABC), Santo André, SP, Brazil

[4]British Columbia's Gynecological Cancer Research (OVCARE) Program and Department of Obstetrics and Gynecology, University of British Columbia, Vancouver General Hospital, Vancouver, British Columbia, Canada

***Corresponding author:** Bianca Ribeiro de Souza. 255, Monteiro Lobato Street, University City - University of Campinas (UNICAMP) - Laboratory of Urogenital Carcinogenesis and Immunotherapy. ZIP/Postal Code: 13083-862, Campinas, São Paulo, Brazil. E-mail: b229237@dac.unicamp.br. Phone: +55 (18) 98193-8916.

ABSTRACT

The term ovarian carcinoma (OC) refers to a heterogeneous collection of five distinct diseases known as histotypes. While histotype-specific treatment is still a clinical challenge, well-characterized models are required for testing new therapies. Here, we assessed whether a chemically-induced animal model was representative of human OC by providing histotype classification. To put animal model characterization into context of new potential OC therapies, we employed OncoTherad®, an interferon (IFN-γ)-stimulating immunotherapy mediated by Toll-like receptors (TLR) 2/4, in association or not with Erythropoietin (EPO). Thirty-five Fischer rats were distributed into 5 groups: Control (Sham surgery); Cancer (7,12-dimethylbenzoanthracene – DMBA injection in the ovarian bursa, 1.25 mg/kg); OncoTherad® (20 mg/kg intraperitoneal); EPO (8.4 µg/kg intraperitoneal); and OncoTherad+EPO (same doses). Ovary specimens were formalin-fixed into paraffin-embedded blocks. TLR pathway and the profile of the inflammatory response were evaluated by immunohistochemistry (IHC). After DNA extraction and tissue microarray construction, we assessed typical gene mutations directly (Sanger sequencing) or indirectly (IHC surrogates) and examined biomarkers typical of different OC histotypes. OC induction decreased immunoreactivities of TLR2, TLR4, and proinflammatory cytokines. OncoTherad® alone or associated with EPO was able to prevent ovarian lesions and modulate the OC microenvironment to a cytotoxic immune profile involving TLR signaling. EPO alone was immunosuppressive. The features analyzed favored interpretation of our DMBA-induced tumor model as low-grade serous carcinoma-like in which treatments with OncoTherad® and EPO showed immunomodulatory properties related to the reduction of ovarian lesions.

Key words: ovarian cancer; immunotherapy; DMBA; erythropoietin; OncoTherad; IHC biomarkers.

HIGHLIGHTS

- The new DMBA-induced ovarian cancer model was morphologically and molecularly characterized as low-grade serous carcinoma-like
- OncoTherad® immunotherapy and Erythropoietin showed immunomodulatory and antitumor properties in the OC model
- OncoTherad® alone or associated with EPO modulated the tumor microenvironment to a cytotoxic profile through TLR2 and TLR4 stimulation, increasing proinflammatory cytokines and M1 macrophages
- EPO alone was immunosuppressive through stimulation of TLR2 and increased M2 macrophages and Tregs
- The association of treatments might have triggered a compensatory effect between both

INTRODUCTION

Ovarian cancer (OC) ranks fifth among cancer deaths in women and remains the deadliest of all gynecological cancers [1,2]. Most patients are diagnosed in stages III or IV, whose 5-year survival is about 27% and 13%, respectively [3,4]. These poor survival rates are associated with the high recurrence rate after standard therapy, absence of early-stage disease markers and its asymptomatic nature, as symptoms that could lead to diagnosis tend to manifest after metastasis has already occurred [5]. The OC poor outcomes highlight the need to develop new clinical approaches and especially a better understanding of this disease.

The term ovarian cancer refers to a heterogeneous group of distinct malignant tumors that differ with respect to morphology, etiology, biological behavior, prognosis, molecular, genetic, and clinical attributes [6–8]. Invasive epithelial ovarian cancer (ovarian carcinoma) comprises five major histopathological subtypes: high-grade serous carcinoma (HGSC), endometrioid carcinoma (EC), clear cell carcinoma (CCC), low-grade serous carcinoma (LGSC), and mucinous carcinoma (MC) [6,9]. HGSC can be characterized by near-ubiquitous *TP53* mutation while in LGSC, *TP53* is altered in less than 10% of cases and usually harbors mitogen-activated protein kinase (MAPK) pathway-activating *KRAS* or *BRAF* mutations [10]. MC is associated with *KRAS* mutation and *HER2* gene amplification [11–13] and CCC or EC harbor defects in *PTEN*, *PIK3CA*, and *ARID1A*, consistent with the shared molecular pathogenesis and etiology [8,14–16]. Despite important differences between OC subtypes, including different levels of chemosensitivity, in many cases standard therapies neglect these differences and treat them as a single disease [8]. New therapeutic approaches must take into account the heterogeneity between, and within, the different OC subtypes since it has shown to have a critical influence on treatment response and clinical outcomes [8].

The 7,12-dimethylbenzoanthracene carcinogen (DMBA) is able to induce the formation of neoplasms of epithelial origin with histological, molecular, and dissemination patterns similar to OC in humans, including epithelial and metabolic markers and *TP53* and *KRAS* mutations [17,18]. Since specific treatment for different OC subtypes is still a clinical challenge, these models are useful to test therapeutic interventions considering the molecular features, components of the tumor microenvironment including aspects of the immune system, and treatment stratification [19]. Further, prior studies in murine models suggest there is some plasticity in the cell of origin that may allow genomic modifications to ovarian surface epithelium to phenotypically mimic a range of ovarian carcinoma histologies [20,21]. Mouse models have been shown to molecularly and phenotypically emulate EC, CCC, and HGSOC

based on modification of ovarian surface epithelium. Yet, their corresponding human disease counterparts are widely accepted to be predominantly from uterine/endometriosis and tubal epithelial origins (respectively) [22–24]. While such models may differ in precise cell of origin, compared to human disease, they are nonetheless useful in preclinical investigations and functional-mechanistic therapeutic evaluations [25,26].

Specific immune activities in the tumor environment have been shown to be associated with positive outcomes in OC [27,28]. OncoTherad® immunotherapy [Biological Response Modifier - Inorganic Phosphate Complex 1 (MRB-CFI-1)] - patents granted in Brazil (BR102017012768B1)[29] and the USA (US11572284B2, US11136242B2)[30] - is a nanostructured inorganic phosphate complex associated to glycosidic protein, developed by University of Campinas, Brazil. This nano-immunotherapy leads to distinct stimulation of the innate immune system mediated by Toll-like receptors (TLRs) 2 and 4, resulting in an increased activation of the interferon (IFN) signaling pathway in preclinical studies and clinical-veterinary trial in dogs [31,32]. In a prospective, single-center, single-arm phase I/ II study (Clinical Trial: RBR-6swqd2) [33] with non-muscle invasive bladder cancer (NMIBC) patients we also demonstrated that OncoTherad® nano-immunotherapy seems a safe and effective treatment option for *Bacillus Calmette-Guérin*-relapsed and/ or intravesical chemotherapy-relapsed NMIBC patients [34,35]. The antitumor and immunomodulatory effects of OncoTherad® are promising and should be analyzed in other cancer types that also establish immunosuppression in the tumor environment, such as OC.

Erythropoietin (EPO) may also play an immunomodulatory role. The anti-inflammatory effects of EPO have been described in different animal models, through the reduction of the expression of pro-inflammatory cytokines and the apoptotic process [36]. In experimental murine models, EPO acted on the activity of B lymphocytes [37], dendritic cells [38], and macrophages [39]. Regarding the ovaries, EPO has shown protective and antioxidant effects in rats and mice, aiding tissue damage and improving follicular survival and functioning [40–42]. The protective effect of EPO has also been reported in female rats undergoing cisplatin chemotherapy, being able to improve ovarian function and prevent infertility [43]. Tamoxifen lipid nanocarriers and surface EPO conjugates have shown promising results with increased cytotoxic activity *in vitro* in human breast adenocarcinoma cells [44] and in rat breast adenocarcinoma models [45]. OC patients are usually of advanced age, postmenopausal, and have low tolerance for anemia [36]. In this way, women with gynecological cancers comprise

a subset of cancer patients who potentially benefit from the use of Erythropoiesis-Stimulating Agents [46].

Given this context, we intended to assess whether a DMBA chemically-induced animal model was representative of human OC. To put animal model characterization into context of new potential OC therapies, we employed OncoTherad® in association or not with Erythropoietin (EPO) and evaluated the TLR pathway and the profile of the inflammatory response. We also assessed both mutational and Immunohistochemistry (IHC) biomarkers routinely used for human OC to provide histotype context in the evaluation of OncoTherad® and EPO effects.

MATERIAL AND METHODS

Drugs and dosages

OncoTherad® (MRB-CFI-1) was synthesized, purified and fully characterized [30,31]. The compounds were suspended in 0.9% saline solution, at a concentration of 20 mg/ml and the established dosage was the therapeutic dose of 20mg/kg, which corresponded to intraperitoneal applications of an average of 0.2ml.

The EPO formulation used was Eritromax®, alpha-epoetin lyophilized powder (rHuEPO, 4,000 IU/ml) from Blau Farmacêutica S.A. (Cotia, SP/Brazil). With 1 µg of the compound being equivalent to approximately 120 I.U., the powder was dissolved in 0.9% saline solution up to a concentration of 33.6 µg/ml (4,000 IU/ml). The dosage used was 1,000 IU/kg or 8.4 µg/kg - adapted from Hardee et al. [47] - corresponding to intraperitoneal applications of an average of 0.05 ml. The association of OncoTherad® (MRB-CFI-1) and Erythropoietin were made in the same doses and diluents as the isolated treatments and the new compounds were characterized by chemical-physical analysis.

Ovarian carcinoma induction and experimental groups

Thirty-five Fischer 344 rats (F344/NTacUnib) with 80 days of age and average weight of 200g, obtained at the Multidisciplinary Center for Biological Research at the University of Campinas (CEMIB/UNICAMP) were used. The animals were kept in a vivarium with adequate and individualized facilities in propylene boxes lined with wood shavings (2 animals/box) and ventilated and sterile mini-isolators, in an appropriate and enriched environment (Supplemental Fig. 1), under controlled conditions of temperature (22 ± 2°C) and light (12h light/dark cycle,

200 lux). All animals received a solid diet consisting of chow (Nuvilab®, Colombo, PR/Brazil) and water *ad libitum*. The experimental protocol followed the ethical principles in animal research according to the National Research Council's Guide for the Care and Use of Laboratory Animals (National Research Council, 2011) and was authorized by the Committee on Ethics in the Use of Animals – CEUA/UNICAMP (**Registration 5555-1/2020**).

The OC chemical induction model consisted of a single injection with 7,12-dimethylbenzoanthracene – DMBA (Sigma Chemical Co, St Louis, Mo) into the ovarian bursa of the left ovary (Chuffa et al. [48]; Supplemental Fig. 2). The animals were anesthetized during the estrus phase, the ovarian bursa was identified and its space filled with a single injection of DMBA at a dose of 1.5 mg/kg of body weight, dissolved in 10 µl of sunflower oil (adapted from Chuffa et al. [48]). Ten rats underwent sham surgery (control), receiving 10 µl of sunflower oil injection under the same procedures as the induced groups. For 150 days on average, the animals were monitored and tumor development was assessed by X-ray computed microtomography (micro-CT). After this period, the animals were divided into five experimental groups (n= 7 animals/group, Fig. 1): **a) Sham Healthy Control (CONTROL):** rats that underwent Sham surgery were treated with 0.3 ml of 0.9% saline solution intraperitoneally, twice a week for 4 weeks; **b) Ovarian Cancer Control (CANCER):** after the development of OC, the rats were treated with 0.3 ml of 0.9% saline solution intraperitoneally, twice a week for 4 weeks; **c) Treated with OncoTherad® (ONCOTHERAD):** after the development of OC, the rats were treated with OncoTherad® (MRB-CFI-1) 20mg/kg, intraperitoneally, twice a week, for 4 weeks; **d) Treated with Erythropoietin (EPO):** after the development of OC, the rats were treated with epoetin alfa (rHuEPO) 1000 IU/kg, intraperitoneally, twice a week, for 4 weeks; **e) Treated with OncoTherad® and Erythropoietin (ONCO+EPO):** after the development of OC, the rats were treated with OncoTherad® (MRB-CFI-1) 20mg/kg and epoetin alfa (rHuEPO) 1000 IU/kg, via intraperitoneal, 2 times a week for 4 weeks.

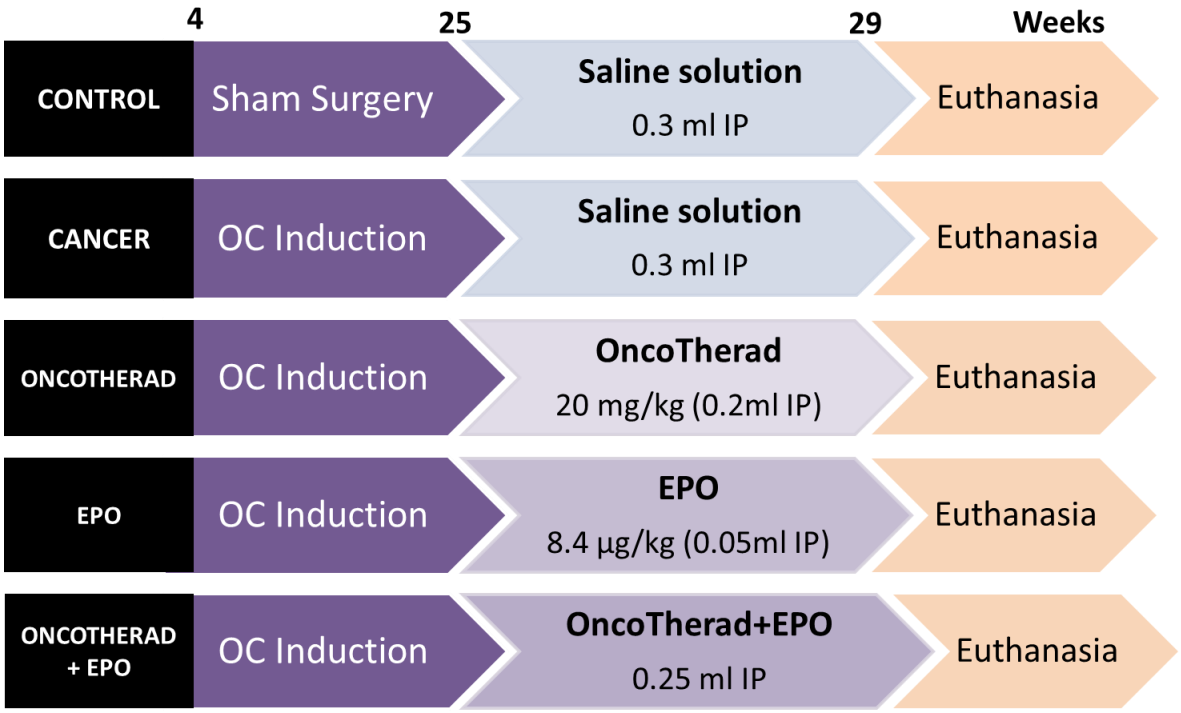

Fig. 1. Experimental protocol according to weeks. In the 3rd and 4th weeks, chemical induction surgeries of OC and Sham surgery were performed. The period between the 4th and 25th week corresponds to the period of tumor development. The period between the 25th and 28th week corresponds to the 4 weeks of treatments with OncoTherad® (20mg/kg); Erythropoietin (EPO, 8.4 µg/kg); OncoTherad® associated with Erythropoietin in the same doses of the isolated treatments. Treatments were carried out twice a week for 4 weeks. The 29th week corresponds to the euthanasia of the animals.

X-ray computed microtomography (micro-CT)

In vivo monitoring and three-dimensional investigation of tumor development were performed in all animals using X-ray computed microtomography (micro-CT) with the Skyscan 1178 device (SkyScan 1178, Bruker, Brussels, Belgium). The microtomography scanner of the Institute of Biology at UNICAMP and is located at the Multiuser Laboratory of Cellular and Molecular Biology, building OCRC – Research Center on Obesity and Comorbidities at UNICAMP. The animals were anesthetized with 10% ketamine (60 mg/kg, via i.p.) and 2% Xylazine (5 mg/kg, via i.p.) and placed in dorsal decubitus on the scanner bed (Supplemental Fig. 3). Capture was performed using the following acquisition parameters: exposure of 480 ms; rotation step 0.18°; 0.5mm aluminum filter; voltage source 65 kV; current voltage 314 uA; 360º rotation and 84.60 µm image pixel size. The images transmitted from the scan were three-

dimensionally reconstructed using the NRecon software version 1.6.10.2 (SkyScan, Bruker), which uses the filtered back-projection algorithm, based on the images acquired by the scanner.

Estrous Cycle Assessment

The estrous cycle was monitored by cytological examination in order to assess the presence of cyclicity during the experimental period. Cytological examination was performed daily at the beginning of the vivarium's light phase, in which the vaginal washing technique was applied [49]. The material was prepared through the usual cytological technique, with fresh analysis and with Shorr and Hematoxylin staining and the corresponding phases of the estrous cycle were analyzed in light microscopy and identified based on the cell types present: a) proestrus, consisting of cells nucleated epithelium; b) estrus, with a predominance of anucleated keratinized cells; c) metestrus, consisting of leukocytes in combination with keratinized cells and mucus; d) diestrus, with predominance of leukocytes and mucus [49,50].

In order to quantitatively and statistically evaluate the estrous cycle of the rats, data from periods of 15 complete and consecutive days were analyzed in 3 specific phases of the experimental period: (1) before surgery for OC induction, (2) after tumor development (before treatment) and (3) after treatments (before euthanasia). The quantitative parameters evaluated over periods of 15 consecutive days were: (1) Cycle Length (number of days between one estrus and the next estrus); (2) Number of Estrus (number of days in the estrus phase); and (3) Number of Diestrus (number of days in the diestrus phase).

Macroscopic Evaluations

Macroscopic analyzes and photographic records with a scale of the reproductive tract were performed at the time of euthanasia of the animals. The absolute weights of the ovaries and uteri were recorded and the relative weight was also calculated (g/100g of body weight).

Survival Analysis

Mortality data were collected throughout the experimental period, considering all spontaneous deaths that occurred during tumor development and the treatment period. For survival analysis, the Kaplan-Meier method was used, which estimates the probability of survival during the period considered and for making the graph. The period considered was after the OC induction surgery until the date of death of the animal (in the case of spontaneous death) or until the moment of euthanasia. The log-rank test was used to assess whether there were differences in survival between experimental groups.

Tissue processing and histology analysis

At the end of the experimental period, the females were euthanized in the diestrus phase for standardized anatomical-morphological analysis. The ovaries were collected and fixed in a 10% formalin buffer solution (in PBS, v/v) for 24 hours. Subsequently, the fixative was removed by bathing in running water and the material was dehydrated in increasing solutions of ethyl alcohol, cleared in xylene and included in Paraplast (Oxford Labware, St. Louis, USA). 5µm-thick sections made in a Leica RM2165 microtome were transferred to silanized slides and stained by Hematoxylin-Eosin (HE) techniques for histopathological analysis under light microscopy performed by a specialized pathologist.

Immunohistochemistry for TLR2, TLR4, IL-6, IFN-γ, iNOS, F4/80, CD163, FOXP3: Quantitative Analysis

5µm sections of the ovaries were also used for immunostaining. The EasyLink One kit (EasyPath EP-12-20504 São Paulo, Brazil) was used for antigen detection according to the manufacturer's instructions. Antigenic retrieval was performed by incubating the sections in citrate buffer (pH 6.0) at 100°C in a microwave oven. The endogenous peroxidase blockade used was the Peroxidase Blocker (EP12-20523) with subsequent incubation in a 5% Goat Serum blocking solution (EP-12-20532) for 10 minutes at room temperature. Subsequently, the TLR2, TLR4, IL-6, IFN-γ, iNOS, F4/80, CD163, FOXP3 antigens were located through specific primary antibodies (Supplemental Table 1), diluted in 1% Goat Serum (EP-12-20532) and stored overnight at 4 ºC. After washing with TBS-T buffer, the sections were incubated with HRP-polymer (EP-12-20503) from the EasyLink One kit for 25 min and, subsequently revealed with diaminobenzidine (DAB), counter-stained with Harris Hematoxylin and evaluated in the DM2500 photomicroscope (Leica, Munich, Germany).

To assess the intensity of antigen immunoreactions, five fields were examined at 100x magnification per animal and for each antibody. The analysis of the immunoreaction was performed globally, that is, considering the sections that included the gonad as a whole, including all the constituent structures (corpora lutea, healthy and atretic follicles of all stages, interstitial tissue, among others) for all groups. Immunoreactivities were quantified using the Image J software (https://imagej.nih.gov/ij/) in the IHC Profile analysis for the quantification of antigen-positive cells [51]. Quantitative data were evaluated in two ways: Total Immunoreactivity and Immunoreactivity Intensity. Total immunoreactivity was obtained as the result of the percentage of ovarian cells negative for a given antibody subtracted from 100%,

that is, the values represent the total number of cells in the field that showed immunoreactivity for the evaluated antibody. The analysis of the Immunoreactivity Intensity was performed from the categorization of the immunoreaction occurring in the cells by intensity criterion. The categories defined in the Image J software were: absent (Negative), weak (Low Positive), moderate (Positive) and strong (High Positive). The values obtained in the different intensity categories were represented in column graphs and are equivalent to the percentage of cells in the field that showed marking at each level (absent, weak, moderate or strong) for each antibody.

Tissue Microarray (TMA) and Immunohistochemistry for histotyping

Tissue microarrays (TMAs) were constructed from the formalin-fixed paraffin-embedded donor blocks containing the left ovary of all animals. Representative lesions cores (1.0 mm, in duplicate when it was possible), previously identified and marked by the pathologist, were punched and then arrayed in a recipient paraffin block using a semi-automated Pathology Devices Tissue micro-Arrayer®. In the case of the Healthy Control Group, representative colors of the normal tissue were also arrayed. Uninvolved rat tissues (spleen kidneys, uterus, mammary gland, and tests from the Center for Comparative Medicine – Animal Care Services of the University of British Columbia (UBC) were also represented on the TMAs to aide in optimization and positive control staining for antibodies. The tissue microarray (TMA) blocks were sectioned using standard microtomy.

Immunohistochemistry (IHC) was carried out using four-micron (4 μm) sections of TMAs that were immunostained on a Leica Bond Rx autostainer (Agilent Technologies). Briefly, sections were deparaffinized in xylene, and dehydrated through an alcohol series with sequential reduction in water content. Heat and pH-based antigen retrieval were used as appropriate for the epitope and antibody. Endogenous peroxidase activity was blocked in 3% hydrogen peroxide. Slides were then incubated with the target antibodies and developed with appropriate secondary detection systems followed by DAB chromogen. Finally, sections were counterstained with hematoxylin and mounted [11]. Sections of the TMAs of positive controls for the antibodies (spleen kidneys, uterus, mammary gland, and testes donated by the Centre for Comparative Medicine - UBC) were used for the optimization and the establishment of the protocol conditions. The primary antibodies used and the final dilutions were represented in Supplemental Table 2.

The IHC Scoring for Wt1, Arid1A, Hnf1b, and Pr considered two types of regions 1) the whole epithelium and 2) abnormal cells in the stroma according to the alterations described in

the previous histopathological analysis. The staining was classified in negative, positive, or heterogeneity. The heterogeneity pattern of staining was defined as a core that showed at least one region where there was positive staining in some cells as well as negative cells for the antigen.

The IHC Scoring for p53 as defined based on the staining pattern found in Control. In this way, the scores were defined as: 1 (Normal) - occasional nuclear positive cells and cytoplasmic positivity; 0 (Abnormal) - complete absence in epithelial cells but "normal" pattern in stroma; 2 (Abnormal) - strong nuclear expression in virtually all epithelial cells and cytoplasmic positivity, normal pattern in stroma; 3 (Abnormal) - cytoplasmic staining in epithelial cells (very rare nuclear positivity), normal pattern in stroma). The same scores were used for the abnormal structures in the ovarian stroma.

CD3 positive cells count

For CD3 positive cell count, immunohistochemistry (IHC) was carried out using four-micron (4 μm) sections of TMAs. The total number of positive cells were counted considering the non-tumor areas (normal) and the abnormal/tumor regions separately. For each core, the area of the two areas was assessed and the final count was the number of CD3 positive cells/μm^2/type of region. All the measurements and counts were performed in the Aperio Image Scope Software version 12.4.6.5003 (Leica Biosystems). The results were evaluated in two ways: 1) Comparison among the groups with Kruskall Wallis test and 2) Comparison between the non-tumor and abnormal/tumor areas inside each experimental group, using T paired Test.

Analysis of ovarian cancer driver mutations

We tried to identify driver mutations in our samples to compliment and corroborate IHC results. While it has been relatively commonplace in human disease, we designed and tested rat-specific primers and short-amplicon sequencing required for testing of DNA from Formalin-fixed, paraffin-embedded (FFPE) tissues.

Primer Design

The equivalent mutation hotspots between human genes and their rat paralogues were researched and *in silico* primer design was undertaken for sequencing assays (detailed information is in the "Primer Design" file attached to this report submission process on Sage website). The primers (Table 1) were designed for *Kras*; *Pik3ca*; and *Ctnnb1* (hotspots only).

Primer 3 Plus web interface - https://www.primer3plus.com/ [52] was used to design the primers from the DNA sequence. BLAT from Genome Browser – https://genome.ucsc.edu/cgi-bin/hgBlat (University of California Santa Cruz, Genomics Institute) was used to check the specificity of the primers to the hotspot only.

Table 1. Primers used for PCR amplification and sequencing.

Gene	Exon	Targets (Codons)	Primer	Sequence
Kras	1	12, 13	Forward	5′ - AGGCCTGCTGAAAATGACTGA - 3′
			Reverse	5′ - AGGGTGGCAGTCATCCTTTGTG - 3′
Pik3ca	9	542, 545	Forward	5′ - AACAGCTCCGAGCACTTTGT - 3′
			Reverse	5′ - ACCCATGAGAGTGACCCAGA - 3′
Pik3ca	20	1043, 1047	Forward	5′ - TCTCCATGATGCTTGGCTCC - 3′
			Reverse	5′ - TGAACTGAGATGGCAGCTGG - 3′
Ctnnb1	2	32, 33, 34, 37, 41, 45	Forward	5′ - AGTTGGACATGGCCATGGAG - 3′
			Reverse	5′ - AGTCCTTCACGCAAGAGCAA - 3′

Microdissection

Five-micron (5 µm) sections of the FFPE blocks were stained with Hematoxylin to facilitate the identification of the abnormal regions. Using a dissection microscope, the tissue of interest was separated and collected using 20G bevel-tip needles and DNase/RNase free H_2O. The tissue was transferred to PCR tubes containing 12µl of Proteinase K buffer each (reconstituted from PicoPure DNA Extraction Kit, Applied Biosystems, Thermo Fisher Scientific) and then kept in a -20ºC freezer.

The dissection of the areas of interest was enriched for abnormal regions (when it was possible) using corresponding Hematoxylin and Eosin (H&E) slides as a reference. In the case of the Healthy Control Group all the ovarian tissue was collected.

DNA Extraction and Quantification

DNA from the ovaries specimens was extracted using the PicoPure DNA Extraction Kit, Thermo Fisher Scientific). For the primers testing, DNA of the uninvolved rat tissues (spleen kidneys, uterus, mammary gland, and testes) donated by UBC were extracted after scrolling and deparaffinization as there was no specific area of interest.

155ul of reconstitution buffer from PicoPure DNA Extraction Kit were added to the tubes containing microdissected tissue and 12µl of ProK buffer. The samples were centrifuged for 15 minutes to pull all tissue pieces from the sides of the tubes. After, the samples were put to digest overnight at 65°C in the MiniAmp™ Plus Thermal Cycler (Thermo Fisher). In the next morning, 3 µl of ProK buffer and 1 µl of ProK solution (20 mg/mL) were added to each tube as well as H_2O up to a total volume of 16 µl (to compensate for evaporation of buffer in the tubes). The digesting was continued at 65°C for another 2-4 hours. Afterwards, the ProK was inactivated by incubating the samples at 90°C for 10 minutes. 1 µl of each sample was reserved for quantification with QuBit assay, while the remainder was stored in a -20°C freezer. DNA concentration was quantified using a Qubit 2.0 Flu-orometer (Thermo Fisher Scientific) and the Qubit™ dsDNA HS Assay Kit (Thermo Fisher Scientific) following the manufacturer's protocol.

PCR

The regions containing the hotspots of *Kras*, *Pik3ca*, and *Ctnnb1* were amplified using the primers described in Table 2. The PCR reaction was performed in a 20 µL volume mixture containing 5 ng of DNA (5ng/µL diluted in Tris 10 µM), 18 µL of Platinum™ PCR SuperMix High Fidelity (Invitrogen, Thermo Fisher), and 1 µL of Primer Working Solution (20 µM of each forward and reverse primer diluted in Tris 10 µM). The PCR amplification was performed in the MiniAmp™ Plus Thermal Cycler (Thermo Fisher) under the following cycling conditions: initial denaturation at 94°C for 10 minutes, followed by 35 cycles of denaturation at 94°C for 10 seconds, annealing at 58°C for 15 seconds, and extension at 68°C for 30 seconds, and final extension at 68°C for 10 minutes.

Gel electrophoresis was performed to confirm the amplicon's presence. The expected PCR product size was ~200 base pairs (bp). We used a 2% agarose gel and GelPilot DNA Molecular Weight Markers 100bp (QIAGEN, Germantown, EUA) as a ladder.

Sample preparation for sanger sequencing and mutation analysis

Ten microliters of amplified products were then purified with 4 µL of ExoSAP-IT PCR Product Clean up (Applied Biosystems, Thermo Fisher). The mixture was treated at 37°C for 15 minutes, followed by enzyme deactivation at 80°C for 15 minutes. DNA concentration was quantified again using a Qubit 2.0 Flu-orometer (Thermo Fisher Scientific) and the Qubit™

dsDNA HS Assay Kit (Thermo Fisher Scientific). Each sample was diluted to 1 ng/µL in a volume of 10 µl per sequencing reaction and 5 µl of CS1 and CS2 primers (5 µM) were added. Four 96 well PCR rigid plates were sent to Azenta Life Sciences (Seattle, EUA) for Sanger DNA Sequencing.

Sequence analysis was performed using Mutation Surveyor® DNA Variant Analysis Software (SoftGenetics, State College, EUA) to compare sample sequences to a reference sequence.

Statistical Analysis

The quantitative data obtained were represented as mean ± standard deviation and evaluated by means of ANOVA parametric analysis of variance, complemented with the Tukey test, when it presented normality and homoscedasticity. In cases of absence of normality, the Kruskal-Wallis non-parametric analysis of variance was used, complemented by the Student-Newman-Keuls test. Estrous cycle data and weights were presented in tables and graphs, and the graphical representation was performed by bar graph and Box Plot graph. The Kaplan-Meier method was used for survival analysis, and the log-rank test (Mantel-Cox) was performed to assess differences in survival between experimental groups. For the quantitative immunohistochemical analyses, the average of the total immunoreactivity for each group and for each antibody was calculated and the data were examined in the above mentioned analysis of variance depending on the characteristics of each set. Immunoreactivities by category of labeling intensity were represented in voice graphs and data were evaluated using two-way analysis of variance (two-way ANOVA), complemented by Tukey's test for each level of immunoreaction (absent, weak, moderate or strong). The results of CD3 positive cells were evaluated in two ways: 1) Comparison among the groups with Kruskall Wallis test and 2) Comparison between the non-tumor and abnormal/tumor areas inside each experimental group, using T paired Test. The softwares used for analysis and creation of graphs were GraphPad Prism, version 7.00 (GraphPad Software Inc., San Diego, California, USA), BioEstat 5.0 (Sociedade Civil Mamirauá/CNPq, Belém, PA, Brazil), and R Statistical Package, version 4.0.2 [53]. Statistical significance was 5% ($p<0.05$) for all applied tests.

RESULTS

DMBA OC induction led to cycle dragging by causing persistent diestrus

Analysis of the estrous cycle of Healthy Control and Cancer Control rats showed that neither Sham surgery nor chemical induction of ovarian cancer with DMBA inhibited cyclicity. Furthermore, treatments with OncoTherad® and Erythropoietin, alone or in association, also did not prevent the cyclicity that was confirmed by the occurrence of the estrus phase recurrently. The rats in the experimental groups exhibited all phases of the estrous cycle (Fig. 2) and it was possible to verify the occurrence of ovulation by the presence of the estrus phase.

Prior to the start of the OC induction surgeries with DMBA, the rats of all groups did not present significant differences ($p>0.05$) in the duration of the estrous cycle, number of days in estrus and in diestrus (Fig. 3). The average duration of the cycle was between six and seven days, and around three days in the estrus phase and 5 to 6 days in the diestrus phase, considering a period of 15 days. At the end of the tumor development period, it was possible to observe an increase in absolute numbers in the duration of the estrous cycle and in the number of days of estrus in the OC-induced rats in comparison with the Healthy group (Fig. 3), although these differences were not statistically significant ($p>0.05$). Regarding the number of diestrus, there were also no significant changes ($p>0.05$) when comparing the groups (Fig. 3).

At the end of the treatment period (before euthanasia of the animals), all groups in which the rats were induced to OC (Cancer, OncoTherad, EPO and OncoTherad+EPO) exhibited an increase ($p<0.05$) in cycle length estrous compared to the Healthy group (Fig. 3). This cycle drag was confirmed by the greater ($p<0.05$) number of days of estrus in these same groups compared to the Healthy Control group (Fig. 3). In addition, it was possible to notice that the treatments did not change the estrous cycle or accentuate the changes resulting from induction, since the same cycle pattern was observed in the Cancer group without treatment before euthanasia. Regarding diestrus, there were no statistically significant differences ($p>0.05$) between groups at the end of treatments (Fig. 3).

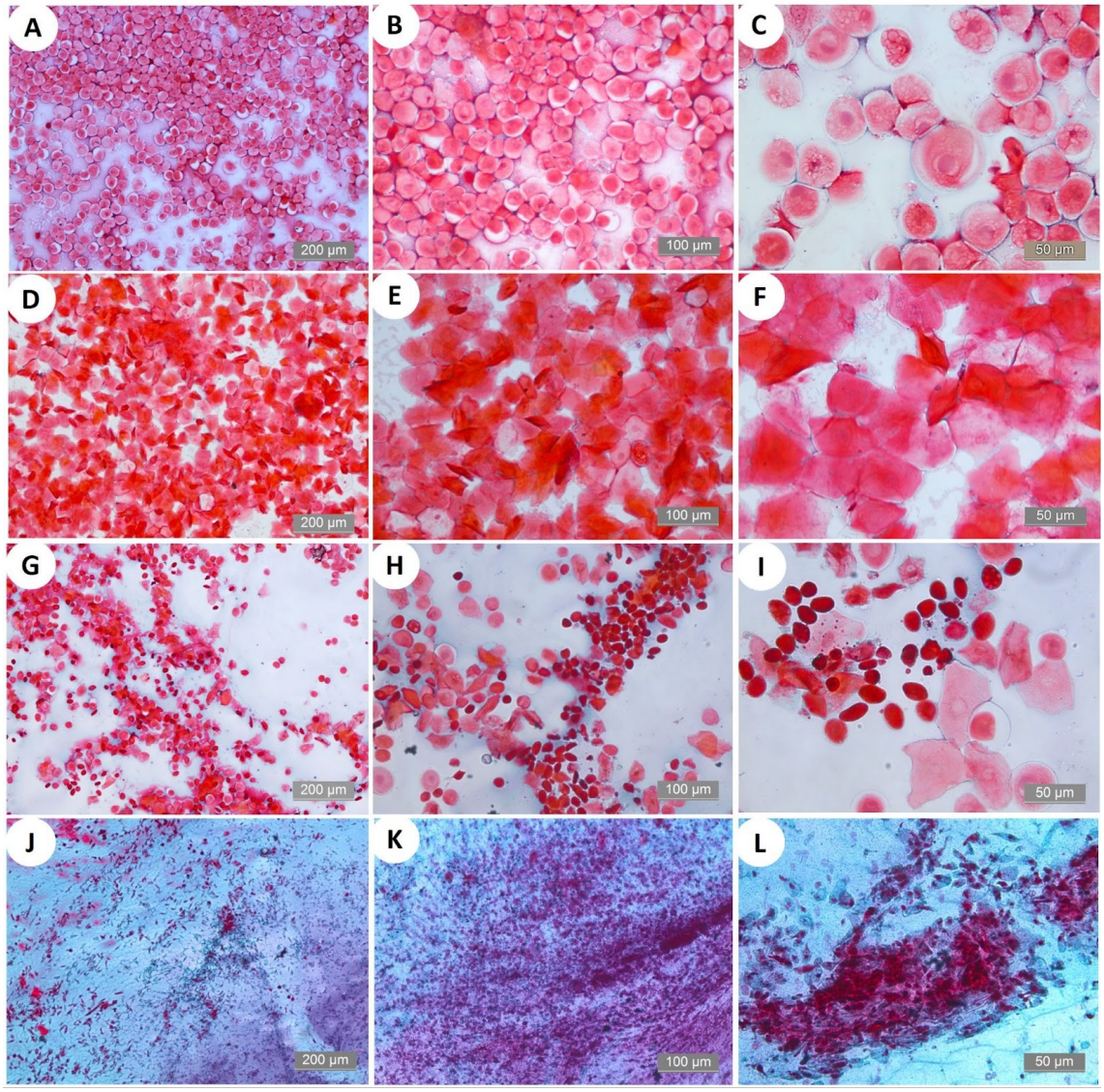

Fig. 2. Phases of the Estrous Cycle. Images obtained after the examination of vaginal cytology for the identification of the phases of the cycle in magnifications of 100x and 200x (visualization of the proportion between the different cell types) and 400x (identification and confirmation of the cell type). (A-C) Proestrus, consisting mostly of nucleated epithelial cells. (D-F) Estrus, with a predominance of anucleated keratinized cells. (G-I) Metaestrus, consisting of leukocytes in combination with keratinized, nucleated epithelial cells, and mucus. (J-L) Diestrus, with predominance of leukocytes and mucus. Shorr stain and Hematoxylin. Bars = 200 µm (A, D, G, J); 100 µm (B, E, H, K) and 50 µm (details in C, F, I, L).

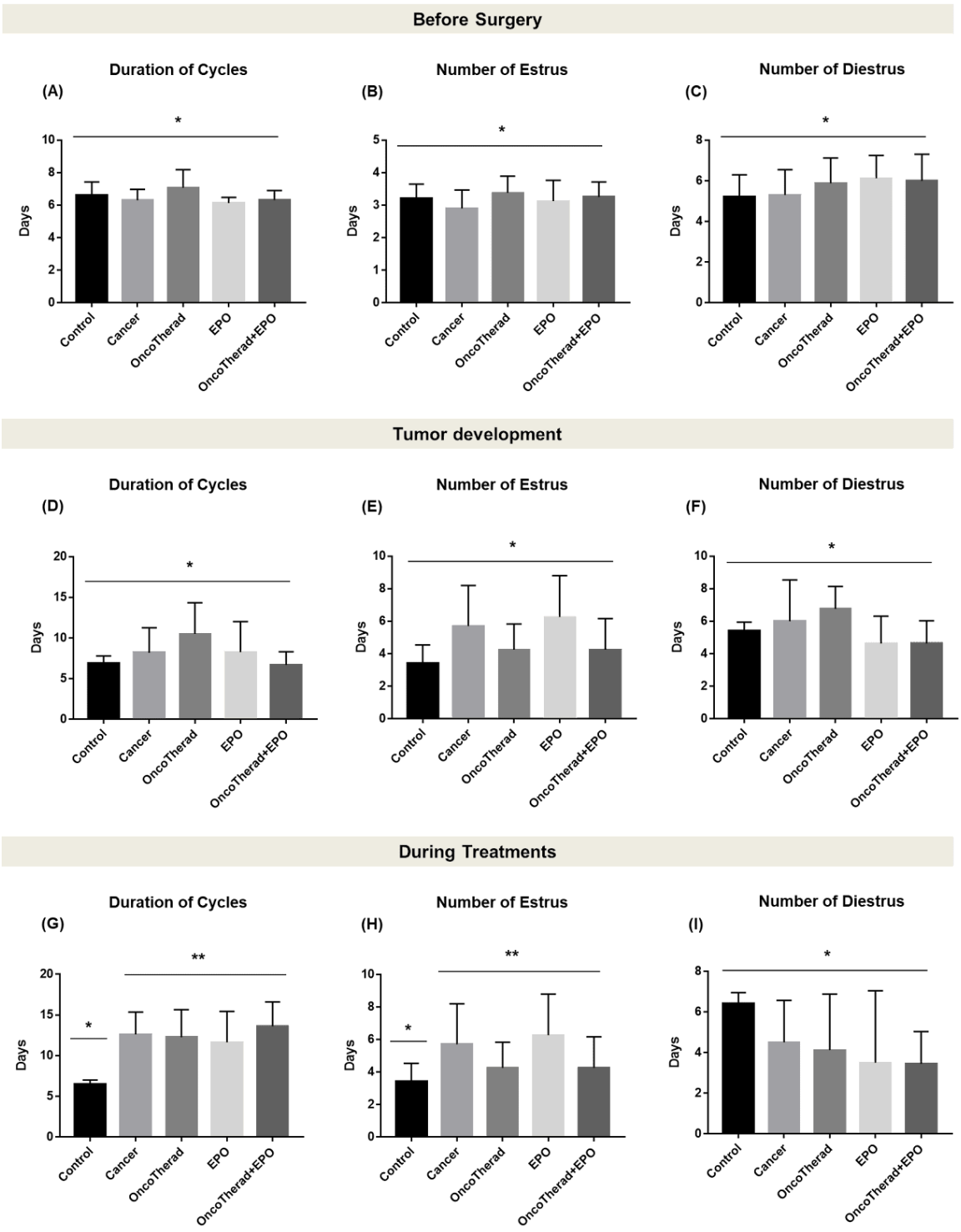

Fig. 3. Estrous Cycle Parameters before OC induction surgery (A-C); before treatments (D-F); and before euthanasia (G-I). (A, D, G) Cycle length in days. (B, E, H) Number of days in the estrus phase in a consecutive 15-day period. (C, F, I) Number of days in the diestrus phase in a consecutive 15-day period. Values expressed as mean ± standard deviation. */** Different symbols indicate statistically significant differences ($p<0.05$). (A, B, D, F, G, H, I) Kruskal-Wallis, Student-Newman-Keuls test. (C, E) ANOVA.

Ovarian weight did not change after OC induction with DMBA

The absolute and relative weights (g/100g of body weight) of the left ovary did not show statistically significant differences ($p>0.05$) between the experimental groups (Fig. 4). Despite this, it is possible to observe in the graphs that the groups that were induced to ovarian cancer have the highest values of absolute and relative weight of the left ovary. Micro-CT examination also showed that most of the rats submitted to OC induction had apparently larger and more visible left ovaries compared to the rats in the Healthy Control group (Supplemental Fig. 4). In the OncoTherad+EPO group, the maximum value due to one animal is very different from the median of the group and the others groups. Regarding the right ovary, the experimental groups did not present significant differences ($p>0.05$) in the absolute and relative weights of the gonad (Fig. 4). It is possible to observe from the graph that the medians of the groups are close and the highest maximum value is found in the cancer group. The rats in the OncoTherad group had a lower ($p<0.05$) uterine weight, both in the analysis of absolute and relative weight, compared to the Cancer and OncoTherad+EPO groups (Fig. 5).

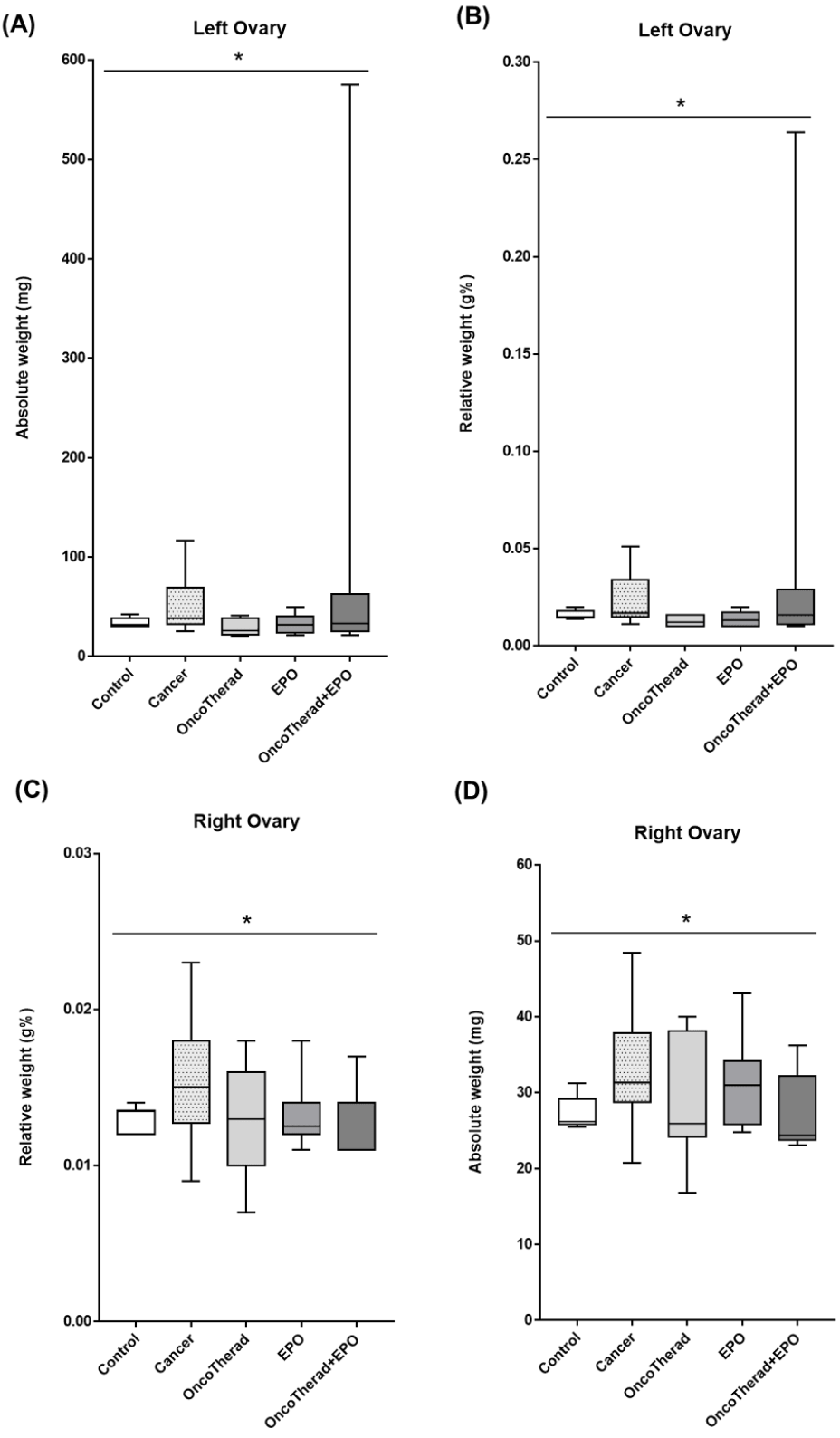

Fig. 4. Absolute and relative weight of the left and right ovaries of the females in the experimental groups. (A, C) Absolute weight in milligrams (mg). (B, D) Relative weight in g% (g/100g of body weight). Kruskal-Wallis Test, Student-Newman-Keuls Test. Equal symbols indicate no significant difference between groups ($p>0.05$).

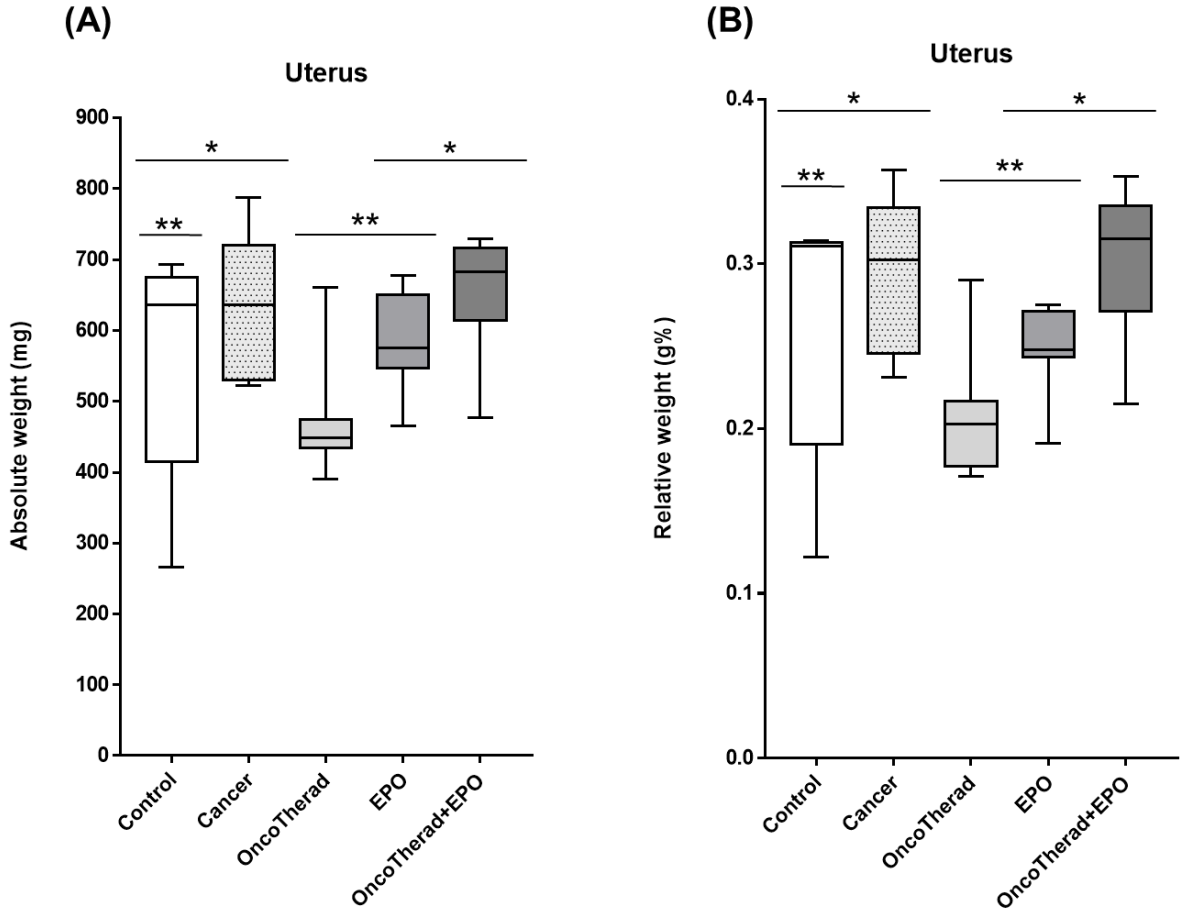

Fig. 5. Absolute and relative weight of the uterus of the females in the experimental groups. (A) Absolute weight in milligrams (mg). (B) Relative weight in g% (g/100g of body weight). Kruskal-Wallis Test, Student-Newman-Keuls Test. Distinct symbols indicate a significant difference between groups ($p<0.05$).

OC chemical induction did not alter the survival of the animals

From the interpretation of the Kaplan-Meier curve (Fig. 6), it was possible to notice that the lowest survival rate was found in the Cancer group, which from the 22nd to the end of the 29th week was on average 83.33%. The OncoTherad group had a survival rate of 87.5% from the 28th week onwards, while in the OncoTherad+EPO group this rate was 90% from the 23rd week onwards. The Healthy Control and EPO groups exhibited 100% survival over the entire period. Possibly, the occurrence of deaths was related to tumor development, since, for example, the incidence of death in the OncoTherad+EPO group occurred from the 23rd week, that is, before treatment with the drugs.

However, these differences in survival rates were not statistically significant (p>0.05) by the log-rank test (Mantel-Cox) (Fig. 6), that is, it is not possible to state that the OC induction performed promoted a reduction of survival compared to healthy animals. In addition, the OC chemical induction also did not alter the body weight, the weekly weight gain, or feed intake (Supplemental Tables 3 and 4; Supplemental Fig. 5). Furthermore, treatments with OncoTherad® and Erythropoietin, alone or in association, did not change the survival of the animals.

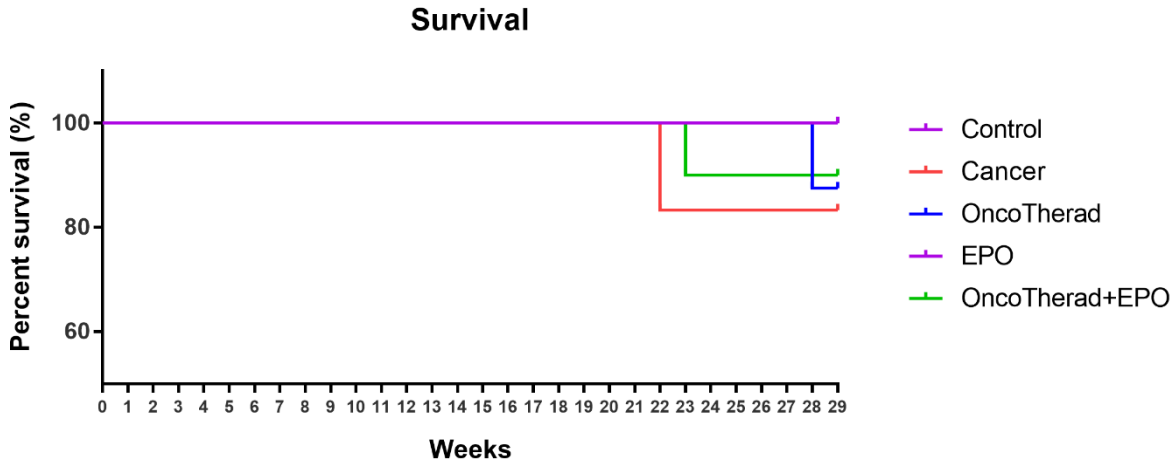

Fig. 6. Kaplan-Meier curve showing the survival rates (%) of the groups over the experimental period. From the 1st to the 2nd week: period before OC induction. In the 3rd and 4th weeks, chemical induction surgeries of OC and Sham surgery were performed. The period between the 4th and 25th week corresponds to the period of tumor development (around 140 days). The 25th and 28th week corresponds to the 4 weeks of treatments with OncoTherad®, Erythropoietin and OncoTherad® associated with Erythropoietin. The 29th week corresponds to the euthanasia of the animals. log-rank test (Mantel-Cox) p=0.639.

OncoTherad® associated with EPO reduced the incidence of macroscopic lesions in OC induced animals

The macroscopic description of the organs of the reproductive tract with due photographic record with scale (Fig. 7) took place at the time of euthanasia. The animals that were part of the Healthy Control group did not present any macroscopically visible structural alteration in the reproductive tract (Table 4, Fig. 7A - C), and in the uterus intrauterine secretion and a wall with a slightly translucent appearance were observed (Fig. 7A, B). The left ovaries presented a

healthy aspect with the presence of visible corpora lutea and a normal-appearing fallopian tube, resembling the right ovaries (Fig. 7C). On the other hand, in the Cancer Control group (Fig. 7D - F) the left ovaries showed diverse alterations such as: presence of cystic nodular lesion (71.4%) and more vascularized aspect (Fig. 7E and F). In general, the lesions observed had a solid appearance with cystic areas around them, yellowish color (with variation in color intensity, darker or lighter yellow), rounded shape with a diameter of less than 3 mm and a diameter greater than 5 mm, approximately (Fig. 7F). Other abnormalities observed in some of the animals submitted to chemical induction of ovarian cancer were: more edematous aspect of the uterus (14.3%) and of the right ovaries (28.6%) as well as the presence of implants in the peritoneum (28.6%) (Table 2).

Regarding the OncoTherad group (Fig. 7G - I), it was possible to notice that most of the left ovaries had no apparent lesions and the presence of corpora lutea (85.7%) and, in some animals (57.1%), the gonad was slightly more atrophied (Fig. 7I). Only one rat differed from the rest of the OncoTherad group, with the presence of a solid mass with cystic areas, brownish in color and measuring around 7 x 10 mm in diameter adhered to the left ovary. With the exception of this animal, in which the right ovary had a more atrophied appearance and had a peritoneal implant, in the other rats the right uteri and ovaries presented a healthy macroscopic appearance (Fig. 7H and I), including some with the presence of functional cysts in the ovary (Fig. 7I).

In the EPO group (Fig. 7J - L), it was possible to identify left ovaries with a more edematous appearance (Fig. 7L) or slightly atrophic (28.6% for both) as well as some with no apparent macroscopic lesions (71.4%). Two rats exhibited possibly neoplastic implants in the intraperitoneal fat, with a cystic nodular appearance and yellowish color or a more solid, heterogeneous and brownish appearance (Fig. 7J), accompanied by more edematous left ovaries with several corpora lutea (Fig. 7L). In general, the right ovaries and uteri of rats treated with Erythropoietin exhibited a healthy macroscopic appearance (Fig. 7K and L).

In the OncoTherad+EPO group (Fig. 7M - O), left ovaries with different aspects were identified, such as macroscopically normal without apparent lesions (57.1%), more edematous (14.3%), slightly atrophic (42.9%) or with adherent nodules (28.6%). Two female rats had cystic nodular lesions, yellowish in color and approximately 3 x 4 mm in diameter, adhered to the left ovary (Fig. 7N and O). Another rat exhibited a solid lesion, with a heterogeneous appearance, with reddish and yellowish regions, measuring 8 x 13 mm, where it was not possible to isolate the left ovary from the lesion. In one rat of the group, a peritoneal implant

was found. In general, the right ovaries and uteri of animals in the OncoTherad+EPO group exhibited a healthy macroscopic appearance (Fig. 7M and N).

Table 2. Frequency of macroscopic changes in different experimental groups.

Anatomopathological features	Experimental Groups (n=7 animals/group)				
	Control	**Cancer**	**OncoTherad**	**EPO**	**OncoTherad+EPO**
Left ovary injury					
Absent	7/7 (100%)	2/7 (28.6%)	6/7 (85.7%)	6/7 (85.7%)	4/7 (57.1%)
nodular cystic	0	5/7 (71.4%)	0	1/7 (14.3%)	2/7 (28.6%)
purely cystic	0	0	0	0	0
solid mass	0	0	1/7 (14.3%)	0	1/7 (14.3%)
Atrophy					
Absent	7/7 (100%)	5/7 (71.4%)	2/7 (28.6%)	5/7 (71.4%)	3/7 (42.9%)
Present in the left ovary	0	2/7 (28.6%)	4/7 (57.1%)	2/7 (28.6%)	3/7 (42.9%)
Present in the right ovary	0	0	1/7 (14.3%)	0	1/7 (14.3%)
Edema					
Absent	7/7 (100%)	3/7 (42.9%)	7/7 (100%)	5/7 (71.4%)	6/7 (85.7%)
Present in the left ovary	0	0	0	2/7 (28.6%)	1/1 (14.3%)
Present in the right ovary	0	2/7 (28.6%)	0	0	0
Present in uterus	0	1/7 (14.3%)	0	0	0
Peritoneal implant					
Absent	7/7 (100%)	5/7 (71.4%)	5/7 (71.4%)	5/7 (71.4%)	6/7 (85.7%)
Present	0	2/7 (28.6%)	2/7 (28.6%)	2/7 (28.6%)	1/7 (14.3%)

The incidence is represented as: number of animals that presented a certain characteristic / total number of animals in the experimental group.

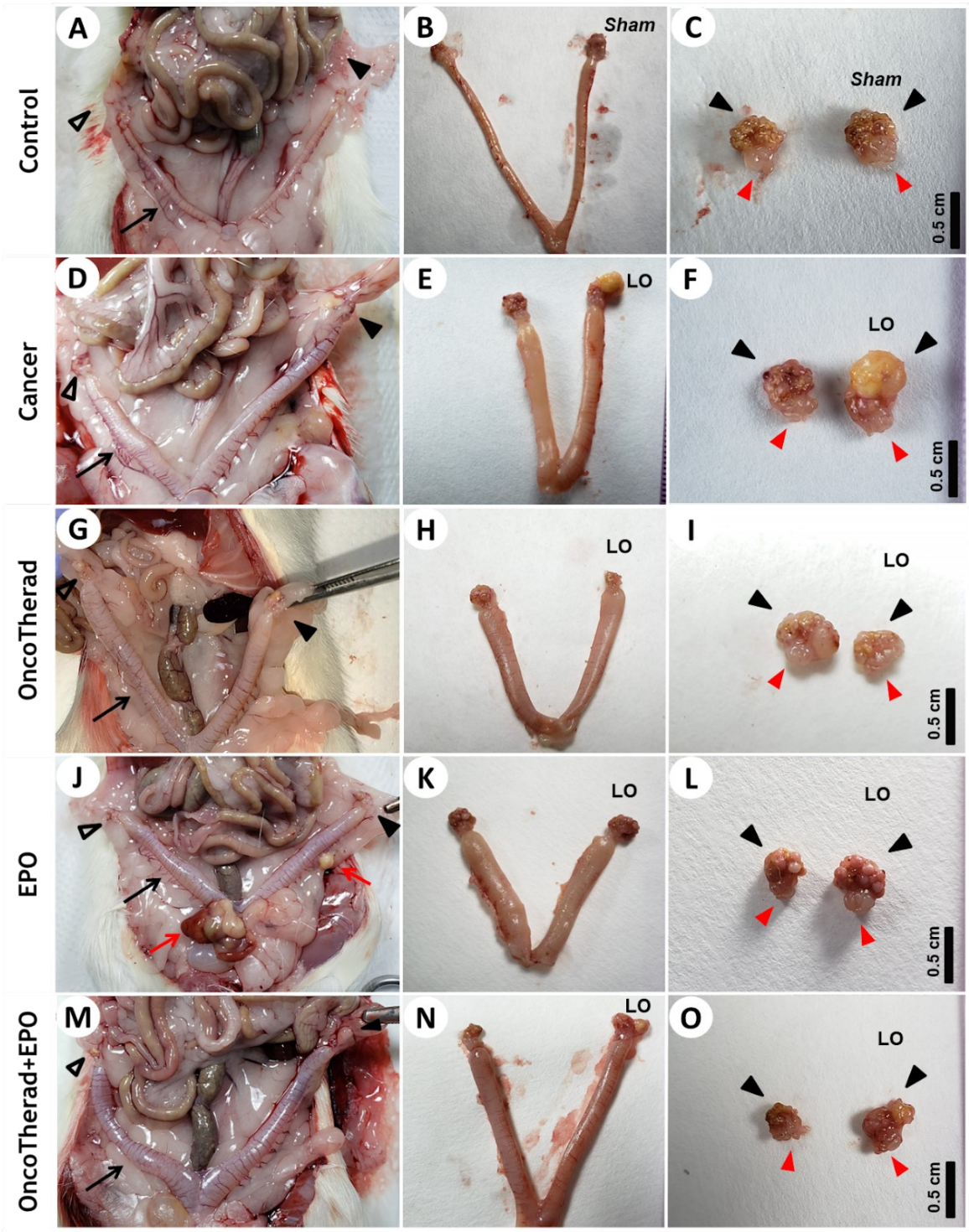

Fig 7. Macroscopic description of the reproductive tract of females from the Healthy Control (A-C), Cancer Control (D-F), OncoTherad (G-I), EPO (J-L) and OncoTherad+EPO (M-O) groups. (A) Exposure of the reproductive tract after incision of the abdominal cavity, highlighting the right ovary (open arrowhead), left ovary submitted to Sham surgery (closed arrowhead) and uterus (arrowhead). (B) Detail of the healthy-looking reproductive tract, with no apparent alterations in the left ovary. (C) Detail of the right and left ovaries (black arrowhead) of normal appearance, with visible corpora lutea and uterine tubes (red arrowhead). (D) Exposure of the

reproductive tract of female rats induced to ovarian cancer, showing the presence of structural alterations in the left ovary (closed arrowhead). (E) Detail of the reproductive tract, the presence of a yellowish cystic nodular lesion on the left ovary (LE) is observed. (F) Detail of the right and left ovaries (black arrowhead) and uterine tubes (red arrowhead), highlighting the difference between the ovary submitted to chemical induction surgery compared to the right ovary. (G) Exposure of the reproductive tract. (H) Detail of the reproductive tract, left ovary (LE). (I) Detail of the ovaries (black arrowhead), the left one shows moderate atrophy and the right one shows a functional cyst; and uterine tubes (red arrowhead). (J) Exposure of the reproductive tract showing the presence of heterogeneous or nodular cystic peritoneal implants (red arrows). (K) Detail of the reproductive tract, left ovary (LE). (L) Detail of the right and left ovaries (black arrowhead) and uterine tubes (red arrowhead), highlighting the more edematous aspect of the left ovary. (M) Exposure of the reproductive tract. (N) Detail of the reproductive tract, note the presence of a yellowish cystic nodule in the left ovary (LE). (O) Detail of the right and left ovaries (black arrowhead) and uterine tubes (yellow arrowhead), highlighting the cystic nodular lesion on the ovary.

OncoTherad® reduced the presence of cystic lesions in the ovaries and recuperated folliculogenesis and luteogenesis impaired by OC induction

The ovaries of the Healthy group rats (Figs. 8A, 9A and 9B) exhibited a morphology characteristic of the estrous cycle phase in which they were euthanized (estrus) with the presence of several smaller growing follicles (Figs. 8A and 9A), but absence of preovulatory (non-atretic) tertiary follicles. The ovarian cortex was well defined with several follicles at different stages of maturation, as well as some atretic follicles (Figs. 8A and 9A). The medulla, consisting of predominantly loose fibrocellular connective tissue, showed rich vascularization. It was also possible to observe corpora lutea from ovulations of previous cycles, with smaller size and presence of degenerative signs such as apoptosis and fibrosis (Figs. 8A and 9B). The lutein cells showed a round nucleus, evident nucleolus and abundant and acidophilic cytoplasm (Fig. 9B). In the stroma, it was possible to observe the presence of interstitial tissue in which the interstitial cells presented pale cytoplasm and a well-stained nucleus. The germinal epithelium appeared normal, as a simple epithelium ranging from cubic to squamous and the tunica albuginea consisting of layers of around six layers of fibroblasts (Fig. 8A).

In the ovaries induced with DMBA in the Cancer group (Figs. 8B, 8C, 9C-F), it was possible to observe several changes in the ovarian cytoarchitecture. In most animals, there was the presence of a cystic nodule filled with serous liquid content, covered with fibrous tissue and with the presence of adipocytes more externally (Figs. 9B and 9C). There were changes

considered pre-neoplastic of epithelial origin such as epithelial hyperplasia, inclusion cysts and degenerative or anomalous follicles (Figs. 9C and 9G). Some areas showed hyperplasia of the germinal epithelium and/or the tunica albuginea (Fig. 9C). Several animals also exhibited poorly differentiated glandular structures, covered by a single epithelial layer ranging from cuboidal to columnar, which defined a lumen, similar to the differentiation of the fallopian tube (endosalpingiosis) (Fig. 9D). Alterations such as inflammatory infiltration, hyperplasia and hypertrophy of interstitial cells were observed, in addition to a drastic decrease in the number of healthy follicles and corpora lutea, the latter not being found in most animals. There was also a clear increase in the incidence of atretic follicles and follicular cysts (Figs. 8B and 8C). Follicular cysts are larger than preovulatory follicles and are surrounded by a thin layer of flattened cells resting on a fibrous capsule (Fig. 8C). It was also possible to verify regions of intense atypia and the presence of pleomorphism that were considered high-grade dysplasias and serous lesions (Fig. 9E), with solid architecture and infiltration of inflammatory cells and accumulation of adipocytes between cells, as well as regions of cells with more acidophilic cytoplasm and hyperchromasia (Fig. 9F).

In the ovaries of the rats from the OncoTherad group (Figs. 8D, 9G and 9H) cysts with serous content or epithelial cysts were not found. Most animals showed an apparent reduction of healthy follicles in more advanced stages of maturation and mainly of corpora lutea in the most atrophied ovaries, with a greater amount of interstitial tissue. However, some animals exhibited follicles at various stages of maturation and active corpora lutea (Fig. 8D). Although less incidents than in the cancer group, anomalous (degenerative) follicles could also be observed (Fig. 9G) and areas of hyperchromasia, nuclear pleomorphism and acidophilic cytoplasm. There was a high incidence of atretic follicles and the presence of several follicular cysts (Fig. 9H). Benign alterations such as interstitial cell hypertrophy, tunica albuginea hyperplasia and immune infiltration also occurred in this group. One rat in the group exhibited single epithelial layer glandular structures and another rat exhibited areas of cells exhibiting intense atypia and nuclear pleomorphism infiltrating the ovarian stroma.

In the EPO group there was an increase in the amount of interstitial tissue inversely proportional to the number of healthy follicles and corpora lutea (Fig. 8E). The interstitial cells showed hypertrophy and vacuolation (Fig. 8I). Some rats exhibited cystic nodules contiguous with the left ovary or very close and adhered to the peritoneum. In these lesions, there was accumulation of adipose tissue, immune infiltrate and cells showing atypia (Fig. 9J). It was possible to observe an apparent increase in vascularity in the ovarian medulla, with the presence

of congested vessels (Fig. 8E). There was also an incidence of anomalous follicles, follicular cysts (Fig. 8E), hyperplasia of the tunica albuginea, immune infiltrate, areas of dysplasia, poorly differentiated glandular structures, cells with more acidophilic cytoplasm, hyperchromasia and pleomorphism in the ovarian stroma.

The ovaries of the rats that received the combined treatment OncoTherad+EPO (Figs. 8F, 9K and 9L) exhibited the alterations verified in the other induced groups, such as the incidence of cystic lesions and accumulation of adipose tissue with immune infiltrate. Most rats showed increased follicular atresia and reduced corpora lutea, while there was an apparent increase in the area with interstitial cells (Fig. 8F). Changes such as follicular cysts, immune infiltrate (Fig. 9K), hypertrophy and hyperplasia of interstitial cells, hyperplasia of the tunica albuginea, and atypical glandular structures were also seen. One rat exhibited areas of nuclear pleomorphism and intense infiltrating atypia in the ovarian stroma (Fig. 9L).

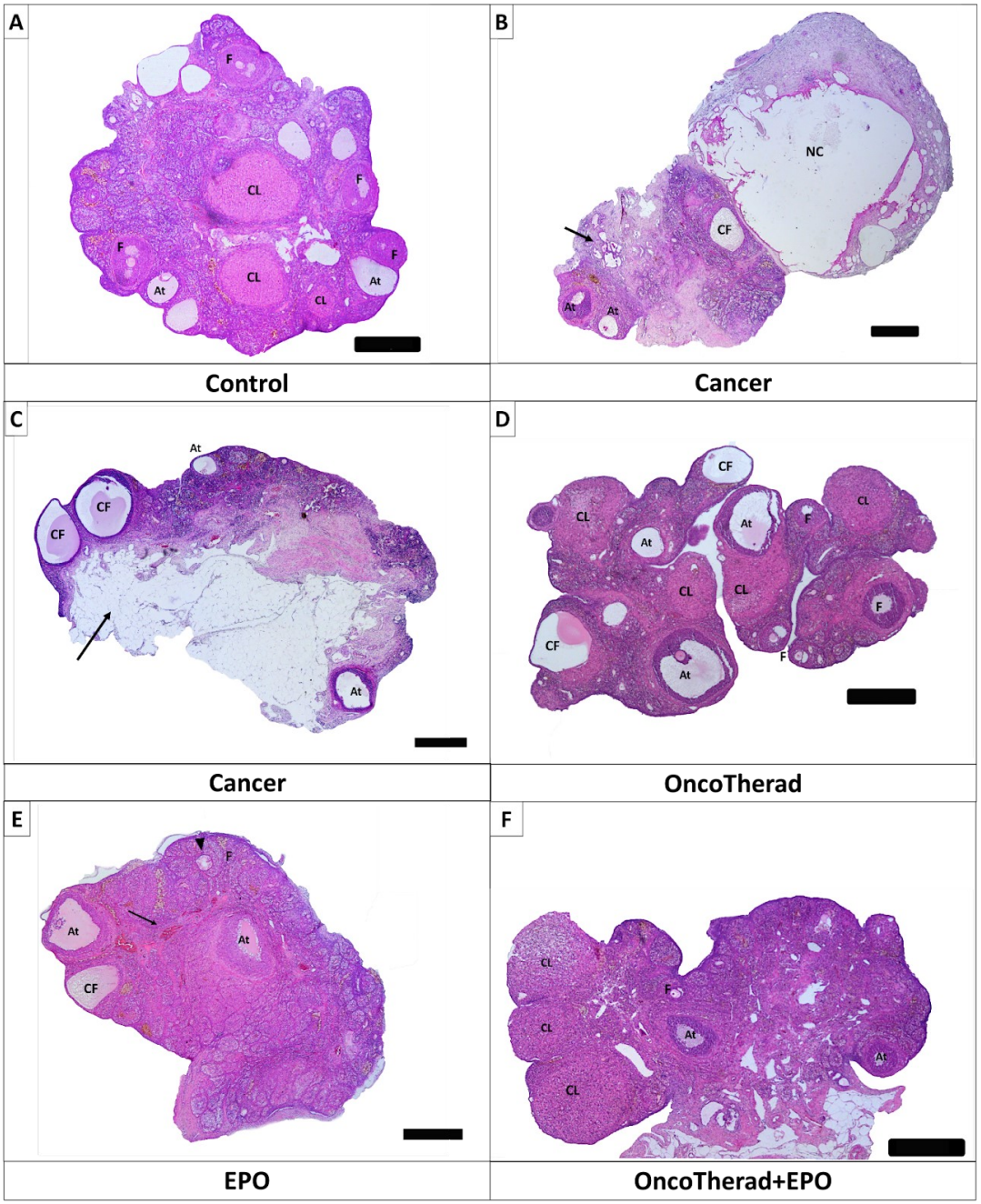

Fig. 8. Photomicrographs of ovaries from Healthy Control (A), Cancer (B and C), OncoTherad (D), EPO (E) and OncoTherad+EPO (F) groups. (A) Observe the morphological aspect of the healthy ovary, with corpora lutea (CL), maturing antral follicles (F) and atretic follicles (At). (B) Ovary with adhered cystic nodular lesion, drastic reduction of follicles and absence of corpora lutea. Presence of atretic follicles (At) and follicular cysts (FC). (C) Ovary with accumulation of adipose tissue (arrow), follicles (F), atretic follicles (At) and follicular cysts (CF). (D) Ovary with the presence of healthy follicles (F), atretic follicles (At), corpora lutea (CL) and follicular cysts (FC). (E) Ovary with hyperplasia of interstitial cells, anomalous follicle (arrowhead), atretic follicles (At), follicular cyst (FC) and more vascularized medulla (arrow). (F) Ovary with depleted corpora lutea, presence of many follicles (At), but also healthy follicles (F). Hematoxylin-Eosin. Bars = 500 µm.

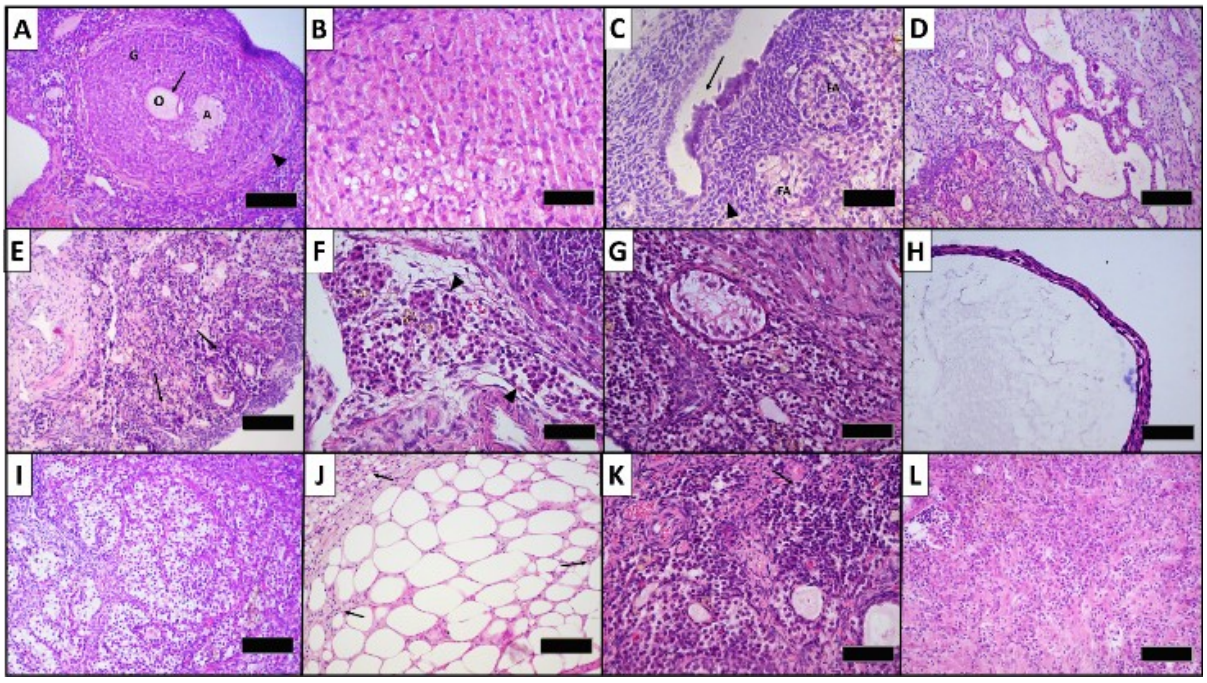

Fig. 9. Details of the histopathological changes found in the ovaries of the Healthy Control (A and B), Cancer (C-F), OncoTherad (G and H), EPO (I and J) and OncoTherad+EPO (K and L) groups. (A) Detail of a tertiary follicle with oocyte (O), zona pellucida (arrow), granulosa cells (G), antrum in formation (A) and theca cells (arrowhead). (B) Luteal cells with rounded nucleus, evident nucleolus and abundant acidophilic cytoplasm in a degenerating corpus luteum. (C) Detail of the hyperplasia of the germinal epithelium (arrow) and the tunica albuginea (arrowhead) as well as anomalous follicles (FA). (D) Atypical glandular structures. (E) Area of high-grade dysplasia with cells showing pleomorphism and atypia (arrows). (F) Cells with hyperchromasia and acidophilic cytoplasm (arrowhead). (G) Detail of anomalous (degenerative) follicle. (H) Detail of follicular cyst wall, a layer of flattened cells over a fibrous capsule. (I) Hypertrophy and vacuolation of interstitial cells. (J) Accumulation of adipocytes with infiltrating immune cells (arrows). (K) Area of cells with acidophilic cytoplasm and immune infiltrate (arrow). (L) Region of intense cellular atypia and pleoformism. Hematoxylin-Eosin. Bars = 200 μm (I); 100 μm (A,D,E,J,L) and 50 μm (B,C,F,G,H,K).

OncoTherad® alone or associated with EPO increased IL-6, IFN-γ, and F4/80+ macrophages with M1 profile (iNOS) through TLR2 and TLR4 stimulation

The total immunoreactivity for the TLR4, IL-6, IFN-γ, iNOS, F4/80, CD163 and FOXP3 antigens in the ovaries are presented in Table 6 and the different intensities of the

immunoreaction in Figs. 10 and 11. The immunolocalization of the antigens in the sections of ovaries is shown in Figs. 12 and 13.

Total TLR2 immunoreactivity was higher ($p<0.05$) in the OncoTherad group compared to the Cancer, control and OncoTherad+EPO groups (Table 3). The EPO group also showed higher ($p<0.05$) total immunoreactivity for TLR2 when compared to the Control and Cancer groups. In the Cancer group, there was the lowest absolute number of immunoreactivity for TLR2, although it did not differ statistically ($p>0.05$) from the Control (Table 3). In the intensity analysis, it was possible to observe that the OncoTherad group presented a stronger TLR2 immunoreactivity pattern ($p<0.05$) in comparison with all other groups, with the highest percentage of strong intensity immunoreactivity, even in comparison with the EPO group (Figures 10A and 12). The EPO group again differed ($p<0.05$) from the Control and Cancer groups in the intensity of TLR2 staining, with a more intense pattern than these groups (Figures 10A and 12).

The total percentage of TLR4 positive cells did not show significant differences ($p>0.05$) between groups, although the lowest absolute percentage was found in the Cancer group and the highest in the OncoTherad+EPO and OncoTherad groups, respectively (Table 3). On the other hand, the intensity analysis was able to capture significant differences between the groups (Figure 10B). In the OncoTherad+EPO group, there was a greater ($p<0.05$) intensity of immunoreaction compared to the Cancer group (Figures 10B and 12).

Total IL-6 immunoreactivity was decreased ($p<0.05$) in the Cancer group compared to the Control group, which had the highest value of IL-6 positive cells among all groups (Table 3). The OncoTherad and OncoTherad+EPO groups also showed lower ($p<0.05$) values of total IL6 immunoreactivity compared to the Control, but with higher absolute values than the Cancer group. However, the EPO and OncoTherad+EPO groups showed significantly higher percentages of IL-6 immunoreactivity ($p<0.05$) compared to the Cancer group (Table 3). The intensity analysis reinforced the total immunoreactivity results for IL-6, as the Cancer showed a weaker immunoreactivity pattern than the Control (Figures 10C and 12). In the three treated groups (OncoTherad, EPO and OncoTherad+EPO), the IL-6 immunoreaction was also more intense ($p<0.05$) compared to the Cancer group (Figures 10C and 12). While the OncoTherad and OncoTherad+EPO groups showed less intense immunoreaction intensities ($p<0.05$) for IL-6 when compared to the Control, the EPO group did not differ statistically from this group (Figures 10C and 12).

Although there were no statistically significant differences ($p<0.05$) in the total IFN-γ immunoreactivity between the groups, it was possible to observe that the lowest value was found in the Cancer group (Table 3). The analysis of immunoreaction intensity revealed significant differences ($p<0.05$) between the OncoTherad group, in which there was a higher percentage of IFN-γ positive cells with strong intensity, compared to the Cancer and EPO groups (Figures 10D and 12).

In the OncoTherad and OncoTherad+EPO groups, there was an increase ($p<0.05$) in iNOS immunoreactivity compared to the Control group, which had the lowest number of iNOS positive cells (Table 3). From the data on the intensity variation of the immunoreaction for iNOS, it was possible to verify more differences between the groups (Figure 11A). The OncoTherad group showed a more intense pattern of iNOS immunostaining ($p<0.05$) than the Control and Cancer groups, predominantly moderate to strong (Figures 11A and 13). The EPO and OncoTherad+EPO groups showed stronger immunoreactivity ($p<0.05$) than the Control, especially in the OncoTherad+EPO group, where the intensity of the immunoreaction for iNOS tended to moderate, in comparison with the Control, which presented immunoreactivity predominantly weak (Figures 11A and 13).

From the analysis of the total immunoreactivity for F4/80, it was possible to observe that the highest values were found in the three treated groups (OncoTherad, EPO and OncoTherad+EPO), and the highest value of immunoreactivity in the OncoTherad+EPO group differed statistically ($p <0.05$) of the Control and Cancer groups (Table 3). Likewise, in the intensity analysis, the OncoTherad+EPO group showed a more intense immunoreaction ($p<0.05$) in relation to the Control and Cancer groups, as well as the EPO group also differed ($p<0.05$) from the Control group, showing stronger immunoreaction (Figures 11B and 13).

The percentage of CD163 positive cells was higher ($p<0.05$) in the EPO and OncoTherad+EPO groups compared to the Control and Cancer groups (Table 3). Comparing the treatment alone with OncoTherad and when associated with erythropoietin, the combined treatment showed the highest ($p<0.05$) total CD163 immunoreactivity (Table 3). The intensity analysis results supported the total immunoreactivity findings, where the OncoTherad+EPO group showed a more intense immunoreaction pattern ($p<0.05$) than all other groups (Figures 11C and 13). Likewise, the EPO group also differed ($p<0.05$) from the Control group, which showed weaker immunoreaction (Figures 11C and 13).

The lowest total FOXP3 immunoreactivity occurred in the Cancer group, which differed statistically ($p<0.05$) from the EPO and OncoTherad groups (Table 3). The EPO group also

showed a higher ($p<0.05$) total FOXP3 immunoreactivity compared to the Control group (Table 3). Through the immunoreaction intensity analysis, it was possible to statistically verify that the EPO group presented a stronger intensity ($p<0.05$) in comparison with the Control and Cancer groups and the OncoTherad group also obtained a more intense immunostaining pattern when compared to the Control (Figures 11D and 13).

Table 3. Total immunoreactivity (%) in groups for different antigens.

Antigens	Experimental groups (n=7/group)				
	Control	**Cancer**	**OncoTherad**	**EPO**	**OncoTherad +EPO**
TLR2	75.64 **a**	71.64 **a**	85.09 **c**	85.91 **bc**	80.23 **ab**
TLR4	77.06 **a**	66.70 **a**	75.06 **a**	68.42 **a**	78.58 **a**
IL-6	85.75 **a**	71.40 **c**	79.22 **bc**	82.40 **ab**	80.40 **b**
IFN-γ	79.91 **a**	71.15 **a**	79.19 **a**	79.01 **a**	79.69 **a**
iNOS	67.51 **a**	70.31 **ab**	78.03 **b**	77.03 **ab**	77.66 **b**
F4/80	66.98 **a**	67.69 **a**	71.70 **ab**	73.52 **ab**	77.47 **b**
CD163*	72.93 **a**	73.40 **a**	76.05 **ab**	79.25 **bc**	83.10 **c**
FOXP3	69.70 **ac**	65.86 **a**	74.64 **bc**	78.29 **b**	73.07 **ab**

Values are equivalent to the mean percentage of urothelial cells positive for the antigens per group (n=5 sections/animal/group). Kruskal-Wallis ANOVA, Student-Newman-Keuls Test. *ANOVA, Tukey Test. Along the same lines, values followed by different letters indicate a significant difference between groups ($p<0.05$).

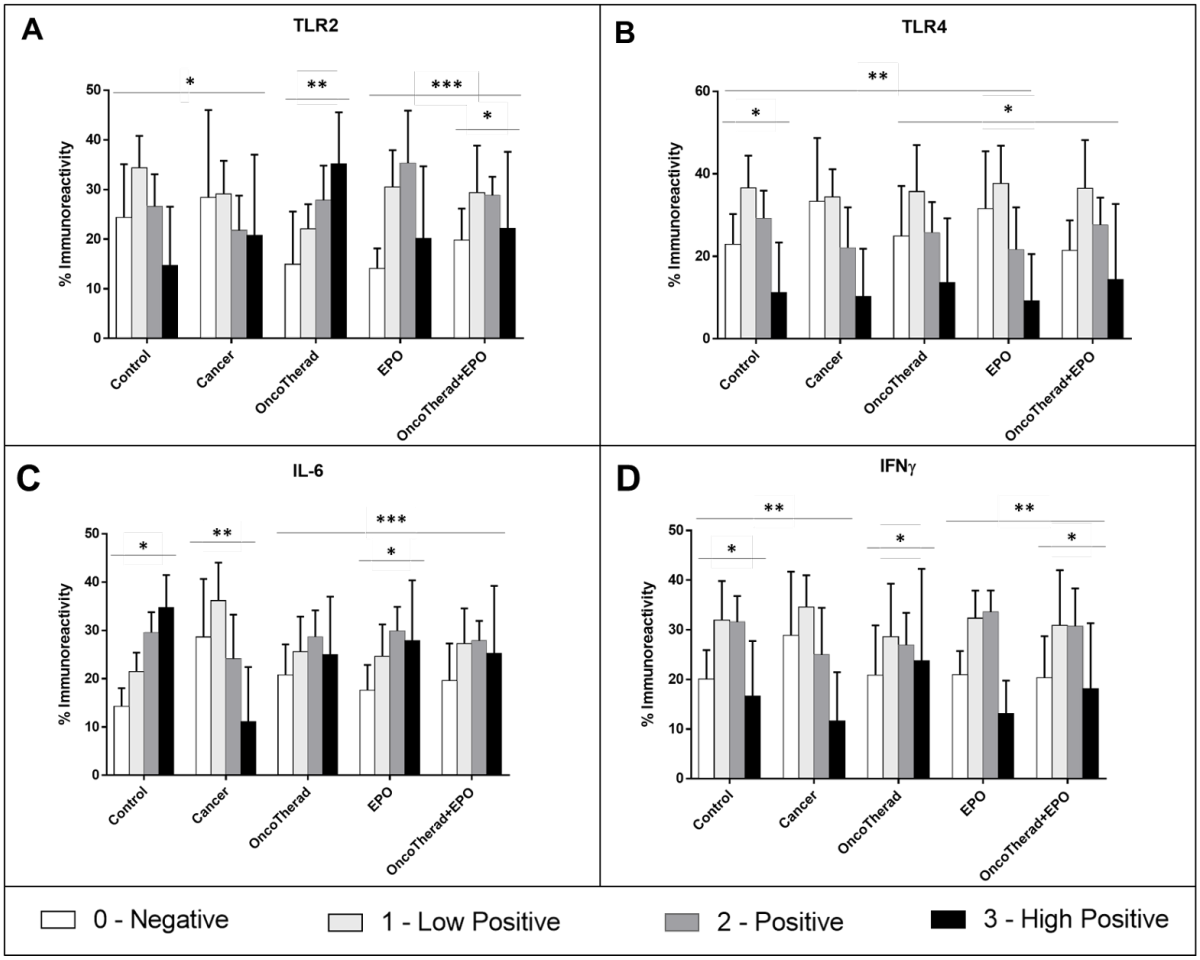

Fig. 10. Immunoreactivity (%) in different intensity categories for antigens: TLR2 (A), TLR4 (B), IL-6 (C) and IFN-γ (D). */**/*** Different symbols indicate a significant difference ($p<0.05$) between groups, when statistically differ in any category of immunoreactivity. ANOVA, Tukey test (n = 5 sections/animal/group). Immunoreactivity was classified into four categories: Negative (0): absence of labeling; Low Positive (1): weak immunoreaction; Positive (2): moderate immunoreaction and High Positive (3) strong immunoreaction.

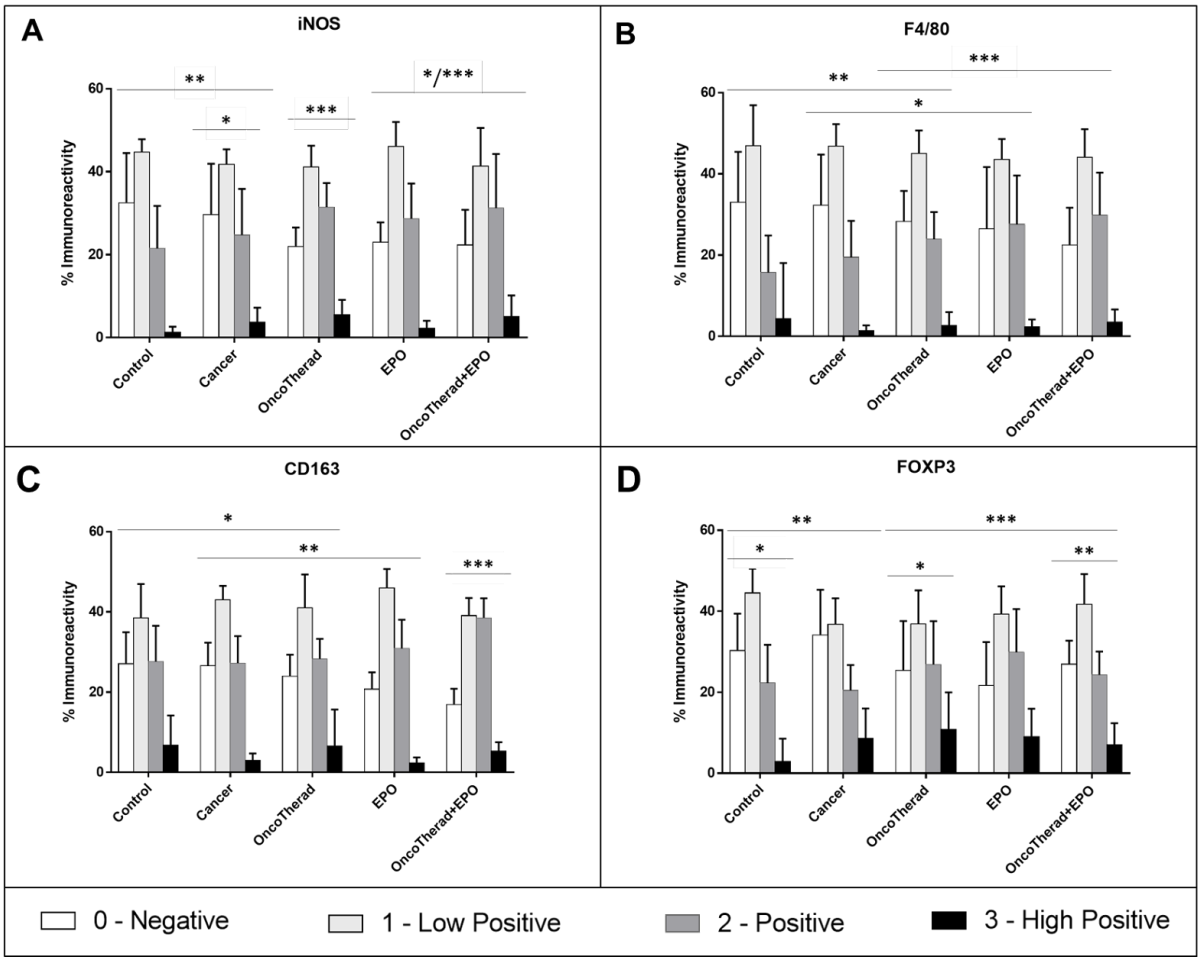

Fig. 11. Immunoreactivity (%) in the different intensity categories for the antigens: iNOS (A), F4/80 (B), CD163 (C) and FOXP3 (D). */**/*** Different symbols indicate a significant difference ($p<0.05$) between groups, when statistically differ in any category of immunoreactivity. ANOVA, Tukey test (n = 5 sections/animal/group). Immunoreactivity was classified into four categories: Negative (0): absence of labeling; Low Positive (1): weak immunoreaction; Positive (2): moderate immunoreaction and High Positive (3) strong immunoreaction.

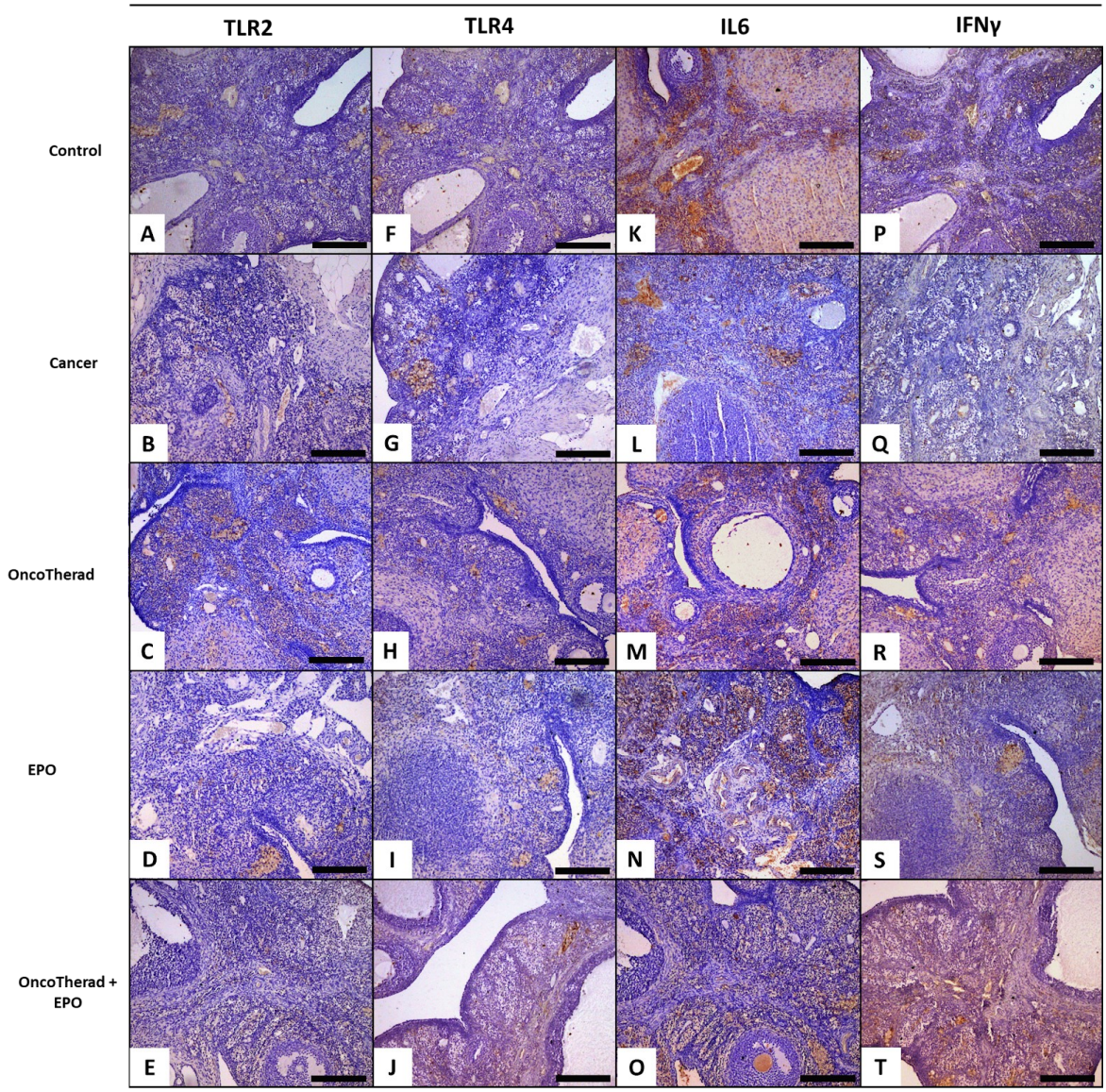

Fig. 12. Immunolocalization of TLR2 (A-E), TLR4 (F-J), IL-6 (K-O) and IFN-γ (P-T) antigens in the ovaries of different experimental groups. Control (A,F,K,P); Cancer (B,G,L,Q); OncoTherad (C,H,M,R); Erythropoietin (D,I,N,S) and OncoTherad+EPO (E,J,O,T). Bars = 200 µm.

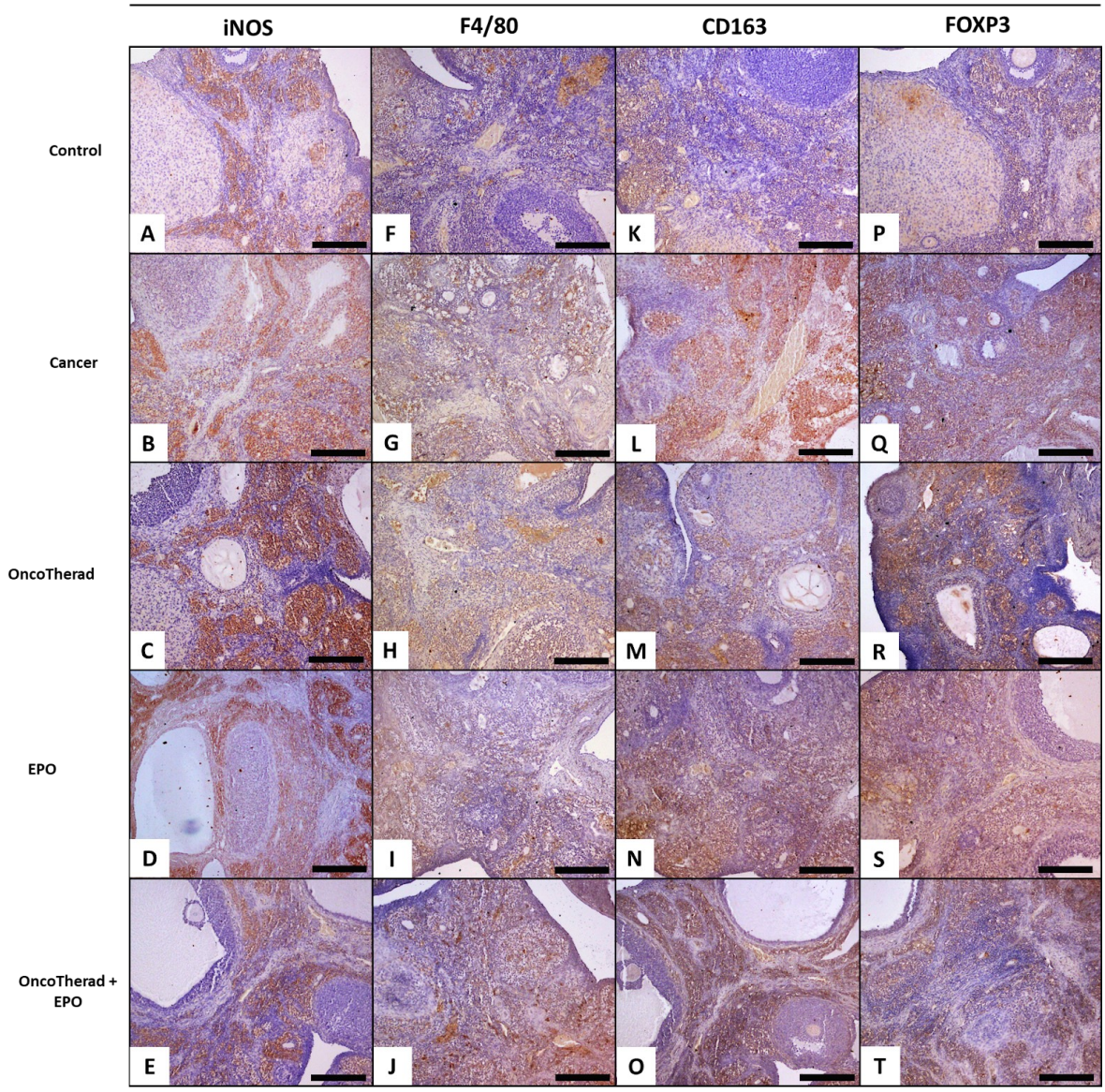

Fig. 13. Immunolocalization of iNOS (A-E), F4/80 (F-J), CD163 (K-O) and FOXP3 (P-T) antigens in the ovaries of different experimental groups. Control (A,F,K,P); Cancer (B,G,L,Q); OncoTherad (C,H,M,R); Erythropoietin (D,I,N,S) and OncoTherad+EPO (E,J,O,T). Bars = 200 µm.

Histotypes biomarkers indicated DMBA induced tumor model as low-grade serous carcinoma-like

The IHC scoring for the histotypes biomarkers were represented in the Heatmap (Figs. 14 and 15) and the photomicrographs of the ovaries in Figs 16, 17, 18, and Supplemental Fig. 6. All the animals of the Healthy Control showed Wt1 positivity in the ovaries (Fig. 14). Healthy ovaries showed positivity in the epithelium and in the granulosa cells of healthy follicles (stronger staining at the low stages of development and absent on the atretic follicles) (Fig.

16A). In the Cancer group, all ovaries also presented positivity in the epithelium and in the most abnormal cells/ abnormal structures in the stroma (Fig. 14). Wt1 was still present in healthy follicles (but weaker compared to the Control group) and was absent in the atretic follicles (Fig. 16B). For the animals treated with OncoTherad, 42.9% of the ovaries presented Wt1 positivity in the epithelium, 42.9% showed heterogeneous pattern of staining, and one animal was Wt1 negative (Fig. 14). In this group, the abnormal cells were Wt1 positive for all animals. Wt1 was present in healthy follicles and absent in the atretic follicles as in the Cancer Group (Fig. 16C). In the EPO Group, 42.9% of the animals presented Wt1 positivity in the epithelium, 42.9% presented negativity, and 14.3% presented heterogeneity in the epithelium. For the abnormal cells, the majority of the animals presented positivity while 28.6% were negative (Figs. 14 and 16D). Like for the other treated groups, OncoTherad+EPO group showed Wt1 positivity in 42.9% of the animals, the same percentage of negativity, and 14.3% presented heterogeneity in the epithelium. For the abnormal cells, 57.1% of the animals presented positivity while 42.9% Wt1 were negative (Figs. 14 and 16E).

Health ovaries showed Arid1a positivity in the epithelium, granulosa cells, interstitial cells, and lutein cells (*corpus luteum*) (Figs. 14 and 16F). In the Cancer group, the majority of the ovaries presented loss of Arid1a expression in the epithelium, 28.6% presented positivity, and one heterogeneity. Regarding the abnormal cells, most of the ovaries showed a heterogeneous pattern of Arid1a staining while 28.6% were positive (Figs. 14 and 16G). 42.9% of the animals of the OncoTherad group showed Arid1a positivity in the epithelium while 28.6% were negative and 28.6% showed heterogeneity. For the abnormal areas, 42.9% of the animals were Arid1a positive, 42.9% showed heterogeneous staining, and one was Arid1a negative (Figs. 14 and 16H). In the EPO Group, some ovaries 57.1% presented loss of Arid1a expression in the epithelium while others showed positivity. For the abnormal cells the most showed heterogeneous staining, 28.6% presented positivity, and one was Arid1a negative (Figs. 14 and 16I). For the animals treated with the combination of OncoTherad® and EPO, the majority was Arid1a positive in the epithelium while 28.6% were negative and 28.6% showed heterogeneous staining. In the abnormal cells the staining was heterogenous for the majority of the ovaries and 28.6% presented positivity (Figs. 14 and 16J).

Healthy ovaries did not show Hnf1b expression (Figs. 14 and 17A). In the same way, in the Cancer groups, ovaries did not present positivity in the epithelium (Fig. 14). Regarding the abnormal cells some of them showed weak cytoplasmic staining (that can be only due to the background) and nuclear staining in some areas (heterogeneity) even though there could be

some types of immune cells (Fig. 17B). The animals treated with OncoTherad did not show any nuclear Hnf1b staining as well (Figs. 14 and 17C). One animal of the group showed Hnf1b positivity in some cells of the stroma which can possibly be immune cells. All the animals of the EPO group were Hnf1b negative in the epithelium. 57.1% showed complete absence of staining in the abnormal cells while 28.6% showed nuclear heterogeneity and cytoplasmic positivity (Figs. 14 and 17D). There was possibly a level of background in the normal cells (granulosa and interstitial cells). Regarding the OncoTherad+EPO group, the ovaries did not present positivity Hnf1b in the epithelium nor in the abnormal cells (Figs. 14 and 17E). There was cytoplasmic background in normal cells (granulosa and interstitial cells).

Ovaries of the Healthy Control group do not present Pr positivity in the epithelium but there was cytoplasmic staining in the interstitial cells (Figs. 14 and 17F). In the Cancer group, the epithelium was Pr negative except by one animal as well as the abnormal cells in the stroma (Figs. 14 and 17G). There was some cytoplasmic staining in the interstitial cells. For the OncoTherad and EPO groups (Figs. 14, 17H, and 17I), the epithelium was also Pr negative like the abnormal cell. The interstitial cells showed cytoplasmic staining. In the OncoTherad+EPO group, just one animal showed Pr positive epithelial cells. Regarding the abnormal cells, 42.9% of the animals showed some Pr positivity (Figs. 14 and 17J). There was some cytoplasmic and rare nuclear staining in the interstitial cells that seems stronger and more common compared with the other experimental groups.

For p53 staining (Figs. 15 and 18), the majority for all the groups was the score 1 (same as healthy ovaries), although specially in the cancer group the staining (in general) was visually stronger and we have the same number of ovaries with score 1 and score 2. For the treated groups, most of the ovaries were classified as score 1, even though some showed score 2 and 3 (Fig. 18).

Fig. 14. Heatmap of the IHC scoring for the histotypes biomarkers (Wt1, Arid1a, Hnf1b, and Pr). The staining was classified in 3 categories (negative, positive, and heterogeneity) and it was analyzed in the epithelium and abnormal areas in the stroma.

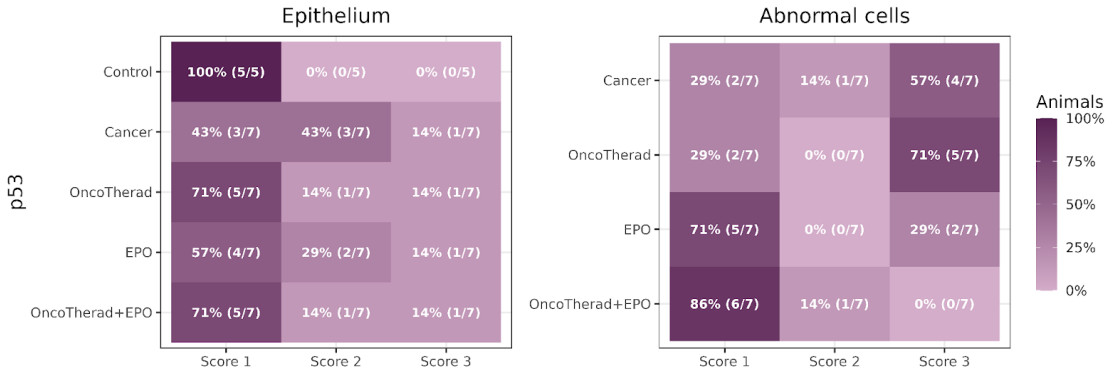

Fig. 15. Heatmap of the IHC scoring for p53. The IHC Scoring for p53 as defined as 1 (Normal) - occasional nuclear positive cells and cytoplasmic positivity; 2 (Abnormal) - strong nuclear expression in virtually all epithelial cells and cytoplasmic positivity, normal pattern in stroma; 3 (Abnormal) - cytoplasmic staining in epithelial cells (very rare nuclear positivity), normal pattern in stroma. The same scores were applied to abnormal structures in the stroma.

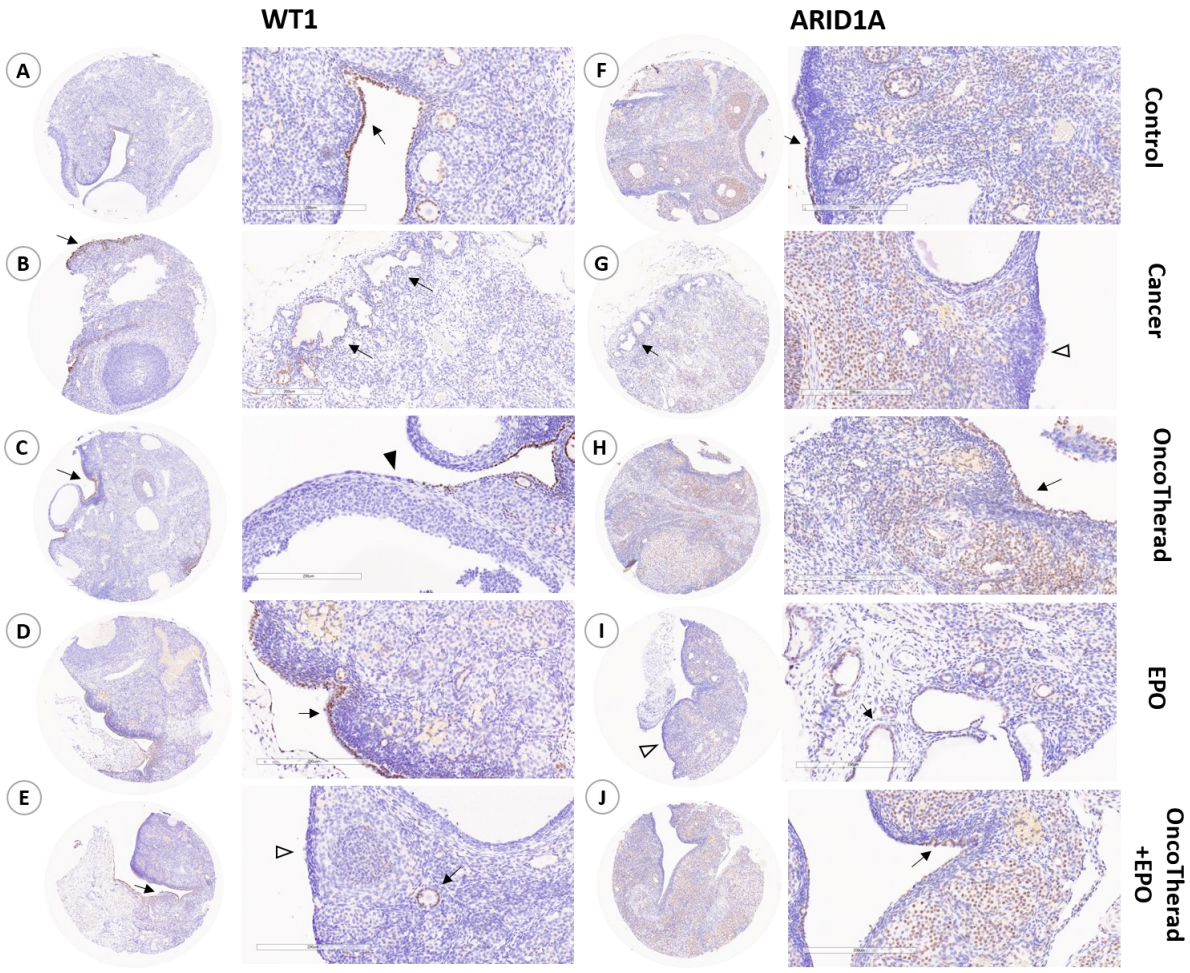

Fig. 16. Photomicrographs of the ovaries immunostained with Wt1 (A-E) and Arid1a (F-J). Healthy control group (A, F); Cancer (B, G); OncoTherad (C, H); EPO (D, I); OncoTherad+EPO (E, J). (A) Healthy ovaries showed Wt1 nuclear positivity in the epithelium (arrow). In the Cancer group (B), the epithelium showed Wt1 positivity (arrow) as well as in the abnormal structures in the stroma (arrows). In the OncoTherad group (C), we could see Wt1 positivity (arrow) and heterogeneity (closed arrowhead) in the epithelium of some ovaries. The EPO group (D) also showed Wt1 positivity (arrow) and heterogeneity. Ovaries of the OncoTherad+EPO group (E) showed Wt1 positivity, heterogeneity, and negativity in the epithelium (arrow) even when they were positive in other cells in the stroma (arrow). For Arid1a, the epithelium of the healthy ovaries (F) was positive (arrow). In the Cancer group (G), some ovaries showed loss of Arid1a in the epithelium (open arrowhead) while the abnormal structures were positive. The majority of the ovaries of the OncoTherad group (H) showed Arid1aA positivity in the epithelium (arrow). In the EPO group (I), some ovaries showed absence of Arid1a expression in the epithelial cells (open arrowhead) and heterogeneous staining in stromal abnormal structures. The OncoTherad+EPO group (J) showed Arid1a positivity in the epithelium for most of the animals. Bars = 200µm.

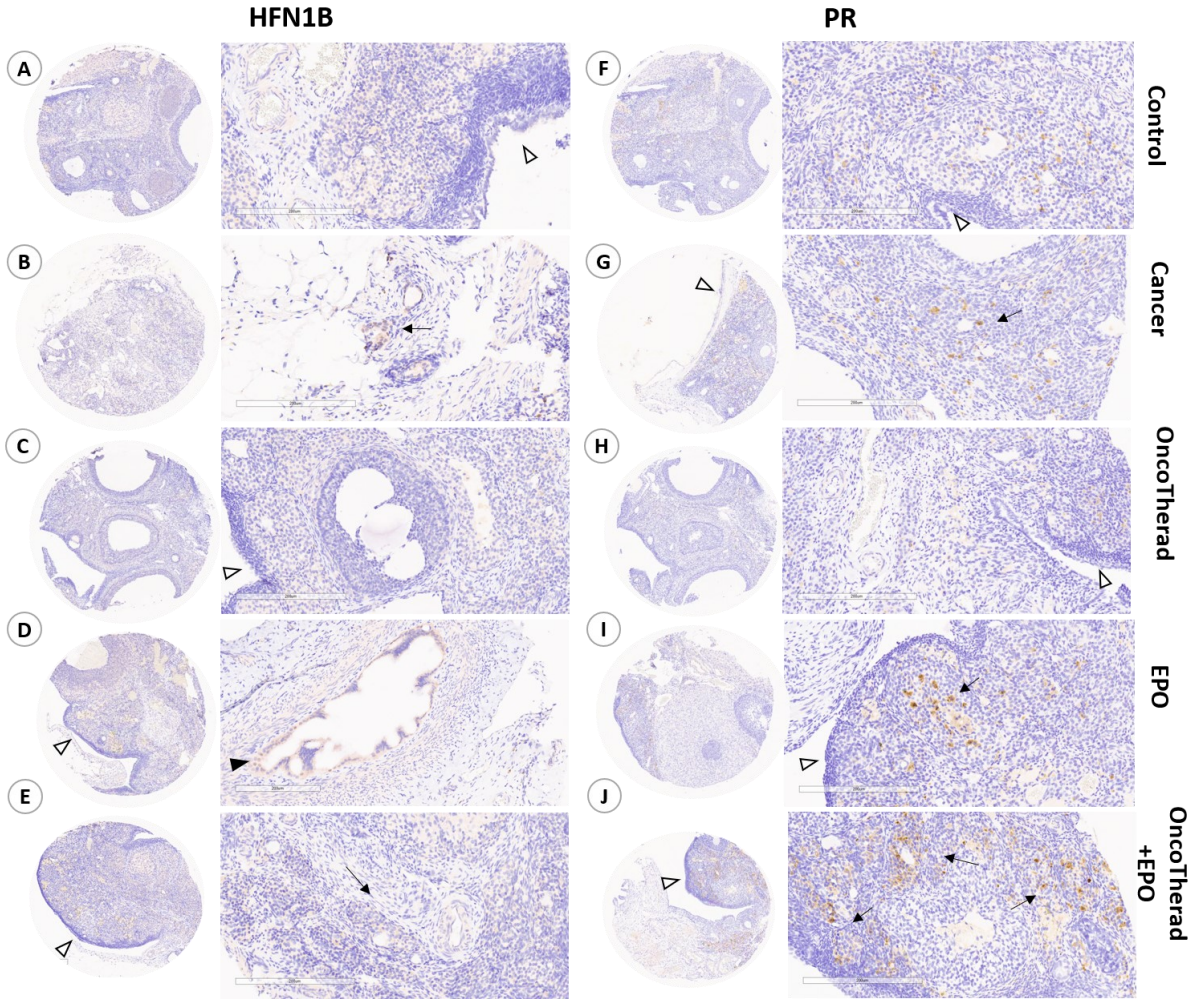

Fig. 17. Photomicrographs of the ovaries immunostained with Hfn1b (A-E) and Pr (F-J). Healthy control group (A, F); Cancer (B, G); OncoTherad (C, H); EPO (D, I); OncoTherad+EPO (E, J). (A) Healthy ovaries were Hfn1b negative in the epithelium (open arrowhead). In the Cancer group (B), the epithelium was Hfn1b negative while some cells in the stroma were positive (arrow). In the OncoTherad group (C), the epithelium was Hfn1b negative (open arrowhead). The EPO group (D) also showed no staining for Hfn1b in the epithelium (open arrowhead) and heterogeneous staining in some structures in the stroma (closed arrowhead). Ovaries of the OncoTherad+EPO (E) group showed no Hfn1b staining in the epithelium (open arrowhead) and some cytoplasmatic staining in the stroma (arrow). For Pr, the epithelium of the healthy ovaries (F) was negative (open arrowhead). In the Cancer group (G), the epithelium was also Pr negative (open arrowhead) and some cells were positive in the stroma. The OncoTherad group (H) showed the epithelium Pr negative (open arrowhead). In the EPO group (I), the ovarian epithelium was Pr negative (open arrowhead) and some cells in the stroma were positive (arrow). The OncoTherad+EPO group (J) showed no staining for Pr in the epithelium (open arrowhead) but some positivity in the stroma (arrows). Bars = 200µm.

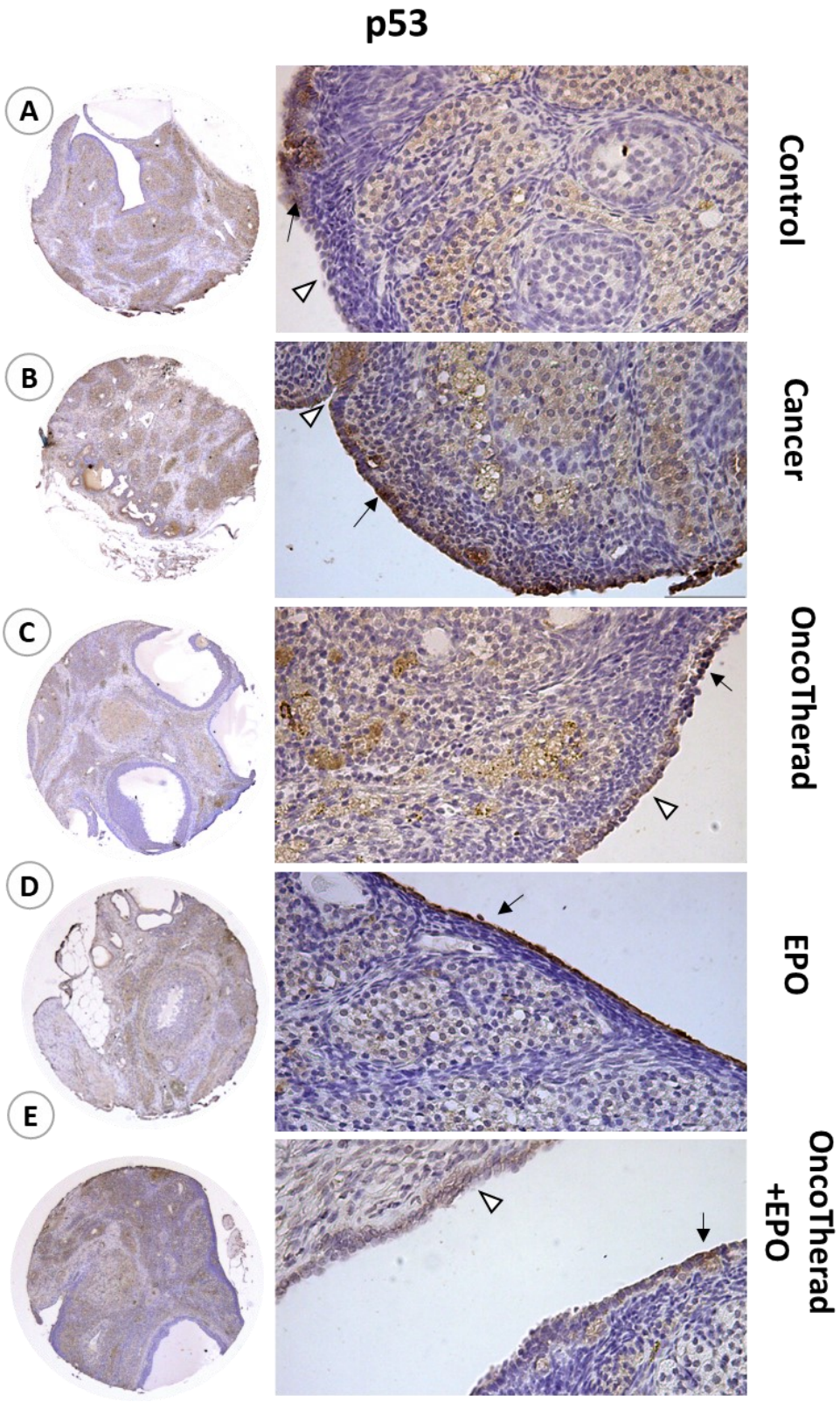

Fig. 18. Photomicrographs of the ovaries immunostained with p53. Healthy control group (A); Cancer (B); OncoTherad (C); EPO (D); OncoTherad+EPO (E). In general, the ovaries were p53 negative in the nucleus of the epithelial cells (open arrowhead) with occasional nuclear positivity (arrow).

EPO treatment increased CD3+ lymphocytes count in the tumor and abnormal areas of ovaries

The number CD3 positive cells/10^6 μm^2 in the experimental groups is represented in Figs. 19 and 20. In the Cancer group, the absolute number of CD3 positive cells in the non-tumor regions was lower than the Healthy Control group (Fig. 19A) as well as in the other treated groups. Although there was no significant difference ($p>0.05$), this could be explained by the immune cells that migrated to the tumor areas. Considering the treated groups, the absolute highest number of CD3 positive cells/10^6 μm^2 in the normal/ non tumor areas was found in the Oncotherad+EPO group (Fig. 19A), even though there was no significant statistical difference. Similarly, considering the abnormal/tumor areas the OncoTherad+EPO group also showed the higher absolute number of CD3 positive lymphocytes (Fig. 19B).

The comparison between the normal/non tumor and abnormal/tumor areas indicated that there was a migration of the immune cells from the normal areas to the regions with lesions (Fig. 20). Significant p value was not found for every experimental group, but it was possible to see a trend. In the EPO group, the number of CD3 positive cells was significantly higher ($p<0.05$) in the abnormal areas compared to the healthy areas. The same happened for the OncoTherad+EPO group, even though the p value was borderline (Fig. 20).

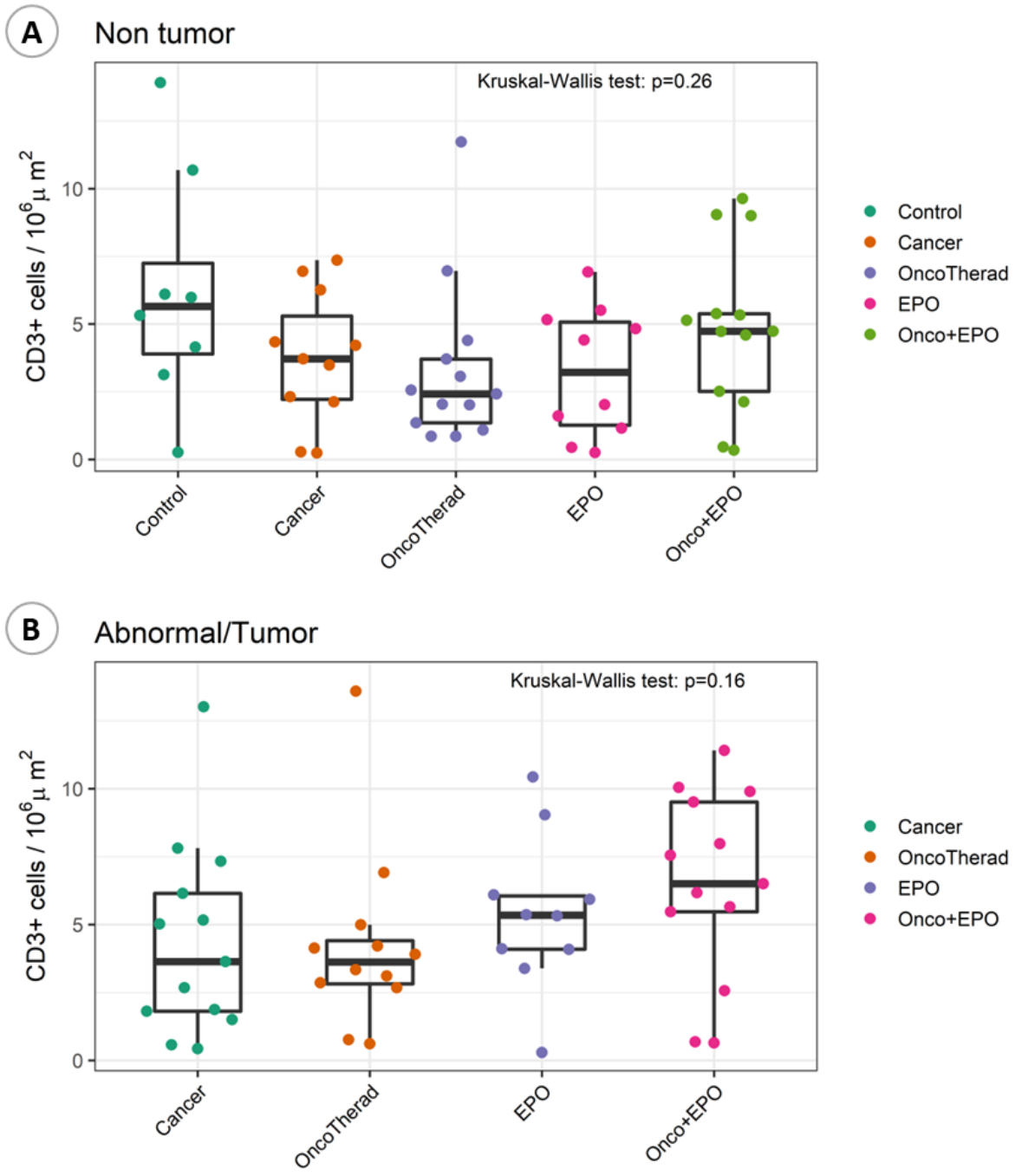

Fig. 19. CD3 positive cells count. CD3 positive cells number/10^6 µm^2 in the normal (non-tumor) areas and abnormal/tumor areas. Comparison among the experimental groups. Kruskal-Wallis test.

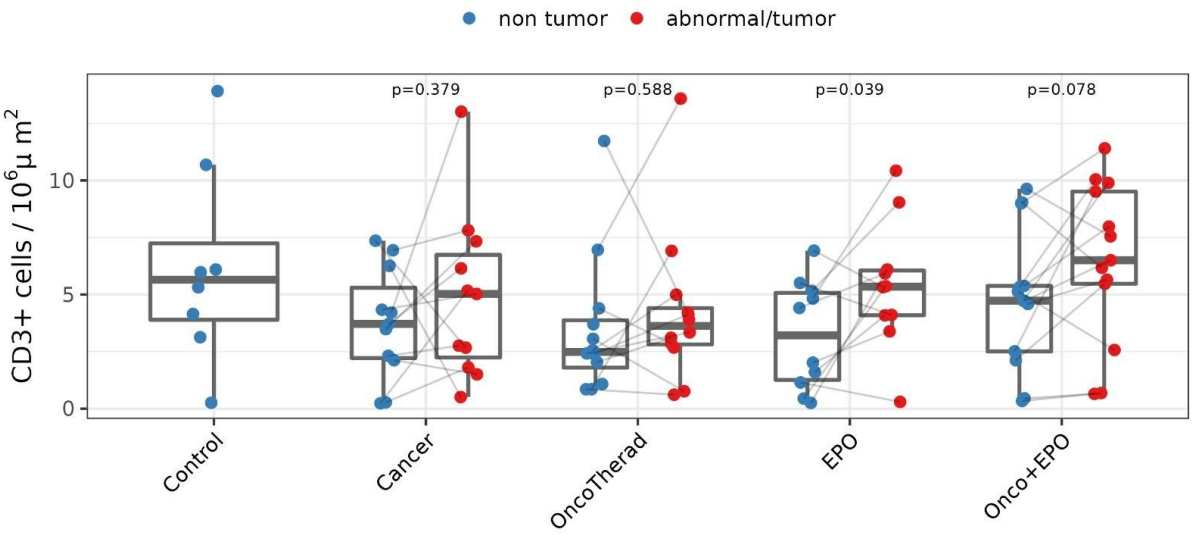

Fig. 20. CD3 positive cells count in two types of ovarian regions. Comparison of CD3 positive cells number/10^6 µm^2 between normal (non-tumor) areas and abnormal/tumor areas in each experimental group. T paired test.

DMBA-induced model did not show driver mutations in *Pik3ca, Ctnnb1*, or *Kras*

The regions containing the hotspots of *Pik3ca*, *Ctnnb1*, and *Kras* were amplified and the presence of the PCR products was confirmed through gel electrophoresis. The amplicons had the expected size of ~200bp. No band was observed in the PCR products of the no template control (NTC) confirming no contamination detected or non-specific amplification. The results of the sequencing analyzed were clear with an acceptable Phred confident/quality score (higher than 20) and little noises. The bases were compared with a human reference sequence (GenBank) using Mutation Surveyor® DNA Variant Analysis Software (SoftGenetics, State College, EUA), focusing on the regions of mutations (hotspots). DNA sequencing did not reveal driver mutations (*Pik3ca, Ctnnb1,* or *Kras*) in any of the sampled specimens.

DISCUSSION

In this study we fully characterized the DMBA-induced OC model and used it to test the antitumor efficacy of OncoTherad® immunotherapy associated with Erythropoietin. According to our results, the chemical induction of OC using DMBA did not inhibit cyclicity. In Fischer rats, estrous acyclicity is associated with cancer cachexia in murine models [54] and food

restriction [55]. However, in the present study, the rats induced to OC did not show cachexia or abnormality with regard to feed intake. On the other hand, the damages caused by OC chemical induction - such as ovarian atrophy - resulted in increase of cycle duration due to the occurrence of persistent estrus. In rats with atrophied ovaries, which exhibit a large number of atretic follicles and follicular cysts and lacks corpora lutea, the vagina may exhibit cornification related to an increase in the 17-beta estradiol/progesterone ratio, causing persistent estrus [56]. Irregularities in the transition of estrous cycle phases, such as prolonged diestrus duration and increase in estrous cycle duration in female rats chemically induced with DMBA were also described [19].

OC induction using DMBA can cause absolute and relative ovarian weight gain in rats [48]. In the present study, most of the ovarian lesions consisted of small cystic nodules, whose diameter did not exceed 5 mm which explains the absence of a statistically difference in gonad weight. Regarding the uterus, there was a reduction in uterine weight of the rats in the OncoTherad group. Yano et al. [57] reported reduction of uterine weight in OC-induced immunodeficient mice through xenographic implants (from OV-1063 ovarian cancer cells). Uterine weight is mainly regulated by estradiol, and the decrease in weight found in this study may be partly related to the atrophy of the left gonad found in the OncoTherad group, which would lead to a possible impact on estrogen synthesis. The decrease in the weight of the uterus may be due to the reduction in the thickness of the uterine layers due to several factors such as changes inherent to the estrous cycle itself [58].

We identified the presence of cysts and several histopathological alterations in OC-induced rats already described in other studies using DMBA-related OC models such as cysts filled with serous secretion histologically identified as cystadenocarcinomas [19], large cysts containing a lot of fat around the ovary [59], serous papillary adenocarcinomas and other serous tumors [59,60] as well as glandular structures, covered by simple cuboidal serous epithelium and similar to the differentiation of the fallopian tube (endosalpingiosis) [17]. Despite these neoplastic and preneoplastic alterations found in the ovaries of the rats in this study, the induction of OC in this study did not decrease the survival of the animals. These results are consistent with the absence of cachexia and with the aspects of the lesions described in the macroscopic analysis. Shao et al. [61] reported that the survival rate of Wistar rats induced to OC with DMBA was 66.7% after 24 weeks of induction. This rate is lower compared to that found in this study (87.5%) after 25 weeks of surgery.

The occurrence of ovarian atrophy may be related to the mechanism of stimulation of the immune system and the antitumor response triggered by OncoTherad®, associated or not with EPO. The more edematous appearance of the ovaries of rats treated mainly with EPO alone may be partly related to the increased expression of angiogenic factors, as well as the maintenance of ovarian function. Mahmoodi et al. [42] showed that EPO administration significantly increased the number of ovarian follicles in female mice due to its antioxidant, protective, and anti-apoptotic effects. In addition, treatments with OncoTherad® associated or not with erythropoietin altered the frequency of histological changes found in the Cancer group.

In humans, TLR2, TLR3, TLR4 and TLR5 are highly expressed in the surface epithelium of the ovary and this pattern is related to the protection against infections and the physiological role of these receptors in stimulating tissue repair after ovulation [62]. Therefore, TLR2 and TLR4 agonists, such as OncoTherad®, have grounds for application targeting gonadal disorders. We could observe that OncoTherad® alone was able to stimulate TLR2 and TLR4 and, when associated with EPO, this effect was potentiated on TLR4. Lau et al. [63] described that paclitaxel induced activation of canonical NF-κB signaling in murine ovarian cancer cells in a TLR4/MyD88 dependent manner, producing anti-tumor immunity. On the other hand, erythropoietin stimulated only TLR2 in ovarian tissue. In consequence of stimulation of TLR2, the three treatment strategies (OncoTherad®, EPO and OncoTherad+EPO) increased IL-6 immunoreactivity, more markedly in animals that received erythropoietin treatment.

In our study, IFN-γ immunoreactivity was reduced in animals induced to OC without treatment, whereas treatments with OncoTherad® alone or associated with EPO increased IFN-γ levels through TLR4 stimulation as well as led the highest rates of immunoreactivity for iNOS. These findings are consistent with previous results from the group reporting the stimulation of TLR4-mediated non-canonical pathway for interferon production by OncoTherad® [31,32,34]. Similarly, Silveira et al. [59] also found an increase in IFN-γ levels in the ovaries of rats with OC treated with the immunomodulator P-MAPA with or without cisplatin. IFN-γ is a cytokine known to have cell proliferation-reducing activity, pro-apoptotic activity and antitumor immunomodulation, produced by T-helper, cytotoxic and natural killer cells and macrophages [64]. In human OC cell lines, IFN-γ administration has been shown to activate SOCS, a family of cytokine signaling inhibitory proteins that inhibit the JAK/STAT signaling pathway which is highly activated in OC and is associated with tumor development and progression [64].

Tumor-associated macrophages (TAMs) with high CD163 expression are associated with anti-inflammatory function (M2 profile) and worse prognosis in malignant tumors [65]. The EPO and OncoTherad+EPO groups showed the highest immunoreactivity for CD163. OncoTherad® alone did not promote an increase in M2 profile macrophages compared to the treatment associated with erythropoietin. Expression of F4/80 on the cell surface still remains one of the best ways to identify macrophages [66]. Our results showed that mainly in the OncoTherad+EPO group, there was an increase in immunoreactivity and in the intensity of immunostaining of F4/80 compared to the Healthy and Cancer groups. These results may be related to immune activity and greater infiltration of macrophages in the ovaries, mainly of the M1 profile (iNOS+).

In OC, blockage of FOXP3+ regulatory T cells (Tregs) recruitment appears to be a therapeutic possibility to suppress ovarian tumor advancement [67] as these cells actively participate in the neoplastic process in ovaries [68]. Our results showed that more markedly with EPO, there was an increase in the number of FOXP3+ cells and the intensity of this receptor's immunoreaction. Yamazaki et al. [69] used bacterial lipopeptides (Pam2) agonists of TLR2 and TLR6 in melanomas *in vivo*, using a murine model. They showed TLR2-dependent production of IL-10 played a role in the expansion of Treg cells *in vivo*. Likewise, treatment with EPO alone stimulated TLR2 but increased Treg cell expansion. Intraepithelial CD3+ tumor-infiltrating lymphocytes count is a significant prognostic factor in epithelial ovarian cancer [70]. However, as CD3 is expressed in all types of lymphocytes, especially in the EPO group, the increase in the number of the CD3 positive cells might be in part explained by the presence of FOXP3+ T reg cells, as IHC analysis showed a significant increase of this type of lymphocytes after EPO treatment which was related with the immunosuppressive effect triggered.

The use of a biomarker immunohistochemical panel to distinguish the five principal histotypes provides a high accuracy and it is well described for human tissues [71,72] and cell lines [73]. This valuable data can make an animal cancer model more relevant clinically and provide a basis for evaluation of experimental treatments. However, the use of the same biomarkers that define the human disease for rat models brings up challenges, since there is not much data characterizing specific DMBA models and the interpretation must be careful.

The histopathological and IHC analyses indicated that the majority of the ovarian lesions induced was of the serous type and this was consistent among all the experimental groups. First,

most of the epithelial lesions induced in the animals showed Wt1 nuclear positivity which is a biomarker of serous type of ovarian carcinoma (can be expressed both in low grade and high grade) [71]. The combination of WT1 and P53 is useful to differentiate the high-grade serous type from the low grade serous [72,74]. Thus, the indication of the serous type of the lesions (in most of the animals) is in agreement with the histopathological results as abnormal patterns of p53 staining were rarely observed. Additionally, we found heterogeneity of Wt1 expression in some ovaries of the three treated experimental groups. A heterogenous WT1 staining was already described in human epithelial ovarian cancer [75,76]. This pattern of expression could be related with a more aggressive phenotype but in this study, this also could be something specific to rats or caused by the treatments.

Inactivation/mutation of *ARID1A* is common in clear cell and endometrioid ovarian carcinoma. If PR is negative and ARID1A is lost, a clear cell carcinoma is likely [71,77]. It is reported an agreement between loss of ARID1A expression assessed by IHC and detection of predicted loss of function *ARID1A* mutations [78]. Considering the lack of previous data about histotype biomarkers in rats and regarding this type of chemically induced ovarian cancer model, the interpretation is not an easy process. The majority of the ovaries were Arid1a+ even though some showed loss of Arid1a expression in the epithelium which could indicate non serous lesions and the heterogeneity of the results obtained with the DMBA. There is also the possibility of epithelial ovarian cancer with mixed-type histology (when 2 or more histotypes are present) nonetheless it is rare in humans [12]. In the cases when WT1 and HNF1B are negative and PR is expressed or overexpressed, it is suggested endometrioid ovarian carcinoma [71]. The Pr staining in the Cancer and treated groups were similar to the healthy control group, with no staining in the epithelium. Pr negativity and Arid1a loss happened in some ovaries but HNF1B is usually positive in case of clear cell ovarian carcinoma [71,77].

Regarding the mutations, for these specific genes and hotspots considered we did not identify mutations and this information is important to characterize this ovarian cancer model. Stewart et al. [17] reported *Kras* mutations in ovarian tumors induced with DMBA, but the method of induction was different since they used DMBA/beeswax suture applied across the ovary. In addition, there are other non KRAS mechanisms of pathway activation that are consistent with low-grade serous pathology as the MAPK pathway [79]. Despite that, reports in the literature are scarce for mutations in rat ovarian cancer models and more studies are needed to evaluate the ovarian carcinogenesis, especially in rats.

The molecular and morphological features analyzed favored interpretation of our DMBA induced tumor model as low-grade serous carcinoma-like in which treatments with OncoTherad® and EPO showed immunomodulatory properties related to the reduction of ovarian lesions. OncoTherad® alone or associated with EPO stimulated TLR2 and TLR4, culminating in the increase of proinflammatory cytokines as IL-6 and IFN-γ, as well as of F4/80+ macrophages with M1 profile (iNOS). EPO alone stimulated TLR2 and increased IL-6, CD163+ (M2) macrophages, and FOXP3+ Tregs. The association of treatments might have triggered a compensatory effect between both. In this way, this work provides a basis for future advancement in OC models as well as deepens our understanding of OncoTherad® antitumor effects in serous-type cancers and assists in correlating data to human trials.

ACKNOWLEDGEMENTS

The present research was carried out with the financial support of the São Paulo Research Foundation (FAPESP). Process Numbers: 2020/15687-5 and 2021/12357-7.

DECLARATION OF COMPETING INTEREST

The authors confirm that they have no conflicts of interest.

DATA STATEMENT

The data supporting the findings of this current study are available from the corresponding author upon reasonable request.

REFERENCES

[1] U. Menon, A. Gentry-Maharaj, M. Burnell, N. Singh, A. Ryan, C. Karpinskyj, G. Carlino, J. Taylor, S.K. Massingham, M. Raikou, J.K. Kalsi, R. Woolas, R. Manchanda, R. Arora, L. Casey, A. Dawnay, S. Dobbs, S. Leeson, T. Mould, M.W. Seif, A. Sharma, K. Williamson, Y. Liu, L. Fallowfield, A.J. McGuire, S. Campbell, S.J. Skates, I.J. Jacobs, M. Parmar, Ovarian cancer population screening and mortality after long-term follow-up in the UK Collaborative Trial of Ovarian Cancer Screening (UKCTOCS): a randomised controlled trial, Lancet. 397 (2021) 2182–2193. https://doi.org/10.1016/S0140-6736(21)00731-5.

[2] Ovarian Cancer Statistics, (n.d.). https://www.cancer.org/cancer/types/ovarian-cancer/about/key-statistics.html (accessed May 19, 2023).

[3] Ovarian Cancer Survival Rates, (n.d.). https://www.cancer.org/cancer/types/ovarian-cancer/detection-diagnosis-staging/survival-rates.html (accessed May 19, 2023).

[4] Ovarian cancer survival statistics, Cancer Research UK. (2015). https://www.cancerresearchuk.org/health-professional/cancer-statistics/statistics-by-cancer-type/ovarian-cancer/survival (accessed May 19, 2023).

[5] M. Jareid, I. Snapkov, M. Holden, L.-T.R. Busund, E. Lund, T.H. Nøst, The blood transcriptome prior to ovarian cancer diagnosis: A case-control study in the NOWAC postgenome cohort, PLoS One. 16 (2021) e0256442. https://doi.org/10.1371/journal.pone.0256442.

[6] R.J. Kurman, I.-M. Shih, The Dualistic Model of Ovarian Carcinogenesis: Revisited, Revised, and Expanded, Am. J. Pathol. 186 (2016) 733–747. https://doi.org/10.1016/j.ajpath.2015.11.011.

[7] A. Talhouk, J. George, C. Wang, T. Budden, T.Z. Tan, D.S. Chiu, S. Kommoss, H.S. Leong, S. Chen, M.P. Intermaggio, B. Gilks, T.M. Nazeran, M. Volchek, W. Elatre, R.C. Bentley, J. Senz, A. Lum, V. Chow, H. Sudderuddin, R. Mackenzie, S.C.Y. Leong, G. Liu, D. Johnson, B. Chen, A. Group, J. Alsop, S.N. Banerjee, S. Behrens, C. Bodelon, A.H. Brand, L. Brinton, M.E. Carney, Y.-E. Chiew, K.L. Cushing-Haugen, C. Cybulski, D. Ennis, S. Fereday, R.T. Fortner, J. García-Donas, A. Gentry-Maharaj, R. Glasspool, T. Goranova, C.S. Greene, P. Haluska, H.R. Harris, J. Hendley, B.Y. Hernandez, E. Herpel, M. Jimenez-Linan, C. Karpinskyj, S.H. Kaufmann, G.L. Keeney, C.J. Kennedy, M. Köbel, J.M. Koziak, M.C. Larson, J. Lester, L.-A. Lewsley, J. Lissowska, J. Lubiński, H. Luk, G. Macintyre, S. Mahner, I.A. McNeish, J. Menkiszak, N. Nevins, A. Osorio, O. Oszurek, J. Palacios, S. Hinsley, C.L. Pearce, M.C. Pike, A.M. Piskorz, I. Ray-Coquard, V. Rhenius, C. Rodriguez-Antona, R. Sharma, M.E. Sherman, D. De Silva, N. Singh, P. Sinn, D. Slamon, H. Song, H. Steed, E.A. Stronach, P.J. Thompson, A. Tołoczko, B. Trabert, N. Traficante, C.-C. Tseng, M. Widschwendter, L.R. Wilkens, S.J. Winham, B. Winterhoff, A. Beeghly-Fadiel, J. Benitez, A. Berchuck, J.D. Brenton, R. Brown, J. Chang-Claude, G. Chenevix-Trench, A. deFazio, P.A. Fasching, M.J. García, S.A. Gayther, M.T. Goodman, J. Gronwald, M.J. Henderson, B.Y. Karlan, L.E. Kelemen, U. Menon, S. Orsulic, P.D.P. Pharoah, N. Wentzensen, A.H. Wu, J.M. Schildkraut, M.A. Rossing, G.E. Konecny, D.G. Huntsman, R.Y.-J. Huang, E.L. Goode, S.J. Ramus, J.A. Doherty, D.D. Bowtell, M.S. Anglesio, Development and Validation of the Gene Expression Predictor of

High-grade Serous Ovarian Carcinoma Molecular SubTYPE (PrOTYPE), Clin. Cancer Res. 26 (2020) 5411–5423. https://doi.org/10.1158/1078-0432.CCR-20-0103.

[8] F. Ravindran, B. Choudhary, Ovarian cancer: Molecular classification and targeted therapy, in: Ovarian Cancer - Updates in Tumour Biology and Therapeutics [Working Title], IntechOpen, 2021. https://doi.org/10.5772/intechopen.95967.

[9] Committee on the State of the Science in Ovarian Cancer Research, Board on Health Care Services, Institute of Medicine, National Academies of Sciences, Engineering, and Medicine, Ovarian Cancers: Evolving Paradigms in Research and Care, National Academies Press (US), Washington (DC), n.d. https://doi.org/10.17226/21841.

[10] B.M. Barnes, L. Nelson, A. Tighe, G.J. Burghel, I.-H. Lin, S. Desai, J.C. McGrail, R.D. Morgan, S.S. Taylor, Distinct transcriptional programs stratify ovarian cancer cell lines into the five major histological subtypes, Genome Med. 13 (2021) 140. https://doi.org/10.1186/s13073-021-00952-5.

[11] M.S. Anglesio, S. Kommoss, M.C. Tolcher, B. Clarke, L. Galletta, H. Porter, S. Damaraju, S. Fereday, B.J. Winterhoff, S.E. Kalloger, J. Senz, W. Yang, H. Steed, G. Allo, S. Ferguson, P. Shaw, A. Teoman, J.J. Garcia, J.K. Schoolmeester, J. Bakkum-Gamez, A.V. Tinker, D.D. Bowtell, D.G. Huntsman, C.B. Gilks, J.N. McAlpine, Molecular characterization of mucinous ovarian tumours supports a stratified treatment approach with HER2 targeting in 19% of carcinomas, J. Pathol. 229 (2013) 111–120. https://doi.org/10.1002/path.4088.

[12] R. Mackenzie, A. Talhouk, S. Eshragh, S. Lau, D. Cheung, C. Chow, N. Le, L.S. Cook, N. Wilkinson, J. McDermott, N. Singh, F. Kommoss, J. Pfisterer, D.G. Huntsman, M. Köbel, S. Kommoss, C.B. Gilks, M.S. Anglesio, Morphologic and Molecular Characteristics of Mixed Epithelial Ovarian Cancers, Am. J. Surg. Pathol. 39 (2015) 1548–1557. https://doi.org/10.1097/PAS.0000000000000476.

[13] D. Cheasley, M.J. Wakefield, G.L. Ryland, P.E. Allan, K. Alsop, K.C. Amarasinghe, S. Ananda, M.S. Anglesio, G. Au-Yeung, M. Böhm, D.D.L. Bowtell, A. Brand, G. Chenevix-Trench, M. Christie, Y.-E. Chiew, M. Churchman, A. DeFazio, R. Demeo, R. Dudley, N. Fairweather, C.G. Fedele, S. Fereday, S.B. Fox, C.B. Gilks, C. Gourley, N.F. Hacker, A.M. Hadley, J. Hendley, G.-Y. Ho, S. Hughes, D.G. Hunstman, S.M. Hunter, T.W. Jobling, K.R. Kalli, S.H. Kaufmann, C.J. Kennedy, M. Köbel, C. Le Page, J. Li, R. Lupat, O.M. McNally,

J.N. McAlpine, A.-M. Mes-Masson, L. Mileshkin, D.M. Provencher, J. Pyman, K. Rahimi, S.M. Rowley, C. Salazar, G. Samimi, H. Saunders, T. Semple, R. Sharma, A.J. Sharpe, A.N. Stephens, N. Thio, M.C. Torres, N. Traficante, Z. Xing, M. Zethoven, Y.C. Antill, C.L. Scott, I.G. Campbell, K.L. Gorringe, The molecular origin and taxonomy of mucinous ovarian carcinoma, Nat. Commun. 10 (2019) 3935. https://doi.org/10.1038/s41467-019-11862-x.

[14] A. Dawson, M.L. Fernandez, M. Anglesio, P.J. Yong, M.S. Carey, Endometriosis and endometriosis-associated cancers: new insights into the molecular mechanisms of ovarian cancer development, Ecancermedicalscience. 12 (2018) 803. https://doi.org/10.3332/ecancer.2018.803.

[15] F.C. Martins, D.-L. Couturier, A. Paterson, A.N. Karnezis, C. Chow, T.M. Nazeran, A. Odunsi, A. Gentry-Maharaj, A. Vrvilo, A. Hein, A. Talhouk, A. Osorio, A.D. Hartkopf, A. Brooks-Wilson, A. DeFazio, A. Fischer, A. Hartmann, B.Y. Hernandez, B.M. McCauley, C. Karpinskyj, C.B. de Sousa, C. Høgdall, D.G. Tiezzi, E. Herpel, F.A. Taran, F. Modugno, G. Keeney, G. Nelson, H. Steed, H. Song, H. Luk, J. Benitez, J. Alsop, J.M. Koziak, J. Lester, J.H. Rothstein, J.M. de Andrade, L. Lundvall, L. Paz-Ares, L. Robles-Díaz, L.R. Wilkens, M.J. Garcia, M.P. Intermaggio, M.-L. Alcaraz, M.A. Brett, M.W. Beckmann, M. Jimenez-Linan, M. Anglesio, M.E. Carney, M. Schneider, N. Traficante, N. Pejovic, N. Singh, N. Le, P. Sinn, P. Ghatage, R. Erber, R. Edwards, R. Vierkant, R.B. Ness, S. Leung, S. Orsulic, S.Y. Brucker, S.H. Kaufmann, S. Fereday, S. Gayther, S.J. Winham, S. Kommoss, T. Pejovic, T.A. Longacre, V. McGuire, V. Rhenius, W. Sieh, Y.B. Shvetsov, A.S. Whittemore, A. Staebler, B.Y. Karlan, C. Rodriguez-Antona, D.D. Bowtell, E.L. Goode, E. Høgdall, F.J. Candido Dos Reis, J. Gronwald, J. Chang-Claude, K.B. Moysich, L.E. Kelemen, L.S. Cook, M.T. Goodman, P.A. Fasching, R. Crawford, S. Deen, U. Menon, D.G. Huntsman, M. Köbel, S.J. Ramus, P.D.P. Pharoah, J.D. Brenton, Clinical and pathological associations of PTEN expression in ovarian cancer: a multicentre study from the Ovarian Tumour Tissue Analysis Consortium, Br. J. Cancer. 123 (2020) 793–802. https://doi.org/10.1038/s41416-020-0900-0.

[16] M.S. Anglesio, P.J. Yong, Endometriosis-associated Ovarian Cancers, Clin. Obstet. Gynecol. 60 (2017) 711. https://doi.org/10.1097/GRF.0000000000000320.

[17] S.L. Stewart, T.D. Querec, A.R. Ochman, B.N. Gruver, R. Bao, J.S. Babb, T.S. Wong, T. Koutroukides, A.D. Pinnola, A. Klein-Szanto, T.C. Hamilton, C. Patriotis, Characterization of

a carcinogenesis rat model of ovarian preneoplasia and neoplasia, Cancer Res. 64 (2004) 8177–8183. https://doi.org/10.1158/0008-5472.CAN-04-1702.

[18] K.A. Crist, Z. Zhang, M. You, W.T. Gunning, P.B. Conran, V.E. Steele, R.A. Lubet, Characterization of rat ovarian adenocarcinomas developed in response to direct instillation of 7,12-dimethylbenz[a]anthracene (DMBA) coated suture, Carcinogenesis. 26 (2005) 951–957. https://doi.org/10.1093/carcin/bgi039.

[19] L.G.A. Chuffa, B.A. Fioruci-Fontanelli, L.O. Mendes, W.J. Fávaro, P.F.F. Pinheiro, M. Martinez, F.E. Martinez, Characterization of Chemically Induced Ovarian Carcinomas in an Ethanol-Preferring Rat Model: Influence of Long-Term Melatonin Treatment, PLoS One. 8 (2013) e81676. https://doi.org/10.1371/journal.pone.0081676.

[20] S. Ganesan, P. Bhattacharya, A.F. Keating, 7,12-Dimethylbenz[a]anthracene exposure induces the DNA repair response in neonatal rat ovaries, Toxicol. Appl. Pharmacol. 272 (2013) 690–696. https://doi.org/10.1016/j.taap.2013.08.013.

[21] J.A. Madden, P.B. Hoyer, P.J. Devine, A.F. Keating, Acute 7,12-dimethylbenz[a]anthracene exposure causes differential concentration-dependent follicle depletion and gene expression in neonatal rat ovaries, Toxicol. Appl. Pharmacol. 276 (2014) 179–187. https://doi.org/10.1016/j.taap.2014.02.011.

[22] R.L. Chandler, J.S. Damrauer, J.R. Raab, J.C. Schisler, M.D. Wilkerson, J.P. Didion, J. Starmer, D. Serber, D. Yee, J. Xiong, D.B. Darr, F. Pardo-Manuel de Villena, W.Y. Kim, T. Magnuson, Coexistent ARID1A-PIK3CA mutations promote ovarian clear-cell tumorigenesis through pro-tumorigenic inflammatory cytokine signalling, Nat. Commun. 6 (2015) 6118. https://doi.org/10.1038/ncomms7118.

[23] K.L. Napoli, B.D. Kahan, Nonselective measurement of cyclosporine for therapeutic drug monitoring by fluorescence polarization immunoassay with a rabbit polyclonal antibody: I. Evaluation of the serum methodology and comparison with a sheep polyclonal antibody in an 3H-tracer mediated radioimmunoassay, Transplant. Proc. 22 (1990) 1175–1180. https://www.ncbi.nlm.nih.gov/pubmed/2190377.

[24] S. Zhang, I. Dolgalev, T. Zhang, H. Ran, D.A. Levine, B.G. Neel, Both fallopian tube and ovarian surface epithelium are cells-of-origin for high-grade serous ovarian carcinoma, Nat. Commun. 10 (2019) 5367. https://doi.org/10.1038/s41467-019-13116-2.

[25] H. Wang, S. Galbán, R. Wu, B.M. Bowman, A. Witte, K. Vetter, C.J. Galbán, B.D. Ross, K.R. Cho, A. Rehemtulla, Molecular imaging reveals a role for AKT in resistance to cisplatin for ovarian endometrioid adenocarcinoma, Clin. Cancer Res. 19 (2013) 158–169. https://doi.org/10.1158/1078-0432.CCR-12-2380.

[26] R.L. Chandler, J.R. Raab, M. Vernon, T. Magnuson, J.C. Schisler, Global gene expression profiling of a mouse model of ovarian clear cell carcinoma caused by ARID1A and PIK3CA mutations implicates a role for inflammatory cytokine signaling, Genom Data. 5 (2015) 329–332. https://doi.org/10.1016/j.gdata.2015.06.027.

[27] K.N. Townsend, J.E. Spowart, H. Huwait, S. Eshragh, N.R. West, M.A. Elrick, S.E. Kalloger, M. Anglesio, P.H. Watson, D.G. Huntsman, J.J. Lum, Markers of T cell infiltration and function associate with favorable outcome in vascularized high-grade serous ovarian carcinoma, PLoS One. 8 (2013) e82406. https://doi.org/10.1371/journal.pone.0082406.

[28] S. Corvigno, J.K. Burks, W. Hu, Y. Zhong, N.B. Jennings, N.D. Fleming, S.N. Westin, B. Fellman, J. Liu, A.K. Sood, Immune microenvironment composition in high-grade serous ovarian cancers based on BRCA mutational status, J. Cancer Res. Clin. Oncol. 147 (2021) 3545–3555. https://doi.org/10.1007/s00432-021-03778-1.

[29] W.J. Fávaro, N.E.D. Caballero, Processo de obtenção de complexo nanoestruturado (cfi-1), complexo nanoestruturado associado a proteína (mrb-cfi-1), BR:102017012768:B1, 2022. https://patentimages.storage.googleapis.com/dd/0e/84/5ce8e5594dd259/BR102017012768B1.pdf (accessed May 19, 2023).

[30] W.J. Favaro, N.E.D. Caballero, Method for producing a nanostructured complex (CFI-1), a protein-associated nanostructured complex (MRB-CFI-1) and use, 11572284, 2023. https://patentimages.storage.googleapis.com/68/24/63/ffa789b92f38b6/US11572284.pdf (accessed May 19, 2023).

[31] W.J. Fávaro, J.C.C. Alonso, B.R. de Souza, I.B. Reis, J.M. Gonçalves, A.C. Deckmann, G. Oliveira, Q.C. Dias, N. Durán, New synthetic nano-immunotherapy (OncoTherad®) for non-

muscle invasive bladder cancer: Its synthesis, characterization and anticancer property, Tissue Cell. 80 (2023) 101988. https://doi.org/10.1016/j.tice.2022.101988.

[32] I.B. Reis, L.H.S. Tibo, E.A.R. Socca, B.R. de Souza, N. Durán, W.J. Fávaro, OncoTherad® (MRB-CFI-1) nano-immunotherapy reduced tumoral progression in non-muscle invasive bladder cancer through activation of Toll-like signaling pathway, Tissue Cell. 76 (2022) 101762. https://doi.org/10.1016/j.tice.2022.101762.

[33] REBEC, (n.d.). https://ensaiosclinicos.gov.br/rg/RBR-6swqd2 (accessed May 19, 2023).

[34] J.C.C. Alonso, B. Ribeiro de Souza, G. Leme, I. Brum Reis, J.M. Gonçalves, A.A. Cintra, L.L.L. de Freitas, F.G. Pereira, A. Billis, W.J. Fávaro, Crosstalk among T-cell CX3CR1, immune checkpoints and toll-like receptor 4 signaling pathway in BCG-unresponsive nonmuscle invasive bladder cancer: Mechanism of action of OncoTherad Nano-Immunotherapy, J. Clin. Oncol. 40 (2022) e16551–e16551. https://doi.org/10.1200/jco.2022.40.16_suppl.e16551.

[35] J.C.C. Alonso, I.B. Reis, J.M. Gonçalves, B.R. de S. Sasaki, A.A. Cintra, N. Duran, A. Billis, W.J. Fávaro, Oncotherad immunotherapy elicits promising responses in Bacillus Calmette-Guérin-unresponsive non–muscle invasive bladder cancer: Results from phase I/ II study, J. Clin. Oncol. 38 (2020) e17048–e17048. https://doi.org/10.1200/jco.2020.38.15_suppl.e17048.

[36] M. Lombardero, K. Kovacs, B.W. Scheithauer, Erythropoietin: a hormone with multiple functions, Pathobiology. 78 (2011) 41–53. https://doi.org/10.1159/000322975.

[37] O. Katz, L. Gil, L. Lifshitz, S. Prutchi-Sagiv, M. Gassmann, M. Mittelman, D. Neumann, Erythropoietin enhances immune responses in mice, Eur. J. Immunol. 37 (2007) 1584–1593. https://doi.org/10.1002/eji.200637025.

[38] L. Lifshitz, S. Prutchi-Sagiv, M. Avneon, M. Gassmann, M. Mittelman, D. Neumann, Non-erythroid activities of erythropoietin: Functional effects on murine dendritic cells, Mol. Immunol. 46 (2009) 713–721. https://doi.org/10.1016/j.molimm.2008.10.004.

[39] L. Lifshitz, G. Tabak, M. Gassmann, M. Mittelman, D. Neumann, Macrophages as novel target cells for erythropoietin, Haematologica. 95 (2010) 1823–1831. https://doi.org/10.3324/haematol.2010.025015.

[40] Y. Ergun, A. Koc, K. Dolapcioglu, Y. Akaydin, G. Dogruer, T. Kontas, T. Kozlu, E. Aslan, The protective effect of erythropoietin and dimethylsulfoxide on ischemia-reperfusion injury in rat ovary, Eur. J. Obstet. Gynecol. Reprod. Biol. 152 (2010) 186–190. https://doi.org/10.1016/j.ejogrb.2010.05.025.

[41] Manizheh, The ovario-protective effect of erythropoietin against oxidative damage associated with reperfusion following ovarian torsion in rat, Am. J. Anim. Vet. Sci. 6 (2011) 18–24. https://doi.org/10.3844/ajavsp.2011.18.24.

[42] M. Mahmoodi, M. Soleimani Mehranjani, S.M.A. Shariatzadeh, H. Eimani, A. Shahverdi, Effects of erythropoietin on ischemia, follicular survival, and ovarian function in ovarian grafts, Reproduction. 147 (2014) 733–741. https://doi.org/10.1530/REP-13-0379.

[43] C. Dayangan Sayan, O.B. Tulmac, G. Karaca, Z.S. Ozkan, S. Yalcin, T. Devrim, N. Dindar Badem, Could erythropoietin reduce the ovarian damage of cisplatin in female rats?, Gynecol. Endocrinol. 34 (2018) 309–313. https://doi.org/10.1080/09513590.2017.1395836.

[44] C.Y. Beh, C.W. How, J.B. Foo, J.N. Foong, G.T. Selvarajah, A. Rasedee, Development of erythropoietin receptor-targeted drug delivery system against breast cancer using tamoxifen-loaded nanostructured lipid carriers, Drug Des. Devel. Ther. 11 (2017) 771–782. https://doi.org/10.2147/DDDT.S123939.

[45] C.Y. Beh, A. Rasedee, G.T. Selvarajah, L.S. Yazan, A.R. Omar, J.N. Foong, C.W. How, J.B. Foo, Enhanced anti-mammary gland cancer activities of tamoxifen-loaded erythropoietin-coated drug delivery system, PLoS One. 14 (2019) e0219285. https://doi.org/10.1371/journal.pone.0219285.

[46] P. Cornes, I. Boiangiu, The role of epoetin beta in the treatment of anaemia in patients with gynaecological malignancies, Anticancer Res. 27 (2007) 513–522. https://www.ncbi.nlm.nih.gov/pubmed/17348435.

[47] M.E. Hardee, J.P. Kirkpatrick, S. Shan, S.A. Snyder, Z. Vujaskovic, Z.N. Rabbani, M.W. Dewhirst, K.L. Blackwell, Human recombinant erythropoietin (rEpo) has no effect on tumour growth or angiogenesis, Br. J. Cancer. 93 (2005) 1350–1355. https://doi.org/10.1038/sj.bjc.6602846.

[48] L.G. de Almeida Chuffa, G. de Moura Ferreira, L.A. Lupi, I. da Silva Nunes, W.J. Fávaro, P-MAPA immunotherapy potentiates the effect of cisplatin on serous ovarian carcinoma through targeting TLR4 signaling, J. Ovarian Res. 11 (2018) 8. https://doi.org/10.1186/s13048-018-0380-5.

[49] F.K. Marcondes, F.J. Bianchi, A.P. Tanno, Determination of the estrous cycle phases of rats: some helpful considerations, Braz. J. Biol. 62 (2002) 609–614. https://doi.org/10.1590/s1519-69842002000400008.

[50] J.M. Goldman, A.S. Murr, R.L. Cooper, The rodent estrous cycle: characterization of vaginal cytology and its utility in toxicological studies, Birth Defects Res. B Dev. Reprod. Toxicol. 80 (2007) 84–97. https://doi.org/10.1002/bdrb.20106.

[51] L.P. Dias, Â.C.M. Luzo, B.B. Volpe, M. Durán, S.E.M. Galdames, L.A.B. Ferreira, N. Durán, W.J. Fávaro, Effects of intravesical therapy with platelet-rich plasma (PRP) and Bacillus Calmette-Guérin (BCG) in non-muscle invasive bladder cancer, Tissue Cell. 52 (2018) 17–27. https://doi.org/10.1016/j.tice.2018.03.011.

[52] A. Untergasser, H. Nijveen, X. Rao, T. Bisseling, R. Geurts, J.A.M. Leunissen, Primer3Plus, an enhanced web interface to Primer3, Nucleic Acids Res. 35 (2007) W71–4. https://doi.org/10.1093/nar/gkm306.

[53] The R Project for Statistical Computing, (n.d.). http://www.r-project.org/index.html (accessed May 19, 2023).

[54] K.L. Hetzler, J.P. Hardee, H.A. LaVoie, E.A. Murphy, J.A. Carson, Ovarian function's role during cancer cachexia progression in the female mouse, Am. J. Physiol. Endocrinol. Metab. 312 (2017) E447–E459. https://doi.org/10.1152/ajpendo.00294.2016.

[55] J. Tropp, E.J. Markus, Effects of mild food deprivation on the estrous cycle of rats, Physiol. Behav. 73 (2001) 553–559. https://doi.org/10.1016/s0031-9384(01)00487-5.

[56] D. Dixon, R. Alison, U. Bach, K. Colman, G.L. Foley, J.H. Harleman, R. Haworth, R. Herbert, A. Heuser, G. Long, M. Mirsky, K. Regan, E. Van Esch, F.R. Westwood, J. Vidal, M. Yoshida, Nonproliferative and proliferative lesions of the rat and mouse female reproductive system, J. Toxicol. Pathol. 27 (2014) 1S–107S. https://doi.org/10.1293/tox.27.1S.

[57] T. Yano, J. Pinski, G. Halmos, K. Szepeshazi, K. Groot, A.V. Schally, Inhibition of growth of OV-1063 human epithelial ovarian cancer xenografts in nude mice by treatment with luteinizing hormone-releasing hormone antagonist SB-75, Proc. Natl. Acad. Sci. U. S. A. 91 (1994) 7090–7094. https://doi.org/10.1073/pnas.91.15.7090.

[58] S. Chattopadhyay, S. Pal Ghosh, D. Ghosh, J. Debnath, Effect of dietary co-administration of sodium selenite on sodium arsenite-induced ovarian and uterine disorders in mature albino rats, Toxicol. Sci. 75 (2003) 412–422. https://doi.org/10.1093/toxsci/kfg194.

[59] H.S. Silveira, L.A. Lupi, G.G. Romagnoli, R. Kaneno, I. da Silva Nunes, W.J. Fávaro, L.G. de Almeida Chuffa, P-MAPA activates TLR2 and TLR4 signaling while its combination with IL-12 stimulates CD4+ and CD8+ effector T cells in ovarian cancer, Life Sci. 254 (2020) 117786. https://doi.org/10.1016/j.lfs.2020.117786.

[60] X.Y. Yang, Y. Li, S.Q. Cai, L. Wang, J.W. Qiang, Optimization of 7,12-dimethylbenz(a)anthracene-induced rat epithelial ovarian tumors, Oncol. Lett. 21 (2021) 206. https://doi.org/10.3892/ol.2021.12467.

[61] Z. Shao, Q. Wen, T. Zhu, W. Jiang, Y. Kang, C. Xu, S. Wang, Preventative effect of celecoxib in dimethylbenz[a]anthracene-induced ovarian cancer in rats, Arch. Gynecol. Obstet. 298 (2018) 981–989. https://doi.org/10.1007/s00404-018-4898-y.

[62] M. Zhou, M.M. McFarland-Mancini, H.M. Funk, N. Husseinzadeh, T. Mounajjed, A.F. Drew, Toll-like receptor expression in normal ovary and ovarian tumors, Cancer Immunol. Immunother. 58 (2009) 1375–1385. https://doi.org/10.1007/s00262-008-0650-y.

[63] T.S. Lau, L.K.Y. Chan, G.C.W. Man, C.H. Wong, J.H.S. Lee, S.F. Yim, T.H. Cheung, I.A. McNeish, J. Kwong, Paclitaxel Induces Immunogenic Cell Death in Ovarian Cancer via TLR4/IKK2/SNARE-Dependent Exocytosis, Cancer Immunol Res. 8 (2020) 1099–1111. https://doi.org/10.1158/2326-6066.CIR-19-0616.

[64] A.H. Gao, Y.R. Hu, W.P. Zhu, IFN-γ inhibits ovarian cancer progression via SOCS1/JAK/STAT signaling pathway, Clin. Transl. Oncol. 24 (2022) 57–65. https://doi.org/10.1007/s12094-021-02668-9.

[65] M.K. Skytthe, J.H. Graversen, S.K. Moestrup, Targeting of CD163 Macrophages in Inflammatory and Malignant Diseases, Int. J. Mol. Sci. 21 (2020). https://doi.org/10.3390/ijms21155497.

[66] A. Dos Anjos Cassado, F4/80 as a Major Macrophage Marker: The Case of the Peritoneum and Spleen, Results Probl. Cell Differ. 62 (2017) 161–179. https://doi.org/10.1007/978-3-319-54090-0_7.

[67] M. Singh, T. Loftus, E. Webb, F. Benencia, Minireview: Regulatory T Cells and Ovarian Cancer, Immunol. Invest. 45 (2016) 712–720. https://doi.org/10.1080/08820139.2016.1186689.

[68] N. Erfani, M. Hamedi-Shahraki, S. Rezaeifard, M. Haghshenas, M. Rasouli, A. Samsami Dehaghani, FoxP3+ regulatory T cells in peripheral blood of patients with epithelial ovarian cancer, Iran. J. Immunol. 11 (2014) 105–112. https://www.ncbi.nlm.nih.gov/pubmed/24975967.

[69] S. Yamazaki, K. Okada, A. Maruyama, M. Matsumoto, H. Yagita, T. Seya, TLR2-dependent induction of IL-10 and Foxp3+ CD25+ CD4+ regulatory T cells prevents effective anti-tumor immunity induced by Pam2 lipopeptides in vivo, PLoS One. 6 (2011) e18833. https://doi.org/10.1371/journal.pone.0018833.

[70] B. Liu, J. Nash, C. Runowicz, H. Swede, R. Stevens, Z. Li, Ovarian cancer immunotherapy: opportunities, progresses and challenges, J. Hematol. Oncol. 3 (2010) 7. https://doi.org/10.1186/1756-8722-3-7.

[71] M. Köbel, J. Bak, B.I. Bertelsen, O. Carpen, A. Grove, E.S. Hansen, A.-M. Levin Jakobsen, M. Lidang, A. Måsbäck, A. Tolf, C.B. Gilks, J.W. Carlson, Ovarian carcinoma histotype determination is highly reproducible, and is improved through the use of immunohistochemistry, Histopathology. 64 (2014) 1004–1013. https://doi.org/10.1111/his.12349.

[72] M. Köbel, E.Y. Kang, The Evolution of Ovarian Carcinoma Subclassification, Cancers . 14 (2022). https://doi.org/10.3390/cancers14020416.

[73] M.S. Anglesio, K.C. Wiegand, N. Melnyk, C. Chow, C. Salamanca, L.M. Prentice, J. Senz, W. Yang, M.A. Spillman, D.R. Cochrane, K. Shumansky, S.P. Shah, S.E. Kalloger, D.G.

Huntsman, Correction: Type-Specific Cell Line Models for Type-Specific Ovarian Cancer Research, PLoS One. 8 (2013). https://doi.org/10.1371/annotation/ffcaf179-872f-470b-8bb6-f06d8ba6d03a.

[74] M. Köbel, A.M. Piskorz, S. Lee, S. Lui, C. LePage, F. Marass, N. Rosenfeld, A.-M. Mes Masson, J.D. Brenton, Optimized p53 immunohistochemistry is an accurate predictor of mutation in ovarian carcinoma, Hip Int. 2 (2016) 247–258. https://doi.org/10.1002/cjp2.53.

[75] B. Hylander, E. Repasky, P. Shrikant, M. Intengan, A. Beck, D. Driscoll, P. Singhal, S. Lele, K. Odunsi, Expression of Wilms tumor gene (WT1) in epithelial ovarian cancer, Gynecol. Oncol. 101 (2006) 12–17. https://doi.org/10.1016/j.ygyno.2005.09.052.

[76] L. Liliac, M.L. Carcangiu, S. Canevari, I.D. Căruntu, D.G. Ciobanu Apostol, M. Danciu, M. Onofriescu, C. Amălinei, The value of PAX8 and WT1 molecules in ovarian cancer diagnosis, Rom. J. Morphol. Embryol. 54 (2013) 17–27. https://www.ncbi.nlm.nih.gov/pubmed/23529305.

[77] O. Fadare, C. Zhao, D. Khabele, V. Parkash, C.M. Quick, K. Gwin, M.M. Desouki, Comparative analysis of Napsin A, alpha-methylacyl-coenzyme A racemase (AMACR, P504S), and hepatocyte nuclear factor 1 beta as diagnostic markers of ovarian clear cell carcinoma: an immunohistochemical study of 279 ovarian tumours, Pathology. 47 (2015) 105–111. https://doi.org/10.1097/PAT.0000000000000223.

[78] M. Köbel, M.S. Anglesio, J.D. Brenton, You won’t believe this old test … that does cheap single-cell mutation detection, Hip Int. 4 (2018) 149–153. https://doi.org/10.1002/cjp2.108.

[79] V. Givant-Horwitz, B. Davidson, P. Lazarovici, E. Schaefer, J.M. Nesland, C.G. Tropé, R. Reich, Mitogen-activated protein kinases (MAPK) as predictors of clinical outcome in serous ovarian carcinoma in effusions, Gynecol. Oncol. 91 (2003) 160–172. https://doi.org/10.1016/S0090-8258(03)00434-7.

SUPPLEMENTARY FILES

Supplemental Fig. 1. Environmental enrichment applied to Fischer rats. Environmental enrichment for rats favors the well-being of experimental animals, with the observation of attitudes more similar to the natural one, with more active behavior, less anxiety and possibly less stress [1].

1. Gozzer, P.; Andrade, E.; Belotto, P. C. P.; Mascarin, A. A. L. Comportamento de ratos Wistar: importância do enriquecimento ambiental. Saúde Rev, v. 18, n. 48, p. 67-77, 2018.

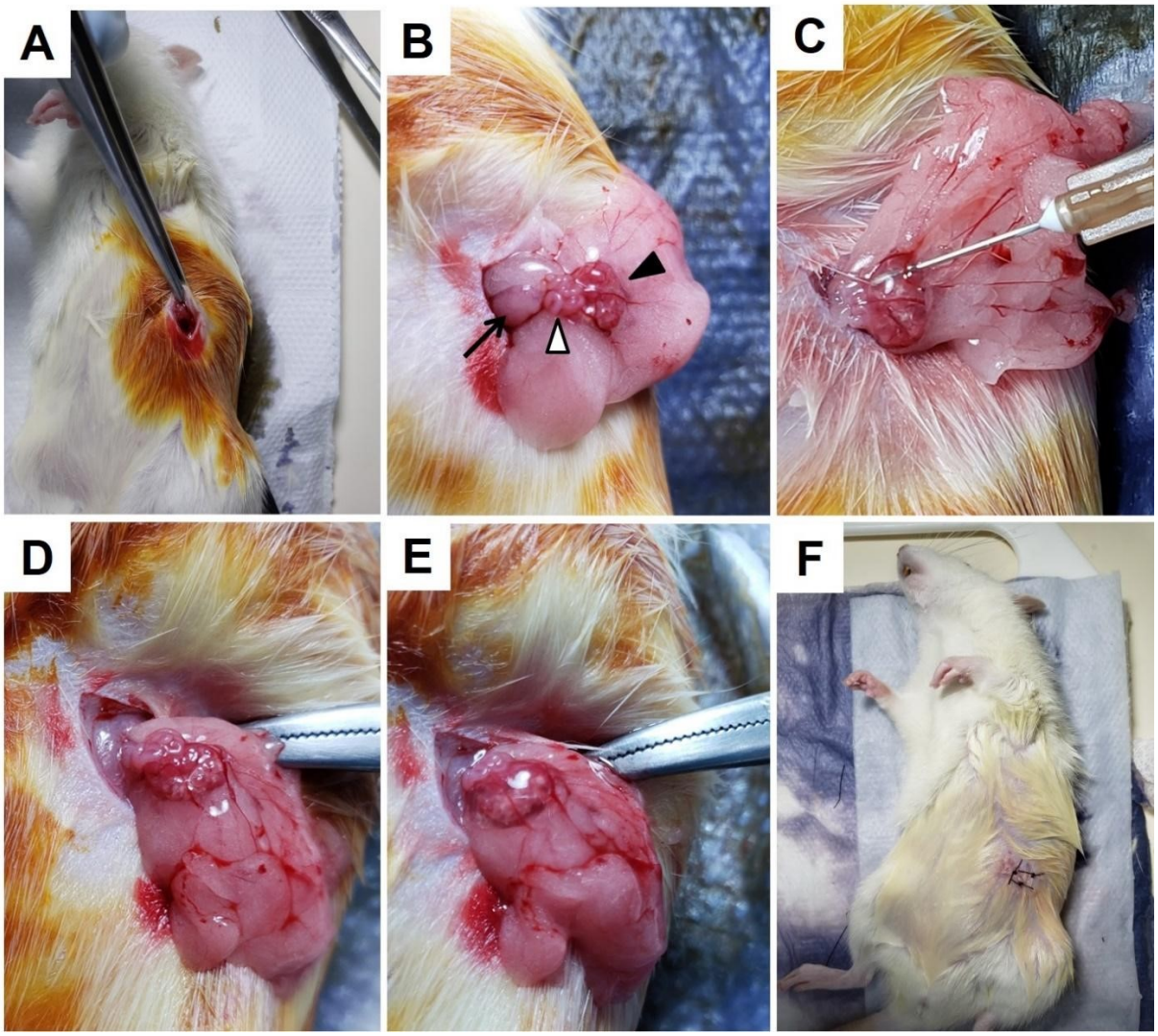

Supplemental Fig. 2. Surgical procedure for inducing ovarian cancer. (A) Initial incision, close to the thoracolumbar junction and iliac crest on the left side. (B) Exposition and identification of the structures of the reproductive tract in the estrus phase: bursa covering the ovary (closed arrowhead); uterine tube (open arrowhead) and end of the uterine horn (arrow). (C) Example of DMBA application in the ovarian bursa. Observe the difference in the ovarian bursa before the application (D) and after its space is filled by the injection with DMBA (E). (F) Examples of sutures performed to close the abdominal wall and skin.

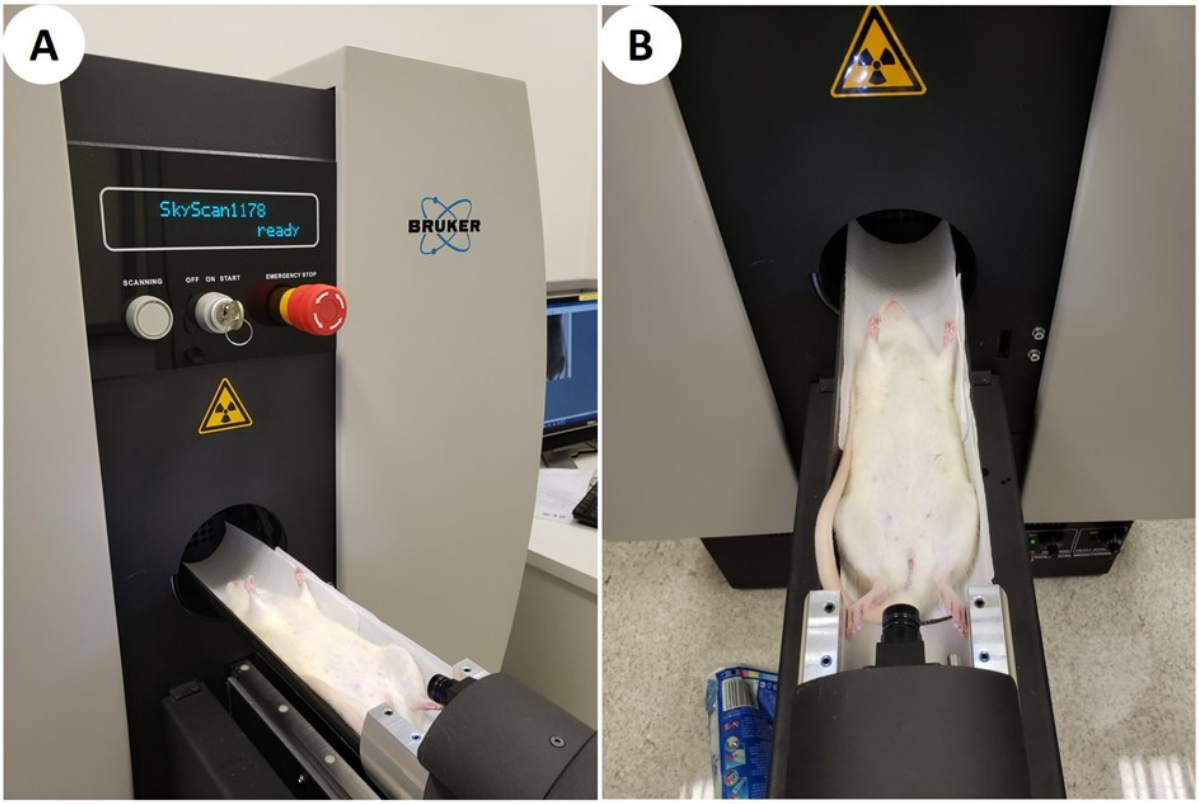

Supplemental Fig. 3. X-ray computed microtomography (micro-CT) examination. (A) Skyscan 1178 microtomography (Bruker) used and anesthetized rat. (B) Detail of positioning the animal in dorsal decubitus on the equipment bed for the image acquisition process.

Supplemental Table 1. Primary antibodies for Immunohistochemistry.

Antibody	Clonality	Code	Distributor	Dilution
TLR2	polyclonal	sc-10739	Santa Cruz Biotechnology, USA	1:100
TLR4	monoclonal	sc-293072	Santa Cruz Biotechnology, USA	1:100
IL-6	polyclonal	sc-1265	Santa Cruz Biotechnology, USA	1:200
IFN-γ	monoclonal	sc-12755	Santa Cruz Biotechnology, USA	1:100
iNOS	polyclonal	ab3523	Abcam, USA	1:100
F4/80	polyclonal	sc-25830	Santa Cruz Biotechnology, USA	1:50
CD163	polyclonal	bs2527R	Bioss, USA	1:150
FOXP3	monoclonal	sc-53876	Santa Cruz Biotechnology, USA	1:200

Supplemental Table 2. Primary antibodies for Histotyping Immunohistochemistry (TMAs).

Antibody	Clone	Clonality	Code	Distributor	Dilution
WT1	[CAN-R9(IHC)-56-2]	monoclonal	ab89901	Abcam	1:300
p53	[PAb 1801]	monoclonal	sc-98	Santa Cruz Biotechnology	1:200
PR	[SP42]	monoclonal	ab101688	Abcam	1:400
HNF1B	HPA 002083	polyclonal	HPA002083	Sigma	1:1200
ARID1A	[EPR13501]	monoclonal	ab182560	Abcam	1:10000
CD3	[SP7]	monoclonal	ab16669	Abcam	1:400

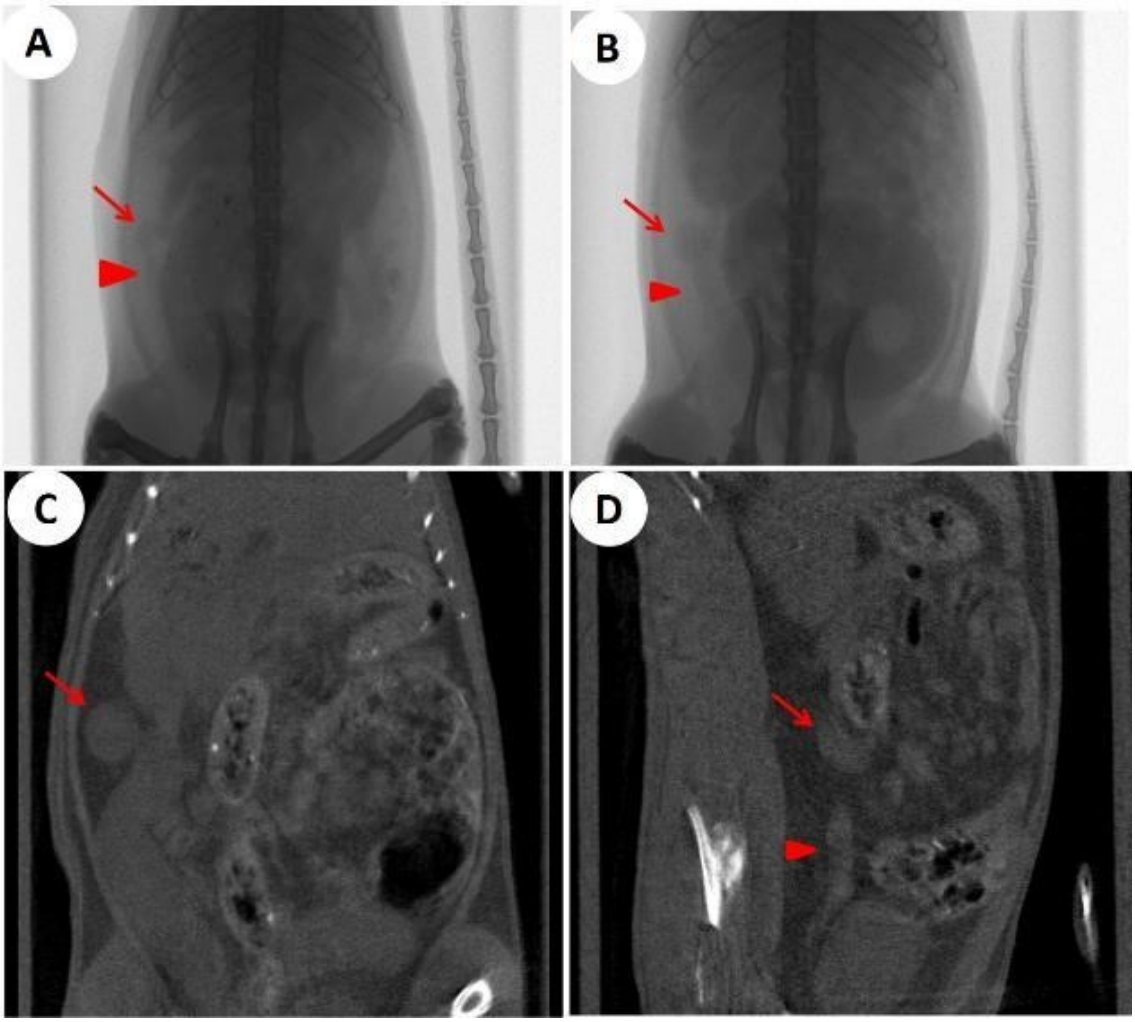

Supplemental Fig. 4. Photographs with X-ray computed microtomography (micro-CT) examination. (A) Healthy Control Rat (uptake without 3D reconstruction), showing the left ovary (arrow) and the left uterine horn (closed arrowhead). (B) Rat induced with ovarian cancer (uptake without 3D reconstruction), note the more pronounced left ovary (arrow) and the left uterine horn (closed arrowhead). (C, D) Images of rats observed at ovarian cancer induction after 3D reconstruction. Left ovary (arrow) and uterine horn (closed arrowhead) in the coronal (C) and sagittal (D) planes. During the exams, visualization difficulties were found due to the size and position of the female gonad, as well as the presence of feces and intestinal gases. However, anatomical structures such as the uterine horns were used to help identify the position of the ovaries. The dimensional differences of the ovaries found in the images captured through microtomography were interpreted together with the other results of macroscopic and histopathological analysis, allowing monitoring of the procedure of chemical OC induction. Equipment used: Microtomography Skyscan 1178.

Supplemental Table 3. Body weight (g) in different periods and weight gain rate (g/week) of experimental groups.

	Experimental groups (n=7 animals/group)				
Parameters	**Control**	**Cancer**	**OncoTherad**	**EPO**	**OncoTherad+EPO**
Initial body weight (g)*	192.8 ± 4.7 **a**	183.4 ± 9.2 **a**	192.8 ± 10.7 **a**	199.4 ± 7.4 **a**	193.4 ± 9.3 **a**
Body weight after OC development (g)	208.4 ± 7.0 **a**	218.6 ± 5.4 **a**	210.0 ± 14.1 **a**	226.7 ± 9.5 **a**	215.4 ± 14.2 **a**
Final body weight (g)*	214.4 ± 6.6 **a**	219.4 ± 8.4 **a**	226.1 ± 15.7 **a**	229.0 ± 12.0 **a**	217.3 ± 12.5 **a**
Weight gain/week (g)	0.98 ± 0.11 **a**	1.41 ± 0.37 **a**	1.39 ± 0.42 **a**	1.08 ± 0.58 **a**	0.88 ± 0.44 **a**

Values expressed as mean ± standard deviation. ANOVA. *Kruskal Wallis test. In the same line, values followed by equal letters indicate absence of statistically significant difference between groups (p>0.05).

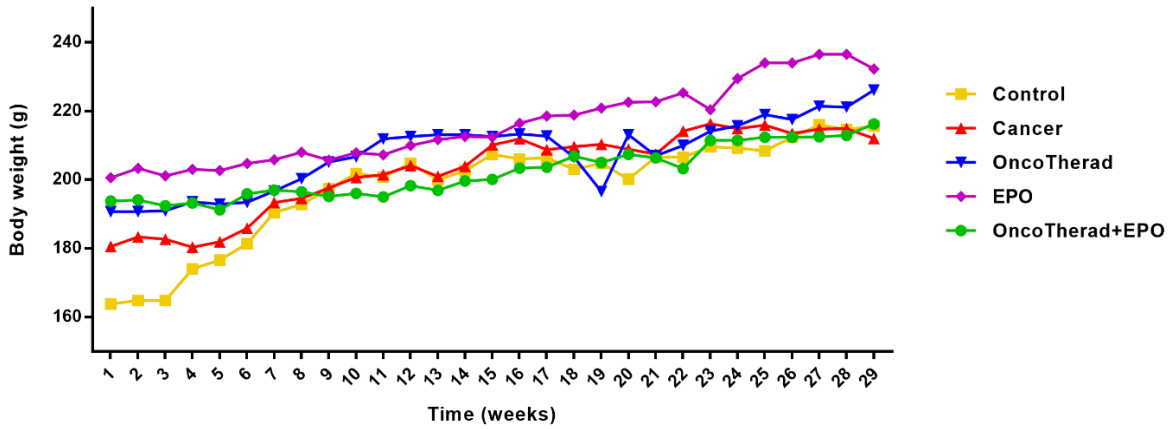

Supplemental Fig. 5. Body weight variation of the groups. Graph of body weight variation from the 1st to the 29th week. In the 3rd and 4th weeks, surgeries of chemical induction of OC. The period between the 4th and 25th week corresponds to the period of tumor development (around 140 days). The period between the 25th and 28th week corresponds to the 4 weeks of treatments with OncoTherad®, Erythropoietin, and OncoTherad® associated with Erythropoietin. The 29th week corresponds to the euthanasia of the animals.

Supplemental Table 4. Feed consumption (g/animal/week) and water consumption (ml/animal/week) of experimental groups in different periods.

	Experimental groups (n=7/group)				
Parameters	**Control**	**Cancer**	**OncoTherad**	**EPO**	**OncoTherad +EPO**
Feed consumption (g/animal/week)					
General (all period)	79.98 ± 16.6 **a**	79.01 ± 9.0 **a**	77.49 ± 18.2 **a**	77.64 ± 7.7 **a**	74.78 ± 8.1 **a**
Before surgery	90.50 ± 30.9 **a**	76.22 ± 3.7 **a**	68.25 ± 20.7 **a**	86.05 ± 9.3 **a**	77.73 ± 3.3 **a**
Tumor development	78.37 ± 13.0 **a**	81.12 ± 9.7 **a**	76.36 ± 6.5 **a**	77.95 ± 8.1 **a**	75.15 ± 8.1 **a**
During the treatments	75.25 ± 3.2 **a**	73.36± 3.7 **a**	91.98 ± 31.4 **a**	74.88 ± 8.5 **a**	72.77 ± 11.1 **a**
Water consumption (ml/animal/week)					
General (all period)	101.8 ± 22.1 **a**	103.0 ± 18.3 **a**	85.3 ± 22.3 **b**	94.4 ± 18.4 **a**	94.5 ± 16.8 **a**
Before surgery*	114.0 ± 19.8 **a**	115.0 ± 17.1 **a**	92.1 ± 27.9 **a**	124.3 ± 6.6 **a**	108.0 ± 11.4 **a**
Tumor development	104.1 ± 22.6 **ac**	102.8 ± 17.2 **a**	80.1 ± 11.76 **d**	88.4 ± 14.0 **b**	90.6 ± 16.7 **bc**
During the treatments	81.3 ± 4.2 **a**	84.2 ± 3.9 **a**	92.9 ± 37.7 **a**	101.3 ± 22.0 **a**	101.7 ± 16.5 **a**

Values expressed as mean ± standard deviation. Kruskal-Wallis, Student-Newman-Keuls test. *ANOVA. In the same line, values followed by different letters indicate statistical difference between groups ($p<0.05$). The differences among the groups during the tumor development period were not related to the OncoTherad® or EPO, since in that period the treatments had not yet been started.

Supplemental Fig. 6. Sections of the TMAs after IHC assays with the histotypes biomarkers. (A) Wt1, (B) Arid1a, (C) Hnf1b, (D) Pr, and (E) p53. Bars = 6mm.

6. CONSIDERAÇÕES FINAIS

Os efeitos antitumorais da imunoterapia OncoTherad® relacionados à indução da produção de IFN-γ foram demonstrados tanto no câncer de bexiga não-músculo invasivo como no carcinoma ovariano do tipo seroso em modelo animal. As associações envolvendo o Plasma Rico em Plaquetas no câncer de bexiga e a Eritropoetina no câncer de ovário mostraram que esses compostos podem modular os efeitos da imunoterapia. Enquanto o PRP polarizou a imunomodulação para o receptor TLR4, a EPO balanceou a estimulação imune através da estimulação de TLR2. Por fim, foi possível descrever novas estratégias para o desenvolvimento de terapias oncológicas para os cânceres do sistema urogenital bem como caracterizar um novo modelo de câncer de ovário para o teste de fármacos considerando o histotipo específico.

7. REFERÊNCIAS

AAPRO, M., JELKMANN, W., CONSTANTINESCU, S. N., LEYLAND-JONES, B. Effects of erythropoietin receptors and erythropoiesis-stimulating agents on disease progression in cancer. **Br J Cancer**, v. 106, n. 7, p. 1249-1258, 2012.

ABBAS, A. K.; LICHTMAN, A. H.; PILLAI, S. H. I. V. Imunologia celular e molecular. 7. ed. Rio de Janeiro: Elsevier, 2012. ADAMS, M. et al. The rationale for combined chemo/immunotherapy using a Toll-like receptor 3 (TLR3) agonist and tumour- derived exosomes in advanced ovarian cancer. **Vaccine**, v. 23, n. 17-18, p. 2374-2378, 2005.

ABULAFIA O. et al. Angiogenesis in primary and metastatic epithelial ovarian carcinoma. **Am J Obstet Gynecol**, v. 177, p. 541–7, 1997.

ABULAFIA O.; SHERER D. M. Angiogenesis in the uterine cervix. **Int J Gynecol Cancer**, v. 10, p.349 – 57, 2000.

ACEBES-HUERTA, A., ARIAS-FERNÁNDEZ, T., BERNARDO, Á., MUÑOZ-TURRILLAS, M.C., FERNÁNDEZ-FUERTES, J., SEGHATCHIAN, J. AND GUTIÉRREZ, L. Platelet-derived bio-products: classification update, applications, concerns and new perspectives. **Transfusion and Apheresis Science**, n. 59, v. 1, p.102716, 2020.

AFZAL, M. Z. et al. Efficacy of metformin in combination with immune checkpoint inhibitors (anti-PD-1/anti-CTLA-4) in metastatic malignant melanoma, **JITC**, v. 6, n. 64, 2018.

AKIRA, S., & TAKEDA, K. Toll-like receptor signalling. **Nat Rev Immunol**, v. 4, n. 7, p. 499-511, 2004.

AKIRA, S.; TAKAEDA, K. Toll-like receptor signalling. **Nat Ver Immunol**,v. 4, n. 7, p. 499-511, 2020.

AKIYAMA H. Control of chondrogenesis by the transcription factor Sox9. **Mod Rheumatol**, v. 18, n. 3, p. 213–219, 2008.

ALONSO, J.C.C. et al. Oncotherad immunotherapy elicits promising responses in Bacillus Calmette-Guérin-unresponsive non–muscle invasive bladder cancer: Results from phase I/II study. **J Clin Oncol**, v. 37, 15 Suppl, 2020.

ALSHAKER, H. A., & MATALKA, K. Z. IFN-gamma, IL-17 and TGF-beta involvement in shaping the tumor microenvironment: The significance of modulating such cytokines in treating malignant solid tumors. **Cancer Cell Int**, v. 11, 2011.

ALVAREZ A. A. et al. The prognostic significance of angiogenesis in epithelial ovarian carcinoma. **Clin Cancer Res**, v. 5, p. 587–91, 1999.

AMERICAN CANCER SOCIETY. **Key Statistics for Blader Cancer**. 2022a. Disponível em: https://www.cancer.org/cancer/bladder-cancer/about/key-statistics.html. Acesso em: 26 dez 2022.

AMERICAN CANCER SOCIETY. **KeyStatistics for Ovarian Cancer**, 2022b. Disponível em:<https://www.cancer.org/cancer/ovarian-cancer/about/key-statistics.html> Acesso em: 28 dez 2022.

AMJADI, F. et al. Variable localization of Toll-like receptors in human fallopian tube epithelial cells. **Clin Exp ReprodMed**, v. 45, n. 1, p. 1-9, 2018.

ANDERSON, R. A. et al. Activation of the aryl hydrocarbon receptor by a component of cigarette smoke reduces germ cellproliferation in the human fetal ovary. **Mol Hum Reprod**, v. 20, n. 1, p. 42-48, 2014.

ANDREWS, L.; MUTCH, D. G. Hereditary Ovarian Cancer and Risk Reduction. **Best Pract Res Clin Obstet Gynaecol**, v.41, p. 31-48, 2017.

ASKELAND, E. J., NEWTON, M. R., O'DONNELL, M. A., & LUO, Y. Bladder Cancer Immunotherapy: BCG and Beyond. **Adv Urol**, v. 2012, ID 181987, 2012.

AYARI, C., BERGERON, A., LARUE, H., MENARD, C., & FRADET, Y. Toll-Like Receptors in Normal and Malignant Human Bladders. **J Urol**, n. 185, v. 5, p. 1915-1921, 2011.

BEH, C. Y. et al. Development of erythropoietin receptor-targeted drug delivery system against breast cancer using tamoxifen-loaded nanostructured lipid carriers. **Drug Des Dev Ther**, v. 11, p. 771 – 782, 2017

BEH, C. Y. et al. Enhanced anti-mammary gland cancer activities of tamoxifen-loaded erythropoietin-coated drug deliverysystem. **PloS One**, v.14, n. 7, p. e0219285, 2019.

BELLORA, F. et al. TLR activation of tumor associated macrophages from ovarian cancer patients triggers cytolytic activityof NK cells. **Eur J Immunol**, v. 44, n. 6, p. 1814-1822, 2014.

BERGER, R. et al. Toll-like receptor 9 expression in breast and ovarian cancer is associated with poorly differentiated tumors. **Cancer Sci**, v. 101, n. 4, p. 1059-1066, 2010.

BERRY, D. L., BLUMENSTEIN, B. A., MAGYARY, D. L., LAMM, D. L., & CRAWFORD, E. D. Local toxicity patterns associated with intravesical bacillus Calmette-Guerin: a Southwest Oncology Group Study. **Int J Urol**, v. 3, n. 2, p. 98-100; discussion 101, 1996.

BHARDWAJ, N.; GNJATIC, S.; SAWHNEY, N. B. TLR AGONISTS: Are They Good Adjuvants? **J Cancer**, v. 16, n. 4, p.382-391, 2010.

BHATTACHARYA, P.; KEATING, A. F. Impact of environmental exposures on ovarian function and role of xenobiotic metabolism during ovotoxicity. **Toxicol Appl Pharmacol**, v. 261, n. 3, p. 227-235, 2012.

BLACKWELL, K. L. et al. Human recombinant erythropoietin significantly improves tumor oxygenation independent of its effects on hemoglobin. **Cancer Res**, v. 63, n. 19, p. 6162-6165, 2003.

BLOCK, M. S. et al. MyD88 and TLR4 Expression in Epithelial Ovarian Cancer. **Mayo Clin Proc**, v. 93, n. 3, p. 307-320, 2018.

BÖCKELMANN, P. K.; TIZZIANI, S. H. S.; DURÁN, N.; FÁVARO, W. J. New Therapeutic Perspective for Bladder Cancer in Dogs: Toxicological and Clinical Effects of OncoTherad Nanostructured Immunotherapy. **J Phys Conf Ser**, v. 1323, n. 1, p. 012022, 2019.

BOEHM, T. et al. Antiangiogenic therapy of experimental cancer does not induce acquired drug resistance. **Nature (Lond.),** v. 390, 1997.

BOHLE, A., & BRANDAU, S. Immune mechanisms in bacillus Calmette-Guerin immunotherapy for superficial bladder cancer. **J Urol**, n. 170, v. 3, p. 964-969, 2003.

BOHLE, A., JOCHAM, D., & BOCK, P. R. Intravesical bacillus Calmette-Guerin versus mitomycin C for superficial bladder cancer: A formal meta-analysis of comparative studies on recurrence and toxicity. **J Urol**, v. 169, n. 1, p. 90-95, 2003.

BRAY, F.; FERLAY, J.; SOERJOMATARAM, I.; SIEGEL, R.L.; TORRE, L.A.; JEMAL, A. Global cancer statistics 2018: GLOBOCAN estimates of incidence and mortality worldwide for 36 cancers in 185 countries. **CA A Cancer J. Clin**. 2018, 68, 394–424.

BROOKS, A. J.; PUTOCZKI, T. JAK-STAT signalling pathway in cancer. **Cancers**, v. 12, n. 7, p. 1971, 2020.

BROOS, K., FEYS, H.B., DE MEYER, S.F., VANHOORELBEKE, K., DECKMYN, H. Platelets at work in primary hemostasis. **Blood reviews**, v. 25, n. 4, p.155-167. 2011.

BRUNELLE, J. L., & GREEN, R. Chapter Twelve - One-dimensional SDS-Polyacrylamide Gel Electrophoresis (1D SDS-PAGE). **In J. Lorsch (Ed.), Methods in Enzymology**, v. 541, p 151-159: Academic Press, 2014.

BURGUER R., SILL M., ZAMARIN, D. NRG Oncology phase II randomized trial of nivolumab with or without ipilimumab in patients with persistent or recurrent ovarian cancer; **Proceedings of the 17th Biennial Meeting of the International Gynecologic Cancer Society**; Kyoto, Japan. 14–16, p. OC11, 2018.

CANNISTRA S. A.; et al. J. Expression and function of β1 and αvβ3 integrins in ovarian cancer. **Gynecol Oncol**, v. 58, 1995.

CANTRELL, L. A.; WESTIN, S. N.; VAN LE, L. The use of recombinant erythropoietin for the treatment of chemotherapy induced anemia in patients with ovarian cancer does not affect progression free or overall survival. **Cancer**, v. 117, n. 6, p. 1220- 1226, 2010.

CECERSKA-HERYĆ, E., GOSZKA, M., SERWIN, N., ROSZAK, M., GRYGORCEWICZ, B., HERYĆ, R. AND DOŁĘGOWSKA, B. Applications of the regenerative capacity of platelets in modern medicine**. Cytokine Growth Factor Rev**, v. 64, p.84-94, 2022.

CESARE, M.; CALCATERRA, C.; PRATESI, G.; GATTI, L. et al. Eradication of ovarian tumor xenografts by locoregional administration of targeted immunotherapy. **Clin Cancer Res**, 14, n. 17, p. 5512-5518, 2008.

CHAMBERS, C. A et al. Lymphoproliferation in CTLA-4–Deficient Mice Is Mediated by Costimulation-Dependent Activation of CD4+ T Cells **Imunity** v. 7, p. 885-895, 1997.

CHATEAUVIEUX, S. et al. Erythropoietin, erythropoiesis and beyond. **Biochem Pharmacol**, v. 82, n. 10, p. 1291-1303. 2011.

CHENG, M. L.; FONG, L. Effects of RANKL-targeted therapy in immunity and cancer. **Front Oncol**, v. 3, p. 329, 2014. CHUANG, C. M. et al. Treatment with LL-37 peptide enhances antitumor effects induced by CpG oligodeoxynucleotides against ovarian cancer. **Hum Gene Ther**, v. 20, n. 4, p. 303-313, 2009.

CHUFFA, L. G. A. et al. Characterization of chemically induced ovarian carcinomas in an ethanol-preferring rat model: influence of long-term melatonin treatment. **PLoS One**, v. 8, n. 12, p. e81676, 2013.

CHUFFA, L. G. A. et al. P-MAPA immunotherapy potentiates the effect of cisplatin on serous ovarian carcinoma through targeting TLR4 signaling. **J Ovarian Res**, v. 11, n. 1, p. 8, 2018.

CLAIRE M. et al. Osteoprotegerin Is a Soluble Decoy Receptor for Tumor Necrosis Factor-related Apoptosis-inducing Ligand/Apo2 Ligand and Can Function as a Paracrine Survival Factor for Human Myeloma Cells, **Cancer res**, v. 63, n. 5, 2003.

CLARKE, B.A.; GILKS, B. Ovarian carcinoma: recent developments in classification of tumour histological subtype. **Can J Pathol**, v. 3, n. 3, 2011.

COHEN, E. D., MARIOL, M. C., WALLACE, R. M. H., WEYERS, J., KAMBEROV, Y. G., PRADEL, J., & WILDER, E. L. DWnt4 regulates cell movement and focal adhesion kinase during Drosophila ovarian morphogenesis. **Dev Cell**, v. 2, n. 4, p. 437-448, 2002.

CONOLLY, D. T. Vascular permeability factor: A unique regulator of blood vessel function, **J Cell Biochem**, v. 47, p. 219-223, 1997.

CORNES P, BOIANGIU I. The role of epoetin beta in the treatment of anemia in patients with gynaecological malignancies. **Anticancer Res.** v. 27, n. 1B, p 513-522. 2007.

CORRALES, L. et al. Direct activation of STING in the tumor microenvironment leads to potent and systemic tumor regression and immunity. **Cell reports**, v. 11, n. 7, p. 1018-1030, 2015.

CORRALES, L., GLICKMAN, L. H., MCWHIRTER, S. M., KANNE, D. B., SIVICK, K. E., KATIBAH, G. E., WOO, S. R., LEMMENS, E., BANDA, T., LEONG, J. J., METCHETTE, K., DUBENSKY, T. W., & GAJEWSKI, T. F. Direct Activation of STING in the Tumor Microenvironment Leads to Potent and Systemic Tumor Regression and Immunity. **Cell Rep**, v. 11, n. 7, p. 1018-1030, 2015.

CORTEZ, A. J.; TUDREJ, P.; KUJAWA, K. A.; LISOWSKA, K. M. Advances in ovarian cancer therapy. **Cancer Chemother Pharmacol**, v. 81, n. 1, p. 17-38, 2018.

CRALLAN, R. A., GEORGOPOULOS, N. T., & SOUTHGATE, J. Experimental models of human bladder carcinogenesis. **Carcinogenesis**, v. 27, n. 3, p. 374-381, 2006.

CRIST, K. A.; ZHANG, Z.; YOU, M.; GUNNING, W. T. et al. Characterization of rat ovarian adenocarcinomas developed inresponse to direct instillation of 7,12-dimethylbenz[a]anthracene (DMBA) coated suture. **Carcinogenesis**, v. 26, n. 5, p. 951-957, 2005.

CUBILLOS-RUIZ, J. R.; RUTKOWSKI, M.; CONEJO-GARCIA, J. R. Blocking ovarian cancer progression by targetingtumor microenvironmental leukocytes. **Cell Cycle**, v. 9, n. 2, p. 260-268, 2010.

CURIEL J. T. et al. Specific recruitment of regulatory T cells in ovarian carcinoma fosters immune privilege and predicts reduced survival. **Nat. Med**. v. 10, p. 942-949, 2004

DAJON, M.; IRIBARREN, K.; CREMER, I. Toll-like receptor stimulation in cancer: A pro- and anti-tumor double-edgedsword. **Immunobiology**, v. 222, n. 1, p. 89-100, 2017.

DAVIDSON B. et al. Macrophage infiltration and angiogenesis in cervical squamous cell carcinoma-clinicopathologic correlation. **Acta Obstet Gynecol Scand**, v. 78, p. 240 – 4, 1999.

DE TONI, E. N. et al. OPG Is Regulated by β-Catenin and Mediates Resistance to TRAIL-Induced Apoptosis in Colon Cancer, **Clin Cancer Res**, v. 14, n. 15, 2008.

DELLAS A. et al. Angiogenesis in cervical neoplasia: microvessel quantitation in precancerous lesions and invasive carcinomas with clinicopathological correlations. **Gynecol Oncol**, vol. 67, p. 27 – 33, 1997.

DIAS, L. P. et al. Effects of Intravesical Therapy with Platelet-Rich Plasma (PRP) and Bacillus Calmette-Guérin (BCG) in Non-Muscle Invasive Bladder Cancer. **Tissue Cell**, v. 52, p. 17-27, 2018.

DIAS, L. P., LUZO, Â. C. M., VOLPE, B. B., DURÁN, M., GALDAMES, S. E. M., FERREIRA, L. A. B., DURÁN, N., & FÁVARO, W. J. Effects of Intravesical Therapy with Platelet-Rich Plasma (PRP) and Bacillus Calmette-Guérin (BCG) in Non-Muscle Invasive Bladder Cancer. **Tissue Cell**, v. 52, p. 17-27, 2018.

DIAS, Q. C., NUNES, I. D., GARCIA, P. V., & FAVARO, W. J. (2016). Potential therapeutic strategies for non - muscle invasive bladder cancer based on association of intravesical immunotherapy with P-MAPA and systemic administration of cisplatin and doxorubicin. **Int Braz J Urol**, v. 42, n. 5, p. 942-954, 2016.

DIAS, Q. C.; NUNES, I. S.; GARCIA, P. V.; FÁVARO, W. J. Potential therapeutic strategies for non - muscle invasive bladdercancer based on association of intravesical immunotherapy

with P-MAPA and systemic administration of cisplatin and doxorubicin. **Int Braz J Urol**, v. 42, p. 942-954, 2016.

DIRK M. et al. A homologue of the TNF receptor and its ligand enhance T-cell growth and dendritic-cell function, **Nature**, v. 390, p. 175–179, 1997.

DISIS, M. L. Immune regulation of cancer. **J Clin Oncol**, v. 28, n. 29, p. 4531, 2010.

DOBRUCH, Jakub et al. Gender and bladder cancer: a collaborative review of etiology, biology, and outcomes. European urology, v. 69, n. 2, p. 300-310, 2016.

DOHAN EHRENFEST, D. M., RASMUSSON, L., & ALBREKTSSON, T. Classification of platelet concentrates: from pure platelet-rich plasma (P-PRP) to leucocyte- and platelet-rich fibrin (L-PRF). **Trends Biotechnol**, v. 27, n. 3, p. 158-167, 2009.

DOUGALL, W. C. et al Molecular Pathways: Osteoclast-Dependent and Osteoclast-Independent Roles of the RANKL/RANK/OPG Pathway in Tumorigenesis and Metastasis. **Clin Cancer Res,** 2012.

DOVIO, A.; ANGELI A. Circulating osteoprotegerin and soluble RANKL: do they have a future in clinical practice? **J Endocrinol Investig**, v. 28(10 Suppl), p.14-22, 2005

DUAN, T. et al. Toll-like receptor signaling and its role in cell-mediated immunity. **Front Immunol**, v. 13, 2022.

DURÁN, N., FÁVARO, W. J. Biogenic synthesis of important environmental minerals: Magnesium phosphate compounds and perspectives. **Quim Nova**, v. 41, n. 5, p. 567-576, 2018.

DURAN, N.; DIAS, Q. C.; FAVARO, W. J. OncoTherad: A New Nanobiological Response Modifier, its Toxicological and Anticancer Activities. **J Phys Conf Ser**, v. 1323, p. 012018, 2019.

Endostatin Associates with Integrin α5β1 and Caveolin-1, and Activates Src via a Tyrosyl WICKSTRÖM S. A. Phosphatase-dependent Pathway in Human Endothelial Cells, **Cancer Research,** 2002.

EPSTEIN, J. I., AMIN, M. B., REUTER, V. R., & MOSTOFI, F. K. The World Health Organization/International Society of Urological Pathology consensus classification of urothelial (transitional cell) neoplasms of the urinary bladder. Bladder Consensus Conference Committee. **Am J Surg Pathol**, v. 22, n. 12, p. 1435-1448, 1998.

ERGUN, Y. et al. The protective effect of erythropoietin and dimethylsulfoxide on ischemia-reperfusion injury in ratovary. **Eur J Obstet Gynecol Reprod Biol**, v. 152, n. 2, p. 186-190, 2010.

FANDREY, J. Erythropoietin receptors on tumor cells: what do they mean?. **The Oncologist**, v. 13, suppl 3, p. 16-20. 2008

FÁVARO, W. et al. Role of OncoTherad immunotherapy in the regulation of toll-like receptors-mediated immune system and RANK/RANKL signaling: New therapeutic perspective for non-muscle invasive bladder cancer. **J Clin Oncol,** 37, n. 15_suppl. 2019.

FÁVARO, W. et al. Single-arm phase I/II study of the safety and efficacy of OncoTherad immunomodulator in patients BCG-refractory or relapsed non-muscle invasive bladder cancer. **J Clin Oncol.** v. 37, 15 Suppl, 2019.

FÁVARO, W. J. et al. Effects of P-MAPA Immunomodulator on Toll-Like Receptors and p53: Potential Therapeutic Strategies for Infectious Diseases and Cancer. **Infect Agent Cancer**, v. 7, n. 1, p. 14, 2012.

FÁVARO, W. J. et al. New synthetic nano-immunotherapy (OncoTherad®) for non-muscle invasive bladder cancer: Its synthesis, characterization and anticancer property. **Tissue Cell**, v. 80, p. 101988, 2023.

FAVARO, W. J., NUNES, O. S., SEIVA, F. R. F., NUNES, I. S., WOOLHISER, L. K., DURAN, N., & LENAERTS, A. J. Effects of P-MAPA Immunomodulator on Toll-Like Receptors and p53: Potential Therapeutic Strategies for Infectious Diseases and Cancer. **Infect Agents Cancer**, v. 7, 2012.

FAVARO, W. J.; NUNES, O. S.; SEIVA, F. R.; NUNES, I. S. et al. Effects of P-MAPA Immunomodulator on Toll-Like Receptors and p53: Potential Therapeutic Strategies for Infectious Diseases and Cancer. **Infect Agent Cancer**, v. 7, n. 1, p. 14, 2012.

FAVARO, W., & DURAN, N. Process of obtaining a nanostructured complex (CFI-1), associated to nanostructured CFI-1 with a protein (MRB-CFI-1) and its use. **Brazil Patent No. PIBR 10.2017.012768.0.** 2017.

FÁVARO, W.; DURAN, N. Process of obtaining a nanostructured complex (CFI-1), associated to nanostructured CFI-1 with a protein (MRB-CFI-1) and its use. Brazil Patent No. PIBR 10.2017.012768.0.

FÁVARO, W.F., DURÁN, N. Patente Brasileira: PIBR 10 2017 012768 0; 2018 **PCT/BR2018/000031**. 2017.

FÁVARO, W.J., DURÁN, N. Process of obtaining a nanostructured complex (CFI-1), associated to nanostructured CFI-1 with a protein (MRB-CFI-1) and its use. **PCT/BR2018/000031**. 2018.

FILARDO, G., KON, E., PEREIRA RUIZ, M. T., VACCARO, F., GUITALDI, R., DI MARTINO, A., CENACCHI, A., FORNASARI, P. M., & MARCACCI, M. Platelet-rich plasma intra-articular injections for cartilage degeneration and osteoarthritis: single- versus double-spinning approach. **Knee Surg Sports Traumatol Arthrosc**, v. 20, n. 10, p. 2082-2091, 2012.

FISHER, J. L. et al. Osteoprotegerin Overexpression by Breast Cancer Cells Enhances Orthotopic and Osseous Tumor Growth and Contrasts with That Delivered Therapeutically. **Cancer** res, v. 66, n. 7, 2006.

FOSTER, T. E., PUSKAS, B. L., MANDELBAUM, B. R., GERHARDT, M. B., & RODEO, S. A. Platelet-rich plasma: from basic science to clinical applications. **Am J Sports Med**, n. 37, n. 11, p. 2259-2272, 2009.

FUJIMURA T., KAMBAYASHI Y., FURUDATE S., ASANO M., KAKIZAKI A., AIBA S. Receptor activator of NF-[kappa]B ligand promotes the production of CCL17 from RANK+ M2 macrophages. **J Invest Dermatol** v. 135, p. 2884–2887, 2015.

GADDUCCI A. et al. Intratumoral microvessel density, response to chemotherapy and clinical outcome of patients with advanced ovarian carcinoma. **Anticancer Res**, v. 23, p. 549–56, 2003.

GALLI, R. et al. TLR stimulation of prostate tumor cells induces chemokine-mediated recruitment of specific immune cell types. **J Immunol**, v. 184, n. 12, p. 6658-6669, 2010.

GALLI, R., STARACE, D., BUSA, R., ANGELINI, D. F., PAONE, A., DE CESARIS, P., FILIPPINI, A., SETTE, C., BATTISTINI, L., ZIPARO, E., & RICCIOLI, A. TLR stimulation of prostate tumor cells induces chemokine-mediated recruitment of specific immune cell types. **J Immunol**, v. 184, n. 12, p. 6658-6669, 2010.

GANESAN, S.; BHATTACHARYA, P.; KEATING, A. F. 7,12-Dimethylbenz[a]anthracene exposure induces the DNArepair response in neonatal rat ovaries. **Toxicol Appl Pharmacol**, v. 272, n. 3, p. 690-696, 2013.

GARCIA, B. A., SMALLEY, D. M., CHO, H., SHABANOWITZ, J., LEY, K., & HUNT, D. F. The platelet microparticle proteome. **J Proteome Res**, v. 4, n. 5, p. 1516-1521, 2005.

GARCIA, P. V. et al. Increased toll-like receptors and p53 levels regulate apoptosis and angiogenesis in non-muscle invasive bladder cancer: mechanism of action of P-MAPA biological response modifier. **BMC Cancer**, v. 16, n. 422, 2016.

GARCIA, P. V., APOLINÁRIO, L. M., BÖCKELMANN, P. K., NUNES, I. S., DURAN, N., & FÁVARO, W. J. Alterations in ubiquitin ligase Siah-2 and its corepressor N-CoR after P-MAPA immunotherapy and anti-androgen therapy: New therapeutic opportunities for non-muscle invasive bladder cancer. **Int J Clin Exp Pathol**, v. 8, n. 5, p. 4427-4443. PMID: 26191134. 2015.

GARCIA, P. V., SEIVA, F. R. F., CARNIATO, A. P., DE MELLO, W., DURAN, N., MACEDO, A. M., DE OLIVEIRA, A. G., ROMIH, R., NUNES, I. D., NUNES, O. D., & FAVARO, W. J. Increased toll-like receptors and p53 levels regulate apoptosis and angiogenesis in non-muscle invasive bladder cancer: mechanism of action of P-MAPA biological response modifier. **BMC Cancer**, v. 16, 2016.

GATA, V.; LAURENTIU, I. F. The role of Toll-like receptors in ovarian cancer. **J buon**, v. 22, n. 5, p. 1092-1096, 2017.

GEN, G. H. et al. Prognostic significance of vascular endothelial growth factor expression in human ovarian carcinoma, **Br J Cancer**, v. 83, p. 196–203, 2000.

GENENTECH PRESS RELEASE. FDA Accepts Genentech's Supplemental Biologics License Application for Avastin as a Front-Line Treatment for Women with Advanced Ovarian Cancer, 2017. Disponível em: <https://www.gene.com/media/press- releases/14685/2017-10-25/fda-accepts-genentechs-supplemental-biol> Acesso em: 15 nov 2022.

GLASPY J, et al. Erythropoiesisstimulating agents in oncology: a study-level meta-analysis of survival and other safety outcomes. **Br J Cancer**. v. 102, p. 301-315, 2010.

GOLDMAN, J. M.; MURR, A. S.; COOPER, R. L. The rodent estrous cycle: characterization of vaginal cytology and its utility in toxicological studies. **Birth Defects Res B: Dev Reprod Toxicol**, v. 80, n. 2, p. 84-97, 2007.

GONG, T. T. et al. Age at menarche and risk of ovarian cancer: a meta-analysis of epidemiological studies. **Int J Cancer**, v.132, n. 12, p. 2894-2900, 2013.

GRIFFITH, T. S. et al. TRAIL Gene Therapy: From Preclinical Development to Clinical Application, **Curr Gen Ther**, v. 9, n. 1, p. 9-19, 2009.

GRISHAM, R. N.; HYMAN, D. M.; IYER, G. Targeted therapies for treatment of recurrent ovarian cancer. **Clin Adv Hematol Oncol**, v. 12, n. 3, p. 158-162, 2014.

GROOT, A. F., APPELMAN-DIJKSTRA, N. M., VAN DER BURG, S. H., KROEP, J. R. The anti-tumor effect of RANKL inhibition in malignant solid tumors–a systematic review. **Cancer Treat Rev**, v. 62, p. 18-28, 2018.

GUALLAR-GARRIDO, Sandra; JULIÁN, Esther. Bacillus Calmette-Guérin (BCG) therapy for bladder cancer: an update. ImmunoTargets and Therapy, v. 9, p. 1, 2020.

GUO J. et al. Microvessel density: correlation with 18F-FDG uptake and prognostic impact in lung adenocarcinomas. **J Nucl Med**, v. 47, p. 419–25, 2006.

HALL, M. C., CHANG, S. S., DALBAGNI, G., PRUTHI, R. S., SEIGNE, J. D., SKINNER, E. C., WOLF, J. S., & SCHELLHAMMER, P. F. Guideline for the management of nonmuscle invasive bladder cancer (Stages Ta, T1, and Tis): 2007 update. **J Urol**, v. 178, n. 6, p. 2314-2330, 2007.

HAMANISHI, J. et al. Programmed cell death 1 ligand 1 and tumor-infiltrating CD8+ T lymphocytes are prognostic factors of human ovarian cancer. **PNAS**, v. 104, n. 9, p. 3360-3365, 2007.

HAN E. et al. Angiogenesis biomarker expression in recurrent or persistent epithelial ovarian cancer and patients with primary peritoneal cancer treated with bevacizumab: a Gynecologic Oncology Group study. **Gynecol Oncol**, v. 108, n. 3, p. S21, 2008.

HAN E. S. et al. Relationship between angiogenic markers and clinicopathologic factors/outcome in GOG-170D, a phase II trial of bevacizumab (Bev) in recurrent or persistent epithelial ovarian cancer (EOC) and primary peritoneal cancer (PPC). **J Clin Oncol**, v. 25, n. 18, 2007.

HANAHAN, D.; FOLKMAN, J. Patterns and emerging mechanisms of angiogenic switch during tumorigenesis. **Cell**, v. 86, 1996.

HARDEE, M. E., et al. Human recombinant erythropoietin (rEpo) has no effect on tumour growth or angiogenesis. **Br J Cancer**, v. 93, n. 12, p. 1350-1355, 2005.

HARRISON, P., ALSOUSOU, J., ANDIA, I., BURNOUF, T., EHRENFEST, D.D., EVERTS, P., LANGER, H., MAGALON, J., MARCK, R. AND GRESELE, P. The use of platelets in regenerative medicine and proposal for a new classification system: guidance from the SSC of the ISTH. **J Thromb Haemost**, v. 16, n. 9, p.1895-1900, 2018.

HEUSKINKVELD, M.; VANDER, B. S. H. Identification and manipulation of tumor associated macrophages in humancancers. **J Transl med**, v. 9, n. 1, p. 216, 2011.

HICKS, R. M., & WAKEFIELD, J. S. Rapid Induction of Bladder Cancer in Rats with N-Methyl-N-Nitrosourea .1. Histology. **Chem Biol Interact**, v. 5, n. 2, p. 139-+, 1972.

HIGUCHI, T. et al. CTLA-4 blockade synergizes therapeutically with PARP inhibition in BRCA1-deficient ovariancancer. **Cancer Immunol Res**, v. 3, n. 11, p. 1257-1268, 2015.

HOFBAUER, L. C. et al. The Roles of Osteoprotegerin and Osteoprotegerin Ligand in the Paracrine Regulation of Bone Resorption, **JBMR**, v. 15, n. 1, 2000.

HOLEN I. et al. Osteoprotegerin (OPG) Is a Survival Factor for Human Prostate Cancer Cells, **Cancer Res**. v. 62, p. 1619–1623, 2002.

HOLEN I; SHIPMAN, C. M. Role of osteoprotegerin (OPG) in cancer, **Clin Sci (Lond).** v. 110, n. 3, p. 279–291, 2006.

HOLEN, I. et al. Osteoprotegerin (OPG) Expression by Breast Cancer Cells in vitro and Breast Tumours in vivo – A Role in Tumour Cell Survival? **Breast Cancer Res Treat,** v. 92, p. 207–215, 2005.

HOLLINGSWORTH H. C. et al. Tumor angiogenesis in advanced stage ovarian carcinoma. **Am J Pathol**, v. 147, p. 33–41, 1995.

HOLSCHNEIDER C. H.; BEREK J.S. Ovarian cancer: epidemiology, biology, and prognostic factors. **Semin Surg Oncol**, v. 19, 2000.

HSU, H. et al. Tumor necrosis factor receptor family member RANK mediates osteoclast differentiation and activation induced by osteoprotegerin ligand. **PNAS**, v. 96, n. 7, p. 3540-3545, 1999.

HU H, et al. RANKL expression in normal and malignant breast tissue responds to progesterone and is up-regulated duringthe luteal phase. **Breast Cancer Res Tr,** v. 146, n. 3, p. 515-23, 2014.

HUA, X., ZENG, Y., ZHANG, R., WANG, H., DIAO, J., & ZHANG, P. Using platelet-rich plasma for the treatment of symptomatic cervical ectopy. **Int J Gynecol Obstet**, v. 119, n. 1, p. 26-29, 2012.

HUANG, Y. et al. Enhanced efficacy and specificity of epithelial ovarian carcinogenesis by embedding a DMBA-coated cloth strip in the ovary of rat. **J Ovarian Res**, v. 5, n. 1, p. 21, 2012.

HUSSEINZADEH, N.; DAVENPORT, S. M. Role of toll-like receptors in cervical, endometrial and ovarian cancers: a review. **Gynecol Oncol**, v. 135, n. 2, p. 359-363, 2014.

INCA - Instituto Nacional do Câncer José de Alencar Gomes da Silva. **Tipos de câncer: Câncer de ovário**. 2020d. Disponível em: <https://www.inca.gov.br/tipos-de-cancer/cancer-de-ovario>. Acesso em: 28 dez 2022.

INCA - Instituto Nacional do Câncer José de Alencar Gomes da Silva. **Estimativa 2023**. 2022a. Disponível em: https://www.gov.br/inca/pt-br/assuntos/cancer/numeros/estimativa. Acesso em: 26 dez 2022.

INCA - Instituto Nacional do Câncer José de Alencar Gomes da Silva. **Atlas on-line de mortalidade**. Rio de Janeiro, 2022b. Disponível em: https://www.inca.gov.br/MortalidadeWeb/pages/Modelo01/consultar.xhtml. Acesso em: 26 dez 2022.

INCA - Instituto Nacional do Câncer José de Alencar Gomes da Silva. **Câncer de Bexiga.** 2022c. Disponível em: https://www.gov.br/inca/pt-br/assuntos/cancer/tipos/bexiga. Acesso em: 26 dez 2022.

JAVADI, S. et al. Ovarian Cancer, the Revised FIGO Staging System, and the Role of Imaging. **AJR Am J Roentgenol**, v. 206, n. 6, p. 1351-1360, 2016.

JELKMANN, W. Erythropoietin. **Sports Endocrinology**. v. 47, p. 115-127. 2016.

JELKMANN, W. Physiology and pharmacology of erythropoietin. **Transfus Med Hemoth**, v. 40, n. 5, p. 302-309, 2013.

JOHN G. Emery, J. G. Osteoprotegerin Is a Receptor for the Cytotoxic Ligand TRAIL, **Cell Metab**, v. 273, 1998.

JONES, R. L. et al. TGF-β superfamily expression and actions in the endometrium and placenta. **Reproduction**, v. 132, n. 2, p. 217–232, 2006.

KAMAT, A. M., COLOMBEL, M., SUNDI, D., LAMM, D., BOEHLE, A., BRAUSI, M., BUCKLEY, R., PERSAD, R., PALOU, J., SOLOWAY, M., & WITJES, J. A. BCG-unresponsive non-muscle-invasive bladder cancer: Recommendations from the IBCG. **Nat Rev Urol**, v. 14, n. 4, p. 244-255, 2017.

KATZ, O. et al. Erythropoietin enhances immune responses in mice. **Eur J Immunol**, v. 37, n. 6, p. 1584-1593, 2007.

KATZ, O. et al. Erythropoietin induced tumour mass reduction in murine lymphoproliferative models. **Acta haematol-basel**, v. 114 n. 3, p. 177-179, 2005.

KAWAI, T.; AKIRA, S. The role of pattern-recognition receptors in innate immunity: update on Toll-like receptors. **NatImmunol**, v. 11, n. 5, p. 373-384, 2010.

KELLY, M. G. et al.TLR-4 signaling promotes tumor growth and paclitaxel chemoresistance in ovarian cancer. **Cancer res**,v. 66, n. 7, p. 3859-3868. 2006.

KEMP, T. J., LUDWIG, A. T., EAREL, J. K., MOORE, J. M., VANOOSTEN, R. L., MOSES, B., LEIDAL, K., NAUSEEF, W. M., & GRIFFITH, T. S. Neutrophil stimulation with Mycobacterium bovis bacillus Calmette-Guerin (BCG) results in the release of functional soluble TRAIL/Apo-2L. **Blood**, v. 106, n. 10, p. 3474-3482, 2005.

KIM Y. M. et al. Endostatin blocks vascular endothelial growth factor-mediated signaling via direct interaction with KDR/Flk-1. **J Biol Chem**, v. 277, p. 27872– 9, 2002.

KIM Y. M. et al. Endostatin inhibits endothelial and tumor cellular invasion by blocking the activation and catalytic activity of matrix metalloproteinase. **Cancer Res**, v. 60, p. 5410– 13, 2000.

KIMÁKOVÁ, P. et al. Erythropoietin Potentiates the Anti-proliferative Effect of Tamoxifen in Ovarian Adenocarcinoma A2780 Cells. **Acta Chim Slov**, v. 65, n.4, p. 842-846. 2018

KONG Y. Y. et al. OPGL is a key regulator of osteoclastogenesis, lymphocyte development and lymph-node organogenesis. **Nature.** v. 397, p.315–2310.1038/16852 1999

KOSTENUIK, P. J. et al. Denosumab, a Fully Human Monoclonal Antibody to RANKL, Inhibits Bone Resorption and Increases BMD in Knock-In Mice That Express Chimeric (Murine/Human) RANKL. **JBMR**, v. 24, n. 2, 2009.

KRISHNAN, V.; BEREK, J. S.; DORIGO, O. Immunotherapy in ovarian cancer. **Curr Probl Cancer**,v. 41, n. 1, p. 48-63, 2017.

KRUMMEL, M. F., ALLISON, J. P. CD28 and CTLA-4 have opposing effects on the response of T cells to stimulation. **J Exp Med,** v. 182, n. 2, p. 459–465, 2005.

KUCUK, L., GUNAY, H., ERBAS, O., KUCUK, U., ATAMAZ, F., & COSKUNOL, E. Effects of platelet-rich plasma on nerve regeneration in a rat model. **Acta Orthop Traumatol Turc**, v. 48, n. 4, p. 449-454, 2014.

KUMAR S. et al. Breast carcinoma: vascular density determined using CD105 antibody correlates with tumor prognosis. **Cancer Res**, v. 59, p.856–61, 1999.

KUMAR, H., KAWAI, T., & AKIRA, S. Pathogen Recognition by the Innate Immune System. **Int Rev Immunol**, v. 30, n. 1, p. 16-34, 2011.

KUMAR, H.; KAWAI, T.; AKIRA, S. Pathogen recognition by the innate immune system. **Int Rev Immunol**, v. 30, n. 1, p.16-34, 2011.

KUMAR, V.; ABBAS, A. K.; FAUSTO, N.; ASTER, J. C. **Robbins & Cotran Patologia - Bases Patológicas das Doenças**. 8 ed. Rio de Janeiro: Elsevier, 2010.

KURMAN R.J.; CARCANGIU M.L.; HERRINGTON C.S.; YOUNG, R.H. WHO **Classification of Tumours of FemaleReproductive Organs**. 4. ed. Lyon: IARC, 2014.

KURMAN, R.J.; SHIH, I.M. The Origin and pathogenesis of epithelial ovarian cancer - a proposed unifying theory. **Am JSurg Pathol**, v. 34, n. 3, p. 433, 2010.

KWON, Y. J.; YE, D. J.; BAEK, H. S.; CHUN, Y. J. 7,12-Dimethylbenz[alpha]anthracene increases cell proliferation andinvasion through induction of Wnt/beta-catenin signaling and EMT process. **Environ Toxicol**, v. 33, n. 7, p. 729-742, 2018.

KYZAS P. A. et al. Endoglin (CD105) as a prognostic factor in head and neck squamous cell carcinoma. **Virchows Arch**, v. 448, p. 768–75, 2006.

LAVOUÉ, V. et al. Immunity of human epithelial ovarian carcinoma: the paradigm of immune suppression in cancer. **J TranslMed**, v. 11, n. 1, p. 147, 2013.

LEDERMANN, J. A. First-line treatment of ovarian cancer: questions and controversies to address. **Ther Adv in Med Oncol**, v. 10, 2018.

LEDERMANN, J. et al. Olaparib Maintenance Therapy in Platinum-Sensitive Relapsed Ovarian Cancer. **New EnglandJournal of Medicine**, v. 366, n. 15, p. 1382–1392, 2012.

LEE J. S. et al. Expression of vascular endothelial growth factor in adenocarcinoma of the uterine cervix and its relation to angiogenesis and p53 and c-erbB-2 protein expression. **Gynecol Oncol,** v. 85, p. 469 – 75, 2002.

LEE J.S. et al. Angiogenesis, cell proliferation and apoptosis in progression of cervical neoplasia. **Anal Quant Cytol Histol**, v. 24, p.103 – 13, 2002.

LEE S. J. et al. Endostatin binds to the catalytic domain of matrix metalloproteinase-2. **FEBS Lett**, v. 519, p. 147– 52, 2002

LEE, H.W., CHOI, K.H., KIM, J.Y., KIM, K.O., HAOTIAN, B., YUXUAN, L. AND NOH, K.C. Proteomic classification and identification of proteins related to tissue healing of platelet-rich plasma. **Clinics in Orthopedic Surgery**, v. 12, n. 1, p.120-129, 2020.

LEIBBRANDT, A., & PENNINGER, J. M. RANK/RANKL: Regulators of immune responses and bone physiology. **Ann N Y Acad Sci**, v. 1143, p. 123-150, 2008.

LENGYEL, E. Ovarian cancer development and metastasis. **Am J Clin Pathol**, v. 177, n. 3, p. 1053-1064, 2010.

LI, Z. G., PRADERA, F., KAMMERTOENS, T., LI, B., LIU, S. B., & QIN, Z. H. Cross-talk between T cells and innate immune cells is crucial for IFN-gamma-dependent tumor rejection. **J Immunol**, v. 179, n. 3, p. 1568-1576, 2007.

LIFSHITZ, L. et al. Non-erythroid activities of erythropoietin: Functional effects on murine dendritic cells. **Mol Immunol,** v. 46, n. 4, p. 713-721, 2009.

LIFSHITZ, L., et al. Macrophages as novel target cells for erythropoietin. **Haematologica**, v. 95, n. 11, p. 1823-1831, 2010. LIU, B. et al. Ovarian cancer immunotherapy: opportunities, progresses and challenges. **J Hematol Oncol**, v. 3, n. 1, p. 1-11,

LIGHTFOOT, A. J., ROSEVEAR, H. M., & O'DONNELL, M. A. Recognition and Treatment of BCG Failure in Bladder Cancer. **Sci World J**, v. 11, p. 602-613, 2011.

LIKHACHEV A.J., IVANOV M.N., BRÉSIL H., PLANCHE-MARTEL G., MONTESANO R., MARGISON G.P. Carcinogenicity of single doses of N-Nitroso-N-methylurea and N-Nitroso-N-ethylurea IN Syrian Golden hamsters and the persistence of alkylated purines in the DNA of various tissues. **Cancer Res**, v. 43, p. 829-833, 1983.

LIU, J.; MATULONIS, U.A. New strategies in ovarian cancer: translating the molecular complexity of ovarian cancer intotreatment advances. **Clin Cancer Res**, v. 20, n. 20, p. 5150-5156, 2014.

LOMBARDERO, M.; KOVACS, K.; SCHEITHAUER, B. W. Erythropoietin: a hormone with multiplefunctions. **Pathobiology**, v. 78, n. 1, p. 41-53, 2011.

LONGACRE M, et al. A comparative analysis of genetic and epigenetic events of breast and ovarian cancer related totumorigenesis. **Int J Mol Sci**. v. 17, n. 5, p. 759, 2016.

LONGACRE, M. et al. A Comparative Analysis of Genetic and Epigenetic Events of Breast and Ovarian Cancer Related to Tumorigenesis, **Int. J. Mol. Sci**. v. 17, n. 5, 759, 2016.

LU, H. et al. VTX-2337 is a novel TLR8 agonist that activates NK cells and augments ADCC. **Clin Cancer Res**, v. 18, n. 2,p. 499-509, 2012.

LUO, J. L., MAEDA, S., HSU, L. C., YAGITA, H., & KARIN, M. Inhibition of NF-kappa B in cancer cells converts inflammation-induced tumor growth mediated by TNF alpha to TRAIL-mediated tumor regression. **Cancer Cell**, v. 6, n. 3, p. 297-305, 2004.

LUVERO, D.; MILANI, A.; LEDERMANN, J. A. Treatment options in recurrent ovarian cancer: latest evidence and clinicalpotential. **Ther. Adv. Med. Oncol**, v. 6, n. 5, p. 229-239, 2014.

LUZO, Â.C.M., LEME, K.C., FÁVARO, W.J., DURÁN, N., BÍSCARO, G.G., DE OLIVEIRA, A.L.R., BOUMEDIENE, K., HAMMAD, M. AND BAUGÉ, C. Platelet-rich plasma, their growth factors, cytokines and clinical use. In **Nanotechnology and Regenerative Medicine**, p. 265-314. Academic Press, 2023.

MAAS, M. et al. Receptor Activator of NF Kappa B (RANK) Expression Indicates Favorable Prognosis in Patients with Muscle-invasive Bladder Cancer. **Eur Urol Focus**, v. 8, n. 3, p. 718-727, 2022.

MADDEN, J. A.; HOYER, P. B.; DEVINE, P. J.; KEATING, A. F. Acute 7,12-dimethylbenz[a]anthracene exposure causes differential concentration-dependent follicle

depletion and gene expression in neonatal rat ovaries. **Toxicol Appl Pharmacol**, v. 276,n. 3, p. 179-187, 2014.

MAHMOODI, M. et al. Effects of erythropoietin on ischemia, follicular survival, and ovarian function in ovarian grafts. **Reproduction**, v. 147, n. 5, p. 733-741, 2014.

MAINE, C. J. et al. Programmed death ligand-1 over-expression correlates with malignancy and contributes to immune regulation in ovarian cancer. **Cancer Immunol Immun**, v. 63, n. 3, p. 215-224, 2014.

MANIZHEH, S. M. et al. The ovario-protective effect of erythropoietin against oxidative damage associated with reperfusion following ovarian torsion in rat. **Am J Anim Vet Sci**, v. 6, n. 1, p. 18-24. 2011

MARCONDES, F. K.; BIANCHI, F. J.; TANNO, A. P. Determination of the estrous cycle phases of rats: some helpful considerations. **Braz J Biol,** v. 62, n. 4a, p. 609-614, 2002.

MARION, S. L. et al. 7,12-Dimethylbenz[a]anthracene-Induced Malignancies in a Mouse Model of Menopause. **Comp Med**,v. 63, p. 6-12, 2013.

MARTINI, M., TESTI, M. G., PASETTO, M., PICCHIO, M. C., INNAMORATI, G., MAZZOCCO, M., UGEL, S., CINGARLINI, S., BRONTE, V., ZANOVELLO, P., KRAMPERA, M., MOSNA, F., CESTARI, T., RIVIERA, A. P., BRUTTI, N., BARBIERI, O., MATERA, L., TRIDENTE, G., COLOMBATTI, M., & SARTORIS, S. IFN-gamma-mediated upmodulation of MHC class I expression activates tumor-specific immune response in a mouse model of prostate cancer. **Vaccine**, v. 28, n. 20, p. 3548-3557, 2010.

MEINHOLD-HEERLEIN, I.; et al. The new WHO classification of ovarian, fallopian tube, and primary peritoneal cancer and its clinical implications. **Arch Gynecol Obstet**, v. 293, n.4, p.695-700, 2016.

MEINHOLD-HEERLEIN, I.; HAUPTMANN, S. The heterogeneity of ovarian cancer. **Arch Gynecol Obstet**, v. 289, n. 2, p.237-239, 2014.

MENDOZA L. et al. Inhibition of cytokine-induced microvascular arrest of tumor cells by recombinant endostatin prevents experimental hepatic melanoma metastasis. **Cancer Res**, v. 64, 2004.

MICHAEL L.; CHENG. M. L.; FONG L. Effects of RANKL-targeted therapy in immunity and cancer, **Front Oncol**, v. 3, 2014.

MIMURA, K. et al. PD-L1 expression is mainly regulated by interferon gamma associated with JAK-STAT pathway in gastric cancer. **Cancer Sci**, v. 109, n. 1, p. 43-53, 2018.

MIN, J. et al. Vascular Endothelial Growth Factor Up-regulates Expression of Receptor Activator of NF-κB (RANK) in Endothelial Cells, **Biol Chem**, v. 278, n. 41, 2003.

MINISTÉRIO DA SAÚDE. Diretrizes Diagnósticas e Terapêuticas de Neoplasia maligna epitelial de ovário.: **CONITEC (Comissão Nacional de Incorporação de tecnologias no SUS)**, n. 401, jan. 2019. Disponível em: <http://conitec.gov.br/images/Relatorios/2019/Relatorio_DDT_NeoplasiaMalignaEpitelialdeOvario_2019.pdf>. Acesso em: 30 dez 2022.

MISHRA, A., HARMON, K., WOODALL, J., VIEIRA, A. Sports medicine applications of platelet rich plasma. **Curr Pharm Biotechnol**, v. 13, n. 7, p.1185-1195, 2012.

MITTELMAN, M., NEUMANN, D., KANTER, P., HARAN-GHERA, N. Erythropoietin induces tumor regression andantitumor immune responses in murine myeloma models. **PNAS**, v. 98, n. 9, p. 5181-5186, 2001.

MITTICA, G., GENTA, S., AGLIETTA, M., VALABREGA, G. Immune checkpoint inhibitors: a new opportunity in thetreatment of ovarian cancer? **Inter J Mol Sci**, v. 17, n. 7, p. 1169, 2016.

MIZUTANI, Y. et al. Prognostic significance of serum osteoprotegerin levels in patients with bladder carcinoma. **Cancer: Interdisciplinary International Journal of the American Cancer Society**, v. 101, n. 8, p. 1794-1802, 2004.

MORALES, A., & EIDINGER, D. Bacillus Calmette-Guerin in the treatment of adenocarcinoma of the kidney. **J Urol**, v. 115, n. 4, p. 377-380, 1976.

MORRISSEY, J. H. Polyphosphate: a link between platelets, coagulation and inflammation. International **J Hematol**, v. 95, n. 4, p. 346-352, 2012.

MORRISSEY, J. H., CHOI, S. H., & SMITH, S. A. Polyphosphate: an ancient molecule that links platelets, coagulation, and inflammation. **Blood**, v. 119, n. 25, p. 5972-5979, 2012.

MORSE, M. A. et al. Phase I study utilizing a novel antigen-presenting cell-targeted vaccine with Toll-like receptor stimulation to induce immunity to self-antigens in cancer patients. **Clin Cancer Res**, v. 17, n. 14, p. 4844-4853, 2011.

MUCCIOLI, M.; BENENCIA, F. Toll-like Receptors in Ovarian Cancer as Targets for Immunotherapies. **Front Immunol**, v.5, p. 341, 2014.

MULLER, F., MUTCH, N. J., SCHENK, W. A., SMITH, S. A., ESTERL, L., SPRONK, H. M., SCHMIDBAUER, S., GAHL, W. A., MORRISSEY, J. H., & RENNE, T. Platelet polyphosphates are proinflammatory and procoagulant mediators in vivo. **Cell,** v. 139, n. 6, p. 1143-1156, 2009.

NEVILLE-WEBBE, H. L. et al. Osteoprotegerin (OPG) Produced by Bone Marrow Stromal Cells Protects Breast Cancer Cells from TRAIL-Induced Apoptosis, **Breast Cancer Res Treat**, v. 86, p. 271–282, 2004.

NISHIDA, T. et al. Histologic characterization of rat ovarian carcinoma induced by intraovarian insertion of a 7,12-dimethylbenz[a]anthracene-coated suture: common epithelial tumors of the ovary in rats? **Cancer**, v. 83, n. 5, p. 965-970, 1998.

NURDEN, A. T. Platelets, inflammation and tissue regeneration. **J Thromb Haemost**, 105 Suppl 1, S13-33, 2011.

O'REILLY, M. S. et al. Endostatin: an endogenous inhibitor of angiogenesis and tumor growth. **Cell**, v. 88, 1997.

O'DONNELL, M. A., & BOEHLE, A. Treatment options for BCG failures. **World J Urol**, v. 24, n. 5, p. 481-487, 2006.

OEHLER, M. K. CAFFIER H. Diagnostic value of serum VEGF in women with ovarian tumors. **Anticancer Res**, v. 19, n. 4A, p. 2519-2522, 1999.

OJEA, A., NOQUEIRA, J. L., SOLSONA, E., FLORES, N., GOMEZ, J. M. F., MOLINA, J. R., CHANTADA, V., CAMACHO, J. E., PINEIRO, L. M., RODRIGUEZ, R. H., ISORNA, S., BLAS, M., MARTINEZ-PINEIRO, J. A., & MADERO, R. A multicentre, randomised prospective trial comparing three intravesical adjuvant therapies for intermediate-risk superficial bladder cancer: Low-dose bacillus Calmette-Guerin (27 mg) versus very low-dose bacillus Calmette-Guerin (13.5 mg) versus mitomycin C. **Eur Urol**, v. 52, n. 5, p. 1398-1406, 2007.

OLIVEIRA, P. A., COLACO, A., DE LA CRUZ, P. L., & LOPES, C. Experimental bladder carcinogenesis-rodent models. **Exp Oncol**, v. 28, n. 1, p. 2-11, 2006.

O'REILLY, M. S. et al. Endostatin: An Endogenous Inhibitor of Angiogenesis and Tumor Growth, **Cell,** v. 88, p. 277-285, 1997.

OWEN, K. L.; BROCKWELL, N. K.; PARKER, B. S. JAK-STAT signaling: a double-edged sword of immune regulation and cancer progression. **Cancers**, v. 11, n. 12, p. 2002, 2019.

PALAFOX, M. et al. RANK induces epithelial-mesenchymal transition and stemness in human mammary epithelial cells and promotes tumorigenesis and metastasis, **Cancer Res**, v. 72, n. 11, p. 2879-88, 2012.

PAMELA J. et al. Alterations in SPARC and VEGF Immunoreactivity in Epithelial Ovarian Cancer. **Gynecol Oncol**, v. 78, n. 3, p. 336-341, 2000.

PATSOUKIS N. et al. Selective effects of PD-1 on Akt and Ras pathways regulate molecular components of the cell cycle and inhibit T cell proliferation. **Sci Signal**, v. 5, n. 230, p. ra46, 2012.

PERABO, F. G. E., WILLERT, P. L., WIRGER, A., SCHMIDT, D. H., VON RUECKER, A., & MUELLER, S. C. Superantigen-activated mononuclear cells induce apoptosis in transitional cell carcinoma. **Anticancer Res**, v. 25, n. 5, p. 3565-3573. PMID: 16101181. 2005.

PEREZ, A. G. M., LICHY, R., LANA, J. F. S. D., RODRIGUES, A. A., LUZO, Â. C. M., BELANGERO, W. D., & SANTANA, M. H. A. Prediction and Modulation of Platelet Recovery by Discontinuous Centrifugation of Whole Blood for the Preparation of Pure Platelet-Rich Plasma. **BioResearch Open Access**, v. 2, n. 4, p. 307-314, 2013.

POON, S. L., HUANG, M. N., CHOO, Y., MCPHERSON, J. R., YU, W., HENG, H. L., GAN, A., MYINT, S. S., SIEW, E. Y., LER, L. D., NG, L. G., WENG, W. H., CHUANG, C. K., YUEN, J. S. P., PANG, S. T., TAN, P., TEH, B. T., & ROZEN, S. G. Mutation signatures implicate aristolochic acid in bladder cancer development. **Genome Med**, n. 7, 2015.

POSTOW, M. A.; CALLAHAN, M. K.; WOLCHOK, J. D. Immune checkpoint blockade in cancer therapy. **J Clin Oncol**, v.33, n. 17, p. 1974, 2015.

POZNAK, V.; ESTILO, C.; C ESTILO. Osteonecrosis of the jaw in cancer patients receiving IV bisphosphonates. **Oncology**, v. 20, n.9, p.1053-62, 2006.

PRAT, J. Ovarian carcinomas: five distinct diseases with different origins, genetic alterations, and clinicopathological features. **Virchows Archiv**, v. 460, n. 3, p. 237-249, 2012.

PRAT, J. Staging Classification for Cancer of the Ovary, Fallopian Tube, and Peritoneum: Abridged Republication of Guidelines from the International Federation of Gynecology and Obstetrics (FIGO). **Obstet Gynecol**, v. 126, n. 1, p. 171-174, 2015.

PRONZATO, P.; JASSEM, J.; MAYORDOMO, J. Epoetin beta therapy in patients with solid tumours. **Crit Rev Oncol Hemat**, v. 58, n. 1, p. 46-52, 2006.

QURESHI, A. H., CHAOJI, V., MAIGUEL, D., FARIDI, M. H., BARTH, C. J., SALEM, S. M., SINGHAL, M., STOUB, D., KRASTINS, B., OGIHARA, M., ZAKI, M. J., & GUPTA, V. Proteomic and phospho-proteomic profile of human platelets in basal, resting state: insights into integrin signaling. **PLOS ONE**, v. 4, n. 10, e7627, 2009.

R CORE TEAM. 'R: A Language and Environment for Statistical Computing'. Vienna, Austria: R Foundation for Statistical Computing, 2022. Available at: https://www.r-project.org/.

RAJABI, H., SHEIKHANI SHAHIN, H., NOROUZIAN, M., MEHRABANI, D., & DEHGHANI NAZHVANI, S. The Healing Effects of Aquatic Activities and Allogenic Injection of Platelet-Rich Plasma (PRP) on Injuries of Achilles Tendon in Experimental Rat. **World J Plast Surg**, v. 4, n. 1, p. 66-73, 2015.

RAMAKRISHNAN, R. et al. Pharmacokinetic and pharmacodynamic modeling of recombinant human erythropoietin after single and multiple doses in healthy volunteers. **J Clin Pharmacol**, v. 44, n. 9, p. 991-1002, 2004.

RANK/RANKL signaling: New therapeutic perspective for non-muscle invasive bladder cancer. **J Clin Oncol**. v. 37, 15 Suppl,2019.

RAWLINGS, J. S., KRISTIN, M., & HARRISON, D. A. The JAK / STAT signaling pathway. **Cell Sci**, n. 1, p. 1281-1283, 2004.

REIS, I. B. et al. OncoTherad® is an immunomodulator of biological response that downregulate RANK/RANKL signaling pathway and PD-1/PD-L1 immune checkpoint in non-muscle invasive bladder cancer. **J Cancer Res Clin Oncol**, p. 1-12, 2022b.

REIS, I. B. et al. OncoTherad®(MRB-CFI-1) nano-immunotherapy reduced tumoral progression in non-muscle invasive bladder cancer through activation of Toll-like signaling pathway. **Tissue Cell**, v. 76, p. 101762, 2022a.

REIS, L. O., FAVARO, W. J., FERREIRA, U., BILLIS, A., FAZUOLI, M. G., & CAGNON, V. H. A. Evolution on experimental animal model for upper urothelium carcinogenesis. **World J Urol**, v. 28, n. 4, p. 499-505, 2010.

REIS, L. O., FERREIRA, U., BILLIS, A., CAGNON, V. H. A., & FAVARO, W. J. Anti-Angiogenic Effects of the Superantigen Staphylococcal Enterotoxin B and Bacillus Calmette-Guerin Immunotherapy for Nonmuscle Invasive Bladder Cancer. **J Urol**, v. 187, n. 2, p. 438-445, 2012.

REIS, L. O., PEREIRA, T. C., FAVARO, W. J., CAGNON, V. H. A., LOPES-CENDES, I., & FERREIRA, U. Experimental animal model and RNA interference: a promising association for bladder cancer research. **World J Urol**, v. 27, n. 3, p. 353-361, 2009.

RENEMA, N. et al. RANK–RANKL signalling in cancer. **Biosc Rep**, v. 36, n. 4, p.e00366. 2016.

RENEMA, N., NAVET, B., HEYMANN, M.-F., LEZOT, F., & HEYMANN, D. RANK-RANKL signalling in cancer. **Biosci Rep**. v. 36, v. 4, 2016.

RIBATTI, D. AND CRIVELLATO, E. Giulio Bizzozero and the discovery of platelets. **Leukemia research**, v. 31, n. 10, p.1339-1341, 2007.

RO, J. Y., STAERKEL, G. A., & AYALA, A. G. Cytologic and Histologic Features of Superficial Bladder-Cancer. **Urol Clin North Am**, n. 19, v. 3, p. 435-453, 1992.

ROBERT, M.D.C. et al. Ipilimumab plus Dacarbazine for Previously Untreated Metastatic Melanoma. **NEJM.** v. 364, p. 2517-2526, 2011.

ROSENBERG, J.E., HOFFMAN-CENSITS, J., POWLES, T., et al. Atezolizumab in patients with locally advanced and metastatic urothelial carcinoma who have progressed following treatment with platinum-based chemotherapy: a single-arm, multicentre, phase 2 trial. **Lancet**, v. 387, p. 1909–1920, 2016.

ROSENQUIST, T. A., & GROLLMAN, A. P. Mutational signature of aristolochic acid: Clue to the recognition of a global disease. **DNA Repair**, v. 44, p. 205-211, 2016.

RUSSELL J. R. et al. Immunostaining for CD31 and CD34 in Kaposi sarcoma. **J Clin Pathol**, v. 48, p.1011 – 6, 1995.

SAIRAH, A. K. et al. The effects of recombinant human erythropoietin and tamoxifen on growth and angiogenesis of mammary tumor in Sprague–Dawley rat. **Am J Pharmacol Toxicol**, v. 4, n. 1, p. 12-16. 2009.

SANDER, B., DAMM, O., GUSTAFSSON, B., ANDERSSON, U., & HAKANSSON, L. Localization of IL-1, IL-2, IL-4, IL-8 and TNF in superficial bladder tumors treated with intravesical Bacillus Calmette-Guerin. **J Urol**, v. 156, n. 2, p. 536-541, 1996.

SANTIN A. D. et al. Secretion of vascular endothelial growth factor in ovarian cancer. **Eur J Gynaecol Oncol,** v. 20, n.3, p.177-181, 1999.

SASAKI T. et al. Structural basis and potential role of heparin/heparan sulfate binding to the angiogenesis inhibitor endostatin. **EMBO J**, v. 18, p. 6240– 8, 1999.

SATO, E. et al. Intraepithelial CD8+ tumor-infiltrating lymphocytes and a high CD8+/regulatory T cell ratio are associated with favorable prognosis in ovarian cancer. **PNAS** vol. 102 (51) 18538-18543, 2005

SATOH, T., & AKIRA, S. Toll-Like Receptor Signaling and Its Inducible Proteins. Microbiology **Spectrum,** v. 4, n. 6, 2016.

SATOH, T.; AKIRA, S. Toll-Like Receptor Signaling and Its Inducible Proteins. **Microbiol Spect** v. 4, n. 6, 2016.

SAYAN, D. C. et al. Could erythropoietin reduce the ovarian damage of cisplatin in female rats? **Gynecol Endocrinol**, v. 34,n.4, p. 309-313, 2018.

SCARLETT, U. K. et al. In situ stimulation of cd40 and toll-like receptor 3 transforms ovarian cancer-infiltrating dendritic cells from immunosuppressive to immunostimulatory cells. **Cancer Res**, v. 69, n. 18, p. 7329-7337, 2009.

SCHAMHART, D. H. J., DE BOER, E. C., DE REIJKE, T. M., & KURTH, K. H. Urinary cytokines reflecting the immunological response in the urinary bladder to biological response modifiers: Their practical use. **Eur Urol**, v. 37, p. 16-23, 2000.

SELIGER, B. et al. The complex role of B7 molecules in tumor immunology. **Trends Mol Med**, v. 14, n. 12, p. 550-559, 2008.

SEMPLE, J. W., & FREEDMAN, J. Platelets and innate immunity. **Cell Mol Life Sci**, v. 67, n. 4, p. 499-511, 2010.

SENGER, D. R. et al. Vascular permeability factor (VPF, VEGF) in tumor biology **Cancer and Metastasis Rev**. v. 12, p. 303–324, 1993.

SESHASAYEE, D. et al. A Novel in Vivo Role for Osteoprotegerin Ligand in Activation of Monocyte Effector Function and Inflammatory Response. **Biol Chem**, v. 12, n. 1, p. 17-25, 2006.

SHANKARAN, V., IKEDA, H., BRUCE, A. T., WHITE, J. M., SWANSON, P. E., OLD, L. J., & SCHREIBER, R. D. IFN gamma and lymphocytes prevent primary tumour development and shape tumour immunogenicity. **Nature**, v. 410, n. 6832, p. 1107-1111, 2001.

SHIMOJO, A. A., PEREZ, A. G., GALDAMES, S. E., BRISSAC, I. C., & SANTANA, M. H. Performance of PRP associated with porous chitosan as a composite scaffold for regenerative medicine. **Sci World J**, v. 2015, ID 396131, 2015.

SHIROTA, Y., SHIROTA, H.; KLINMAN, D. M. Intratumoral injection of CpG oligonucleotides induces the differentiation and reduces the immunosuppressive activity of myeloid-derived suppressor cells. **J Immunol**, v. 188, n. 4, p. 1592-1599, 2012.

SIGL V, et al. RANKL/RANK control Brca1 mutation-driven mammary tumors. **Cell research**, v. 26, n. 7, p.761-74, 2016 STEWART, C.; RALYEA, C.; LOCKWOOD, S. Ovarian Cancer: An Integrated Review. **Semin Oncol Nurs**, v. 35, n. 2, p.151-156, 2019.

SILVEIRA H.S. et al. P-MAPA activates TLR2 and TLR4 signaling while its combination with IL-12 stimulates CD4+ and CD8+ effector T cells in ovarian cancer. **Life Sci**, v. 254, p. 117786, 2020.

SMYTH, M. J. et al. Combination cancer immunotherapies tailored to the tumour microenvironment, **Nat Rev Clin Oncol**, v. 13, p. 143–158, 2015.

SOLOWAY, M. S., NISSENKORN, I., & MCCALLUM, L. Urothelial Susceptibility to Tumor-Cell Implantation - Comparison of Cauterization with N-Methyl-N-Nitrosourea. **Urology**, v. 21, n. 2, p. 159-161, 1983.

STEINBERG, G. D., BRENDLER, C. B., ICHIKAWA, T., SQUIRE, R. A., & ISAACS, J. T. Characterization of an N-Methyl-N-Nitrosourea-Induced Autochthonous Rat Bladder-Cancer Model. **Cancer Res**, v. 50, n. 20, p. 6668-6674. Pubmed: 2208131. 1990.

STEINBERG, G. D., SMITH, N. D., RYDER, K., STRANGMAN, N. M., & SLATER, S. J. Factors Affecting Valrubicin Response in Patients with Bacillus Calmette-Guerin-Refractory Bladder Carcinoma In Situ. **Postgrad Med**, v. 123, n. 3, p. 28-34, 2011.

STEWART, S. L. et al. Characterization of a carcinogenesis rat model of ovarian preneoplasia and neoplasia. **Cancer Res**, v.64, n. 22, p. 8177-8183, 2004.

STOPIGLIA, R. M., MATHEUS, W. E., GARCIA, P. V., BILLIS, A., CASTILHO, M. A., HUGO, V., & JESUS, F. D. Molecular Assessment of Non-Muscle Invasive and Muscle Invasive Bladder Tumors : Mapping of Putative Urothelial Stem Cells and Toll-Like Receptors (TLR) Signaling. (February), **J Cancer Ther**, v. 6, n. 2, p. 129-140, 2015.

SWIFT, S. et al. Absence of functional EpoR expression in human tumor cell lines. **Am J Hematol**, v. 115, n. 21, p. 4254- 4263, 2010.

TADDEI, L. et al. Inhibitory effect of full-length human endostatin on in vitro angiogenesis. **Biochem. Biophys. Res. Commun**., v. 263, 1999.

TAKEDA, K., & AKIRA, S. TLR signaling pathways. **Semin Immunol**, v. 16, n. 1, p. 3-9, 2004.

TANOS T, et al. Progesterone/RANKL is a major regulatory axis in the human breast. **Sci Transl Med**. v. 5, n. 182, p.182ra55, 2013.

TASKIRAN C. et al. The prognostic value of endoglin (CD105) expression in ovarian carcinoma. **Int J Gynecol Cancer**, v. 16, p.1789–93, 2006.

TATE, D. J., PATTERSON, J. R., VELASCO-GONZALEZ, C., CARROLL, E. N., TRINH, J., EDWARDS, D., AIYAR, A., FINKEL-JIMENEZ, B., & ZEA, A. H. Interferon-Gamma-Induced Nitric Oxide Inhibits the Proliferation of Murine Renal Cell Carcinoma Cells. **Int J Biol Sci**, n. 8, v. 8, p. 1109-1120, 2012.

TAUBE, J.M. et al. Implications of the tumor immune microenvironment for staging and therapeutics. **Modern Pathol**, v. 3, p. 214-234, 2017.

TAUBE, J.M., ANDERS, R.A., YOUNG, G.D., et al. Colocalization of inflammatory response with B7-h1 expression in human melanocytic lesions supports an adaptive resistance mechanism of immune escape. **Sci Transl Med**, v. 4, 127ra137, 2012.

TAUBE, J.M., GALON, J., SHOLL, L.M., RODIG, S.J., COTTRELL, T.R., GIRALDO, N.A., BARAS, A.S., PATEL, S.S., ANDERS, R.A., RIMM, D.L., CIMINO-MATHEWS, A. Implications of the tumor immune microenvironment for staging and therapeutics. **Mod Pathol**, 3, 214-234, 2018.

TE VELDE E. A. et al. Early endostatin treatment inhibits metastatic seeding of murine colorectal cancer cells in the liver and their adhesion to endothelial cells. **Br J Cancer**, v. 62, 2005.

TEFFERI, A. JAK and MPL mutations in myeloid malignancies. **J Leuk Lymphoma**, v. 49, n. 3, p. 388-397, 2008.

TEW, W. P. et al. PARP inhibitors in the management of ovarian cancer: ASCO guideline. **Obst Gynecol Surv**, v. 75, n. 12, p. 739-741, 2020.

THERESA L. et al. CTLA-4 can function as a negative regulator of T cell activation. **Immunity.** v. 1, p. 405-413, 1994.

THOMAS, S. J., SNOWDEN, J. A., ZEIDLER, M. P., & DANSON, S. J. The role of JAK/STAT signalling in the pathogenesis, prognosis and treatment of solid tumours. **Br J Cancer**, v. 113, n. 3, p. 365-371, 2015.

TING, A. Y. et al. Characterization of a preclinical model of simultaneous breast and ovarian cancer progression. **Carcinogenesis**, v. 28, n. 1, p. 130-135, 2007.

TJALMA W. et al. Quantification and prognostic relevance of angiogenic parameters in invasive cervical cancer. **Br J Cancer**, v. 78, p.170 – 4, 1998.

TSAI-TURTON, M.; NAKAMURA, B. N.; LUDERER, U. Induction of apoptosis by 9,10-dimethyl-1,2-benzanthracene in cultured preovulatory rat follicles is preceded by a rise in reactive oxygen species and is prevented by glutathione. **Biol Reprod**, v. 77, n. 3, p. 442-451, 2007.

UBEZIO, G., GHIO, M., CONTINI, P., BERTORELLO, R., MARINO, G., TOMASINI, A., & TRIPODI, G. Bio-modulators in platelet-rich plasma: a comparison of the amounts in products from healthy donors and patients produced with three different techniques. **Blood Transfus**, 12 Suppl 1, s214-220, 2014.

VAN DAM, P. A. et al. RANK-RANKL Signaling in Cancer of the Uterine Cervix: A Review, Int **J Mol Sci**, v. 20, n.9, p. 2183, 2019.

VAN DAM, P.A. et al. RANK/RANKL signaling inhibition may improve the effectiveness of checkpoint blockade in cancer treatment. **Crit Rev Oncol Hematol**, v. 133, p.85-91, 2019.

VENDRAMIN, F. S., FRANCO, D., NOGUEIRA, C. M., PEREIRA, M. S., & FRANCO, T. R. Plasma rico em plaquetas e fatores de crescimento: técnica de preparo e utilização em cirurgia plástica. **Rev Col Bras Cir**, v. 33, p. 24-28, 2006.

VERMEULEN P. B. et al. Quantification of angiogenesis in solid human tumors: an international consensus on the methodology and criteria of evaluation. **Eur J Cancer**, v. 32, p. 2474 – 84, 1996.

VIEIRA, S. C. Quantification of angiogenesis in cervical cancer: a comparison among three endothelial cell markers. **Gynecol. Oncol**. v. 93, p.121-124, 2004.

VIGNATI, S. et al. Trail activity in human ovarian cancer cells: potentiation of the action of cytotoxic drugs, **Eur J Cancer**, v. 38, n. 1, p. 177-183. 2002.

VINANICA, N. et al. Specific stimulation of T lymphocytes with erythropoietin for adoptive immunotherapy. **Am JHematol**, v. 135, n. 9, p. 668-679, 2020.

WADA, T. et al. RANKL–RANK signaling in osteoclastogenesis and bone disease. **Trends Mol Med0**, v. 12, n. 1, p. 17-25, 2006.

WALKER, L. S. K. SANSOM, D. M. The emerging role of CTLA4 as a cell-extrinsic regulator of T cell responses. **Nat. Rev. Immunol**. v. 11, p. 852–863, 2011.

WANG, Jia et al. Human FOXP3 and tumour microenvironment. **Immunology**, 2022.

WAT, J. M., FOLEY, J. H., KRISINGER, M. J., OCARIZA, L. M., LEI, V., WASNEY, G. A., LAMEIGNERE, E., STRYNADKA, N. C., SMITH, S. A., MORRISSEY, J. H., & CONWAY, E. M. (2014). Polyphosphate suppresses complement via the terminal pathway. **Blood**, v. 123, n. 5, p. 768-776, 2014.

WATERHOUSE, P. et al. Lymphoproliferative Disorders with Early Lethality in Mice Deficient in Ctla-4. **SCIENCE.** v. 270, p. 985-988, 1995

WEBB, P. M.; JORDAN, S. J. Epidemiology of epithelial ovarian cancer. **Best Pract Res Clin Obstet Gynaecol**, v. 41, p. 3-14, 2017.

WEIDNER N. et al. Tumor angiogenesis and metastasis correlation in invasive breast cancer. **N Engl J Med.** v.324, p.1 – 8, 1991.

WELDON, T. E., & SOLOWAY, M. S. Susceptibility of urothelium to neoplastic cellular implantation. **Urology**, v. 5, n. 6, p. 824-827, 1975.

WICKSTROM, S. A.; ALITALO, K.; KESKI-OJA, J. Endostatin associates with integrin α5β1 and caveolin-1, and activates Src via a tyrosyl phosphatase-dependent pathway in human endothelial cells. **Cancer Res.** v. 62, n.19, p.5580-9, 2002.

WIESER, V., et al. Clinical Impact of RANK Signalling in Ovarian Cancer. **Cancers**, v. 11, n. 6, p.791. 2019.

WONG B. R. et al. TRANCE (tumor necrosis factor [TNF]-related activation-induced cytokine), a new TNF family member predominantly expressed in T cells, is a dendritic cell-specific survival factor. **J Exp Med,** v. 186, n. 12, p. 2075–2080, 1997.

WOO, S. R., FUERTES, M. B., CORRALES, L., SPRANGER, S., FURDYNA, M. J., LEUNG, M. Y., DUGGAN, R., WANG, Y., BARBER, G. N., FITZGERALD, K. A., ALEGRE, M. L., & GAJEWSKI, T. F. STING-dependent cytosolic DNA sensing mediates innate immune recognition of immunogenic tumors. **Immunity**, v. 41, n. 5, p. 830-842, 2014.

YANG, X.Y. et al. Optimization of 7,12-dimethylbenz(a)anthracene-induced rat epithelial ovarian tumors. **Oncol Lett**, v. 21, n. 3, p. 206, 2021.

YANG, Y. Cancer immunotherapy: harnessing the immune system to battle cancer. **J Clin Invest**, v. 125, n. 9, p. 3335-3337, 2015.

YASUDA, Y. et al. Expression of erythropoietin in human female reproductive organs. **Ital J Anat Embryol**, v. 106, n. 2, Suppl 2, p. 215-222, 2001.

YOKOYAMA Y.; RAMAKRISHNAN S. Binding of endostatin to human ovarian cancer cells inhibits cell attachment**. Int J Cancer**, v. 121, 2007.

YU, D. S., LEE, C. F., & CHANG, S. Y. Immunotherapy for orthotopic murine bladder cancer using bacillus Calmette-Guerin recombinant protein Mpt-64. **J Urol**, v. 177, n. 2, p. 738-742, 2007.

ZEEGERS, M. P. A., TAN, F. E. S., DORANT, E., & VAN DEN BRANDT, P. A. The impact of characteristics of cigarette smoking on urinary tract cancer risk - A meta-analysis of epidemiologic studies. **Cancer**, n. 89, n. 3, p. 630-639, 2000.

ZENG X. et al. Endostatin binds biglycan and LDL and interferes with LDL retention to subendothelial matrix during atherosclerosis. **J Lipid Res** v. 46, 2005.

ZHANG, L.; CONEJO-GARCIA, J. R.; KATSAROS, D.; GIMOTTY, P. A. et al. Intratumoral T cells, recurrence, and survival in epithelial ovarian cancer. **N Engl J Med**, v. 348, n. 3, p. 203-213, 2003.

ZHANG, S. et al. Analysis of CD8+ Treg cells in patients with ovarian cancer: a possible mechanism for immune impairment. **Cel Mol Immunol**, v. 12, n. 5, p. 580-591, 2015.

ZHAO, S., ZHANG, Y. F., ZHANG, Q. Y., WANG, F., & ZHANG, D. K. Toll-like receptors and prostate cancer. **Front Immunol**, n. 5. 2014.

ZHOU, H.; YOUNG, C. J.; LOCH-CARUSO, R.; SHIKANOV, A. Detection of lindane and 7,12-dimethylbenz[a]anthracene toxicity at low concentrations in a three-dimensional ovarian follicle culture system. **Reprod Toxicol**, v. 78, p. 141-149, 2018.

ZHOU, M. et al. Toll-like receptor expression in normal ovary and ovarian tumors. **Cancer Immunol Immunother**, v. 58, n. 9, p.1375-1385, 2009.

ZONTA, Y. R. et al. Melatonin Reduces Angiogenesis in Serous Papillary Ovarian Carcinoma of Ethanol-Preferring Rats. **IntJ Mol Sci**, v. 18, n. 4, 2017.

ZSIROS, E., TANYI, J., BALINT, K., KANDALAFT, L. E. Immunotherapy for ovarian cancer: recent advances and perspectives. **Cur Op Oncol**, v. 26, n. 5, p. 492-500, 2014.

8. ANEXOS

8.1. Certificado de Bioética e Biossegurança: Projeto Câncer de Bexiga (Capítulo I)

UNICAMP

CEUA/UNICAMP

CERTIFICADO

Certificamos que a proposta intitulada **Nova Perspectiva Terapêutica para o Câncer de Bexiga Não-Músculo Invasivo (CBNMI): Associação Intravesical do Plasma Rico em Plaquetas (PRP) e Imunoterapia com o Modificador de Resposta Biológica – Complexo Fosfato Inorgânico 1 (MRB-CFI-1)**, registrada com o nº **4871-1/2018**, sob a responsabilidade de **Prof. Dr. Wagner José Fávaro / Prof. Dr. Nelson Eduardo Durán Caballero / Murilo Izidoro Santos**, que envolve a produção, manutenção ou utilização de animais pertencentes ao filo *Chordata*, subfilo *Vertebrata* (exceto o homem) para fins de pesquisa científica (ou ensino), encontra-se de acordo com os preceitos da **LEI Nº 11.794, DE 8 DE OUTUBRO DE 2008**, que estabelece procedimentos para o uso científico de animais, do **DECRETO Nº 6.899, DE 15 DE JULHO DE 2009**, e com as normas editadas pelo **Conselho Nacional de Controle da Experimentação Animal (CONCEA), tendo sido** aprovada pela **Comissão de Ética no Uso de Animais** da **Universidade Estadual de Campinas - CEUA/UNICAMP,** em **16 de abril de 2018**.

Finalidade:	**( ) Ensino (X) Pesquisa Científica**
Vigência do projeto:	**17/05/2018-17/04/2021**
Vigência da autorização para manipulação animal:	**17/05/2018-17/04/2021**
Espécie / linhagem/ raça:	**Camundongo isogênico / C57BL/6JUnib**
No. de animais:	**120**
Idade/Peso:	**07 semanas / 40g**
Sexo:	**Fêmeas**
Origem:	**CEMIB/UNICAMP**
Biotério onde serão mantidos os animais:	**Biotério da Anatomia, Área de Anatomia, DBEF, IB/UNICAMP**

A aprovação pela CEUA/UNICAMP não dispensa autorização prévia junto ao **IBAMA**, **SISBIO** ou **CIBio** e é **restrita** a protocolos desenvolvidos em biotérios e laboratórios da Universidade Estadual de Campinas.

Campinas, 16 de abril de 2018.

Profa. Dra. Raquel Franco Leal
Vice Coordenadora

Fátima Alonso
Secretária Executiva

IMPORTANTE: Pedimos atenção ao prazo para envio do relatório final de atividades referente a este protocolo: até 30 dias após o encerramento de sua vigência. O formulário encontra-se disponível na página da CEUA/UNICAMP, área do pesquisador responsável. A não apresentação de relatório no prazo estabelecido impedirá que novos protocolos sejam submetidos.

UNICAMP

CEUA/Unicamp

Comissão de Ética no Uso de Animais
CEUA/Unicamp

CERTIFICADO

Certificamos que o projeto de pesquisa intitulado **Nova Perspectiva Terapêutica para o Câncer de Bexiga Não-Músculo Invasivo (CBNMI): Associação Intravesical do Plasma Rico em Plaquetas (PRP) e Imunoterapia com o Modificador de Resposta Biológica – Complexo Fosfato Inorgânico 1 (MRB-CFI-1)** (protocolo CEUA/UNICAMP nº **4871-1/2018**), de responsabilidade do **Prof. Dr. Wagner José Fávaro** e **Murilo Izidoro Santos**, teve aprovada a inclusão da executora **Bianca Ribeiro de Souza Sasaki**.

Este documento é válido apenas se apresentado junto com o certificado emitido originalmente pela CEUA/UNICAMP em 16/04/2018.

Campinas, 13 de setembro de 2018.

Profa. Dra. Liana M. C. Verinaud
Membro

Fátima Alonso
Secretária Executiva

CEUA/UNICAMP
Caixa Postal 6109
13083-970 Campinas, SP – Brasil

Telefone: (19) 3521-6359
E-mail: comisib@unicamp.br
http://www.ib.unicamp.br/ceea/

8.2. Certificado de Bioética e Biossegurança: Projeto Câncer de Ovário (Capítulo II)

UNICAMP

CEUA/UNICAMP

CERTIFICADO

Certificamos que a proposta intitulada **Associação da Imunoterapia com OncoTherad® (MRB-CFI-1) e Eritropoetina no Tratamento do Câncer de Ovário Quimicamente Induzido em Ratas: Avaliação da Resposta Inflamatória Citotóxica, Angiogênese e Checkpoints Imunológicos**, registrada com o nº **5555-1/2020**, sob a responsabilidade de **Prof. Dr. Ana Carolina Deckmann e Bianca Ribeiro de Souza Sasaki, Gabriela de Oliveira, Felippe Augusto Tossini Cabral, Juliane Lima Baggio de Paula**, que envolve a produção, manutenção ou utilização de animais pertencentes ao filo *Chordata*, subfilo *Vertebrata* (exceto o homem) para fins de pesquisa científica (ou ensino), encontra-se de acordo com os preceitos da **LEI Nº 11.794, DE 8 DE OUTUBRO DE 2008**, que estabelece procedimentos para o uso científico de animais, do **DECRETO Nº 6.899, DE 15 DE JULHO DE 2009**, e com as normas editadas pelo **Conselho Nacional de Controle da Experimentação Animal (CONCEA), tendo sido** aprovada pela **Comissão de Ética no Uso de Animais** da **Universidade Estadual de Campinas - CEUA/UNICAMP**, em reunião de **18/06/2020**.

Finalidade:	**( ) Ensino (X) Pesquisa Científica**
Vigência do projeto:	01/07/2020 a 01/07/2022
Vigência da autorização para manipulação animal:	18/06/2020 a 01/07/2022
Espécie / linhagem/ raça:	Rato isogênico / F344/NTacUnib
No. de animais:	10
Idade/Peso:	28.00 Dias / 100.00 Gramas
Sexo:	10 Fêmeas
Espécie / linhagem/ raça:	Rato isogênico / F344/NTacUnib
No. de animais:	10
Idade/Peso:	28.00 Dias / 100.00 Gramas
Sexo:	10 Fêmeas
Espécie / linhagem/ raça:	Rato isogênico / F344/NTacUnib
No. de animais:	10
Idade/Peso:	28.00 Dias / 100.00 Gramas
Sexo:	10 Fêmeas
Espécie / linhagem/ raça:	Rato isogênico / F344/NTacUnib
No. de animais:	10
Idade/Peso:	28.00 Dias / 100.00 Gramas
Sexo:	10 Fêmeas
Espécie / linhagem/ raça:	Rato isogênico / F344/NTacUnib
No. de animais:	10
Idade/Peso:	28.00 Dias / 100.00 Gramas
Sexo:	10 Fêmeas
Espécie / linhagem/ raça:	Rato isogênico / F344/NTacUnib
No. de animais:	10
Idade/Peso:	28.00 Dias / 100.00 Gramas
Sexo:	10 Fêmeas
Espécie / linhagem/ raça:	Rato isogênico / F344/NTacUnib
No. de animais:	10
Idade/Peso:	28.00 Dias / 100.00 Gramas
Sexo:	10 Fêmeas
Origem:	CEMIB – Centro Multidisciplinar para Investigação Biológica na Área da Ciência em Animais de Laboratório - UNICAMP
Biotério onde serão mantidos os animais:	Biotério da Anatomia, Área de Anatomia, DBEF, IB/UNICAMP

A aprovação pela CEUA/UNICAMP não dispensa autorização a junto ao **IBAMA,SISBIO** ou **CIBio** e é **restrita** a protocolos desenvolvidos em biotérios e laboratórios da Universidade Estadual de Campinas.

Campinas, **06 de julho de 2020**.

p/ Cinthia Baú Betim Cazarin

Prof. Dr. Wagner José Fávaro
Presidente

Rosangela dos Santos
Secretária Executiva

IMPORTANTE: Pedimos atenção ao prazo para envio do relatório final de atividades referente a este protocolo: até 30 dias após o encerramento de sua vigência. O formulário encontra-se disponível na página da CEUA/UNICAMP, área do pesquisador responsável. A não apresentação de relatório no prazo estabelecido impedirá que novos protocolos sejam submetidos.

8.3. Declaração de Direitos Autorais

Declaração

As cópias de artigos de minha autoria ou de minha co-autoria, já publicados ou submetidos para publicação em revistas científicas ou anais de congressos sujeitos a arbitragem, que constam da minha Dissertação/Tese de Mestrado/Doutorado, intitulada **AVALIAÇÃO DA IMUNOTERAPIA COM O ONCOTHERAD® (MRB-CFI-1) E ASSOCIAÇÕES NO TRATAMENTO ONCOLÓGICO: CÂNCER DE BEXIGA E CÂNCER DE OVÁRIO**, não infringem os dispositivos da Lei n.° 9.610/98, nem o direito autoral de qualquer editora.

Campinas, 07 de julho de 2023

Assinatura : _____
Nome do(a) autor(a): **Bianca Ribeiro de Souza**
RG n.° 48.884.327-3

Assinatura : _____
Nome do(a) orientador(a): **Wagner José Fávaro**
RG n.° 33.478.777-4